Investigating long-term temporal variability of soil moisture and differences in dynamics in wet and dry periods

Rita Duzzo Grohs

Submitted in total fulfilment of the requirements of the degree of

Doctor of Philosophy

November 2022

STATEMENT OF ORIGINALITY

I hereby certify that the work embodied in the thesis is my own work, conducted under normal supervision. The thesis contains no material which has been accepted, or is being examined, for the award of any other degree or diploma in any university or other tertiary institution and, to the best of my knowledge and belief, contains no material previously published or written by another person, except where due reference has been made. I give consent to the final version of my thesis being made available worldwide when deposited in the University's Digital Repository, subject to the provisions of the Copyright Act 1968 and any approved embargo.

Rita Duzzo Grohs

Acknowledgments

I would like to thank my supervisors that were crucial for the completion of this PhD. Professor Garry Willgoose (*in memoriam*), thank you for all the support you gave me, for always believing in me and encouraging me. Your passion for teaching was inspiring. Associate Professor Patricia Saco, thank you for your support since day one and for the feedback you gave me along the way. Dr Kelsey McDonough, thank you for all the encouragement and conversations we had. Associate Professor Jose Rodriguez, your guidance was super valuable and helpful, thank you. Associate Professor Greg Hancock, thank you for the good inputs and conversations we had. Thank you all the staff from the University of Newcastle for all the assistance provided. I acknowledge the Australian Government Research Training Program Scholarship, thank you for making this possible. I would like to thank the thesis examiners for their comments, they contributed for an improved final version of the thesis.

I would like to thank my colleagues that made my day better and became good friends. Thank you also for all the help along this long and challenging journey. Thank you Angelo, Juan, Eliana, Elham, Samira, Armin and Natã.

Thank you to my close friends that gave me support in different stages of this PhD journey. Thank you to all my friends from Feijão com arroz, you are my safety net here. A special thanks to Tamy, Marina, Glei, Babi, Pri, Cintia, Monica, Leticia and Lynn. Thank you to my family and friends that are present in my life even so far away, I love you. Thank you to my psychologist, Patricia Lima de Oliveira, that provided help when I most needed.

Thank you to my amazing partner, Guilherme, for being by my side, for making me laugh and for being so patient.

I dedicate this thesis to my family: pai, mãe e Lavi, amo vocês demais!

Abstract

Soil moisture represents a reservoir of water in the soil, that is crucial to the hydrologic cycle and land-atmosphere interactions. Soil moisture allows vegetation to grow, affects evapotranspiration, water distribution, and food production. Because of its high spatial and temporal variability, and uncertainties on its future availability, studies on long-term soil moisture trend are important to manage and allocate water, and to help to develop strategies for water security (McDonough et al., 2020). The main attributes (e.g., topography, soil properties) that drive the spatial organization of soil moisture change according to the wetness period (e.g., dry or wet), and are also dependent on the climate in which the catchment is inserted. Previous work analysed soil moisture spatial and temporal variability in dry and wet conditions in a temperate climate (Grayson et al., 1997; Western et al., 1999) and in a humid-subtropical climate (Famiglietti et al., 1998) and found that soil properties (e.g., porosity and hydraulic conductivity) governed soil moisture temporal variability in wet conditions, while elevation, aspect, and clay content dictated governed soil moisture variability in dry conditions (Famiglietti et al., 1998). This work investigates soil moisture temporal and spatial variability in conditions that are wetter and drier than average, in two Australian catchments located in a semiarid subhumid climate, through the comparison of physical drivers of soil moisture using in-situ dataset in clay and sandy soils.

Preferential flow is known to contribute for spatial soil moisture variability. It allows water and solutes to move faster along the soil profile than they would with uniform infiltration (Hendrickx & Flury, 2001; Hardie et al., 2013). Macropore flow is one form of preferential flow, characterised for the flow in fissures or cracks (Gerke, 2006). Our study area encompasses a region characterised by Vertisols, that is, soils rich in expansive clay and the presence of cracks in the soil mentioned in other studies (Rüdiger, 2006; Martinez, 2010). An investigation on macropore preferential flow was never carried in the site, thus, this study aims to apply a dual-porosity model to assess how a model that accounts for preferential paths perform in the site.

Along with soil moisture temporal and spatial variability, climate change adds uncertainty to climate and consequently to soil moisture modelling. Soil moisture has an

important role in land-atmosphere feedback mechanisms (Koster et al., 2004; Zhang et al., 2008; Seneviratne et al., 2010; Whan et al., 2015; Lo et al., 2021) and it represents an important influence in climate-change projections (Seneviratne et al., 2010). Long periods of soil moisture data (e.g., greater than 10-15 years) are necessary to investigate temporal anomalies and to be able to evaluate the impact of those anomalies within a hydrological context (Brocca et al., 2014; Brocca et al., 2017). Studies on long-term soil moisture trends are predominantly carried on a global scale, with a coarse spatial resolution dataset (25 to 100 km pixel) (Sheffield & Wood, 2008a; Dorigo et al., 2012; Albergel et al., 2013; Deng et al., 2020) that mask local and regional trends. The global scale studies on soil moisture trends usually analyse surface soil moisture (~7 cm) trends (Sheffield & Wood, 2008a; Dorigo et al., 2012; Feng & Zhang, 2015; Deng et al., 2020), and not the profile layer (~100 cm). Surface and profile soil layers impact differently the soil moisture processes, i.e., the surface layer is where the flux of mass and energy with the atmosphere occurs (Brocca et al., 2009), while the profile soil moisture is a better representation of vegetation (Wigneron et al., 1999; Santos et al., 2014). This study investigates the long-term variability of soil moisture in New South Wales, Australia, both in the surface (0-10 cm) and the profile layers of soil (0-100 cm), in a finer spatial resolution (5×5 km pixel).

Contents

List of figures

List of tables

Chapter 1. Introduction

Soil moisture is an important freshwater reservoir and has substantial importance at local, regional and global scales. At a global scale, soil moisture is key in global hydrologic cycle, through the evaporation from bare soil and transpiration from plants, and in climate cycles, by the partitioning of the incoming energy into latent and sensible heat (Seneviratne et al., 2010; Lo et al., 2021). At a regional scale, soil moisture has impact on inter-basin water allocation by evapotranspiration and an influence on regional flooding and drought by affecting the surplus or deficit of water in an aquifer (Famiglietti & Rodell, 2013). Regional soil moisture trends are driven by small-scale land-atmosphere interactions, and to understand the patterns of these regional soil moisture is crucial for local agricultural and industrial needs (McDonough et al., 2020). At a local scale, the amount of water local soil moisture present in the rooting zone of a vegetated soil profile, the water movement dynamics and soil properties as the water-holding capacity (Romano, 2014) are the focus of study of hydrologists, scientists and modellers. To understand local soil moisture patterns is crucial for the better understanding of regional and global soil moisture behaviour.

Soil moisture can vary significantly over space and time, even within a single catchment. The governing forces that drive soil moisture behaviour can vary depending on the season, predominant rainfall regime and the scale of analysis. At the local scale, preferential flow, that is when water bypasses a fraction of the porous soil matrix, is a great contributor to soil moisture spatial variability (Hendrickx & Flury, 2001; Simunek et al., 2003; Gerke, 2006). Further at this local scale, soil moisture can vary vertically, depending on the depth of the soil layer. Surface (top 10 cm) and profile layers (root zone) represent different processes that happen in the soil, the first is representative of climatic processes (Brocca et al., 2009), and the second is a better representation of vegetation (Cai et al., 2009; Santos et al., 2014). Several approaches have been developed to quantify and understand soil moisture variability, including statistical (Famiglietti et al., 2008; Brocca et al., 2010; Zucco et al., 2014), geostatistical (Western et al., 1998; Brocca et al., 2007; Korres et al., 2015) and fractal (Korres et al., 2015) studies.

The availability of long-term data sets of fine resolution is still missing. Soil moisture data can be obtained by in-situ measurements, modelling or via satellite, each method has its advantages and disadvantages. For instance, in-situ data is the most reliable data but only gives point measurement and to have a large area is costly, whereas satellite data can cover large areas but usually give a coarser spatial resolution (~25 km) and provide data from the top layer of the soil. Due to the complexity and uncertainties surrounding the drivers of soil moisture variability over space and time and the major implications soil moisture has in numerous applications, including agricultural and city management, weather and climate forecasting (Famiglietti et al., 1998; Rhodin et al., 1999; Koster et al., 2003; Daly & Porporato, 2005; Kerr, 2007; Huang et al., 2016; McDonough et al., 2020) studies on soil moisture are needed. The gaps in soil moisture knowledge that require scientific and technological developments include, but are not restricted to, the advance in the current understanding of the interactions between elements that control the spatiotemporal soil moisture distribution (i.e., vegetation, soil texture, preferential flow, seasonality) and studies on soil moisture trend in a regional scale for both surface and profile layers.

1.1 Motivation

Soil moisture is generally ascribed to the water stored in the unsaturated zone or the region of the soil profile from the surface to the top of the water table. Soil moisture is an important freshwater reservoir that is crucial for sustaining vegetation and represents 0.15% of the total liquid or available freshwater on Earth (Dingman, 1994; Western et al., 2002). Soil moisture is a key climate variable (Albergel et al., 2013) that determines the availability of water for plant transpiration and soil evaporation (Jung et al., 2010; Seneviratne et al., 2010) and plays a critical role in the hydrological cycle by determining whether precipitation will infiltrate or flow superficially (Rüdiger et al., 2007). Furthermore, soil moisture influences both the energy and biogeochemical cycles, and understanding soil moisture-climate interactions has been gaining more attention (Seneviratne et al., 2010). A key characteristic of soil moisture is its variability over both space and time. Physical environmental factors, such as topography, vegetation and soil type, influence soil moisture dynamics, although they may be more or less important depending on the characteristics of the catchment, location, climate and weather. Soil moisture spatial and temporal variability has been explored over the years (Bell et al., 1980; Vachaud et al., 1985; Famiglietti et al., 1998; Grayson & Western, 1998; Brocca et al., 2012; Zucco et al., 2014; Korres et al., 2015) and several approaches have been developed to quantify and understand soil moisture variability, including statistical, geostatistical and fractal methodologies. However, the complexity of soil moisture variability over space and time continues to make characterisation of soil moisture behaviour a challenge.

Seasonal differences in rainfall patterns can change the main attributes (e.g., topography, soil properties) that will drive the spatial organisation of soil moisture. In wet areas, lateral distribution is present (Western et al., 2002; Brocca et al., 2007), whereas in dry conditions, lateral distribution is almost non-existent and vertical fluxes predominate (Grayson et al., 1997; Western et al., 2004; Korres et al., 2015). Grayson et al. (1997) found that soil moisture has two preferred states: the dry state and the wet state, and that in the dry state spatiotemporal patterns are driven by the local characteristics of soil and vegetation and in the wet state, because of the lateral flow, soil moisture at one point has a connection with its upslope area. This change in soil moisture dynamics in different wetness periods, i.e., dry and wet, also depends on the climate that the catchment is inserted into. In an arid catchment the dry state prevails, so even if a saturated state is approached the evapotranspiration is generally high enough to prevent the soil from fully saturating (Grayson et al., 1997). In a catchment located in a temperate climate, terrain index, which represents the terrain convergence, was the major predictor for spatial organisation of soil moisture during wet periods, while the potential radiation index was a better predictor in dry periods (Western et al., 1999). In a humid-subtropical area, Famiglietti et al. (1998) found that soil properties (e.g., porosity and hydraulic conductivity) dictated the surface soil moisture temporal variability in wet conditions, while in dry conditions this regulation was driven by elevation, aspect and clay content.

A great contributor to spatial soil moisture variability is preferential flow, which is characterised by water and solutes moving along certain pathways and bypassing a fraction of the porous soil matrix (Hendrickx & Flury, 2001; Simunek et al., 2003; Gerke, 2006). Preferential flow is considered to be a common phenomenon in soils (Flury et al., 1994; Hardie et al., 2011) and in the last twenty years the study of preferential flow through the use of hydrological models that account for nonequilibrium flow has become more popular (Šimůnek & van Genuchten, 2008). In loamy to clay soils, water may move along cracks or fissures (Beven & Germann, 1982) which allows water to move faster along the soil profile than it would with uniform infiltration (Hendrickx & Flury, 2001; Hardie et al., 2013). Along with soil moisture temporal and spatial variability, climate change adds uncertainty to climate and consequently to soil moisture modelling. Soil moisture has an important role in land–atmosphere feedback mechanisms (Koster et al., 2004; Zhang et al., 2008; Seneviratne et al., 2010; Whan et al., 2015; Lo et al., 2021) and it represents an important influence in climate-change projections (Seneviratne et al., 2010). In Australia, despite the fact that the rainfall variability is affected by natural drivers, such as El Niño, La Niña, Indian Ocean Dipole and Southern Annular Mode, the State of Climate Report CSIRO and BoM (2020) reveals a long-term trend of drier conditions, i.e., less rainfall in the cooler months, across the country's south-west and south-east regions. The State of Climate Report (CSIRO & BoM, 2020) also shows that temperatures in Australia have increased, on average, by 1.44 ± 0.24 °C since 1910. The strong interactions between soil moisture and climate, and climate change impacts also driving a global trend toward extremes (e.g., rainfall and temperature) (Meehl & Tebaldi, 2004; Sillmann & Roeckner, 2007; Stott, 2016), reinforce the need for studies investigating soil moisture in wetter and drier conditions.

Despite the multitude of studies on soil moisture, there remains a lot to understand about soil moisture dynamics, particularly because the widespread availability of long-term data sets of fine resolution is missing. High resolution temporal soil moisture data (e.g., daily or sub-daily) is necessary for a more detailed hydrological modelling (Parinussa et al., 2012; de Jeu et al., 2014), while long periods of soil moisture data (e.g., greater than 10-15 years) are necessary to investigate temporal anomalies and to be able to evaluate the impact of those anomalies within a hydrological context (Brocca et al., 2014; Brocca et al., 2017). Also, long-term, high-resolution datasets are important to advance our current understanding of the interactions between elements that control the spatiotemporal soil moisture distribution (i.e., vegetation, soil, topography) (Teuling & Troch, 2005). Studies of long-term soil moisture trends are predominantly carried out on a global scale, with a coarse spatial resolution dataset (25 to 100 km pixel) (Sheffield & Wood, 2008a; Dorigo et al., 2012; Albergel et al., 2013; Deng et al., 2020) that masks local and regional trends. The global scale studies of soil moisture trends usually analyse surface soil moisture (0-10 cm) trends (Sheffield & Wood, 2008a; Dorigo et al., 2012; Feng & Zhang, 2015; Deng et al., 2020), and not the profile layer (0-100 cm). It is important to investigate both the surface and the profile layers of soil because they impact the soil moisture processes differently, i.e., the surface layer is where the flux of mass and energy with the atmosphere occurs (Brocca et al., 2009), while the profile soil moisture is a better representation of vegetation (Wigneron et al., 1999; Santos et al., 2014).

1.2 Objectives

The overall objective of this thesis is to refine the knowledge about temporal and spatial soil moisture variability at a catchment and regional scale in Australia.

1. Explore how the main drivers of soil moisture dynamics in a semi-arid subhumid catchment in Australia, i.e., soil parameters and vegetation, are affecting the temporal differences in soil moisture behaviour between wet and dry periods in two different soil types: clay and sandy.
2. To evaluate whether a dual-porosity model is able to better simulate the profile soil moisture dynamics of a clay-loam soil in a semi-arid subhumid catchment to improve the understanding of soil moisture physics and preferential flow in that area.
3. To investigate the long-term soil moisture trend in New South Wales for both profile and surface soil moisture layers and its drivers, i.e., temperature and rainfall.

1.3 Thesis outline

This thesis contains six chapters. Chapter 1 starts by outlining the problem of soil moisture temporal and spatial variability, the motivation to do this research, and the objectives of thesis. The literature review, Chapter 2, shows the current knowledge about soil moisture spatial and temporal dynamics, exposing the complexity of soil moisture variability in different climates, at different scales of analysis, in different parts of the same catchments, in different layers of the soil, and a number of methods used by researchers to develop the understanding of soil variability. It covers preferential flow effects in the soil, why it happens and how researchers study this matter. On soil moisture temporal variability, this chapter encompasses seasonal differences and their influence on soil moisture dynamics, and a long-term variability of soil moisture that shows behavioural trends of the water in the soil. Chapter 3 investigates the changes in soil moisture dynamics in dry and wet periods through the analysis of changes in soil properties and vegetation index between the periods using a Monte Carlo approach associated with a one-dimensional model to address objective 1. Chapter 3 also describes the study area, the field data used, the model applied and the methodology used to assess the results. Chapter 4 briefly exposes the soil data and study site that are also part of Chapter 3. Chapter 4 shows the dual-porosity model and the methodology used to analyse the results, and it evaluates how a dual-porosity model simulates the profile soil moisture dynamics of a clay-loam soil in order to meet objective 2. Chapter 5 investigates the long-term soil moisture trend in NSW in order to tackle objective 3. Chapter 5 presents the study area, the dataset used, and the model applied to generate the results. Chapter 6 exhibits the conclusions from the results of Chapters 3, 4 and 5, including the limitations of the work and possibilities for future research.

Chapter 2. Literature review

This chapter starts by describing the known governing processes that influence soil moisture in dry and wet conditions, and then discusses the current state of understanding of soil moisture variability over space and time scales. It covers the main approaches used to evaluate soil moisture dynamics, including numerical modelling, statistics, geostatistics and remotely sensed data.

2.1 Soil moisture dynamics in semi-arid and humid regions

Soil moisture in semi-arid regions has been extensively studied (Castillo et al., 2003; Cosh et al., 2008; Zribi et al., 2010; Chen et al., 2014a), particularly due to water scarcity in those areas, which can be a limiting factor for vegetation growth and population settlement (Goodrich et al., 2000). The impact of soil moisture on the climate in dry areas is mainly due to evapotranspiration reduction, when there is no more water available in the soil for uptake (Seneviratne et al., 2010).

Soil moisture dynamics are characteristically different in semi-arid and humid areas. The upper and lower bounds of soil moisture, i.e., the wilting point for dry conditions and maximum porosity for wet, are responsible for driving differences in spatiotemporal soil moisture patterns (Western et al., 2002; Korres et al., 2015). In a hillslope transect in a subtropical-humid climate, topography, hydraulic conductivity and porosity are principally responsible for soil moisture distribution in wet conditions, whereas during dry conditions elevation, aspect and clay content have more influence (Famiglietti et al., 1998). In wet areas, lateral distribution is present (Western et al., 2002; Brocca et al., 2007), whereas in dry conditions lateral distribution is almost non-existent and vertical fluxes predominate (Grayson et al., 1997; Western et al., 2004; Korres et al., 2015). In a dry regime, even if a saturated state is approached, the evapotranspiration is generally high enough to prevent the soil from fully saturating (Grayson et al., 1997). In this drier state the local characteristics, like soil and vegetation, control the spatiotemporal patterns of water (Grayson et al., 1997).

Runoff generation in humid catchments is usually through saturation excess runoff, where the antecedent moisture condition of the soil plays a decisive role in the runoff response. Although the main runoff mechanism in semi-arid areas is infiltration excess runoff, which is governed by rainfall intensity and the soil conductivity relationship, the soil moisture content prior to rainfall still plays an important role in the determination of runoff in semi-arid catchments (Castillo et al., 2003).

2.2 Variability of soil moisture

Soil moisture can vary significantly over both space and time, and the factors that influence these patterns have been explored extensively (Bell et al., 1980; Vachaud et al., 1985; Grayson & Western, 1998; Famiglietti et al., 2008; Brocca et al., 2012; Zucco et al., 2014; Korres et al., 2015). The physical properties that influence soil moisture variability, such as topography, land cover, vegetation and soil type, can change depending on the local catchment characteristics. However, even within a single catchment, the governing forces that drive soil moisture behaviour can vary depending on the season, predominant rainfall regime and the scale of analysis. A complete understanding of soil moisture behaviour and the forces that influence it are critical for numerous applications, including improved agricultural management, weather and climate forecasting, city planning and more (Famiglietti et al., 1998; Rhodin et al., 1999; Koster et al., 2003; Daly & Porporato, 2005; Kerr, 2007; Huang et al., 2016; McDonough et al., 2020). Therefore, in numerous attempts to clarify some of the uncertainties surrounding the drivers of soil moisture variability, hydrologists have utilised a variety of methods, including statistical, geostatistical, and fractal analysis, pattern analysis, modelling and more.

2.2.1 Spatial variability of soil moisture

A common approach used when there is a constraint in the number of samples is statistical analysis (Cromer, 1996). Many studies have investigated the spatial variability of soil moisture using statistical analysis due to limited data availability (Brocca et al., 2007;

Famiglietti et al., 2008; Brocca et al., 2010; Zucco et al., 2014) and have found a decrease in spatial variability when soil moisture content increased in both humid and semi-humid areas (Western et al., 2004; Brocca et al., 2007; Famiglietti et al., 2008). However, in dry areas the pattern was the opposite: an increase in the coefficient of variation was observed when soil moisture content increased (Brocca et al., 2007; Martinez et al., 2008). These results are consistent with an analysis of the probability density functions of catchments with varying climates, from humid to semi-arid, by Western et al. (2002). For a medium state of moisture (i.e., between arid and humid), Western at al. (2002) reported a distinct pattern in soil moisture spatial variability: variability increased from wilting point to a maximum value of variability and then the variability decreased until soil saturation.

When saturated, soil moisture content over space is typically more homogeneous, but when the soil moisture begins to dry, the spatial differences of soil hydraulic conductivity and porosity become more evident, thus increasing the spatial variability of moisture in the soil (Korres et al., 2015). However, the drying of soil from an intermediate moisture state to a very dry condition results in a more homogeneous state again, though the spatial differences in soil moisture are now due mainly to physical soil properties, since the soil is not wetter in some parts and drier in others as it was in the medium states of saturation (Famiglietti et al., 1998; Korres et al., 2015). This type of behaviour is largely expected to occur in arid and semi-arid areas. For example, in a semi-arid region in Spain, after consecutive low intensity rainfall events, the soil reached a close to saturation state that created a more homogeneous state within the catchment, leading the soil moisture spatial correlation to double its length (Fitzjohn et al., 1998). In a separate study, Korres et al. (2015) reported an increase in the coefficient of variability associated with decreasing soil moisture for both the drier agricultural portion of the catchment and the wetter forested catchment area. Brocca et al. (2007) found that an increase in soil moisture brings a more homogeneous state for semi-humid areas.

The patterns of probability density functions of soil moisture spatial distribution have also been explored (Bell et al., 1980; Famiglietti et al., 1999; Western et al., 2002; Brocca et al., 2007; Brocca et al., 2010) and a normal distribution was generally assumed in a diverse number of studies. Brocca et al. (2010) considered a normal distribution in soil moisture spatial distribution, since more than 80% of the measurements in the study followed this pattern, although Brocca et al. (2007) reported that in only one out of the three catchments, characterised by a topography with flat relief, a normal distribution could be assumed. When the distribution becomes skewed, i.e., the probability density function (PDF) is less variable, the distribution is concentrated in one boundary and is affected by that boundary (Western et al., 2002). Bell et al. (1980) and Famiglietti et al. (1999) found a positive skew in the distribution for low values of soil moisture and a negative skew for higher values of soil moisture. This positive skew in the soil moisture distribution in dry conditions was also found in a study by Western et al. (2002).

The statistical behaviour of earth sciences data sets is usually skewed and the samples are spatially correlated (Cromer, 1996), thus geostatistics could be more appropriate than traditional statistics for soil moisture studies. The geostatistical approach consists of creating a variogram from measured soil moisture data and fitting it to a theoretical variogram (e.g., exponential) to be able to analyse the sample variability related to the distance between measured points (Brocca et al., 2007). The range is the distance in which samples are influenced by each other, i.e., that they are considered dependent, and the sill is the variance correspondent to the range (Figure 2.1).

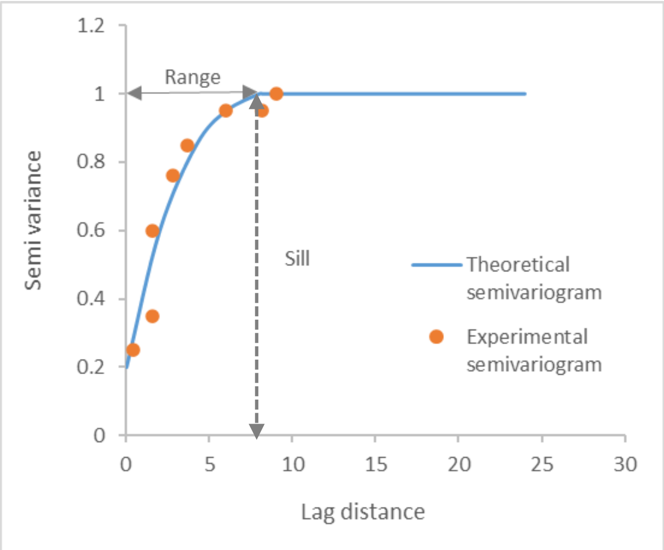

Figure 2.1 – Theoretical and experimental semi-variogram. Source: modified from Western et al. (2004).

Several studies that have examined soil moisture spatial variability have used geostatistical analysis (Western et al., 1998; Western et al., 2004; Brocca et al., 2007; Korres et al., 2015). Western et al. (1998) studied seasonal influence on soil moisture spatial variability in a temperate catchment and found a lower variability (sill) in summer (dry) than in winter (wet), as well as a higher correlation length (range) for dry conditions. In a separate study, Brocca et al. (2007) reported that topography was likely to be governing the soil moisture pattern in their sample sites, and they found no correlation length for flat areas. For Tarrawarra catchment (Australia), which is located in a temperate climate with evapotranspiration surpassing rainfall from October to March, Western et al. (2004) revealed that soil moisture temporal variability increased with increasing moisture, and the correlation length increased with increasing moisture. Korres et al. (2015) used statistical, geostatistical and a fractal analysis to study soil moisture patterns, and found that soil moisture has a multifractal behaviour, thus a multifractal model would be better to describe the variations of soil moisture for their dataset.

The scale of which the analysis is done is important in soil moisture and studies tried to find representative sites inside the catchment, that is, sites that can have values of soil moisture that are similar to the catchment mean (Warrick et al., 1977). Based on this concept, numerous studies have explored the idea of point measurements that could represent the catchment mean soil moisture to try to optimise the number of samples necessary for research or monitoring (Grayson & Western, 1998; Cosh et al., 2004; Brocca et al., 2012). Intuitively, catchment representative sites would be places that have the general, average physical characteristics of the catchment, such as a site with average soil properties and not located at the top or bottom of a hill (Grayson & Western, 1998). For Cosh et al. (2006), only one out of the four representative sites found in their study was located in a centre area of the catchment. Depending on which attribute influences soil moisture distribution the most in a catchment (e.g. topography, vegetation, soil type), this feature will have greater weight on the location of the representative sites (Vachaud et al., 1985). Brocca et al. (2012) found that two random measurements would be enough to obtain the catchment mean soil moisture with low absolute errors, within an area up to

100 km^2. While analysing soil moisture spatial variability at five sites in central Italy, Zucco et al. (2014) found that a higher number of samples was necessary for the intermediate state of wetness.

2.2.2 Temporal variability of soil moisture

Throughout the calendar year, temporal patterns of soil moisture can change in a single catchment due to differences in the net balance of water input and output (i.e., precipitation and evapotranspiration). These seasonal differences lead to different governing forces that predominate throughout the year and influence soil moisture dynamics. As stated previously (Section 2.1), the dynamics of soil moisture in dry conditions, where evapotranspiration surpasses precipitation, is characterised by vertical fluxes, while the dynamics of soil moisture in humid conditions are characterised by long periods of rainfall where lateral fluxes are predominant (Grayson et al., 1997; Western et al., 2002). Seasonal differences in rainfall patterns can change which of the main attributes (e.g., topography, soil properties) will drive the spatial organisation of soil moisture. For example, Western et al. (1999) reported that terrain index, which represents the terrain convergence, was the major predictor for spatial organisation of soil moisture during wet periods, while the potential radiation index was a better predictor in dry periods. In a different study, Famiglietti et al. (1998) concluded that in wet conditions, soil properties (e.g., porosity and hydraulic conductivity) dictated the surface soil moisture temporal variability, while in dry conditions this regulation was driven by elevation, aspect and clay content.

The concept of the temporal stability of soil moisture was created by Vachaud et al. (1985), who introduced the idea that within a catchment there are areas that have a more constant temporal behaviour (i.e., the soil moisture is more consistently dry or wet). For example, Grayson and Western (1998) applied the concepts of time stability to catchments with significant relief and found a number of time-stable sites in the catchments, although they could not find a time stability of the complete soil moisture pattern in the catchments analysed. If a site is temporally stable but is wetter or drier than the catchment mean, it could still be used to estimate the catchment mean, whereas high standard deviation sites are not useful for estimating the catchment mean (Grayson & Western, 1998; Cosh et al., 2006; Cosh et al., 2008).

2.2.3 Soil moisture variability across scales

Soil moisture is not only highly variable in space and time, but it is also affected by the scale at which soil moisture behaviour is being analysed. Within soil moisture data sets, it is common to have monitored data at one temporal scale (e.g., daily), while modelled soil moisture data will be available at a differing temporal scale (e.g., hourly). Regarding differences in the spatial resolution of soil moisture data, it is common to collect monitored data at a single point in space and often extend that value to be applicable across a catchment. It is not uncommon to have differences in scales of data measurement: other spatially and temporally dependent variables, such as precipitation and vegetation, are also measured at varying scales. Unfortunately, the scale effect on these variables is not linear, so comparing measured values across scales is not straightforward, making the study of these parameters and their behaviour even more complex (Western et al., 2002).

The importance of scales in hydrology has been discussed for years (Dooge, 1986; Sivapalan, 1995), with multiple studies exploring differences in the variability of soil moisture across scales (Western et al., 1999; Famiglietti et al., 2008; Martinez et al., 2008; Brocca et al., 2012; Zucco et al., 2014). Western and Blöschl (1999) found that the spatial variance of soil moisture increases as extent (total coverage of the area) increases. Similarly, Zucco et al. (2014) reported a higher coefficient of spatial variation for soil moisture at their catchment scale (6 km^2) than at their field scale (20 m^2). In contrast, Brocca et al. (2007) reported that the variability of soil moisture increased to an area around 10 km^2. Famiglietti et al. (2008) explored spatial soil moisture variation using six extent scales and found a general increase in standard deviation, coefficient of variation, and skewness with increasing spatial scale. Western et al. (2002) highlighted that, generally, spatial soil moisture is stationary for small (<1 km^2) and large-scale catchments

(>100s+km^2), but there is still a need for further investigation of soil moisture patterns at intermediate scales.

2.2.4 Long-term variability of soil moisture

Due to the importance of soil moisture in the global climate and for its highly spatial and temporal variability, the study of soil moisture dynamics is of interest for hydrologists, climatologists, and the agricultural sector. Most studies of soil moisture temporal trend analysis have been conducted at global scales (Sheffield & Wood, 2008a; Dorigo et al., 2012; Albergel et al., 2013) that mask local and regional trends driven by small-scale land–atmosphere interactions. Studies of global soil moisture temporal trends do not always lead to converging conclusions, which can be due to the different datasets and periods analysed. Some studies of the global soil moisture trend found that dry locations will become drier while wet regions will become wetter (Held & Soden, 2006; Feng & Zhang, 2015), while others indicated a general drying trend globally (Dai, 2011; Dorigo et al., 2012; Albergel et al., 2013; Gu et al., 2019; Deng et al., 2020).

In the study of the hydrological cycle response to global warming, Held and Soden (2006) found that an increase of lower-tropospheric water vapour and an increase in horizontal moisture transport will intensify the associated evaporation minus precipitation pattern, making wet regions wetter and dry regions drier. The hydrological assessment of trends in land surface (1948-2005) by Greve et al. (2014) applied a 0.5×0.5° (~55×55 km^2) spatial resolution dataset and found that only 11% of the global land area follows the 'dry gets drier, wet gets wetter' (DGDWGW) concept, while 9.5% of global land area shows the opposite, i.e., dry places getting wetter and wet places getting drier. Feng and Zhang (2015) examined global moisture trends using satellite soil moisture (active and passive microwave merged data at 25 km resolution, at surface 0-10 cm) for 1978 to 2013 and found that only 15% of the land areas have followed the DGDWGW paradigm, whereas 8% have experienced the opposite trend. Despite some agreement on regions that will become drier and regions that will become wetter, the differences in the results exist among the studies.

There are studies that found a predominance of a drying trend globally (Sheffield & Wood, 2008b; Dai, 2011; Dorigo et al., 2012; Albergel et al., 2013; Deng et al., 2020). Sheffield and Wood (2008b), using the IPCC AR4 General Circulation Model on a 220 km regular grid, projected decreases in soil moisture globally and an increase in frequency of short-term (4 to 6-month) droughts for the period of ~2050 to 2100. Dorigo et al. (2012) conducted a global trend analysis of soil moisture (1988-2010) with three surface soil moisture datasets: merged microwave surface soil moisture dataset (SM-MW) (top 2 cm of soil at a 27 km resolution), ERA Interim reanalysis dataset (0-7 cm at 80 km resolution) and the Global Land Data Assimilation System (GLDAS) Noah model (0-10 cm at 111 km resolution). They found a predominance of a drying trend in the three datasets, although there were spatial distribution divergences in the trends, highlighting the importance of evaluating the limitations and uncertainties of soil moisture products (Dorigo et al., 2012; Deng et al., 2020). An example of the contradiction is a wetting trend in the north of Australia and a drying a trend in the south-east shown in the ERA and GLDAS dataset, and the opposite presented by SM-MW (Dorigo et al., 2012). As mentioned, soil moisture temporal trends can show different results depending on the different datasets, soil layer and period analysed.

In a study of global soil moisture trends analysis (1988-2010), Albergel et al. (2013) used three soil moisture products: the ECMWF Interim Re-Analysis (ERA-Land) (80 km pixel resolution), the NASA Modern-Era Retrospective Analysis for Research and Applications (MERRA) (5574 km spatial resolution), and the merged microwave surface soil moisture dataset (SM-MW) (27 km pixel resolution). A contradiction in the results was also found, since they identified a predominance of drying surface soil moisture trends for ERA-Land and SM-MW datasets, and a predominance of wetting trends for MERRA-Land (Albergel et al., 2013). A drying trend for south-eastern Australia was identified in ERA and MERRA products for the surface layer (0-7 cm for ERA-L and 0-2 cm for MERRA) and the root-zone (0-100 cm) for the period (Albergel et al., 2013).

Using the ERA Interim dataset (55 km pixel resolution), Deng et al. (2020) found a general drying trend in surface soil moisture (0-7 cm) globally for the period 1979 to

2017 that appeared to be accelerated from 2001. The east coast of Australia, though, showed a wetting trend for surface soil moisture (0-7 cm) in the same period. A global study using the IPCC AR4 General Circulation Model (GCM), estimated that mean drought duration will increase in Australia (Sheffield & Wood, 2008b). Greve et al. (2014) observed trends towards more arid conditions in different places of the world, including eastern Australia, for the period 1948 to 2005.

In Australia, the study of spatiotemporal soil moisture behaviour and associated drivers has been the focus of recent research (Gibson et al., 2019; Kirono et al., 2020; Lockart et al., 2020; Wasko et al., 2021). The importance of soil moisture on Australian climate was reinforced by Timbal et al. (2002), who showed that the variation in soil moisture increased the potential predictability of rainfall and surface temperature. Analysing the rainfall and soil moisture simulations from the CMIP5 global climate model in Australia at a 150 km pixel resolution, for past (1900-2005) and future (2006-2100) time windows, Kirono et al. (2020) showed significant increases in drought intensity and duration for Australia, with harsher drought conditions over southern and eastern Australia. Using a 25 km spatial resolution merged microwave surface soil moisture dataset (SM-MW) for the period 1991 to 2009, Chen et al. (2014b) found a general decrease in surface soil moisture for the study period.

A recent work from Wasko et al. (2021) using a dataset at a finer resolution (5×5 km^2 pixel) assessed profile soil moisture trends in Australia (1960-2017) and reported a decrease in profile soil moisture in the south-west and south-east coast of Australia (Wasko et al., 2021). In two catchments in the Hunter Region (NSW), Gibson et al. (2019) used modelled soil moisture data from AWRA-L (Australian Water Resources Assessment - Landscape) and AWAP (Australian Water Availability Project) at a 5 km spatial resolution for the period 1908 to 2015 and did not find a significant trend in soil moisture for the catchments. The studies of temporal trends in soil moisture point to a general drying trend globally. Deng et al. (2020) highlight that "under dry conditions, the depth of soil water exchange decreases, and the regulating capacity of soil reservoirs is weakened". Studies of surface and profile soil moisture trends at a finer scale are needed for better local agriculture management and to understand the changes in small-scale land–atmosphere interactions that are often masked by spatially coarser datasets.

Another approach to better understand trends in soil moisture is to study climate variables that affect soil moisture spatially and temporally, like precipitation, temperature, vegetation and evapotranspiration, and compare them to soil moisture trends (Sheffield & Wood, 2008b; Jung et al., 2010; Alexander, 2011; Dorigo et al., 2012; Deng et al., 2020; McDonough et al., 2020). Temperature appeared as a key influence on soil moisture trends in many studies (Mueller & Seneviratne, 2012; Deng et al., 2020; McDonough et al., 2020). Deng et al. (2020) found that temperature rise has an explanatory power of 65% over the global surface soil moisture (0-10 cm) drying trend. Increasing temperature appeared to be the cause of a global soil moisture drying trend in the period 1970 to 2000 (Sheffield & Wood, 2008a). Another global study identified Australia, among other regions, as a region of strong correlation between surface moisture deficits and temperature extremes (Mueller & Seneviratne, 2012). Dai (2011) observed that many of the global soil moisture drying trends would not exist without the recent temperature changes, pointing to temperature as a key factor. In the Great Plains region in the USA (1987-2016), McDonough et al. (2020) investigated surface (0-10 cm) soil moisture trends at a 3 km pixel resolution and identified that temperature dominated soil moisture trends over a major part of the study area, and more than precipitation or elevation. Applying climate models, Alexander (2011) found that for dry regions, deficits in soil moisture can lead to higher temperatures.

The role of precipitation in the soil moisture trend was explored by global-scale studies (Dai, 2011; Dorigo et al., 2012; Feng & Zhang, 2015; Deng et al., 2020). Dai (2011) explains that, despite the increasing temperature being pointed to as the main influence on decreasing soil moisture, places like eastern Australia and East Asia appeared to have precipitation decrease as the main driver of soil moisture drying. Global surface soil moisture (~2 cm) trends from SM-MW data were compared to precipitation and a positive relationship for precipitation and soil moisture was found in locations of drying soil moisture trends (Dorigo et al., 2012). Dorigo et al. (2012) highlighted that despite precipitation’s crucial role in soil moisture variation, its impact depends on other factors, like evaporation, soil type, vegetation and topography. In drier areas, Feng and Zhang (2015) described how low precipitation and evapotranspiration were the main factors affecting soil moisture, with the dry soil driving an increase in sensible heat flux and temperature, which, consequentially, would lead to potential evapotranspiration increase and thus decrease soil moisture. Despite the majority of studies finding a relationship between precipitation and soil moisture drying trends (Dai, 2011; Dorigo et al., 2012; Feng & Zhang, 2015), Deng et al. (2020) found that precipitation had the strongest correlation with soil moisture in the wetting areas. There is general agreement among local and global studies that precipitation and temperature are the key influences on soil moisture trend analysis, thus this study will explore the trends in temperature and precipitation and relate these to soil moisture trends.

2.3 Soil moisture in surface and profile layers

Profile and surface soil layers correspond to different soil moisture processes. The surface layer of the soil (top 5 cm) is where the flux of mass and energy with the atmosphere occurs, which makes this layer key for climatological processes (Brocca et al., 2009), while the deeper layer of the soil is a better representation of vegetation (Wigneron et al., 1999; Santos et al., 2014). The profile layer of the soil, also known as the root zone, represents the water availability for plant transpiration, and it has a 'longer memory' due to the large soil water capacitance of the lower layer (Wu & Dickinson, 2004; Cai et al., 2009). This longer memory of the deeper layers represents the slower time of response of the soil to rainfall, in contrast to the upper layer that has the rainfall quickly depleted through evaporation to atmosphere and penetration to the lower soil layer (Cai et al., 2009). Thus, near surface and root zone soil moisture have different time responses to atmospheric conditions, as the surface responds quicker to rainfall and sunlight than deeper layers.

Martinez et al. (2008) explored the different mechanisms involved in soil moisture distribution in the near surface and root zone layers and found that near surface measurements could be used to estimate root zone soil moisture with acceptable levels of confidence. Applying an exponential filter proposed by Wagner et al. (1999), studies inferred profile soil moisture values (5, 10, 20 and 30 cm) from satellite soil moisture data (2 cm) (Albergel et al., 2008; Brocca et al., 2011). A study under three different land uses found no strong correlation between near surface (0-2.5 cm) and root zone soil moisture (0-1.2 m), and suggested that the temporal distribution of soil moisture over the soil layers is a function of soils, land use and prevailing hydroclimatic conditions (Mahmood & Hubbard, 2007).

2.4 Preferential flow effects in soil moisture

Preferential flow is a great contributor to spatial soil moisture variability. Preferential flow is characterised by water and solutes moving along certain pathways and bypassing a fraction of the porous soil matrix (Hendrickx & Flury, 2001; Simunek et al., 2003; Gerke, 2006). There are different reasons for preferential flow to occur, and these can be separated into three big groups: 1) Macropore flow: preferential flow in continuous root channels, earthworm burrows, fissures or cracks; 2) Unstable flow: usually in coarse-textured soils, can be induced by fine-over-coarse textural layers, water repellency, or air entrapment; and 3) Funnel flow: redirection caused by textural boundaries – water follows where there is the least resistance, bypassing less permeable zones (Gerke, 2006). Macropore flow can be classified according to the macropore morphology: 1) Pores formed by soil fauna, 2) Pores formed by plants roots, 3) Cracks and fissures, and 4) Natural soil pipes (Beven & Germann, 1982).

Preferential flow allows water and solutes to move faster along the soil profile than they would with uniform infiltration (Hendrickx & Flury, 2001; Hardie et al., 2013). One major concern with preferential flow is the increasing risk of groundwater contamination by agrochemicals short-circuiting the soil matrix (Tyner et al., 2007; Hardie et al., 2013). Direct measurement of bypass flow is difficult due to great spatial and temporal variability involved in water movement in field soil (Flury et al., 1994). Studies of preferential flow can involve different methods of investigation: laboratory analysis using soil columns (Köhne & Mohanty, 2005; Köhne et al., 2006; Stumpp et al., 2009; Arora et al., 2011; Iversen et al., 2011), field experiments that can involve the use of dye tracers, time domain reflectometry probes, lysimeters, and piezometers (Flury et al., 1994; Weiler & Flühler, 2004; Tyner et al., 2007; Garg et al., 2009; Rimon et al., 2011; Zeng et al., 2014; Blackmore et al., 2018; Feng et al., 2018) and the use of models that are usually associated with measured soil moisture data (Köhne et al., 2006; Garg et al., 2009; Rimon et al., 2011; Arora et al., 2012; Zeng et al., 2014; Feng et al., 2018). Studies applying models are usually interested in solute transportation, like pesticides (Köhne & Mohanty, 2005; Tyner et al., 2007; Pontedeiro et al., 2010; Iversen et al., 2011; Jaynes et al., 2016).

The use of dye tracers is a common way to study preferential flow by staining flow pathways (Flury et al., 1994; Weiler & Flühler, 2004; Hardie et al., 2011). The dye is usually added to water and the infiltration pattern can be observed at excavated soil sections (Weiler & Flühler, 2004). When analysing the role of antecedent soil moisture in preferential flow, Hardie et al. (2011) found lower preferential flow associated with higher antecedent soil moisture, which was contrary to what was found by Jaynes et al. (2001). The contrasting result is linked to the different soils examined, i.e., shrinkage cracks soils and macropores in silt dominant soils (Hardie et al., 2011).

The use of hydrological models has become a frequent approach to the study of preferential flows. Models that account for the presence of macropores or cracks can use different equations to calculate preferential flow, such as the Darcy equation, Richards equation and kinematic wave equation (Gerke, 2006). Despite criticisms that the Darcy and Richards equations do not properly represent the preferential flow effect, a large number of studies of preferential flow rely on Darcy and Richards equations (Beven & Germann, 2013). A model that has been extensively used to simulate preferential flow is HYDRUS-1D, which uses the Richards equation and simulates preferential flow with a dual-porosity or a dual-permeability flow model. To model preferential flow, a number of studies applied HYDRUS-1D with the dual-porosity model (Garg et al., 2009; Stumpp et al., 2009; Jiang et al., 2010; Pontedeiro et al., 2010; Rimon et al., 2011; Jaynes et al., 2016) and also with the dual-permeability model (Köhne et al., 2004; Kodešová et al., 2006; Arora et al., 2012; Feng et al., 2018).

In HYDRUS-1D, the dual-porosity model allows water and solutes to flow through the macropores but not through the matrix of the soil (Figure 2.2-b). The matrix can exchange, retain, and store water. The water exchanged between soil matrix and macropores is calculated with a mass transfer rate that is set to be proportional to the difference in effective water content or pressure heads between the two domains (Simunek et al., 2013). In the dual-porosity model, Richards' equation is applied to the macropore domain only. Another approach to simulate preferential flow in HYDRUS-1D uses the dual permeability model (Figure 2.2-c), which considers that water flows relatively fast in the macropore domain (when close to full saturation), and slowly in the matrix domain, also referred to as the micropore domain (Šimůnek & van Genuchten, 2008). As in the dual-porosity model, the dual-permeability model allows the transfer of water and solutes between macropores and the soil matrix. In the dual permeability model, Richards' equation is applied to the macropore domain and to the micropore domain, which results in a large number of parameters. In HYDRUS-1D, the traditional flow model is the uniform flow (Figure 2.2-a) that considers a porous medium as a grouping of impermeable soil particles separated by pores or fractures through which flow occurs (Šimůnek & van Genuchten, 2008). The uniform flow model uses Richards' equation to describe the flow. The dual-porosity and the dual permeability models are nonequilibrium flow models that were derived from the uniform flow model. When compared to the uniform flow model that has six soil parameters, the dual-porosity model adds three parameters (or five, if the macropore-matrix transfer rate is to be proportional to pressure heads instead of water content) and the dual permeability adds eleven parameters, giving a total of 17 soil parameters.

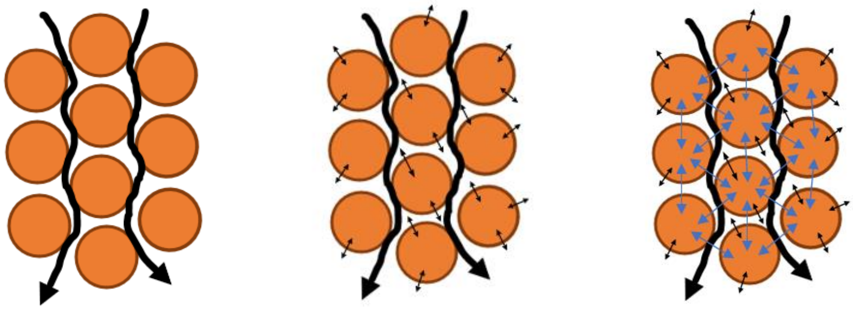

(a) (b) (c)

Figure 2.2 – HYDRUS-1D conceptual physical models for water flow and solute transport in (a) a uniform flow model, (b) a nonequilibrium dual-porosity model and (c) a nonequilibrium dual permeability model. Source: modified from Šimůnek and van Genuchten (2008).

The dual-porosity model was applied with water transfer between matrix and macropore based on difference in effective saturation (water content) and pressure head and it was found that physical nonequilibrium was more pronounced for wet and dry soils than for intermediate initial water content (Kohne et al., 2004). Jiang et al. (2010) applied HYDRUS-1D to simulate leaching of faecal coliforms and bromide through sandy loam soil lysimeters and found that the single-porosity model was satisfactory to simulate water movement under natural climatic conditions and with an irrigation of 25 mm/week, but with the doubling of irrigation, the dual-porosity model was better because preferential flow paths become more significant. Although in some cases preferential flow becomes greater with increasing wetness, Nimmo (2012) points out that there are cases of preferential flow occurring in media much drier than saturation, and Kladivko et al. (2001) explain that the predominance of preferential flow can be reduced in cracks of heavy clay soils with wetter conditions.

When analysing preferential flow in a paddy field (flooded soil), Garg et al. (2009) found similar results using HYDRUS-1D single (uniform flow) and dual-porosity flow models. Using HYDRUS-1D in a dual-porosity model with exchange rate between mobile and immobile domains (macropore and matrix, respectively) based in the difference in pressure head, Zeng et al. (2014) investigated salt leaching in a loamy sand soil under 15 irrigation scenarios. They found that increasing irrigation would accelerate salt leaching but that irrigation amount had an insignificant effect on soil water storage (Zeng et al., 2014).

To explore the effects of macropores on the infiltration rate, Kodešová et al. (2006) applied HYDRUS-1D in a uniform flow model and dual-permeability model to simulate one-hour ponded infiltration into clay soils with and without macropores. They found that the cumulative infiltration differed by two or more orders of magnitude when the simulations were made with and without macropores (Kodešová et al., 2006). The large number of input parameters is a challenge to the dual-porosity and dual-permeability application (Simunek et al., 2003). Köhne et al. (2006) explored the practicability of the inverse solution (Levenberg-Marquardt) to dual-permeability model parameters. They found good matches of bulk infiltration and outflow of the hydrograph but not for Br breakthrough simulation (Köhne et al., 2006). In order to tackle the challenge of working with a model that has a large number of input parameters, Arora et al. (2012) tests the usefulness of Bayesian methods in evaluating parameter uncertainty and in dual-permeability models. Considering 10 out of 17 parameters to be random, their result indicates that adaptive Markov chain Monte Carlo (AMCMC) resolves parameter correlations and has faster convergence for all dual-permeability parameters (Arora et al., 2012).

2.5 Satellite-derived soil moisture data

The availability of satellite-based soil moisture products is considerably recent, with the most common method to retrieve surface soil moisture data through the use of passive or active microwave sensors. The active radar sends a signal from the sensor and reads what returns, while the passive one captures what is naturally emitted from the surface (Western et al., 2002). The active radiometers are divided into the Synthetic Aperture Radars (SARs) and scatterometers. The scatterometers and the passive radars provide data at a coarse spatial resolution (~ 20 km) and with high temporal resolution (~daily) (Brocca et al., 2017). On the other hand, the SAR can give high spatial resolution with low temporal resolution. However, until January 2017, these high spatial resolution data were still not available, highlighted by Brocca et al. (2017). Using soil moisture satellite-derived products is a convenient way to obtain data, since it eliminates the necessity of going to the field, and it is cheaper when it is necessary to cover a broader area. Despite those advantages, there are three main constraints for satellite-derived data: it only measures near surface soil moisture (a few centimetres), it may present low quality depending on soil coverage (e.g. dense vegetation and mountainous terrain), and it uses coarse resolution (~20 km) (Brocca et al., 2017). Furthermore, satellite data needs to be calibrated and validated, and the discrepancy between the satellite footprint (>10 km) and ground measurements (~ 5 cm) is one of the main challenges of this validation process (Cosh et al., 2004).

Many recent studies have explored the soil moisture satellite-derived data (Goodrich et al., 2000; Cosh et al., 2004; Cosh et al., 2006; Martinez et al., 2008; Albergel et al., 2009; Brocca et al., 2011; Paulik et al., 2014; Dorigo et al., 2015; Korres et al., 2015). To validate remotely sensed data, Crow et al. (2005) tested upscaling point-scale data, combining modelling with field-collected data, and found better results than when using the observed data alone. Soil moisture data from passive and active satellite measures were shown to have a good performance when compared to in-situ measured and modelled data in a range of sites in Europe (Brocca et al., 2011).

An important remote sensing project focused on soil moisture was the Soil Moisture Active Passive (SMAP) of the National Aeronautics and Space Administration (NASA) (Entekhabi et al., 2008; Entekhabi et al., 2010). It was launched on January 2015 but it stopped working six months after being launched due to a failure in one component of the radar (Das et al., 2018). Despite that, Das et al. (2018), could work with a 3 km spatial resolution soil moisture product for the 2.5 months available when the data was validated and available to the public for research purposes. Chan et al. (2018) explains that SMAP can still deliver high spatial resolution data by combining the coarse resolution of passive observations with the high resolution of synthetic aperture radars (SARs) from the European Space Agency. Santi et al. (2018) created an algorithm to retrieve soil moisture data from SMAP, Sentinel-1 and AMSR-2. Another important sensor used for soil moisture purposes on-board NASA's Aqua satellite is the Advanced Microwave Scanning Radiometer for Earth Observing System, AMSR-E (Brocca et al., 2011). The Soil Moisture and Ocean Salinity (SMOS) radiometer, launched by the ESA, is an L-band radiometer (passive microwaves) with spatial resolution of 50 km able to capture 0-5 cm surface soil moisture (Kerr et al., 2001). On-board the MetOp (Meteorological Operational) satellite there is a widely used active microwave sensor, the Advanced SCATterometer (ASCAT), a C-band scatterometer operating since 2006 (Brocca et al., 2011). Chen et al. (2018) made a global-scale evaluation using active and passive soil moisture products with an independent soil moisture estimates via land surface modelling and found a better anomaly correlation for soil moisture for SMAP than for SMOS and ASCAT.

2.6 Field measurements

It is worth mentioning projects and catchments around the world in which soil moisture is the target, such as the Global Soil Wetness Project (GSWP), an interdisciplinary initiative that covers all surface components of water balance with a focus on soil moisture (Dirmeyer, 2011). The Semi-Arid Land-Surface-Atmosphere (SALSA) project is a long-term, integrated program in the Upper San Pedro Basin (USA) that investigates environmental changes in semi-arid regions based on water balance and ecological studies (Goodrich et al., 2000). The Walnut Creek Watershed, a tributary of the San Pedro River (USA), was part of the Southern Great Plains 1997 and 1999 (SGP97, SGP99), and Soil Moisture Experiments in 2003 (SMEX03), and its soil moisture data was used to validate satellite data from the Advanced Microwave Scanning Radiometer (AMSR) (Cosh et al., 2004; Cosh et al., 2008; Famiglietti et al., 2008). The Little Washita River watershed, Oklahoma (USA), where soil moisture has been extensively studied, was the experiment site for the SGP97, SGP99 and SMEX02 (Jackson et al., 1999; Cosh et al., 2006; Famiglietti et al., 2008). The Rür catchment (Germany) is located in one of the four observatories of the Terrestrial Environmental Observation (TERENO) project, which is a multidisciplinary project for which soil moisture monitoring is one part (Bogena et al., 2010; Rosenbaum et al., 2012; Zacharias et al., 2013; Korres et al., 2015).

In Australia, the Scaling and Assimilation of Soil Moisture and Streamflow (SASMAS) project in the Goulburn River catchment (NSW) has relied on continuous monitoring of soil moisture and meteorological data, with high temporal resolution, since 2004 (Rüdiger et al., 2007; Martinez et al., 2008; Chen et al., 2014a). Another important soil moisture study in Australia was in the Tarrawarra catchment (VIC), where the spatial and temporal dynamics of soil moisture has been explored (Grayson et al., 1997; Grayson & Western, 1998; Western et al., 2004). Still in Australia, the Murrumbidgee Soil Moisture Monitoring Network (MSMMN) has a total of 38 soil moisture monitoring sites within the Murrumbidgee Catchment, located in southern New South Wales (Smith et al., 2012). A validation study of SMAP soil moisture products was held in the Yanco site, a densely monitored area in the Murrumbidgee River catchment (Yee et al., 2016). In 2010, the calibration and validation of SMOS was taken across the Murrumbidgee River catchment as part of the Australian Airborne Cal/val Experiments for SMOS (AACES) (Peischl et al., 2012).

Chapter 3. Investigating changes in soil moisture predictability during wet and dry periods

3.1 Introduction

It was described in the introduction that wet and dry periods may have different impacts on soil moisture spatial and temporal dynamics, so this chapter explores the temporal and spatial differences in soil moisture dynamics in a semi-arid to subhumid Australian catchment where vertical flow is dominant over lateral flow (Chen et al., 2014a). The differences in soil moisture dynamics between periods that are wetter and drier than the average will be explored in two soil types using a one-dimensional model, HYDRUS-1D, through analysis of the changes in soil properties and vegetation between the periods. The study was carried out using long-term (2005-2015) high temporal resolution data (point measurement), which is one of the few datasets available. A Monte Carlo (GLUE) approach associated with HYDRUS-1D will be used to obtain the parameter set (i.e., soil properties and vegetation) for calibration of the HYDRUS-1D model, in an attempt to derive the "best" set of physical parameters to characterise soil moisture behaviour in wet and dry periods. The best parameter set will be selected by applying goodness-of-fit indices, including the Pearson Correlation Coefficient (R), scaled Root Mean Squared Error (sRMSE), and Nash–Sutcliffe Efficiency (NSE), as well as through visual analysis. From this evaluation it is hypothesised that a strong relationship will exist, driving soil moisture dynamics, between soil moisture and vegetation (Leaf Area Index - LAI) and soil moisture and soil properties (e.g., saturated and residual soil water content) in two temporal periods: a dry period (2005-2006) and a wet period (2008 and 2010). This study, thus, will contribute to refining the knowledge about soil moisture temporal variability through the identification of physical drivers of soil moisture variability in varying periods of wetness in two different soil types (clay and sandy) in an Australian catchment.

3.2 Study area

The study area is part of the Scaling and Assimilation of Soil Moisture and Streamflow (SASMAS) project (Rüdiger et al., 2007) situated in the Upper Hunter Valley in New South Wales, Australia. Study sites correspond to two catchments, Merriwa and Krui, and a microcatchment, Stanley, located in the Goulburn River catchment (6540 km^2) (Figure 3.1). The area is characterised by a temperate or subhumid climate, with approximate average annual rainfall of 650 mm, varying from 500 to 1100 mm depending on the altitude (Stern et al., 2000; Rüdiger et al., 2007). The Goulburn River flows mainly from west to east, and its main tributaries are from north or south. Merriwa (651 km^2) and Krui (562 km^2) are two of the major sub-catchments of the Goulburn River catchment and are located in the north part of the catchment (Martinez, 2010). The soil moisture stations in Krui and Stanley (S2, S3 and K2) are located in an elevation between 300 and 500 m, whereas the station located in Merriwa (M1) is in a 150-300 m elevation (Figure 3.2).

Rüdiger et al. (2007), citing Story et al. (1963) explains that the geological formation of Merriwa and Krui are the Merriwa Plateau and the Liverpool Range beds on the head, both lying on Tertiary Basalt. The soils and the terrain characteristics differ in the geological formations. The Liverpool Range presents rugged relief, clay humic soil, and has more than half of its area covered by wood, while in the Merriwa Plateau the relief is more undulating, the soil usually is dark cracking clays, with low tree coverage (Rüdiger et al., 2007; Chen, 2013).

The Merriwa Plateau, geological formation where the soil moisture stations applied in this study (S2, S3, K2 and M1) are located, was dominated by woodlands with Grey Box (*Eucalyptus moluccana*), Blakely's Red Gum (*E. blakelyi*), Yellow Box (*E. melliodora*), Forest Red Gum (*E. tereticornis*), Rough-barked Apple (*Angophora floribunda*) and Kurrajong (*Brachychiton populneus*), prior to European settlement (Martinez, 2010). After the European settlement, a significant part of the original vegetation has been cleared (Banks, 1998; Martinez, 2010) and beef cattle grazing is dominant in the Upper Hunter Valley (DIP, 2013). Following grazing, irrigated cropping, especially lucerne hay, is an important growth in the Upper Hunter Valley (DIP, 2013).

From the aerial image it is possible to see that the vegetation is not dense in most of Krui and Merriwa catchments (Figure 3.4), the north of Krui and south of Merriwa present a denser vegetation. The land use map (Figure 3.3) shows grazing as dominant land use followed by cropping in both catchments. The aerial photos of the soil moisture stations show a sparse tree coverage east of K2 and a denser tree coverage west of the monitoring station (Figure 3.5-b), while M1 station appears to be in a denser tree coverage area (Figure 3.5-c). Despite the aerial image showing tree coverage around M1 soil moisture station, the photo taken on-site shows that M1 station is in an open, free of tree, location (Figure 3.10) and the same is noted in Krui-K2 (Figure 3.9). Merriwa-M1 and Krui-K2 stations have a high sand percentage (70%) soils (Figure 3.6-b).

Stanley catchment (1.75 km^2) is located in the lower reach of Krui catchment and it has a sparse tree coverage (~ 5%) (Figure 3.5-a). Stanley catchment used to be a cropping area (until 2003) and is now a biodynamic beef cattle grazing property (Figure 3.8) with its native grass (Martinez et al., 2008). Stanley dominant grass species are plains grass (*Austrostipa aristiglumis*), wiregrass (*Aristida ramosa*), wallaby grasses (*Danthonia spp*.), red grass (*Bothriochloa macra*) and blue grass (*Dicanthium spp.*) Mitchell (2002) cited in Martinez et al. (2008). The average annual rainfall recorded from a local gauge was 572 mm (2005-2015), and long-term average annual rainfall (1882-2007) was 617 mm, estimated by Chen (2013) using linear regression in two nearby weather stations (Gumnun and Terragong) from the Bureau of Meteorology (BoM). Figure 3.7 shows the meteorological station in Stanley-S2. Because it is densely monitored, Stanley has been studied in previous hydrologic works (Martinez et al., 2008; Chen et al., 2014a). The soil in station S2 and S3 is predominately clay (35-40%) (Figure 3.6-a).

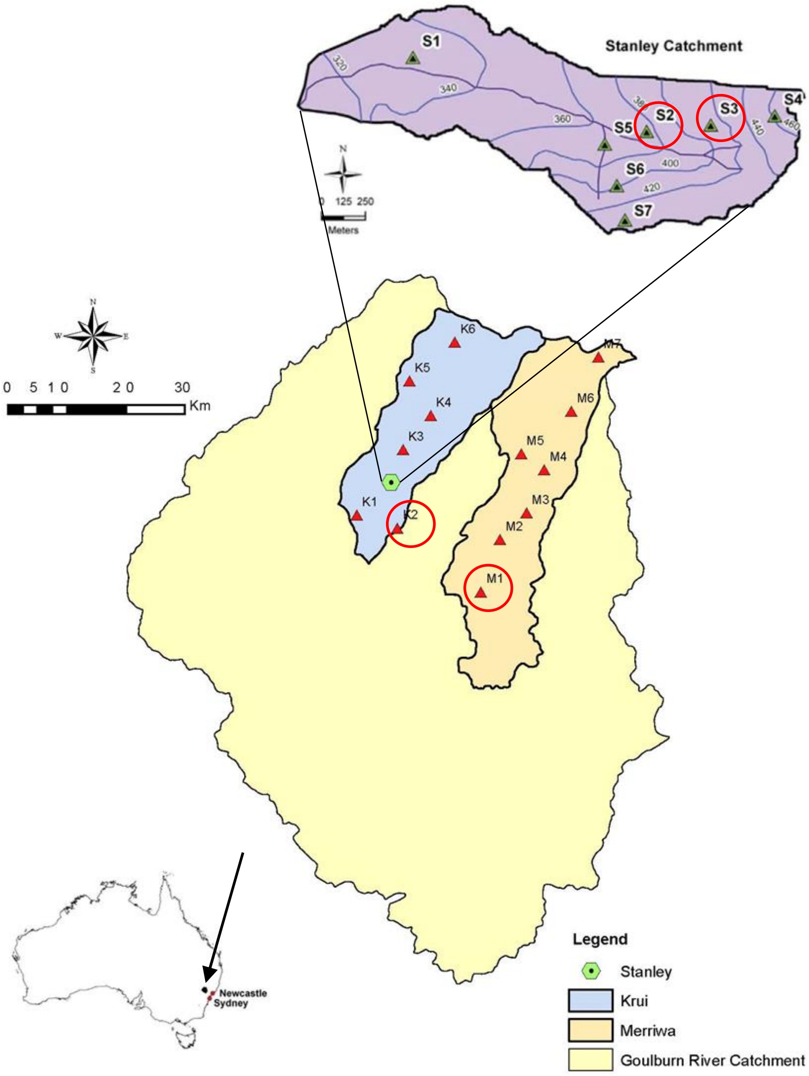

Figure 3.1 – Location of Merriwa, Krui and Stanley catchment within the larger Goulburn River catchment. Soil moisture stations are indicated by the triangular points.

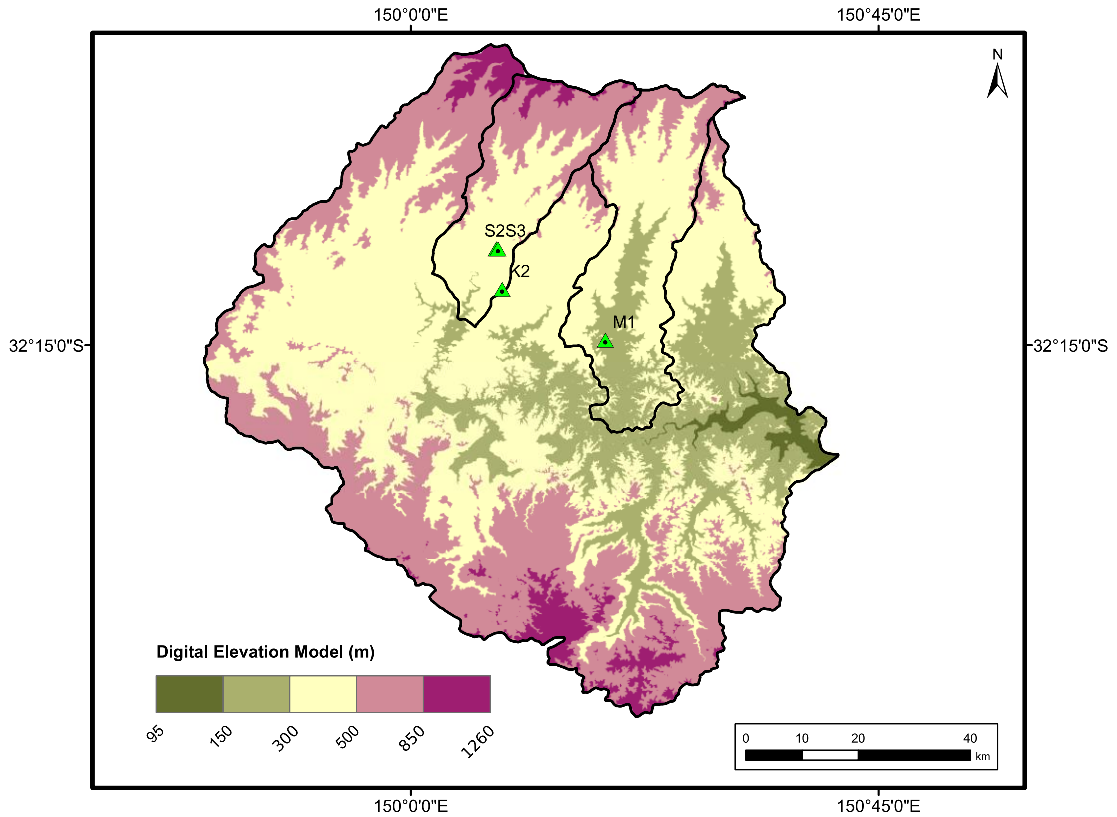

Figure 3.2 – Digital elevation model for Goulburn River Catchment and soil moisture stations (S2, S3, K2 and M1), Krui (left) and Merriwa catchments. *(Source: Gallant et al, 2011).*

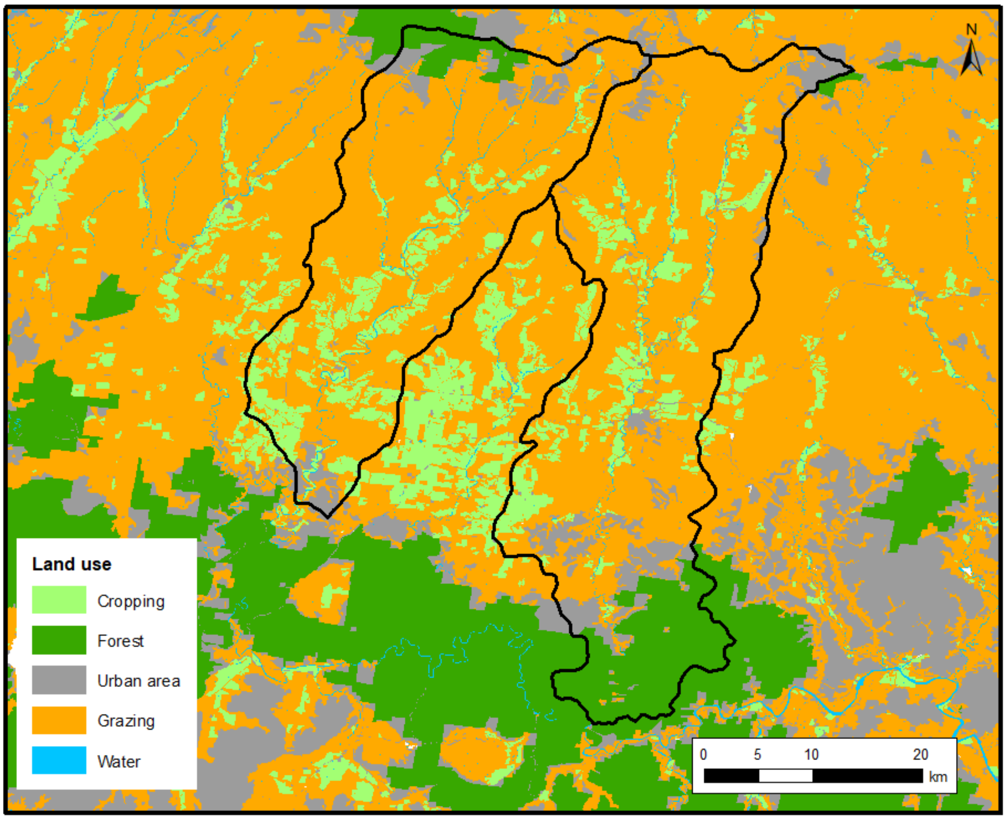

Figure 3.3 – Land use in Krui (left) and Merriwa catchments. (*Source: Department of Planning, Industry and Environment, NSW*).

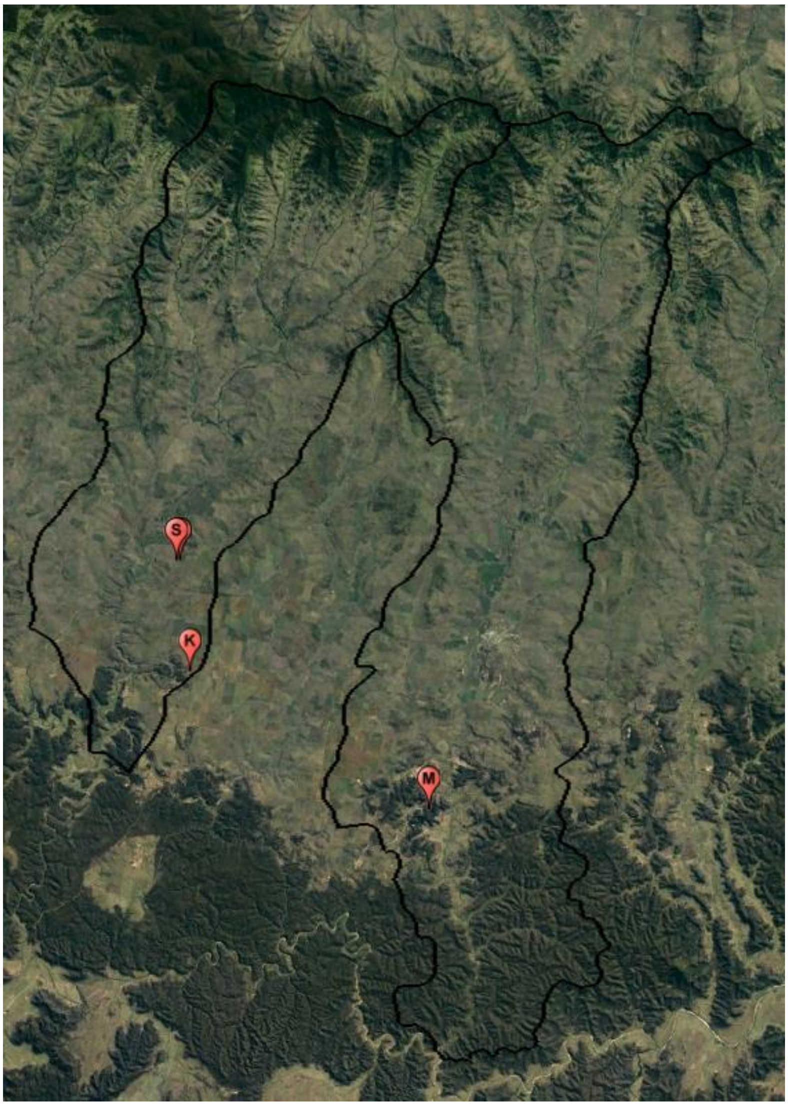

Figure 3.4 – Aerial image of Krui (left) and Merriwa catchments and the soil moisture stations (*Source: Google Earth*).

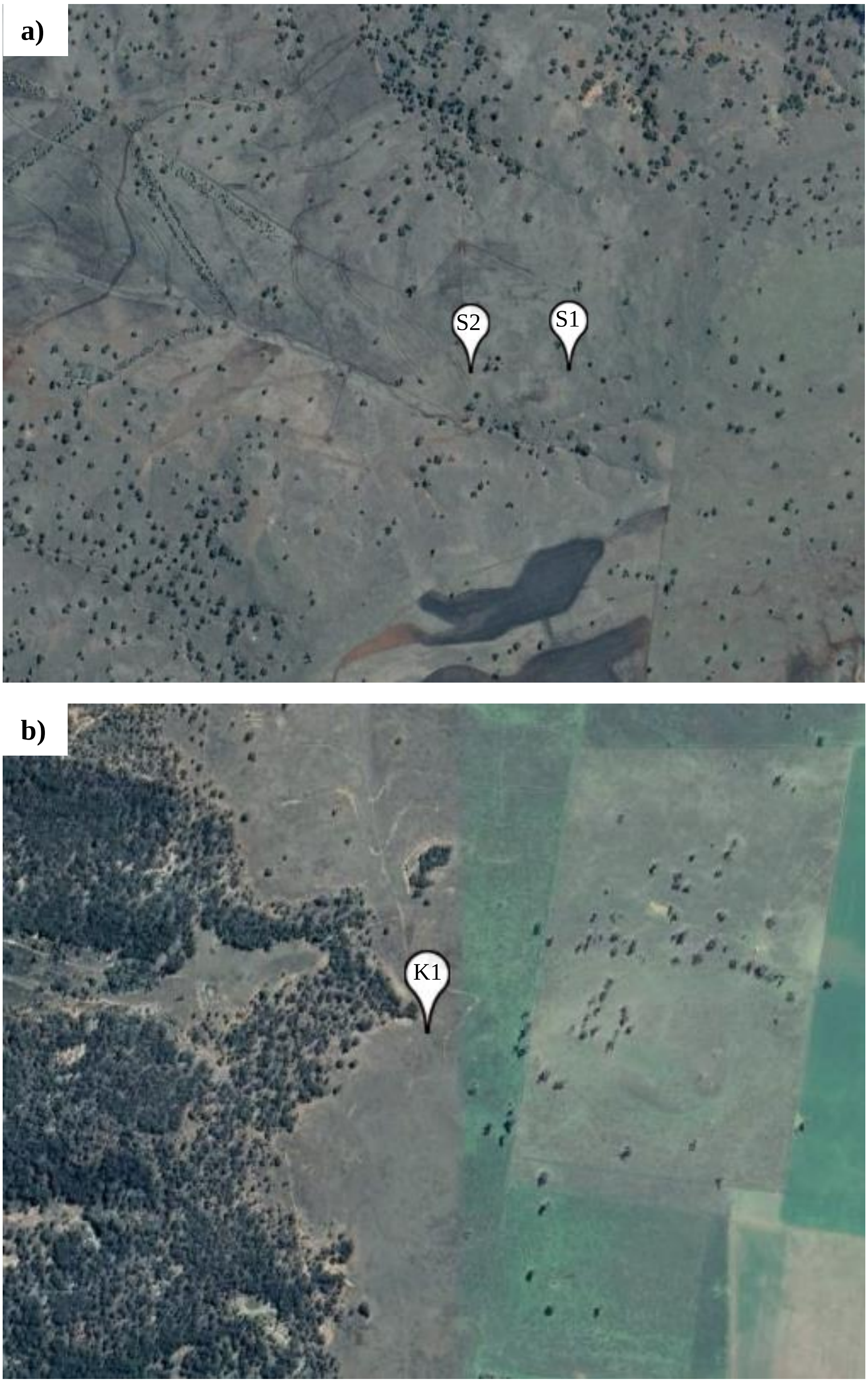
a)
S2
S1
b)
K1

Figure 3.5 – Aerial image of soil moisture stations: S2 and S3 (a), K2 (b) and M1 (c). Images are from 2018 (S2, S3 and K1) and 2021 (M1) (*Source: Google Earth*).

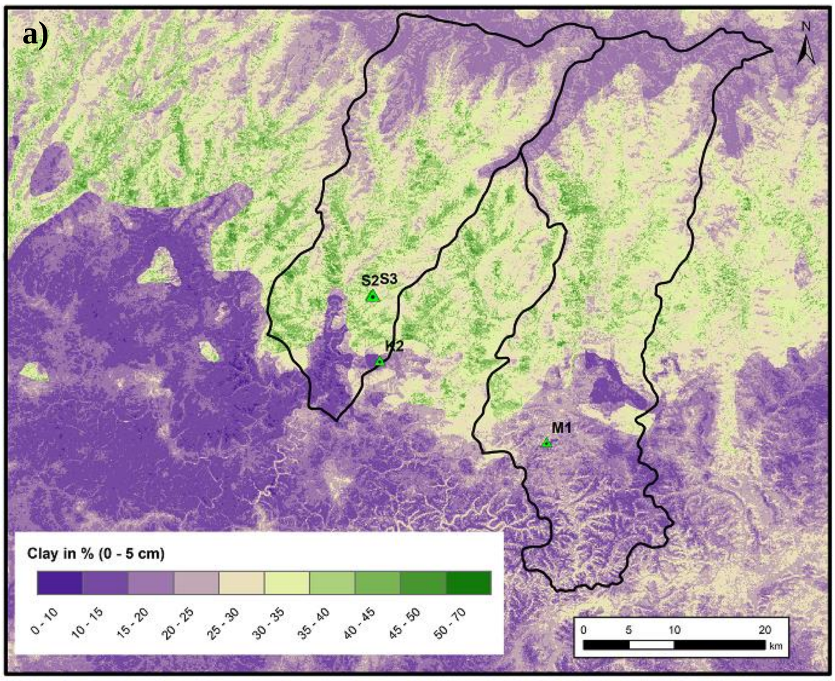

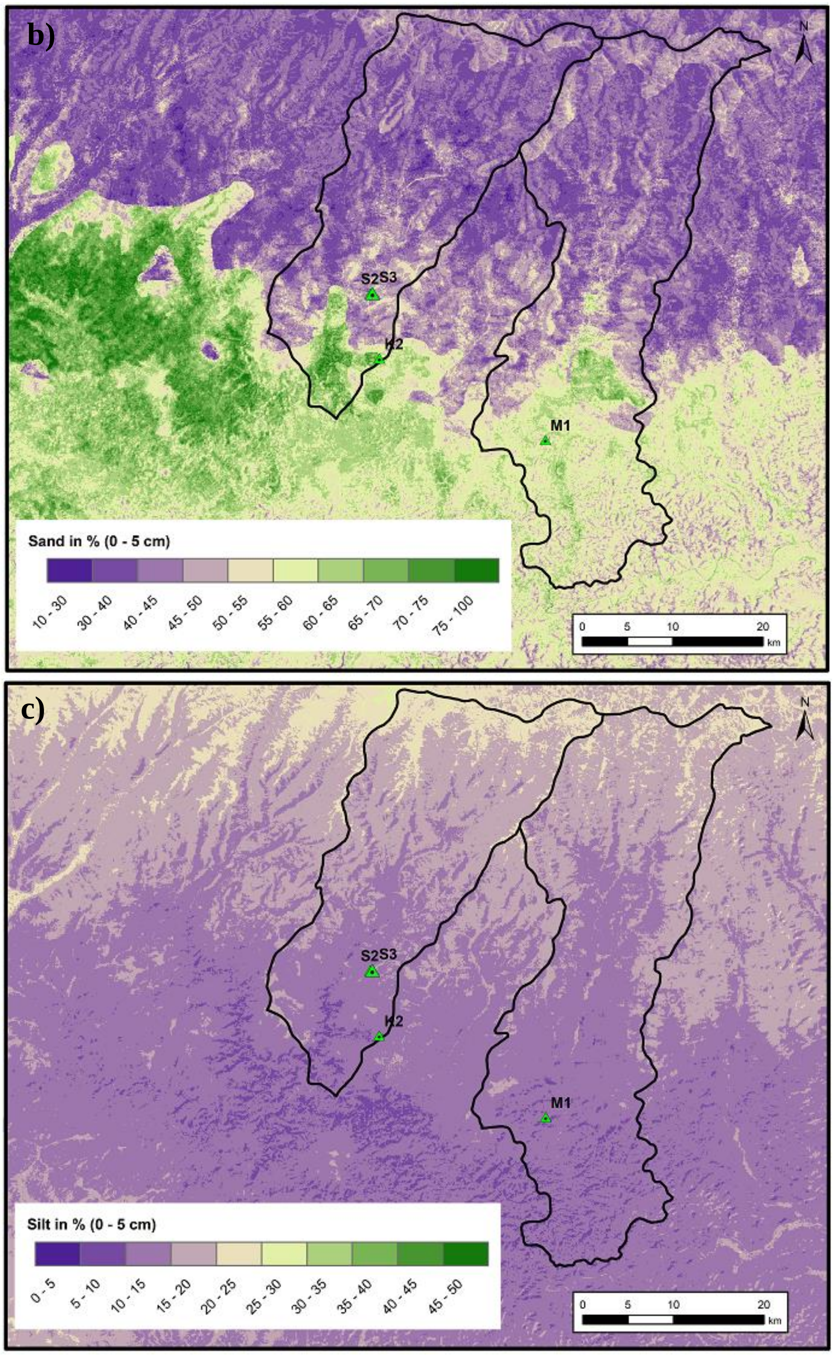

Figure 3.6 – Soil texture in Krui (left) and Merriwa catchments, percentage of (a) clay, (b) sand and (c) silt.

Figure 3.7 – Meteorological station (S2) in the Stanley micro-catchment, photo taken by the author on October 2017.

Figure 3.8 – Biodynamic beef cattle grazing in Stanley catchment, photo taken by the author on October 2017.

Figure 3.9 – Soil moisture station (K2) in Krui catchment, photo taken by Tony Wells on November 2018.

Figure 3.10 – Soil moisture station (M1) in Merriwa catchment, photo taken by Tony Wells on November 2020.

3.3 Materials and Methods

This section presents the collected data, the numerical model, and the method to assess the results. The measured in situ data includes soil moisture, precipitation and the meteorological dataset for sites in the Merriwa, Krui and Stanley catchments in the study period (2005-2015). Precipitation and meteorological data were applied as input data to simulate the vertical fluxes of soil moisture using the HYDRUS-1D model. The GLUE approach was used to assess the feasible distribution of the model parameters and the evaluation of the model calibrations was done by visual analysis and applying goodness-of-fit indices.

3.3.1 Field data

3.3.1.1. Soil moisture data

Rüdiger et al. (2010) calibrated and installed Campbell Scientific CS616 water content reflectometers (Campbell Scientific Inc., 2002) to measure the volumetric water content of the soil at three depths: 0-30 cm, 30-60 cm and 60-90 cm, although some sensors did not reach 90 cm due to the bedrock depth (Rüdiger et al., 2007). Each of the sensors collected soil moisture data every 20 minutes, though the data was averaged to an hourly interval for the purpose of this study. The accuracy of the instrument is 0.025 v/v according to the manufacturer (Campbell Scientific Inc., 2002) and Rüdiger (2006) found an error of 0.022 v/v, considerably close to the accuracy of the instrument.

Soil temperature sensors (Campbell Scientific T107) were also installed at each location due to the sensitivity of soil moisture to oscillations in soil temperature so that appropriate corrections could be made (Rüdiger et al., 2007). The soil temperature sensors were located 15 cm below the soil surface and provided a continuous soil temperature measurement for each monitoring station. The monitoring sites were selected to be representative of average catchment conditions, taking into consideration factors such as vegetation, slope, soil and aspect, following Grayson and Western (1998) (Rüdiger et al., 2010).

There are seven monitoring stations in Merriwa (M1-M7) in a NNE-SSW transect, Krui has six stations (K1-K6) in a NE-SW transect, and Stanley has seven soil moisture monitoring stations (S1-S7) disposed WNW-ESE. In order to explore the soil moisture dynamics in different soil compositions, two clay-predominant (S2 and S3) and two sand-predominant (M1 and K2) stations were selected. Those stations had the lowest proportion of missing data. Soil moisture dynamics in the top layer of the soil (0-30 cm) will be analysed in this chapter. The location of the stations is indicated by the triangular points in the study area figure (Figure 3.1).

3.3.1.2 Soil data

The soil texture and soil type for the 0-30 cm layer was obtained based on laboratory analyses (Rüdiger et al., 2010), which revealed that clay soils are the predominant soil type throughout the catchments, although sandy soils were found in the south of the Krui and Merriwa catchments. The area where the Stanley catchment is located is characterised by Vertisols, or soils rich in expansive clay (Hillel, 1998; Martinez, 2010). These soils shrink and swell after wetting and drying, forming deep cracks in the soil profile that work to create preferential paths for water movement (Hillel, 1998). Soils in the study area consist mainly of Tertiary basalt (Story et al., 1963; Rüdiger, 2006) and the characteristic cracks in the clay soil of the region have been pointed out by other studies (Rüdiger, 2006; Martinez, 2010; Chen et al., 2014a).

In clay soils (stations S2 and S3) the porosity is highly variable because the soil alternately swells, shrinks, aggregates, disperses, compacts and cracks (Hillel, 1998). Porosity generally ranges from 0.3 to 0.7 (30-70%) (Nimmo, 2013). The saturated soil water content (θ_s) in clay soils can approach 60% (Hillel, 1998), and the soil water potential curve for clay soils shows that the saturated soil water content varies from 0.55 to 0.60 v/v for poorly to well-structured soil, respectively (Brady & Weil, 1999). According to Carsel and Parrish (1988), the typical saturated and residual soil water content values for clay loam soil are 0.41 v/v and 0.095 v/v, respectively, while for sandy soils (stations M1 and K2), Carsel and Parrish (1988) found an average value for saturated soil moisture (θ_s) content of 0.41 v/v for loamy sand and sandy loam soils, and an average of 0.057 v/v of residual soil moisture content (θ_r) for loamy sand soil and 0.065 v/v for sandy loam soil. The soil texture and soil type (Table 3.1) for the 30 cm layer was obtained based on laboratory analyses (Rüdiger et al., 2010).

Table 3.1 – Soil type for the Stanley, Krui and Merriwa sites at station depth: 0 to 30 cm (Rüdiger et al., 2010).

Catchment	**Station**	**Soil type**	**Clay (%)**	**Silt (%)**	**Sand (%)**
Stanley	S2	Clay loam	39	35	26
Stanley	S3	Clay loam	-	-	-
Krui	K2	Loamy sand	6.5	8.5	85
Merriwa	M1	Sandy loam	6.5	21.5	72

3.3.1.3 Meteorological data

Meteorological data was obtained from the weather station located in the Stanley microcatchment (at station S2) at an elevation of 376 m (Table 3.2). The meteorological weather station measures air temperature, relative humidity, wind speed and direction, rainfall and soil temperature. The station includes a pyranometer and measures the soil temperature at eight depths (25, 50, 100, 150, 300, 450, 600, and 750 mm) (Rüdiger et al., 2007). There is a meteorological station in the north of Krui at station K6, but because it does not measure solar radiation, the meteorological data used for all stations was from Stanley S2 station.

To analyse the effect of using meteorological data from a single station (located in Stanley-S2), point data from SILO (Jeffrey et al., 2001) was retrieved for the four stations (https://www.longpaddock.qld.gov.au/silo/point-data/). Meteorological data (radiation, relative humidity, wind and air temperature - minimum and maximum) is used by HYDRUS to calculate potential evapotranspiration. From the analysis of daily radiation, relative humidity, and minimum and maximum air temperature for the years 2005, 2006, 2008 and 2010, it was found that daily differences of meteorological data between S2 and K2 and S2 and M1 was low. The maximum difference between S2 and K2 maximum and minimum daily temperature (°C) was 0.4 and 0.3, respectively, relative humidity (%) had the maximum daily difference of 1.2 and radiation (MJ/m^2) 0.5. comparing S2 and M1, the maximum daily differences were slightly higher, 1.1 °C for both maximum and minimum temperature, 4.2 % for relative humidity, and 1.8 MJ/m^2 for radiation. The average difference between S2 and K2 for the period analysed was less 1% for radiation, relative humidity, maximum and minimum air temperature. The average difference between S2 and M1 was 1.8 % for radiation, 1% for relative humidity, 1.8 % for maximum temperature and 4.7% for minimum temperature. Although wind data could not be compared, differences of radiation, relative humidity and air temperature data between stations were not significant. It is believed that the impact on the calculation of potential evapotranspiration is small but it needs to be acknowledged as a limitation.

Tipping bucket rain gauges are present at two stations in Stanley (S1 and S2), and at all stations in the Merriwa and Krui catchments. The rainfall from S2 was used as the input for S3 due to their proximity, as they are 230 metres apart. In Stanley S2, for the year 2009, there were signs of missing rainfall data which was evidenced by the occurrence of soil moisture peaks without concurrent rainfall (e.g., day 150 to day 180) (Figure 3.11). When comparing the S2 rainfall data to another local station, S1, the difference in recorded rainfall was significant: S1 recorded 528 mm for 2009 while S2 recorded only 260 mm for that year. In addition to that, Bureau of Meteorology stations (Terragong and Mar-Lea) that are located close to Stanley S1 and S2 stations recorded values closer to S1 than to S2. Furthermore, rainfall in S1 and S2 have very similar behaviour, evidenced by the double mass plot for the years 2006-2008 (Figure 3.12 - a) and 2010-2015 (Figure 3.12 – b). For the abovementioned reason, the rainfall for 2009 from S2 was substituted by rainfall from S1 multiplied by a correction factor of 0.9 identified in the double mass method.

For Krui K2 station and Merriwa M1 station, the days of missing rainfall were substituted with rainfall from the Terragong station, a station from the Bureau of Meteorology (BoM) that is close (~20 km) to both Krui-K2 and Merriwa-M1. Rainfall from Terragong has a good fit (i.e., R^2) with Krui-K2 (Figure 3.12 - a) and Merriwa-M1 (Figure 3.12 - b).

Table 3.2 – Geographical coordinates and elevation of soil moisture stations (Rüdiger, 2006).

Catchment	Station	Elevation (m)	Latitude	Longitude
Stanley	S2	376	32° 05' 44"S	150° 08' 13"E
Stanley	S3	412	32° 05' 44"S	150° 08' 22"E
Krui	K2	424	32° 09' 38"S	150° 08' 46"E
Merriwa	M1	242	32° 14' 30"S	150° 18' 41"E

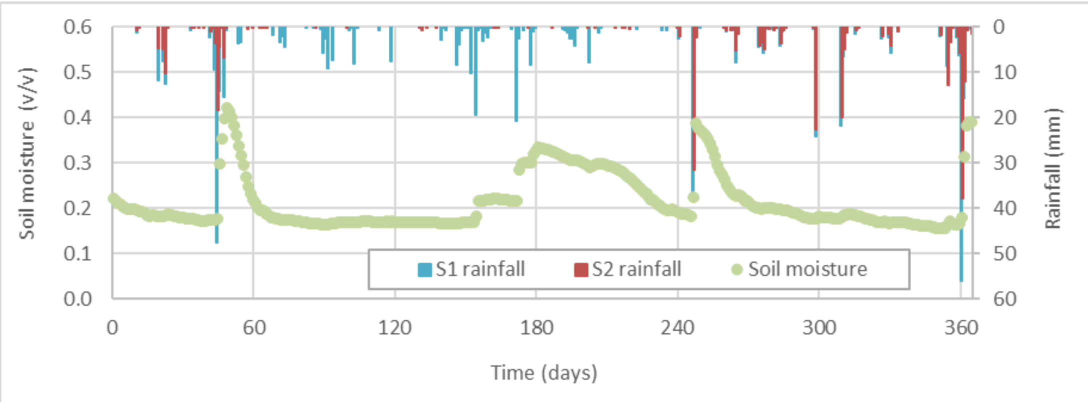

Figure 3.11 – Soil moisture (v/v) in the top 30 cm of soil at station S2, and rainfall recorded at stations S1 and S2 for the year 2009.

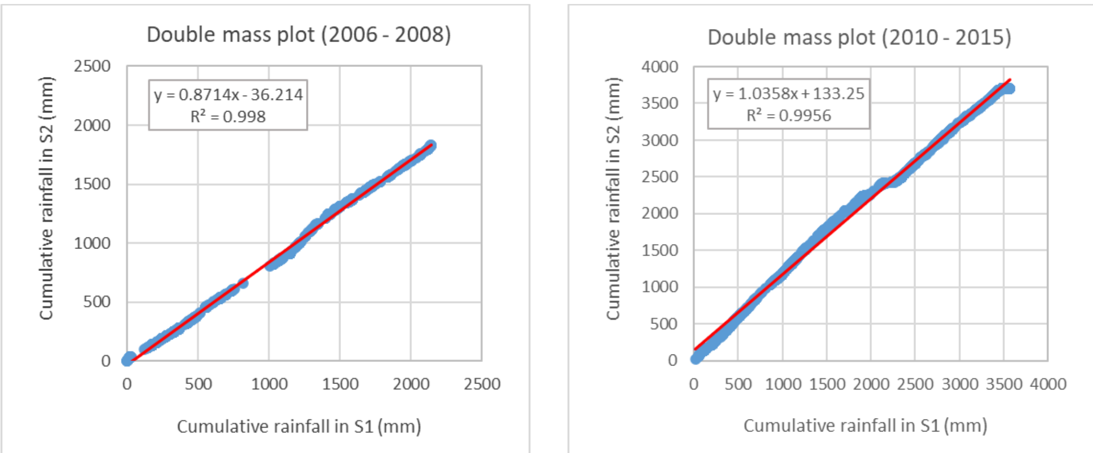

(a)

(b)

Figure 3.12 – Double mass plot of accumulated rainfall in Stanley S1 and S2 stations for the period (a) 2006-2008 and (b) 2010-2015.

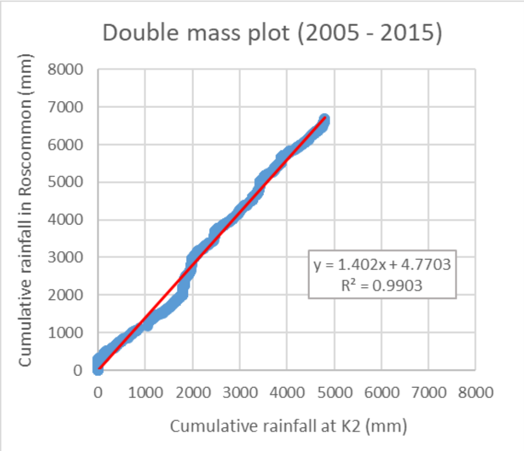

(a)

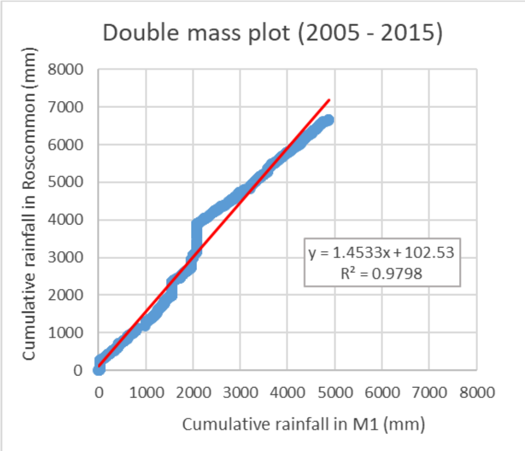

(b)

Figure 3.13 – Double mass plot of Roscommon (BoM station) rainfall and (a) Krui-K2, and (b) Merriwa-M1 for the period 2005-2015.

3.3.2 HYDRUS-1D – Uniform flow model

The model selected for this study is HYDRUS-1D, as it has been successfully used for Stanley for the period 2005 to 2007 in previous work (Chen et al., 2014a), and because vertical fluxes prevail most of the time in this area, i.e., potential evaporation surpasses the precipitation (Rüdiger, 2006), which reinforces the choice of a one-dimensional model for the area. In addition, this is a relatively simple model and was considered to capture all relevant processes while avoiding overparameterization (Beven, 2006; Blöschl, 2006). The key parameters affecting HYDRUS-1D performance are soil parameters and vegetation. The latter are mostly characterised by the leaf area index (LAI) (Chen et al., 2014a). The bottom condition is 'free drainage' since the soil is deeper than 30 cm, i.e., 90 cm for S2 and K2, and 60 cm for S3 and M1.

3.3.2.1 Model structure

The version of HYDRUS-1D used in this study is V4.14 (Simunek et al., 2013), which is the same version used by Chen (2013). The model is one-dimensional and uses the modified Richards equation for simulating the water flow (Equation 3-1), which assumes no liquid flow due to thermal gradients and no interference of air phase in the liquid flow (Simunek et al., 2013).

$$\frac{\partial\theta}{\partial t}=\frac{\partial}{\partial x}\left[K\left(\frac{\partial h}{\partial x}+1\right)\right]-S \qquad 3\text{-}1$$

where θ is the volumetric water content [L^3L^{-3}], t is time [T], x is the spatial coordinate [L] (increases with depth), K(h) is the hydraulic conductivity [LT^{-1}], h is the water pressure head [L], and S is the water sink term [$L^3L^{-3}T^{-1}$] (Simunek et al., 2013). The Van Genuchten (1980) model describes the unsaturated soil hydraulic properties in terms of soil water retention parameters, using Mualem (1976) pore-size distribution model (Simunek et al., 2013). Van Genuchten (1980) (Equations 3-2 to 3-5) contain five independent parameters: residual soil water content (θr), saturated soil water content (θs), pore size distribution parameter (n), saturated hydraulic conductivity (Ks) and pore discontinuity (L).

$$\theta(h)=\theta_r+\frac{\theta_s-\theta_r}{[1+|\alpha h|^n]^m} \qquad \text{when } h<0 \qquad 3\text{-}2$$

$$\theta(h)=\theta_s \qquad \text{when } h\geq 0 \qquad 3\text{-}3$$

$$K(h)=K_s\,S_e^L\left[1-\left(1-S_e^{\frac{1}{m}}\right)^m\right]^2 \qquad 3\text{-}4$$

$$m=1-1/n \qquad n>1 \qquad 3\text{-}5$$

When the water pressure head is negative (h < 0), the soil water retention equation (θ (h)), is calculated by Equation 3-2, whereas when the pressure head is equal to or greater than zero, the volumetric water content is equal to the saturated soil water content (θs) (Equation 3-3). In Equation 3-2, the volumetric water content is calculated using the residual (θr) and saturated (θs) volumetric water content, α, n (related to pore-size distribution). The hydraulic conductivity, K(h) (Equation 3-4), is dependent on the saturated hydraulic conductivity (Ks), the effective saturation (Se), α, n, and L, and are considered empirical coefficients that alter the shape of the hydraulic functions (Arora et al., 2011). The shaping parameter (m) (Equation 3-5) is a function of the empirical coefficient (n).

The effective saturation (Equation 3-6) is a function of the residual and saturated soil water content. The value of the residual soil water content (θr) corresponds to the condition when water stops flowing through the soil (usually lower than wilting point) (Van Genuchten, 1980; Kirkham, 2014).

$$S_e = \frac{\theta - \theta_r}{\theta_s - \theta_r} \qquad 3\text{-}6$$

There are ways to infer the van Genuchten-Mualem soil parameters in HYDRUS, if the soil texture is known, by using the soil-textural-class pedotransfer function (Carsel & Parrish, 1988). Another way is to use a computational program, such as Rosetta code (Schaap et al., 2001) which is a continuous pedotransfer function. The third and last way is to apply the HYDRUS built-in calibration tool, the Levenberg-Marquardt inverse method (Marquardt, 1963).

To calculate the evapotranspiration, HYDRUS-1D utilises the Penman-Monteith equation (Equation 3-7).

$$ET_p = \frac{1}{\lambda} + \frac{\Delta\,(R_n - G) + \rho c_p (e_a - e_d)/r_a}{\Delta + \gamma\,(1 + r_c/r_a)} \qquad 3\text{-}7$$

where ET_p is the potential evapotranspiration rate [mm d^{-1}], λ is the latent heat of vaporization [MJ kg^{-1}], R_n is the radiation net of a surface [MJ $m^{-2}d^{-1}$], G is the soil heat flux at surface [MJ $m^{-2}d^{-1}$] (e_a-e_d), is the saturation vapour pressure deficit [kPa], r_a is the aerodynamic resistance [s m^{-1}], is the canopy resistance [s m^{-1}], Δ is the slope of the vapour pressure curve [kPa °C^{-1}], γ is the psychrometric constant [kPa °C^{-1}], and the ρ is the mass density of water [kg m^{-3}].

The canopy resistance (r_c) is calculated from the leaf area index and from the average daily single-leaf stomatal resistance (Equation 3-8).

$$r_c = \frac{R_l}{0.5 \times LAI} = \frac{200}{LAI} \qquad 3\text{-}8$$

Where R_l is the average daily single-leaf stomata resistance (assumed to be 100 s m^{-1}) and LAI is the leaf area index [-].

Potential evapotranspiration (ET_p) is divided into potential transpiration (T_p) [mm d^{-1}], and potential evaporation (E_p) [mm d^{-1}], using Beer's law (Equation 3-9 and 3-10). It divides the solar radiation component of the energy budget via interception by the canopy.

$$T_p = ET_p \times SCF \qquad 3\text{-}9$$

$$E_p = ET_p \times (1 - SCF) \qquad 3\text{-}10$$

Where SCF is the soil cover fraction (SCF) (Equation 3-11).

$$SCF = 1 - e^{-rExtinct \times LAI} \qquad 3\text{-}11$$

where rExtinct is the constant for the radiation extinction by the canopy, set to 0.463 [-] and the LAI is the leaf area index [-] a calibrated parameter.

Interception loss by vegetation can be calculated in HYDRUS-1D, but in this work, it will not be considered due to very low tree coverage in the study area (as shown in Section 3.2, Figure 3.7, Figure 3.9 and Figure 3.10). The water in the root-zone is depleted by evaporation of bare soil, by transpiration of the leaves, or by percolation to deeper layers. The water sink term S(h) from Equation 3-1, represents the water extracted from the soil per unit time due to plant water uptake. Equation 3-12 is defined by Feddes equation (Feddes, 1978) cited in Simunek et al. (2008).

$$S(h)= \alpha(h)\ S_p \qquad 3\text{-}12$$

where $\alpha(h)$ [-] is the root-water uptake water stress response function of the soil water pressure head ($0 \leq \alpha \leq 1$) (Figure 3.14), and S_p is the potential water uptake rate [T^{-1}].

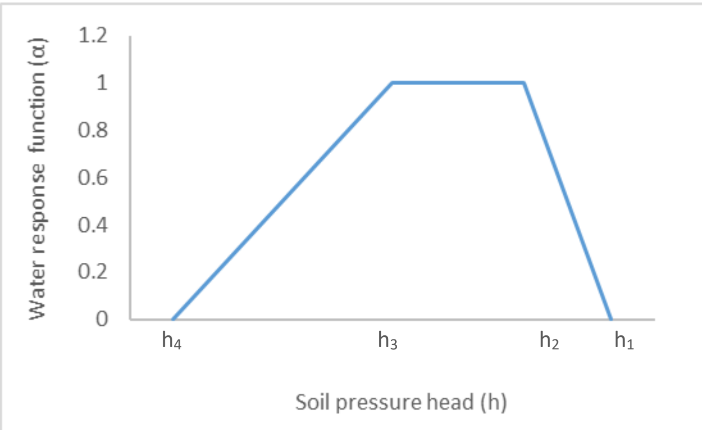

Figure 3.14 – Schematic plant water stress response function, α(h), by Feddes (1978) (Simunek et al., 2008).

From the plant water stress response function (Figure 3.14) the water uptake is assumed to be zero close to saturation (i.e., wetter than an arbitrary "anaerobiosis point", $h > h_1$). When the pressure head is less than the wilting point, i.e., $h < h_4$, water uptake is also assumed to be zero. Optimal water uptake is undertaken between pressure heads h_2 and h_3. When the pressure head is between h_3 and h_4, or between h_1 and h_2, water uptake decreases or increases linearly with h. When there is no water stress, i.e., $\alpha(h) = 1$, the water uptake rate (S(h)) is equal to potential water uptake rate (S_p) (Equation 3-12). The potential root-water-uptake rate (S_p) is derived from potential transpiration rate, T_p.

$$S_p = b(x)T_p \qquad 3\text{-}13$$

where b(x) is the normalised root water uptake distribution. It expresses the variation in space of the potential extraction term (S_p) over the soil profile, and it can assume different functions, e.g. linear or exponential (Simunek et al., 2013). The root water uptake rate is proportional to b(x), and the integral of b(x) over the soil profile is equal to 1 (Simunek et al., 2013).

3.3.2.2 Input parameters

HYDRUS-1D has six parameters that represent the soil and greatly influence the modelling of the behaviour of water in the soil (Table 3.3). The parameter sensitivity analysis will guide which parameters affect the model outputs the most.

Table 3.3 – Soil parameters in HYDRUS

Parameter	**Symbol**	**Unit**	**Description**
Residual soil water content	θr	$[L^3L^{-3}]$	It is the moisture content where water flow ceases (for sandy soils, the wilting point is a good approximation, but for clay soils, θr is lower than the wilting point) (Van Genuchten, 1980; Kirkham, 2014).

Saturated soil water content	θs	$[L^3L^{-3}]$	It is the maximum moisture content of a soil. It is usually 5 to 10% smaller than the porosity because of entrapped or dissolved air (Van Genuchten et al., 1991).
Parameter from the soil water retention function	α	$[L^{-1}]$	It is a parameter related to soil pore-size distribution; it is the inverse of the air-entry value (Simunek et al., 2013).
Parameter from the soil water retention function	n	[-]	It is a measure of the pore-size distribution (Arora et al., 2011); it has a small value for fine-textured soils (Simunek et al., 2013).
Saturated hydraulic conductivity	Ks	$[LT^{-1}]$	It expresses the ability of the saturated soil to transmit water when subjected to a hydraulic gradient (USDA, 2017).
Parameter from the soil water retention function	L	[-]	It represents the pore discontinuity and tortuosity of the flow path (Arora et al., 2011).

The vegetation in HYDRUS-1D is mainly expressed by LAI since interception and root growth were not considered in this application. LAI was defined by Watson (1947) as the ratio between the sum of the foliar area and the unit of soil surface (LAI = leaf area / ground area, m^2/m^2). It characterises plant canopies and can be related to photosynthesis, evaporation and transpiration, rainfall interception and carbon flux (Zheng & Moskal, 2009). There are different methods to estimate LAI; they can be ground-based measurements or indirect, for instance with the use of remote sensing imagery (Asner et al., 2003). In this study, 'residual soil water content' and 'saturated soil water content' will be used interchangeably by 'residual water content' and 'saturated soil content', respectively.

3.3.3 GLUE analysis

Strong parameter interactions and overparameterization can lead to multiple combinations of parameters that reproduce soil moisture observations equally well, otherwise known as equifinality (Beven, 2012). The Monte Carlo-based approach of the

Generalised Likelihood Uncertainty Estimation (GLUE) deals with the issue of equifinality. This method was not well accepted when released, but it gained attention over time, as uncertainty estimation increased in popularity in the field of hydrology (Beven & Binley, 2014). Beven (2012) explains that the bad or good results obtained from a parameter set is due to their interaction as a whole, rather than due to an individual parameter value. GLUE has been successfully applied in land-surface modelling (LSM) studies, which include complex land-surface modelling (Prihodko et al., 2008), soil moisture modelling (Hossain et al., 2004b; Chen et al., 2015), canopy modelling (Mo & Beven, 2004), flood prediction uncertainty (Hossain et al., 2004a) and evaporative fluxes (Schulz & Beven, 2003; McCabe et al., 2005).

The calibration process is based on single-objective and multi-objective approaches. The single-objective approach finds a unique "best" parameter set that ensures a "global optimum" fitting of the modelled and observed data, and it has been a common practice in hydrological modelling (Efstratiadis & Koutsoyiannis, 2010; Chen et al., 2014a). The multi-objective approach accepts the existence of multiple "behavioural" parameter sets, and it is more consistent with most hydrological models since they have a number of non-linear interacting parameters (Wagener & Gupta, 2005). The need to establish an approach that considers the multi-objective nature of the calibration problem has been stressed in several studies (McCabe et al., 2005; Efstratiadis & Koutsoyiannis, 2010). GLUE handles these non-linear interactions and can find a number of parameter set values that generate simulation using a good data fit (Efstratiadis & Koutsoyiannis, 2010). The selection of parameter sets in GLUE starts by defining the upper and lower limit for each parameter, then GLUE randomly selects a value between the limits (Willgoose & Sharmeen, 2006). There is no parameter correlation in GLUE since each parameter is assumed independent from the others (Willgoose & Sharmeen, 2006).

3.3.3.1 Parameter sensitivity

An elemental part of modelling is to evaluate how sensitive the model outputs are to a change of input parameters (Ahmed et al., 2007). A sensitivity analysis helps to better understand the model structure; it finds the parameters that are most sensitive to model output, and the principal sources of output uncertainty (Ratto et al., 2001; Yan et al., 2020). GLUE has been broadly applied to hydrological studies to understand the parameters' sensitivity and the uncertainty of the outputs (Ahmed et al., 2007; Blasone et al., 2008; Vázquez et al., 2009; Sun et al., 2016). The sensitivity analysis determines the most important parameters for the calibration process, that is, the parameters that need to be carefully adjusted to obtain a better fit of the model simulations to the observation values (Reusser et al., 2011).

In hydrology the sensitivity analysis is frequently conducted using an objective function (Reusser et al., 2011), e.g., the root mean square error (RMSE) or Nash–Sutcliffe Efficiency (Nash & Sutcliffe, 1970). Here, the Nash–Sutcliffe Efficiency (NSE) coefficient was applied to assess HYDRUS-1D parameter sensitivity. Parameters that are more sensitive will display a graph with a defined peak, which corresponds to a parameter value that generates a higher NSE (Chen et al., 2016) (e.g., Figure 3.15-a). Parameters that do not show a well-defined peak in the graph (e.g., Figure 3.15-b) are considered sensitive with weak identifiability because they have a small range of values corresponding to high NSE. When the response surface is flat (e.g., Figure 3.15-c), it means that the change in parameter does not impact the NSE result, thus the parameter is not affecting the model performance, nor is its effect compensated by another parameter. In this study, the NSE was applied to assess HYDRUS-1D parameter sensitivity because it is a widely used goodness-of-fit index in hydrology.

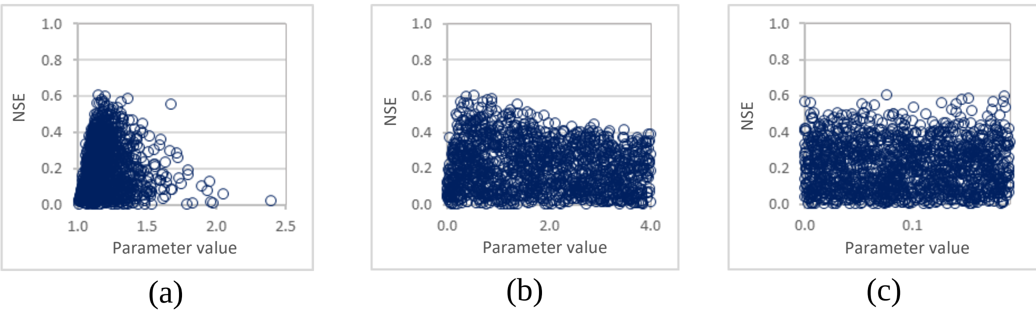

Figure 3.15 – HYDRUS-1D parameter sensitivity – Nash–Sutcliffe Efficiency (NSE) likelihood function.

3.3.3.2 HYDRUS GLUE calibration

The parameter range for the wet and dry calibration at each station was defined by the literature (Brooks & Corey, 1964; Carsel & Parrish, 1988; Brady & Weil, 1999; Asner et al., 2003). For each parameter, the average values of soil hydraulic properties that are found for clay soils (e.g., residual soil water content, saturated conductivity) were taken, and higher and lower values characterise the maximum and minimum limits. The parameter range is shown in Table 3.4.

Table 3.4 – Parameter range for GLUE analysis

Parameter	**θr** **[L^3L^{-3}]**	**θs** **[L^3L^{-3}]**	**α** **[L^{-1}]**	**n** **[-]**	**Ks** **[LT^{-1}]**	**L** **[-]**	**LAI** **[-]**
Min	0.01	0.3	0.01	1	10^{-8}	-3	0
Max	0.2	0.6	0.2	2.5	10^{-4}	3	4

The residual soil water content (θr) is usually higher for fine soils than for coarser soils, such as sand (Van Genuchten, 1980). Carsel and Parrish (1988) developed probability density functions for soil moisture parameters, reporting a residual soil water content that is, on average, 0.068 (v/v) for clay soils and 0.095 (v/v) for clay loam soils. For the Monte Carlo GLUE analysis, the range of residual soil water content was set to vary between 0.01 to 0.2 (v/v). Physically meaningful values of saturated soil water content (θs) in clay soils can be as high as 60% (Hillel, 1998; Brady & Weil, 1999), and are on average 0.38 v/v (Carsel & Parrish, 1988). Therefore, the saturated soil water content was set to vary between 0.3 and 0.6 v/v for the Monte Carlo GLUE analysis.

The shape parameter, α, from the soil water retention is the inverse of the air-entry value (or bubbling pressure) (Arora et al., 2011; Simunek et al., 2013). Carsel and Parrish (1988) found a mean value of 0.008 cm^{-1} for clay soils and 0.145 cm^{-1} for sandy soils. For the Monte Carlo simulation it ranged from 0.01 to 0.2. The parameter n from the soil water retention function is an experimentally determined parameter; it is a measure of the pore-size distribution (Arora et al., 2011). Fine-textured soils (e.g. clay) have small values for pore-size distribution (1-1.3) (Simunek et al., 2013). For the Monte

Carlo analysis, n ranges between 1 and 2.5. The saturated hydraulic conductivity (Ks) constant varies for sandy soils (10^{-5}-10^{-4} m/s) and clay soils (10^{-9}-10^{-6} m/s) (Hillel, 1998). For clay soils, Carsel and Parrish (1988) found an average saturated hydraulic conductivity of 7.210^{-7} m/s for clay loam soils and 4.110^{-5} m/s for loam sand soils. For the Monte Carlo simulation analysis, Ks was set to range between 10^{-8} to 10^{-4} m/s. Schaap et al. (2001) explains that for finer textured soils, i.e., clay, α, n and Ks decrease while θr increases. The pore-connectivity parameter (L) in the hydraulic conductivity function was assumed to be 2 in Brooks and Corey (1964) study and it was found to be around 0.5 for many soils by Mualem (1976). Yates et al. (1992) found that L varied between -3 and values greater than 100. For Schaap and Leij (2000), L was often negative, with smaller values for finer textured soils, and an optimum value of -1 across the soil types. In this analysis the pore-connectivity parameter ranges from -3 to 3.

A study based on measurements of plant canopy leaf area index (LAI) from around the world reported a mean LAI for grassland of 2.5 (Asner et al., 2003), whereas Ramírez-García et al. (2012) found an average of 2.5 and 3 from direct measurement and estimations, respectively. Additional work using different methods (LAI200, Accupar and destructive) reported average values of LAI in grasslands of 1.71, 1.44 and 2.02 (He et al., 2007). For this reason, the range of LAI values for the GLUE analysis was set as 0 to 4.

3.3.4 Goodness-of-fit indices

Calibration is usually necessary prior to application of hydrological models, with the results of calibration acquired using goodness-of-fit measures, such as the likelihood and objective function (McCuen et al., 2006). To analyse the goodness-of-fit of observed and simulated data, this study applies four statistics: Pearson's correlation coefficient (R) (Equation 3-14), root mean square error (RMSE) (Equation 3-15), scaled root mean square error (sRMSE) (Equation 3-16) and Nash-Sutcliffe Efficiency (NSE) (Equation 3-17).

$$R= \frac{\sum_{i=1}^{n}(S_i- \bar{S})(O_i- \bar{O})}{\sqrt{\sum_{i=1}^{n}(S_i- \bar{S})^2}\ \sqrt{\sum_{i=1}^{n}(O_i- \bar{O})^2}} \tag{3-14}$$

$$RMSE= \sqrt{\frac{\sum_{i=1}^{n}(S_i- O_i)^2}{n}} \tag{3-15}$$

$$sRMSE= \sqrt{\frac{\sum_{i=1}^{n}\left(\frac{S_i- O_i}{O_i}\right)^2}{n}} \tag{3-16}$$

$$NSE=1- \frac{\sum_{i=1}^{n}(O_i- S_i)^2}{\sum_{i=1}^{n}(O_i- \bar{O})^2} \tag{3-17}$$

where n is the number of observations, S_i and O_i are the simulated and observed data, respectively, at time i.

The Pearson's correlation coefficient (R) indicates the strength of the linear relationship between two random variables, that are accumulated and the scales of the variables are adjusted by the denominator to have equal units, and a strong correlation between the two variables has a value close to one (Rodgers & Nicewander, 1988; Benesty et al., 2009). RMSE "represents the sample standard deviation of the differences between modelled and observed values" (Shamsi & Koran, 2017). RMSE is a computation of the differences between observed and modelled values; it is a widely used criteria and good simulations have RMSE close to one (Shamsi & Koran, 2017). The sRMSE is the RMSE divided by the mean of observed values; it admits lower errors for dry soil conditions and larger errors for high soil moisture peaks, and it ranges from 0 to ∞, with best values closer to 0 (Shamsi & Koran, 2017). One of the most widely used goodness-of-fit indices is the coefficient of efficiency by Nash and Sutcliffe (1970). The NSE is "sensitive to differences in the observed and model simulated means and variances" (Legates & McCabe, 1999). NSE may assume negative numbers when RMSE exceeds the variance of the observed flows (Hall, 2001). "NSE can range from −∞ to 1. An NSE value of 1 represents a perfect match between the observed and modelled hydrographs” (Shamsi & Koran, 2017). In this study, some of the analysed stations had missing soil moisture data, so the indices were calculated only for the days with existing measured data.

3.3.5 Model calibration

The key parameters affecting the ability of HYDRUS-1D to simulate soil moisture are physical soil parameters and vegetation (Chen et al., 2014a). The vegetation data in HYDRUS-1D is represented by the leaf area index (LAI) and the soil is described by six parameters, explained in section 3.3.2.2. Both LAI and soil parameters will be calibrated in HYDRUS-1D to find the parameter set that best simulates soil moisture during the dry and wet the periods. To calibrate HYDRUS-1D, the Monte Carlo GLUE analysis (Beven & Binley, 1992) will be used. The selection of the best parameter set will be by statistical (R, sRMSE and NSE) and visual analysis. The soil profile in HYDRUS-1D was described with 50 nodes evenly distributed in the 30 cm soil layer. The number of nodes was tested by Chen (2013) who found that a further increase in the spatial discretisation did not make notable impact on the results. The root distribution in the soil profile was determined according to Jackson et al. (1996) that recommended, for grasslands, an exponential root distribution with depth.

3.3.6 Wet and dry periods

To explore the difference in soil moisture dynamics between dry and wet periods, local rainfall measurements were used to define the periods that will be used later for calibration and validation of the stations. The average for the 11 years (2005-2015) was calculated for S2, K2 and M1 (Figure 3.16). The dry period corresponds to years below the average and the wet period to years above the average. The only two consecutive years below the average that were coincident in the three stations were 2005 and 2006. In S2 those two years were considerably drier (~36%) than the average, whereas in K2, 2005 was quite close to the average. For the wet period there were no two consecutive wetter than average years, and the year 2007 was not considered because, despite being higher than the average, it was an atypical year. In 2007 there was an extreme event, known as Pasha Bulker storm, that over four days (06 to 09 of June) precipitated 221 mm, corresponding to 25% of the total in that year. 2010 was the wettest year in this period, 62% higher than the average in S2, 55% higher than the average in M1 and 33% higher than the average in K2. The second wettest year (apart from 2007) was 2008, ~4% above the average in the three stations. The wet period was defined, then, as 2008 and 2010.

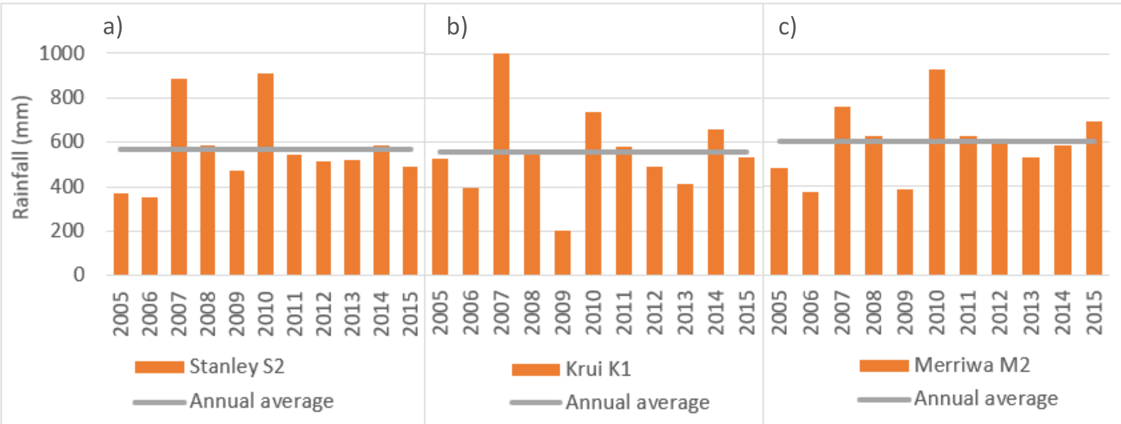

Figure 3.16 – Annual rainfall at Stanley-S2 (a), Krui-K1 (b) and Merriwa-M2 (c) stations (2005-2015).

3.4 Results

The results show the validation of an existing HYDRUS-1D soil moisture model for Stanley-S2 station, and an evolution of how the soil moisture drivers, i.e., soil parameters and vegetation, are affecting the temporal and spatial differences in soil moisture behaviour in wet and dry periods, in three catchments in New South Wales, Australia.

3.4.1 Validation of existing model

The objective of the first part of this study was to validate an existing HYDRUS-1D soil moisture model for the Stanley micro-catchment (Figure 3.18) (Chen et al., 2014a). This model was calibrated for a three-year calibration period (2005-2007), but there was no validation in that study. Validation was pursued using data for the period (2008-2015). The best parameter set found by Chen et al. (2014a) for the three years (Table 3.5) generated high values for each of the goodness-of-fit indices (Table 3.6). It is important to note that the measured soil moisture dataset used at that time had some small errors, and this study uses the corrected data, which corresponds to version 3 of the calibrated dataset from SASMAS monitoring stations (Rüdiger et al., 2010). Figure 3.17 shows the simulated soil moisture at Stanley station S2 (2005-2007) using the calibration parameters from Chen et al. (2014a). The calibration period (2005-2007) was considerably dry in the first two years (around 36% drier than the average for 2005-2015). However, in 2007, an extreme rainfall event, concentrated over a four-day period, contributed to the annual rainfall totals for this year being wetter than the eleven-year average.

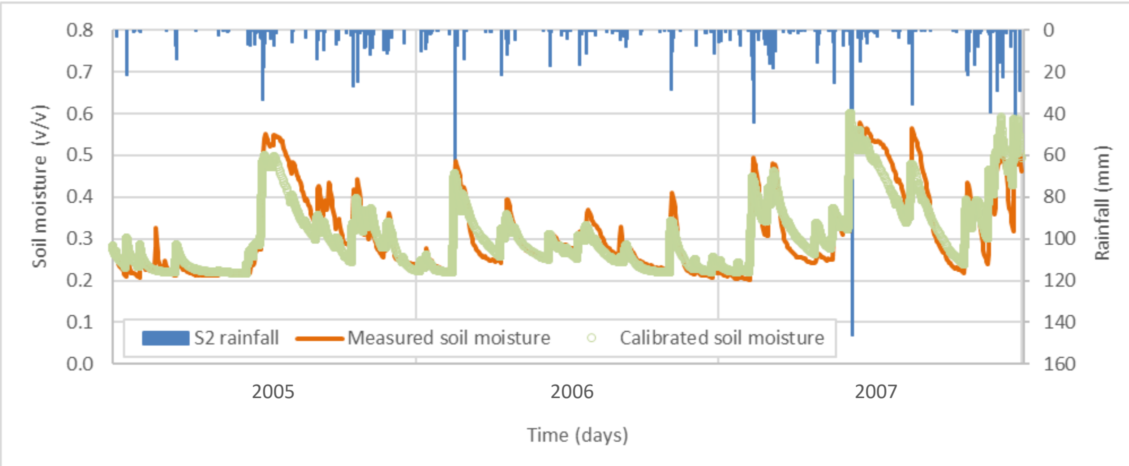

Figure 3.17 – Measured and simulated profile soil moisture data (0-30 cm) at Stanley station S2 for the period 2005-2007 (Chen et al., 2014a).

Table 3.5 – Best parameter set for Stanley (S2) for the period 2005-2007 (Chen et al., 2014a).

θr (v/v)	**θs (v/v)**	**α (cm^{-1})**	**n (-)**	**log Ks (m/s)**	**L (-)**	**LAI (-)**
0.0362	0.6	0.0164	1.2262	-5.87	0.1322	1

Comparison of simulated and observed values for the validation period 2008-2015 shows that the soil moisture variability was well simulated (Figure 3.18). In general, the wet and dry fluctuations of simulated and measured soil moisture were matched, although the simulated soil moisture was overestimated in some of the peaks, i.e., 2010-2014, and lows, i.e., 2010-2015. Because the calibration period was mainly dry (2005-2006), when there was higher rainfall, the model typically overestimated the soil moisture peaks. The overestimation of soil moisture recession values is linked to a change in the measured soil moisture behaviour; from 2009 the recession values are around 0.15 v/v whereas in the calibration period (2005-2007) they were around 0.2 v/v. The maximum difference between measured and simulated soil moisture was about 0.20 v/v (i.e., 23%) but only for 0.3% of the time; for 84% of the time the difference between simulated and measured soil moisture was less than 0.1 v/v. This difference between measured and simulated soil moisture of 0.20 v/v is lower than the uncertainty of the observed soil moisture value of 0.022 v/v (Rüdiger, 2006). Results show that the calibration parameter set applied to a longer period of simulation (2008-2015) were still within an acceptable range (Table 3.6). The NSE for the validation period decreased 40%, and 22% for the Pearson correlation (R) when comparing to the indices from the calibration period.

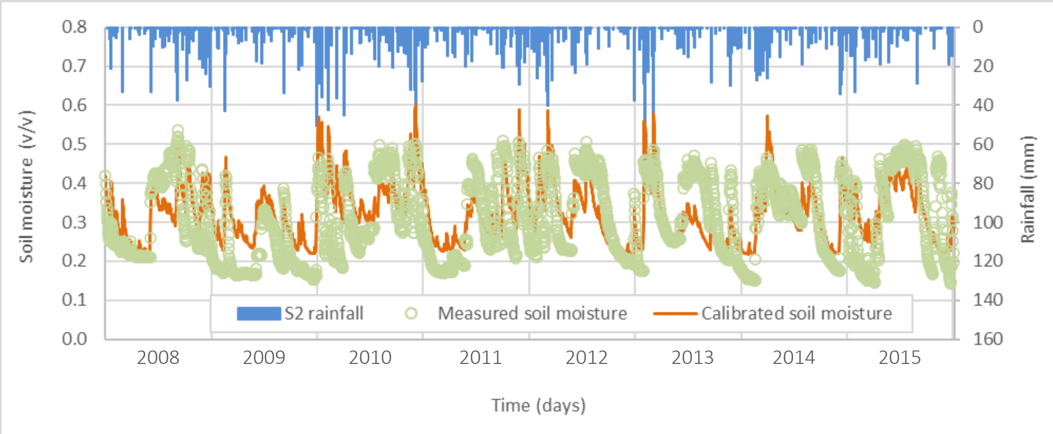

Figure 3.18 – Measured and simulated profile soil moisture data (0-30 cm) at Stanley station S2 for the period 2008-2015, using the calibration parameters from Chen et al. (2014a).

Table 3.6 – Goodness-of-fit values for Stanley (S2) for calibration (2005-2007) and validation (2008-2015)

	Period	**R**	**RMSE (v/v)**	**sRMSE**	**NSE**
Calibration (Chen et al., 2014a)	2005-2007	0.936	0.037	0.104	0.866
Validation	2008-2015	0.731	0.073	0.287	0.512

3.4.2 Calibration for wet and dry periods in multiple sites

For a temporal and spatial investigation of soil moisture dynamics, the model HYDRUS-1D was calibrated for distinct periods of wetness that were characterised by being above or below the precipitation average (2005-2015) for two soil textures: clay and sand. Two stations were located in a predominantly clay soil (S2 and S3 – clay loam soil) and two in sandy soils (loamy sand – K2, and sandy loam – M1) (Figure 3.1) which enabled an analysis of the influence of the soil's physical parameters on soil moisture spatial and temporal variability. For each station and wetness period, 15,000 Monte Carlo simulations were run, for a total of 120,000 simulations. The Monte Carlo GLUE analysis generated several combinations of parameter sets (consisting of physical soil parameters and LAI). Two individual parameter sets for each station (for wet and dry periods), using those that reached a high NSE, are then used to run HYDRUS-1D and simulate soil moisture behaviour. Modelled soil moisture was compared against observed soil moisture data and the physical meaning of vegetation and soil parameters were explored. The parameter set that generated the best goodness-of-fit for both the wet and dry calibration was applied to the eleven-year (2005-2015) simulation period to assess if a dry or a wet calibration could better capture the soil dynamics of a longer period.

3.4.2.1 Clay soil stations

For the S2 station in Stanley, characterised by a clay soil, the Monte Carlo GLUE analysis that generated runs with NSE greater than zero are shown in Figure 3.19.

Dry simulations

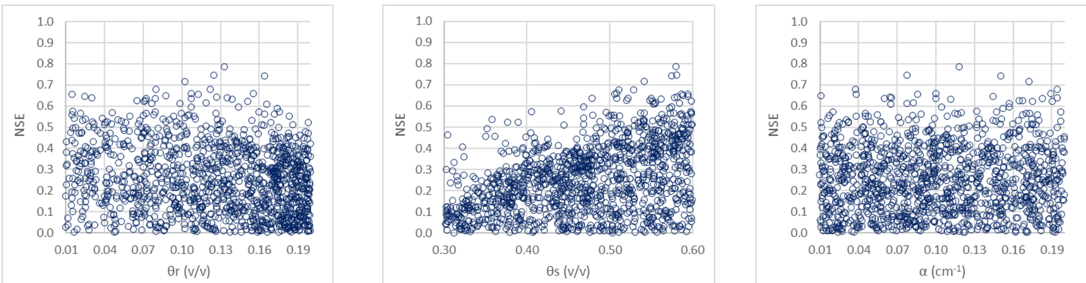

(a) (b) (c)

Wet simulations

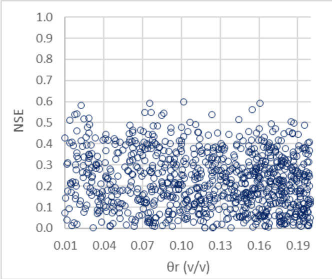

(d)

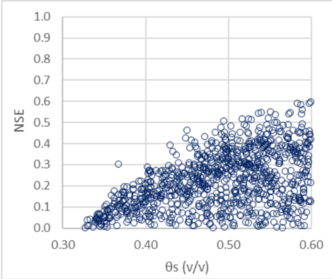

(e)

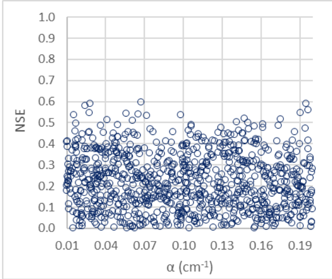

(f)

Dry simulations

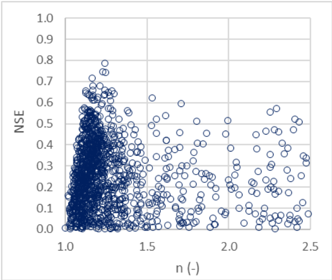

(g)

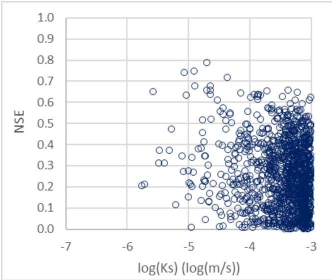

(h)

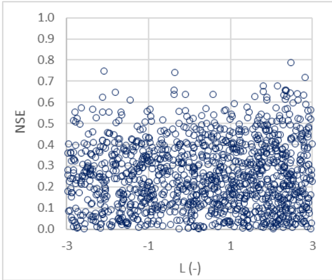

(i)

Wet simulations

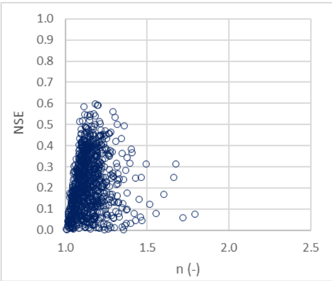

(j)

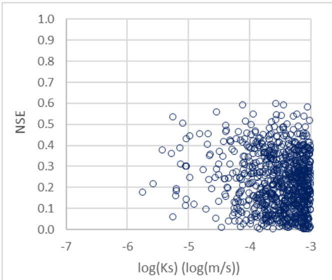

(k)

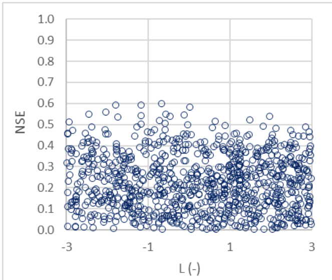

(l)

Dry simulations

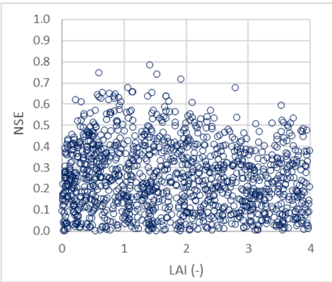

(m)

Wet simulations

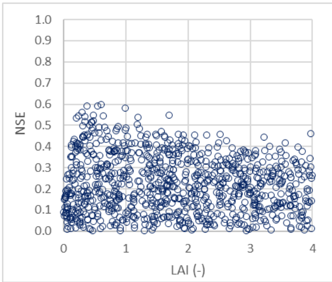

(n)

Figure 3.19 – Dotty plots from Monte Carlo GLUE analysis for the dry (2005-2006) and wet (2008 and 2010) calibration periods at station S2 for the parameters: (a, d) residual soil water content – θr, (b, e) saturated soil water content – θs, (c, f) inverse of the air-entry value – α, (g, j) soil pore-size distribution – n, (h, k) logarithm of saturated hydraulic conductivity – logKs, (i, l) pore discontinuity – L, and (m, n) Leaf Area Index – LAI.

The dry simulations reached higher NSE than the wet simulations; 20% of the valid runs for the dry simulations had NSE above 0.4, whereas in the wet simulations 10% of the valid runs had NSE above 0.4. The highest NSE for the dry and wet simulation was 0.8 and 0.6, respectively. The most sensitive parameter in both dry and wet periods is the soil pore distribution (n), with a defined peak around 1.2 (Figure 3.19 – g and j) (Grohs et al., 2019). The saturated soil moisture content (θs) presented higher values of NSE towards high values of θs for the dry and wet simulations (Figure 3.19 – b and e). The saturated soil moisture content relates to the porosity of the soil, although usually 5 to 10% smaller than the porosity (Van Genuchten et al., 1991). A high value of θs implies less drainage, since there is more space for water in the soil. In the wet calibration period, there were no runs with θs below 0.32 v/v, even though the limit was set to 0.30 v/v, indicating the wet period needs additional space for water in the soil. The residual water content (θr) in the dry and in the wet calibrations did not show a well-defined peak, although there is a concentration of runs towards higher values of θr, i.e., higher than 0.13 v/v for both periods (Figure 3.19 – a and d). The α parameter, that is, the inverse of the air-entry value, also did not show a well-defined peak but it is possible to see a slight tendency to higher NSE values towards higher α values, especially in the dry period (Figure 3.19 – c and f). The parameter L represents the pore discontinuity (Arora et al., 2011), for both periods did not show a well-defined peak, but there is a subtle peak around -1 for the wet period of calibration (Figure 3.19 – i and l).

An important difference between dry and wet periods is observed in the values of Ks. The saturated hydraulic conductivity (Ks) has a wide range, i.e., from 0.864 to

8640 cm/d (1 e^{-7} to 1 e^{-3} m/s), and for that reason the values were shown in a logarithm scale (logKs). The majority of dry and wet simulations were concentrated in high values of Ks (Figure 3.19 – h and k), with 87% of the valid runs, for both wet and dry, corresponding to a range of -4 to -3 log(m/s) (i.e., 864 to 8640 cm/d). Despite the predominance of high Ks values among the simulations, in the dry period there is a tendency to obtain higher NSE with lower Ks (i.e., from -6 to -4, or 8.64 to 864 cm/d), whereas in the wet simulations the opposite occurs (i.e., from -4 to -3, or 864 to 8640 cm/d). A high saturated hydraulic conductivity (Ks) generates high drainage, making the soil dry faster, whereas lower values of Ks make the soil hold water, leading to less drainage.

The LAI presented a concentration of runs between 0 and 1 for the dry and wet simulations (Figure 3.19 – m and n). The peak of the dotty plots for LAI was around 0.5, for both dry and wet simulations, although in the dry simulations some of the highest NSE runs were above that peak, e.g., 1.42, 1.53 and 1.92. The LAI has a big influence in the potential and actual transpiration; the higher the LAI, the more water will be extracted from the soil by transpiration of the plants, thus the faster the soil will dry. Although it is expected that a wet period would have higher LAI than a dry period (Grohs et al., 2019), a high LAI works on extracting the water from the soil and because the dry period has a lower quantity of water in the soil, the model tries to compensate by assigning high LAI to drier periods.

The best parameter set of the dry calibration period for Stanley-S2 generated a good match between simulated and measured values (Figure 3.20 – a) and was able to reproduce the wetting and drying dynamics of soil moisture in this period (Figure 3.21). Peaks and recessions were well fitted, and the highest difference between a measured and a simulated peak happened in November 2006, with a value of 0.065 v/v. It is worth to mention that the confidence interval of the soil moisture probes is +/- 0.022 v/v (Rüdiger, 2006) which is of similar magnitude of the confidence can slightly influence the match of simulated and observed values. In a semi-arid region, such as the Stanley micro-catchment, the temporal variation of soil moisture is lower during a dry period compared to rainy periods, which makes soil moisture behaviour more constant than during the wet calibration period (Figure 3.22). The wet calibration at Stanley-S2 obtained a satisfactory fit of simulated and measured values (Figure 3.20 – b) although worse than in the dry calibration. The highest difference between simulated and measured peak was 0.14 v/v in August 2008. The parameter sets that generated the best wet and dry calibrations are shown in Table 3.7.

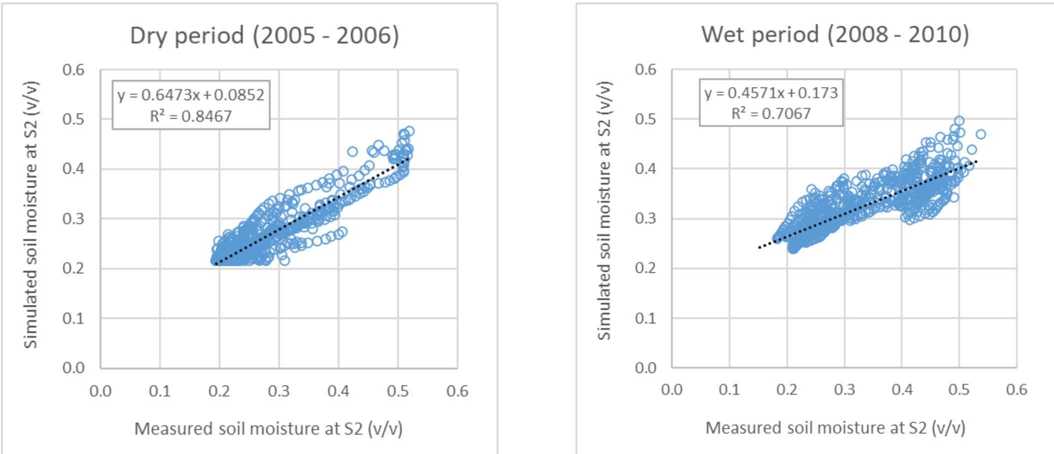

(a) (b)

Figure 3.20 – Scatter plot of the measured and simulated soil moisture (0-30 cm) at Stanley clay station - S2 for the dry (2005-2006) (a) and wet (2008 and 2010) (b) calibration period.

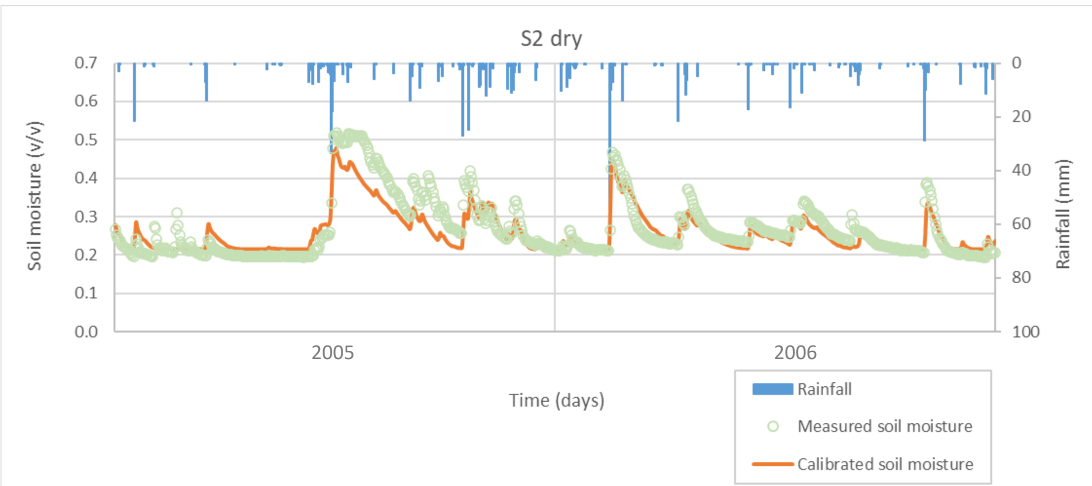

Figure 3.21 – Dry calibration (2005-2006) in S2 station.

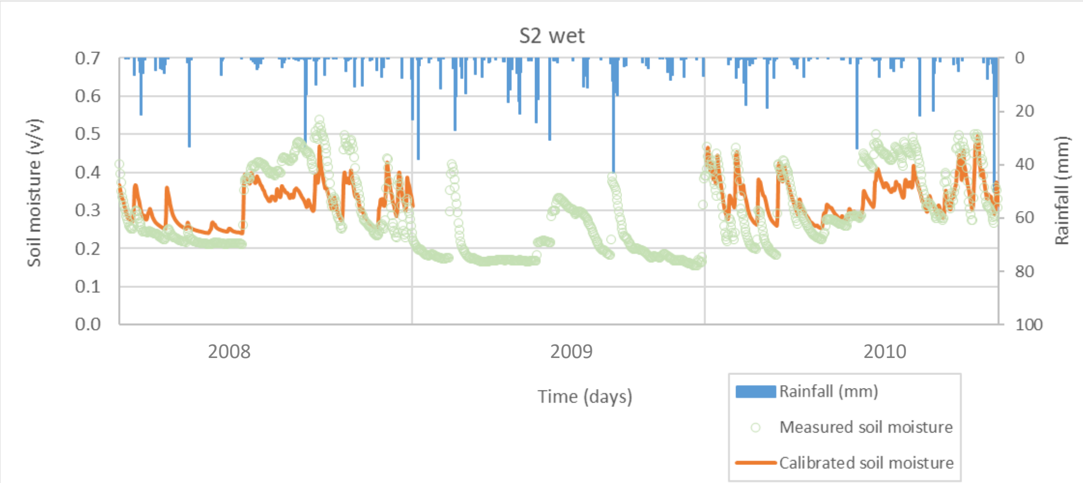

Figure 3.22 – Wet calibration (2008 and 2010) in S2 station.

Table 3.7 – Best parameter set for Stanley (S2) clay station for dry (2005-2006) and wet (2008 and 2010) calibration period.

Calibration period	**θr (v/v)**	**θs (v/v)**	**α (cm^{-1})**	**n (-)**	**log Ks (m/s)**	**L (-)**	**LAI (-)**
Dry	0.133	0.580	0.118	1.245	-4.702	2.476	1.42
Wet	0.102	0.599	0.067	1.186	-3.568	-0.655	0.61

Despite the differences in rainfall, i.e., an annual average of 360 mm in the dry period and 830 mm in the wet, some of the parameters that best calibrated the two wetness periods were very similar, i.e., residual soils water content (θr), saturated soils water content (θs) and pore-size distribution parameter (n). The LAI, the tortuosity parameter (L), the saturated hydraulic conductivity (log Ks) and the inverse of the air-entry (α) were counteracting each other in the wet and the dry calibration. A higher LAI, i.e., the case of dry calibration, increases the plants' transpiration, drying the soil faster, whereas a lower LAI decreases the transpiration, which would better represent soils with more water. A higher tortuosity parameter (L) makes water stay longer in the soil, thus the dry calibration period that has a high L may be compensated by the high LAI, since the first is keeping water in the soil and the second is losing water to the atmosphere. In the same way, the lower saturated conductivity (Ks) of the dry period that keeps the water in the soil for longer is counterbalanced by the higher α that drains the water faster, and this mechanism occurs in the wet period in the opposite way. The goodness-of-fit for the Stanley-S2 station in the dry calibration reached better indices, e.g., higher R and NSE, than the wet period (Table 3.8).

Table 3.8 – Goodness-of-fit values for Stanley (S2) clay station for dry (2005-2006) and wet (2008 and 2010) calibration periods.

Calibration period	**R**	**RMSE (v/v)**	**sRMSE**	**NSE**
Dry	0.920	0.036	0.111	0.785
Wet	0.815	0.060	0.183	0.597

The calibration parameters from the dry period (2005-2006) (Table 3.7) generated excellent indices of goodness-of-fit when applied to the eleven-year period at station S2 in Stanley (Table 3.9), where NSE decreased by only 20%. When using wet calibration parameters for the eleven-year period, NSE did not deteriorate much, i.e., 0.597 for wet calibration and 0.553 for the eleven-year period. Simulations using the wet calibration parameters for the eleven-year period did not match the soil moisture value recessions (Figure 3.24) as well as when using the dry calibration parameters. The parameters from the wet calibration closely produced values of soil moisture peaks throughout the eleven years, with the exception of 2012, 2013 and 2015 (Figure 3.24).

The scatter plot of the eleven-year simulation results (Figure 3.25) shows that the wet parameter data set generated higher soil moisture values (y axis) than the dry parameter set, except for high soil moisture contents, i.e., soil moisture peaks, where the dry parameters generated higher simulated values. It is expected that a calibration in drier conditions would produce lower simulated values than a calibration in wetter conditions.

Table 3.9 – Goodness-of-fit values for Stanley (S2) for the period 2005-2015 using parameter set from the dry (2005-2006) and wet (2008 and 2010) calibration periods.

Calibration period	**R**	**RMSE (v/v)**	**sRMSE**	**NSE**
Dry calibration	0.808	0.063	0.213	0.625
Wet calibration	0.794	0.068	0.256	0.553

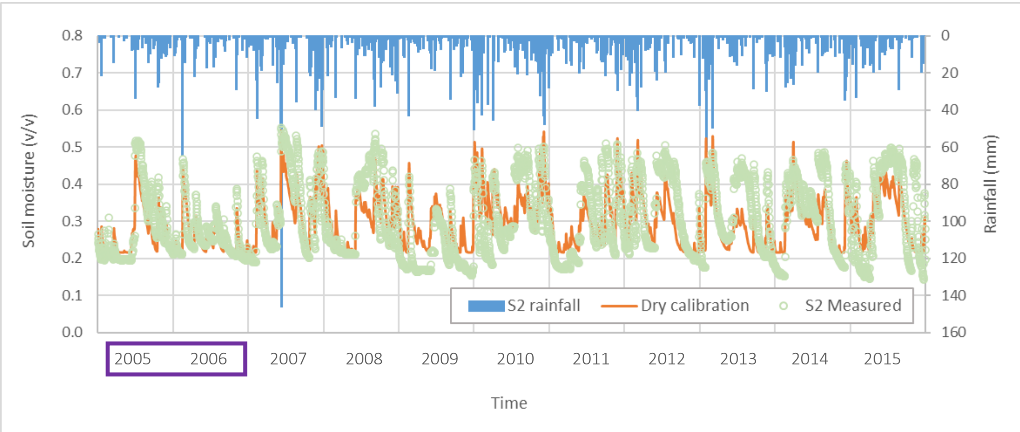

Figure 3.23 – Measured and simulated soil moisture (0-30 cm) at S2 for the period 2005-2015, using parameters from the dry calibration (2005-2006).

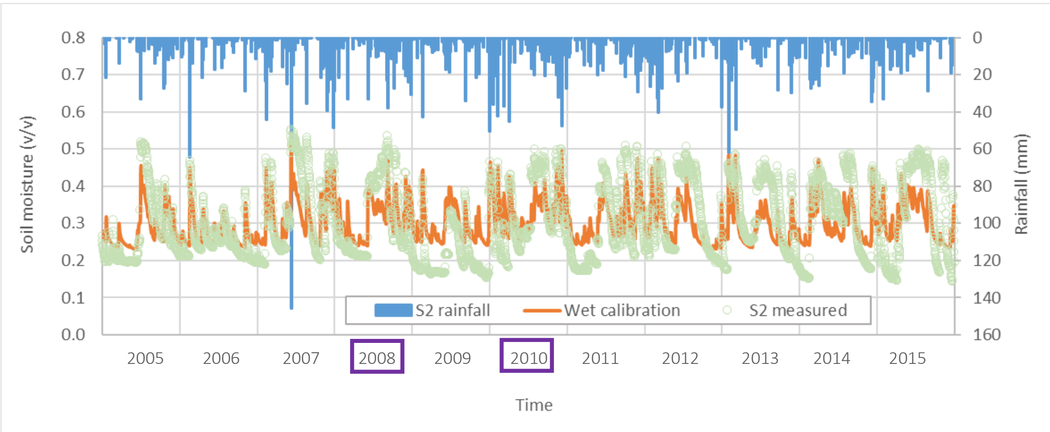

Figure 3.24 – Measured and simulated soil moisture (0-30 cm) at S2 for the period 2005-2015, using parameters from the wet calibration (2008 and 2010).

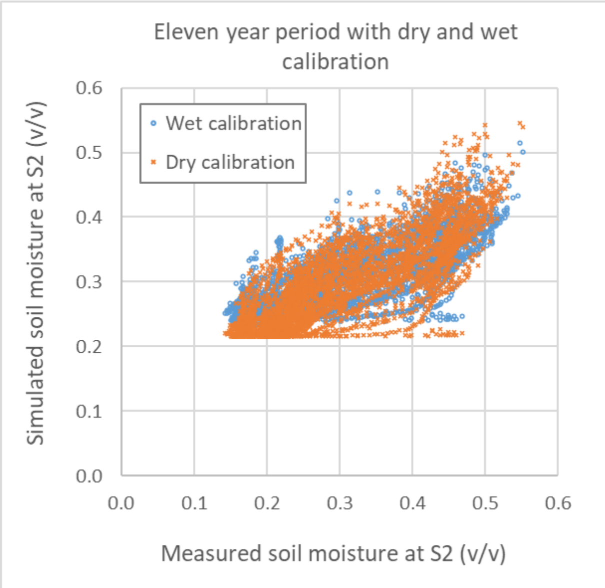

Figure 3.25 – Scatter plot of the measured and simulated soil moisture (0-30 cm) at Stanley station S2 for the period 2005-2015, using parameters from the dry calibration (2005-2006) and from the wet calibration (2008 and 2010).

For the S3 station in Stanley, characterised by a clay soil, the Monte Carlo GLUE analysis plots for the dry and wet period that generated runs with NSE greater than zero are shown in Figure 3.26.

Dry simulations

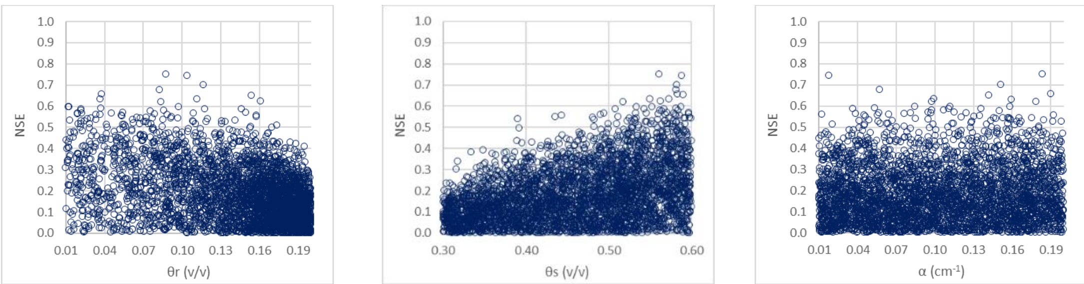

(a) (b) (c)

Wet simulations

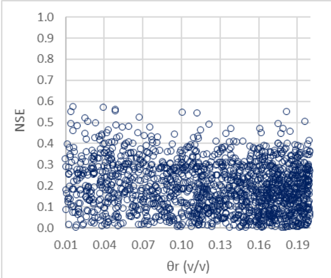

(d)

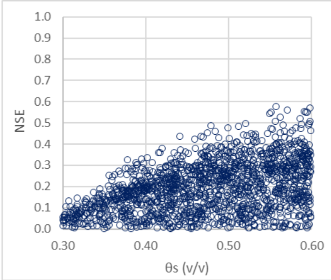

(e)

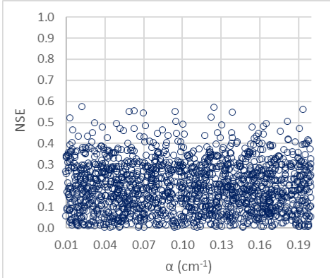

(f)

Dry simulations

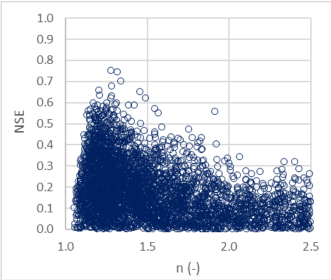

(g)

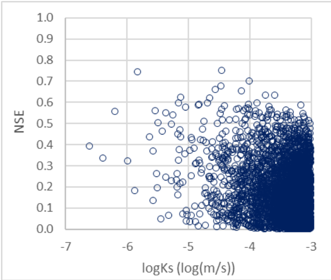

(h)

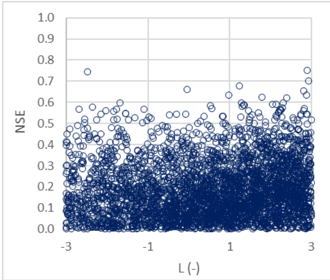

(i)

Wet simulations

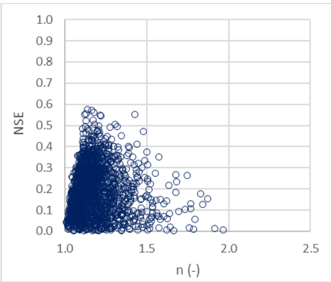

(j)

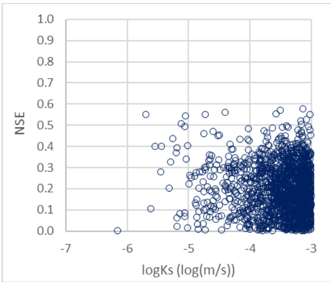

(k)

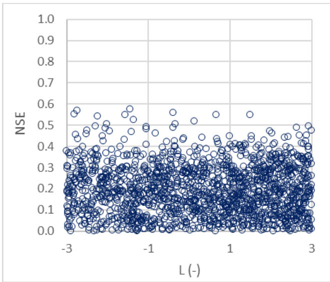

(l)

Dry simulations

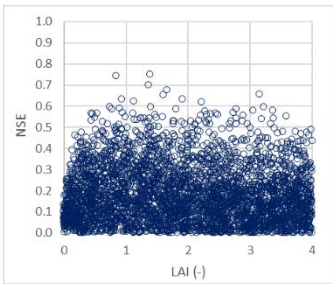

(m)

Wet simulations

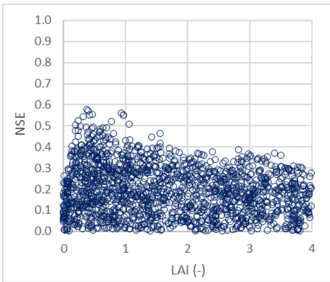

(n)

Figure 3.26 – Dotty plots from Monte Carlo GLUE analysis for the dry (2005-2006) and wet (2008 and 2010) calibration periods at station S3 for the parameters: (a, d) residual soil water content – θr, (b, e) saturated soil water content – θs, (c, f) inverse of the air-entry value – α, (g, j) soil pore-size distribution – n, (h, k) logarithm of saturated hydraulic conductivity – logKs, (i, l) pore discontinuity – L, and (m, n) Leaf Area Index – LAI.

For S3 station, the results from the Monte Carlo simulations show that the parameter sets from the dry period generated a higher NSE than the wet period (Figure 3.26). The soil pore distribution (n) had a defined peak around 1.2 in the dry and wet simulations (Figure 3.26 – g and j) and there were no simulations for n>2 in the wet period. There was a tendency for high values of θs to generate high NSE for the dry and wet simulations (Figure 3.26 – c and f). The same happened with the saturated hydraulic conductivity (Ks), where the simulations were concentrated in the high values (-4 to -3 log(m/s)) (Figure 3.26 – h and k). For the dry period, higher NSE was found in the middle range of Ks, i.e., -6 to -4 log(m/s). The residual water content (θr) showed a concentration of runs toward higher values (> 0.15 v/v) for wet and dry simulations, although the highest NSEs were located in this range (Figure 3.26 – a and d). The LAI presented a peak between 0 and 1 for the wet simulations (Figure 3.26 – n) and a subtle concentration of higher NSE peaks between 0.5 and 1.5 for the dry simulations (Figure 3.26 – m). The inverse of the air-entry value (α) showed a flat response, which indicates that this parameter was not sensitive in wet and dry simulations (Figure 3.26 – c and f). The tortuosity parameter (L) did not present a definable peak (Figure 3.26 – i and l), and the highest NSE for the dry period were a high (2.9) and a low (-2.5) value of L. In general, the dotty plots of S2 and S3 had similar distribution for all the parameters, except for θr, θs and n. The soil pore distribution (n) in the dry simulations had considerably lower NSE, corresponding to the higher range of n (2-2.5) in S3 (Figure 3.26 – g) than in S2 (Figure 3.20 – g). In the dry simulations, the two highest NSEs of the residual water content (θr) for S3 were between 0.07 to 0.11 v/v (Figure 3.26 – a) whereas S2 presented the two best runs between 0.13 and 0.17 v/v for the dry simulations (Figure 3.20 – a). The wet simulations of saturated water content (θs) for S2 did not have runs for θs below 0.32 v/v (Figure 3.20 – e), while S3 did have (Figure 3.26 – e). These differences in θs and θr simulations between the clay stations reflects how the model captured the overall difference in wetness between S2 and S3, i.e., S2 has higher field values of soil moisture than S3.

The scatter plot of measured against simulated soil moisture for Stanley-S3 shows that the dry calibration period had a superior coefficient of determination (Figure 3.27 – a) than the wet period (Figure 3.27 – b). The dry calibration best parameter set could capture the peaks, despite two underestimations in 2005, and recessions in the two years (Figure 3.28) which generated a high NSE (Table 3.11). The wet calibration period presented a lot of missing measured soil moisture data (51%), and the parameter set achieved a poorer NSE (Table 3.11). The parameter set from the wet calibration could not capture the soil moisture behaviour very well, especially in 2010 (Figure 3.29). The parameter sets that generated the best wet and dry calibrations are shown in Table 3.10.

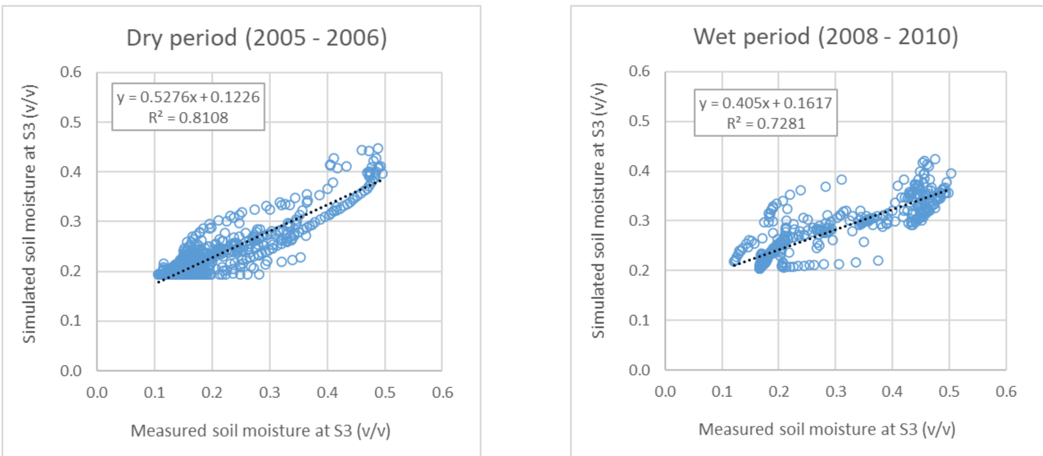

(a) (b)

Figure 3.27 – Scatter plot of the measured and simulated soil moisture (0-30 cm) at Stanley clay station – S3 for the dry (2005-2006) (a) and wet (2008 and 2010) (b) calibration period.

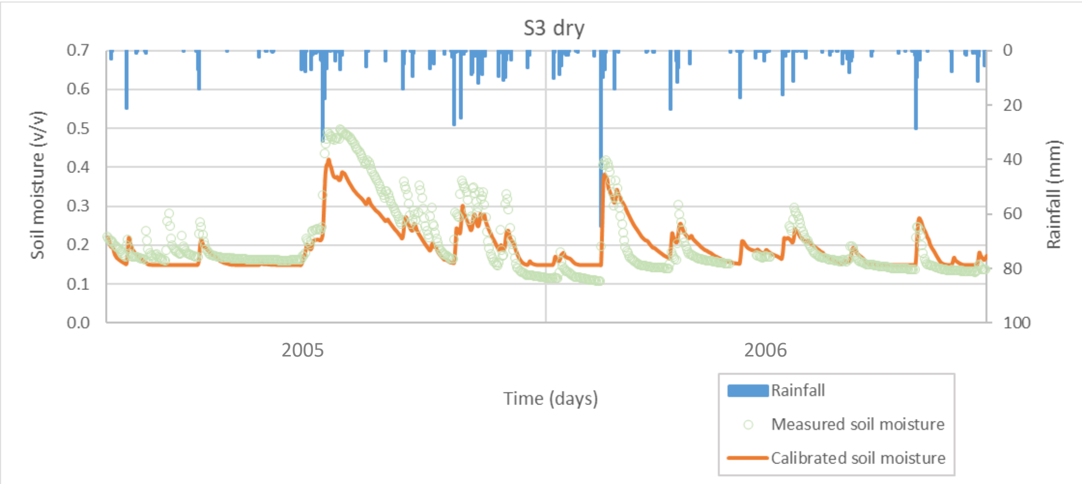

Figure 3.28 – Dry calibration (2005-2006) in S3 station.

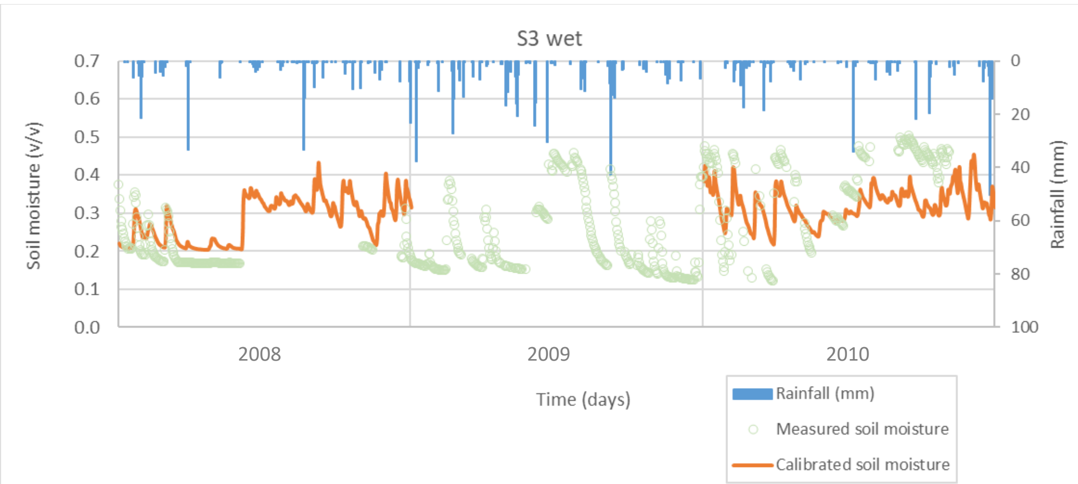

Figure 3.29 – Wet calibration (2008 and 2010) in S3 station.

Table 3.10 – Best parameter set for Stanley (S3) clay station for dry (2005-2006) and wet (2008 and 2010) calibration period.

Calibration period	**θr (v/v)**	**θs (v/v)**	**α (cm^{-1})**	**n (-)**	**log Ks (m/s)**	**L (-)**	**LAI (-)**
Dry	0.088	0.561	0.184	1.282	-4.45	2.898	1.38
Wet	0.016	0.558	0.022	1.138	-3.13	-1.453	0.38

Similar to what happened to S2-station, the best parameter set for the dry and the wet period in S3-station (Table 3.10) differs mainly on LAI, tortuosity parameter (L), saturated hydraulic conductivity (log Ks) and inverse of the air-entry (α). As mentioned above, LAI and L can compensate each other, in the same way as Ks and α. A low LAI in the wet period decreases the transpiration; thus, less water is being lost to the atmosphere, and a low L increases the drainage of water to lower layers. For the dry period the opposite occurs, and the high LAI is compensated with the high L. The goodness-of-fit for Stanley-S3 presented higher NSE for the dry period (Table 3.11).

Table 3.11 – Goodness-of-fit values for Stanley (S3) clay station for dry (2005-2006) and wet (2008 and 2010) calibration periods.

Calibration period	**R**	**RMSE (v/v)**	**sRMSE**	**NSE**
Dry	0.899	0.045	0.201	0.750
Wet	0.853	0.079	0.296	0.575

Stanley-S3 parameters from the dry and wet periods resulted in lower goodness-of-fit when applied to the eleven-year simulation period (Table 3.12). The NSE for the dry period decreased 26% while the NSE for the wet period decreased 16%. Using the parameter sets from the dry and wet periods, the model was able to capture the soil moisture peaks throughout the eleven years. While the model could match closely the recession values along the whole period using the dry calibration parameters (Figure 3.31) the model overestimated the recessions during the eleven years when applying the wet calibration parameters (Figure 3.31). The scatter plot of the eleven-year simulation period (Figure 3.32) using the dry and the wet calibration parameters shows that the low values of soil moisture in the wet simulation (blue) are higher than the dry simulation (orange); the plots have similar behaviour, but the wet simulation is shifted 0.05 v/v upward.

Table 3.12 – Goodness-of-fit values for Stanley (S3) for the period 2005-2015 using parameter set from the dry (2005-2006) and wet (2008 and 2010) calibration period.

Calibration period	R	RMSE (v/v)	sRMSE	NSE
Dry calibration	0.794	0.079	0.295	0.554
Wet calibration	0.760	0.085	0.477	0.481

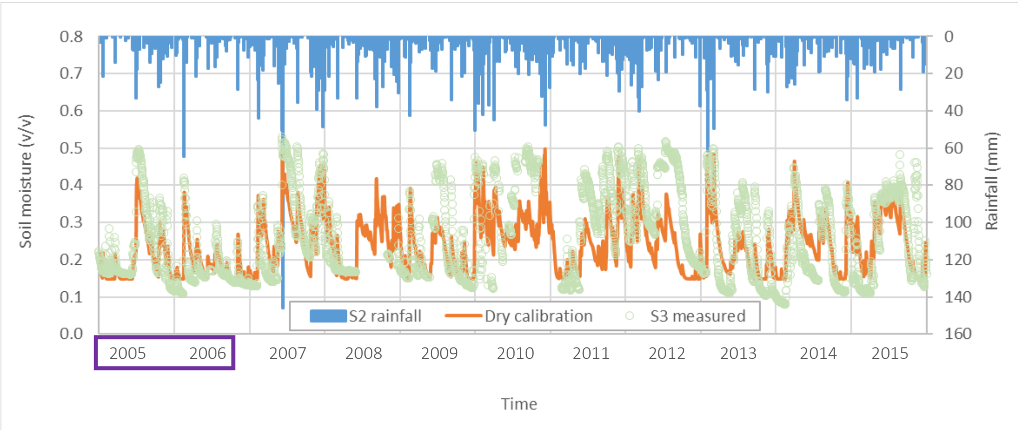

Figure 3.30 – Measured and simulated soil moisture (0-30 cm) at S3 for the period 2005-2015, using parameters from the dry calibration (2005-2006).

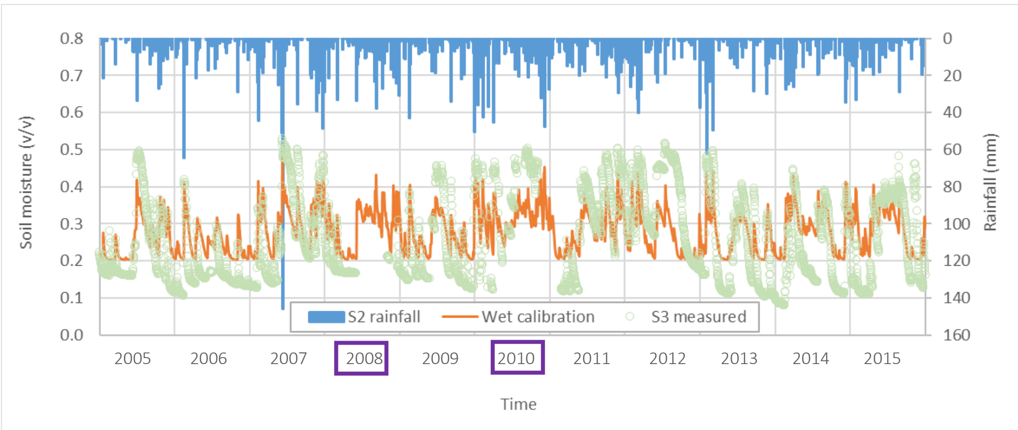

Figure 3.31 – Measured and simulated soil moisture (0-30 cm) at S3 for the period 2005-2015, using parameters from the wet calibration (2008 and 2010).

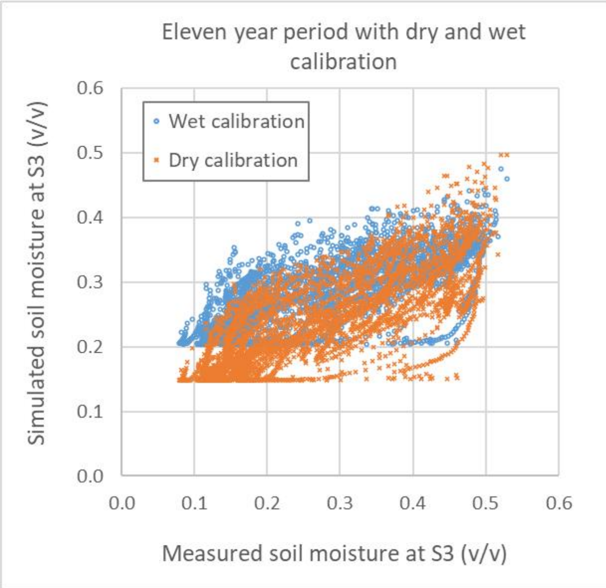

Figure 3.32 – Scatter plot of the measured and simulated soil moisture (0-30 cm) at Stanley station S3 for the period 2005-2015, using parameters from the dry calibration (2005-2006) and from the wet calibration (2008 and 2010).

3.4.2.2 Sandy soil stations

For the Krui-K2 station, characterised by a sandy soil, the Monte Carlo GLUE analysis for dry and wet periods that generated runs with NSE greater than zero are shown in Figure 3.33.

Dry simulations

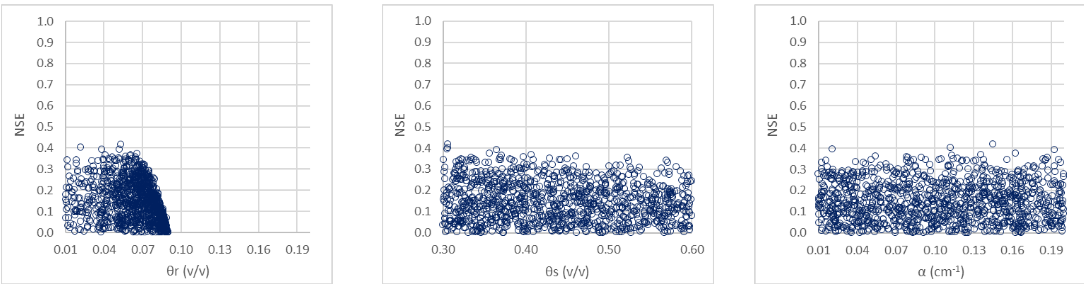

(a) (b) (c)

Wet simulations

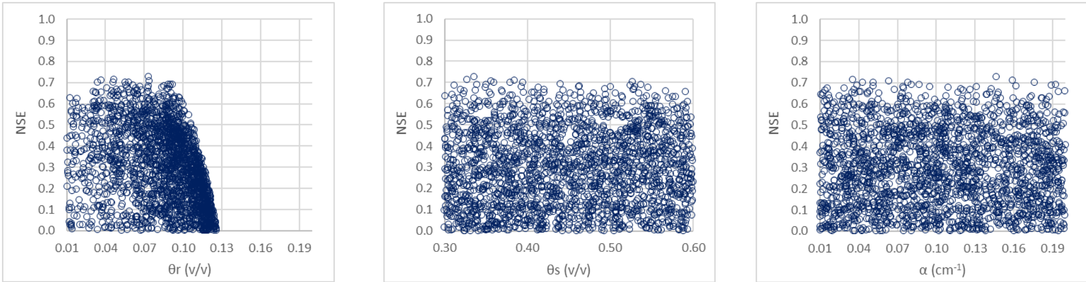

(d) (e) (f)

Dry simulations

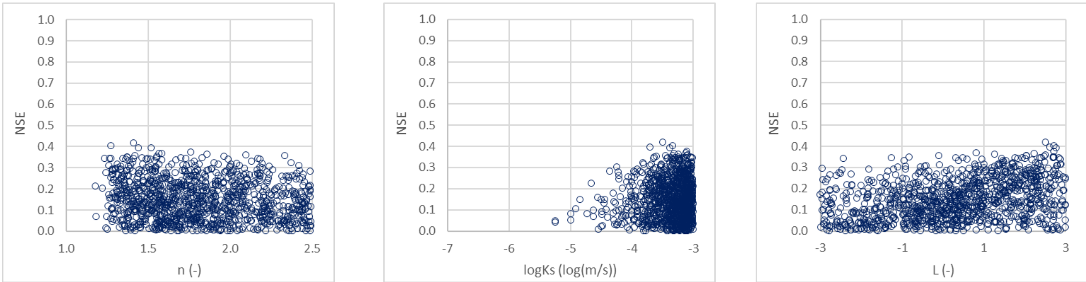

(g) (h) (i)

Wet simulations

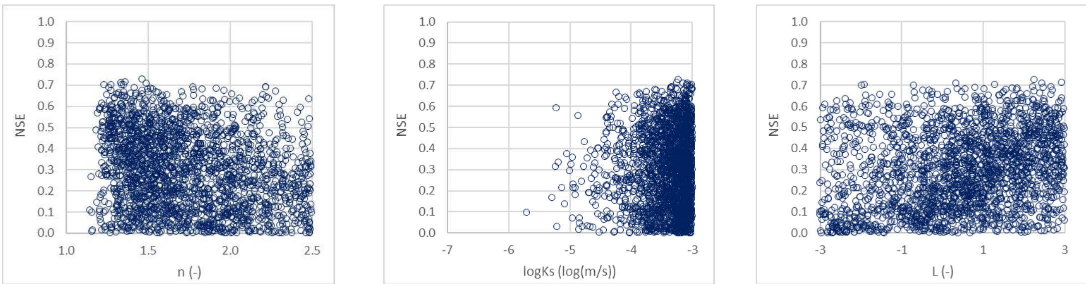

(j) (k) (l)

Dry simulations

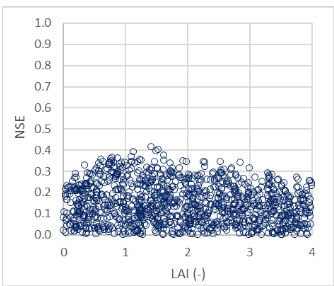

(m)

Wet simulations

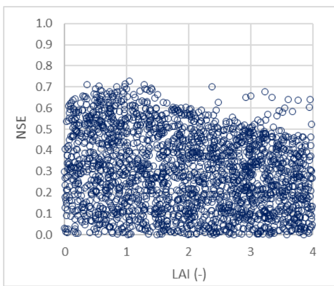

(n)

Figure 3.33 – Dotty plots from Monte Carlo GLUE analysis for the dry (2005-2006) and wet (2008 and 2010) calibration periods at station K2 for the parameters: (a, d) residual soil water content – θr, (b, e) saturated soil water content – θs, (c, f) inverse of the air-entry value – α, (g, j) soil pore-size distribution – n, (h, k) logarithm of saturated hydraulic conductivity – logKs, (i, l) pore discontinuity – L, and (m, n) Leaf Area Index – LAI.

The dotty plots from the Monte Carlo GLUE analysis showed that the wet period reached considerably higher NSE values than the dry period, with a maximum of 0.73 for the wet period and 0.42 for the dry. The most sensitive parameters in both dry and wet periods was the residual water content (θr) (Figure 3.33 – a and d) and the saturated hydraulic conductivity (Ks) (Figure 3.33 – h and k). The vast majority (93%) of dry and wet simulations were concentrated in high values of Ks (i.e., -4 to -3 log(m/s) or 864 to 8640 cm/d) which is linked to a faster drying of the soil. The residual water content (θr), the moisture content where water flow ceases, is expected to be low in sandy soils. The dry calibration period presented θr lower than 0.10 v/v in all simulations, whereas in the wet period θr was a bit higher, but always lower than 0.13 v/v.

The saturated soil moisture content (θs) presented a very subtle peak towards lower values, i.e., 0.3-0.4 v/v, in both wet and dry periods (Figure 3.33 – b and e). The saturated soil moisture content corresponds to the maximum moisture content of a soil, so the results are in accordance with what is known for sandy soils' weak capacity for holding water. The LAI also showed a subtle peak for values around 1 (i.e., 0.5 to 1.5) in both dry and wet simulations (Figure 3.33 – m and n). The soil pore distribution (n) had almost a flat response but with a very slight peak in 1.25-1.5 (Figure 3.33 – g and j) and only 2% of the simulations had n less than 1.25. This is consistent with what is found in the literature for this parameter, where sandy soils have higher values of n, and fine-textured soils (e.g. clay) have small values of pore-size distribution (1-1.3) (Simunek et al., 2013). The α parameter (Figure 3.33 – c and f), the inverse of the air-entry value, showed a flat response, which indicates that this parameter was not sensitive in the K2 wet and dry simulations. The pore discontinuity parameter (L) graph also showed a flat response in both dry and wet periods (Figure 3.33 – i and l).

The scatter plot of Krui-K2 soil moisture for the dry and wet calibration period (Figure 3.34 – a and b) shows that the wet calibration had a better regression model. The best parameter set for the wet calibration period was also able to match the general soil moisture dynamics, although the wet period had 54% of missing data, which interfered in the results, since there were only a few days of soil moisture behaviour that could be analysed for this station in this period (Figure 3.36). In the dry calibration, the best parameter set was able to generate a good match in the soil moisture recession but the peaks were overestimated throughout the two years (Figure 3.35).

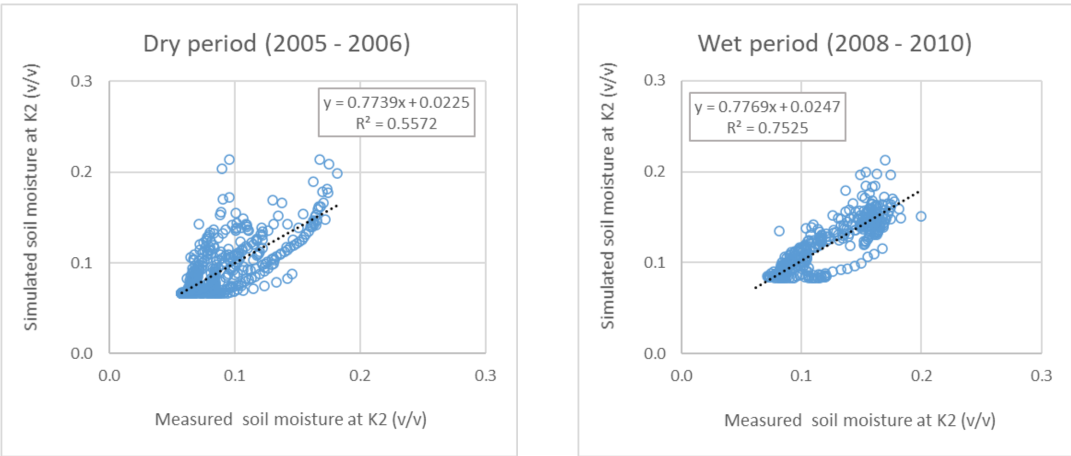

(a) (b)

Figure 3.34 – Scatter plot of the measured and simulated soil moisture (0-30 cm) at Krui sandy station - K2 for the (a) dry (2005-2006) and (b) wet (2008 and 2010) calibration period.

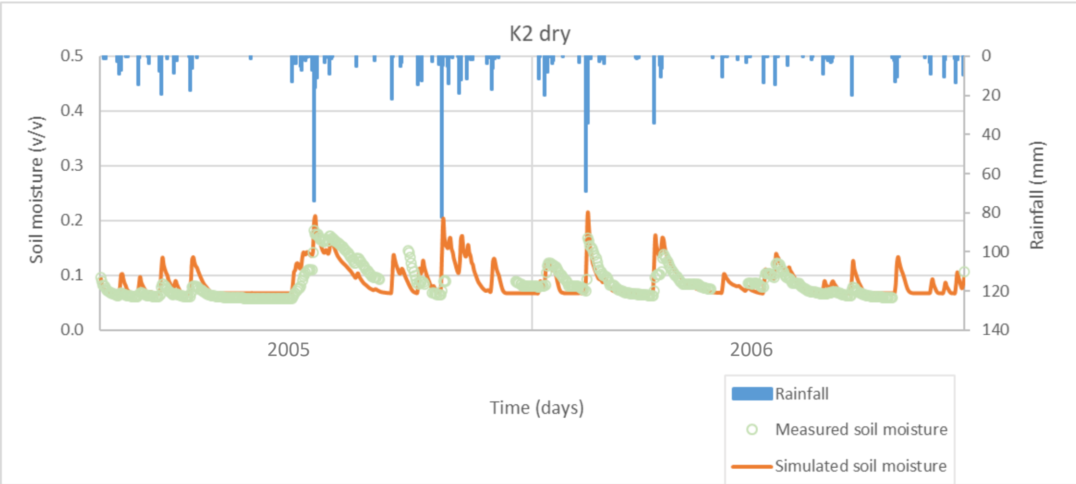

Figure 3.35 – Dry calibration (2005-2006) in K2 station.

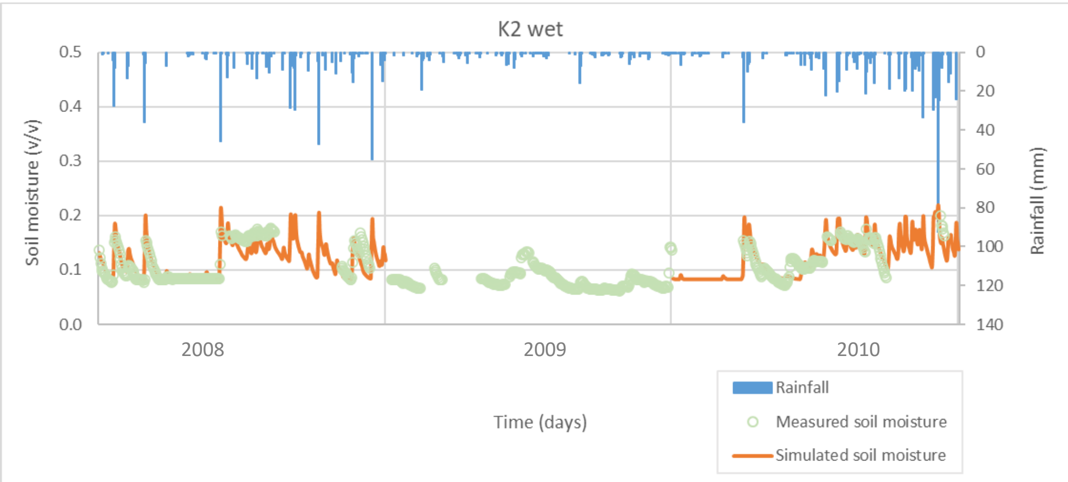

Figure 3.36 – Wet calibration (2008 and 2010) in K2 station.

Table 3.13 – Best parameter set for Krui (K2) sandy station for dry (2005-2006) and wet (2008 and 2010) calibration periods.

Calibration period	**θr (v/v)**	**θs (v/v)**	**α (cm^{-1})**	**n (-)**	**log Ks (m/s)**	**L (-)**	**LAI (-)**
Dry	0.053	0.306	0.145	1.412	-3.488	2.519	1.41
Wet	0.073	0.336	0.147	1.463	-3.222	2.245	1.05

All parameters for the dry and wet calibration are very close to each other (Table 3.13), which can be attributed to the small difference in annual average rainfall between the two periods, i.e., 461 and 656 mm. The higher LAI in the dry period contributes to depletion of water in the soil by evaporation so that the simulated soil moisture can reach the low values of soil moisture measured at the site. The wet calibration period achieved considerably better goodness-of-fit than the dry calibration for Krui (K2) (Table 3.14). The wet period had a high amount of missing soil moisture data (43%) which could have influenced the results, i.e., fewer days to analyse the soil moisture behaviour in this period.

Table 3.14 – Goodness-of-fit values for Krui (K2) sandy station for dry (2005-2006) and wet (2008 and 2010) calibration periods.

Calibration period	**R**	**RMSE (v/v)**	**sRMSE**	**NSE**
Dry	0.727	0.021	0.233	0.417
Wet	0.853	0.017	0.142	0.727

The goodness-of-fit from the dry calibration was minimally affected when applying the best dry parameter set to the eleven-year period, whereas for the wet period, NSE decreased by 33% (Table 3.15). The eleven-year simulation using the dry calibration parameter set could match the soil moisture recessions well but overestimated the peaks throughout the whole period. When using the wet calibration parameter set for the whole period, the soil moisture peaks, as well as the recession values, were overestimated. This is easy to see in the scatter plot of the eleven-year simulation period (Figure 3.39), where the dry and wet plots have the same behaviour, but the wet plot is shifted 0.02 v/v higher than the dry, which is lower than the soil moisture sensor confidence interval (Rüdiger, 2006).

Table 3.15 – Goodness-of-fit values for Krui (K2) for the period 2005-2015 using parameter set from the dry (2005-2006) and wet (2008 and 2010) calibration period.

Calibration period	**R**	**RMSE (v/v)**	**sRMSE**	**NSE**
Dry calibration	0.749	0.026	0.233	0.443
Wet calibration	0.736	0.025	0.264	0.490

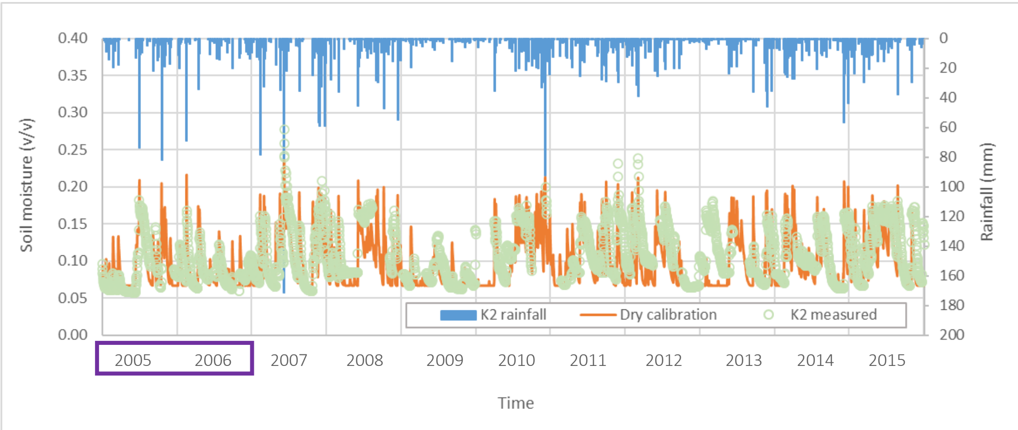

Figure 3.37 – Measured and simulated soil moisture (0-30 cm) at Krui station K2 for the period 2005-2015, using parameters from the dry calibration (2005-2006).

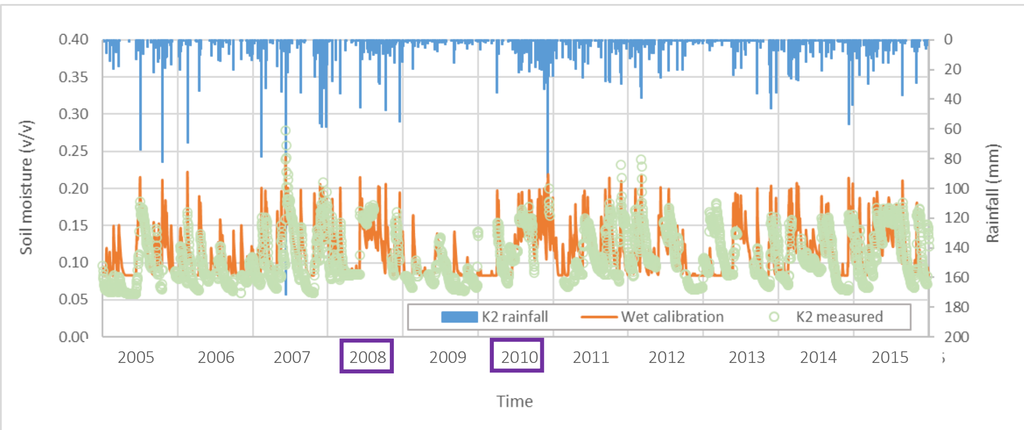

Figure 3.38 – Measured and simulated soil moisture (0-30 cm) at Krui station K2 for the period 2005-2015, using parameters from the wet calibration (2008 and 2010).

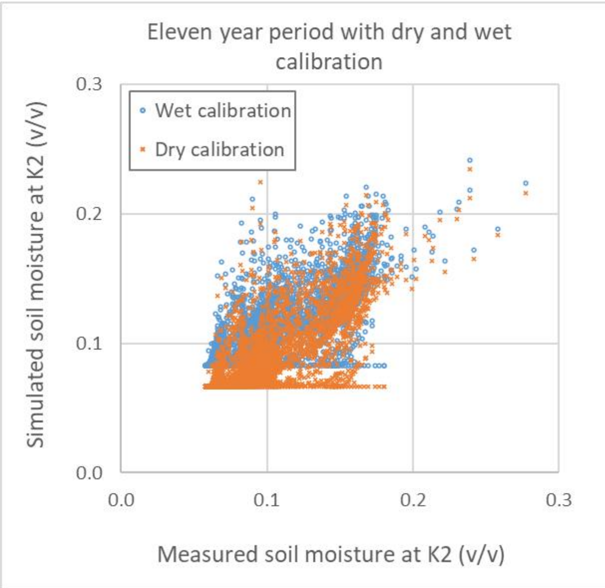

Figure 3.39 – Scatter plot of the measured and simulated soil moisture (0-30 cm) at Krui station K2 for the period 2005-2015, using parameters from the dry calibration (2005-2006) and from the wet calibration (2008 and 2010).

For the Merriwa-M1 station, characterised by a sandy soil, the Monte Carlo GLUE analysis for dry and wet periods that generated runs with NSE greater than zero are shown in Figure 3.40.

Dry simulations

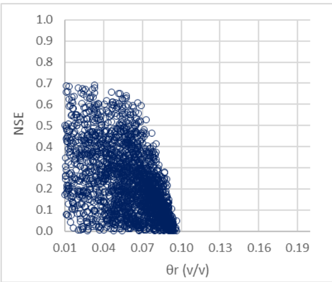

(a)

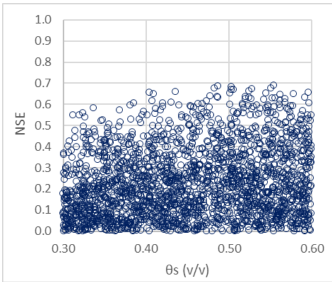

(b)

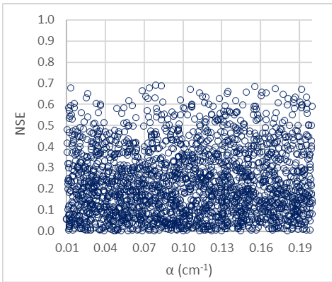

(c)

Wet simulations

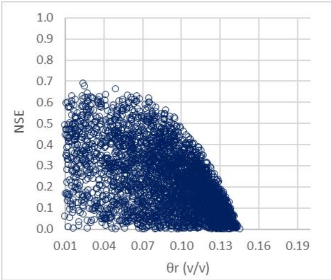

(d)

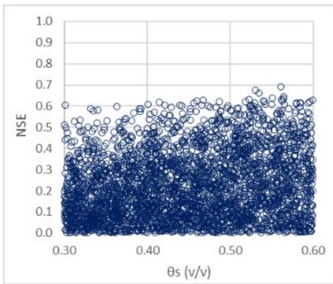

(e)

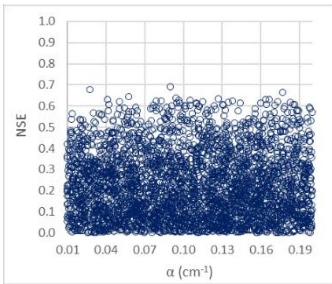

(f)

Dry simulations

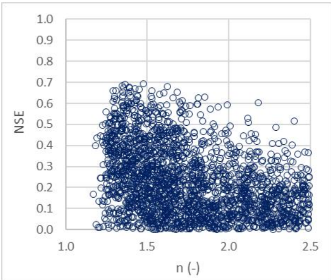

(g)

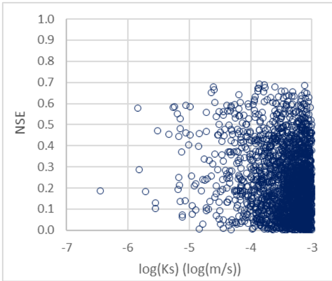

(h)

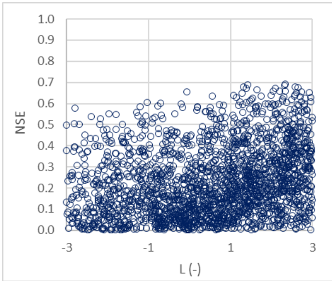

(i)

Wet simulations

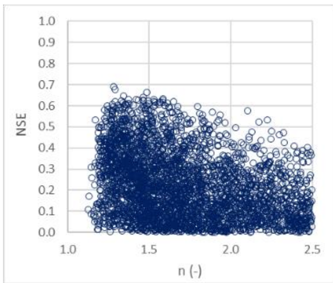

(j)

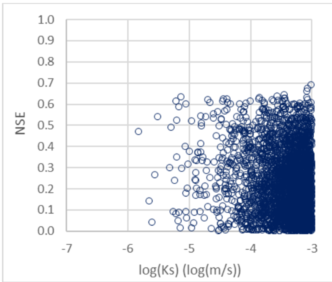

(k)

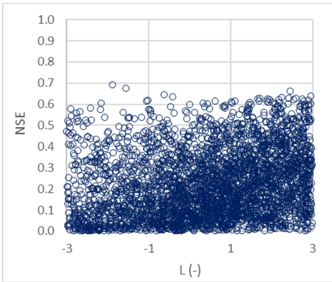

(l)

Dry simulations

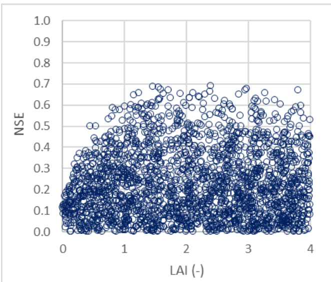

(m)

Wet simulations

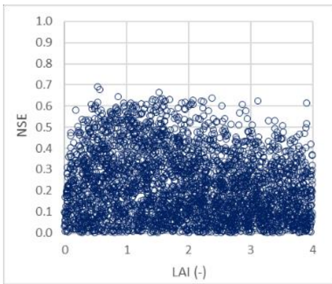

(n)

Figure 3.40 – Dotty plots from Monte Carlo GLUE analysis for the dry (2005-2006) and wet (2008 and 2010) calibration periods at station M1 for the parameters: (a, d) residual soil water content – θr, (b, e) saturated soil water content – θs, (c, f) inverse of the air-entry value – α, (g, j) soil pore-size distribution – n, (h, k) logarithm of saturated hydraulic conductivity – logKs, (i, l) pore discontinuity – L, and (m, n) Leaf Area Index – LAI.

Both wet and dry Monte Carlo simulations reached high NSE (Figure 3.40). NSE was higher than 0.4 in 15% of the simulations in the wet period, and in 17% of the simulations of the dry. The dotty plots' behaviour shows that the residual water content (θr) (Figure 3.40 – a and d) and the saturated hydraulic conductivity (Ks) (Figure 3.40 – h and k) were the most sensitive parameters in both dry and wet periods. For sandy soils like M1 and K2, the residual water content (θr) is expected to be lower than in clay soils, and in the dry period the θr was considerably low; there were no simulations with θr higher than 0.10 v/v. For the wet period simulations, θr is still low but higher than in the dry period, with θr no higher than 0.15 v/v. The saturated hydraulic conductivity (Ks) was once again marked by higher values, i.e., -4 to -3 log(m/s) or 864 to 8640 cm/d, which is linked to a fast drying of the soil.

The saturated water content (θs) (Figure 3.40 – b and e) and the tortuosity parameter (L) (Figure 3.40 – i and l) have higher NSE linked with higher ranges of these parameters for both dry and wet periods. Higher values of θs and L result in more water in the soil, since the high tortuosity of the soil makes drainage slower and a high saturated water content allows for a greater volume of water to stay in the soil. The α parameter, the inverse of the air-entry value (Figure 3.40 – c and f), did not show a peak, which indicates that this parameter was not sensitive in Merriwa-M1 wet and dry simulations. The soil pore distribution (n) presented higher NSE for values between 1.25 and 1.5 (Figure 3.40 – g and j), and no simulations with n less than 1.17, which is consistent with what is found for coarser soils like those at M1 station. The Monte Carlo simulations for LAI show that the dry period has higher NSE corresponding to LAI between 1 and 2, whereas for the wet period, this range is for smaller values, between 0.2 and 1. The dotty plots in the sandy soil stations (K2 and M1) had overall the same behaviour, with a difference between the soil pore distribution (n) and the saturated hydraulic conductivity (Ks). M1 had values of NSE deteriorate for n higher than 1.6 in dry and wet periods (Figure 3.40 – g and j) whereas K2 had an almost flat response for this parameter in both periods (Figure 3.33 – g and j). The Ks had NSE depreciate when lower than -4 log(m/s) for K2 dry and wet periods (Figure 3.33 – h and k), while M1 obtained a flat response for both periods (Figure 3.40 – h and k).

The scatter plots show a slightly better regression model for the wet period for Merriwa-M1 (Figure 3.41 – a and b). The dry calibration shows that the parameter set could meet the recession period well, although the two higher peaks were overestimated (Figure 3.42). Just as for Krui-K2, the wet period in M1 station had a considerably high amount of missing soil moisture data (68%), which influenced the results, i.e., only a few days of soil moisture behaviour could be explored for this station in this period (Table 3.16).

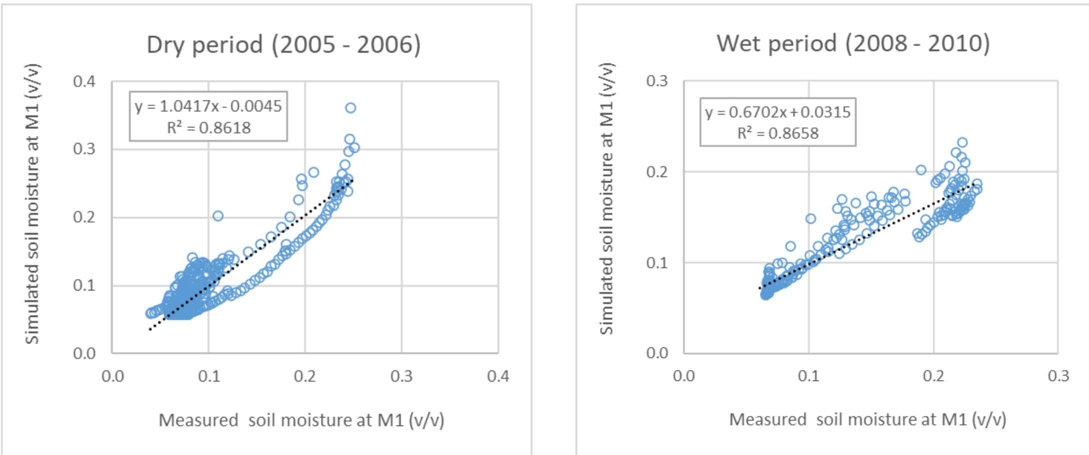

(a) (b)

Figure 3.41 – Scatter plot of the measured and simulated soil moisture (0-30 cm) at Merriwa sandy station – M1 for the (a) dry (2005-2006) and (b) wet (2008 and 2010) calibration period.

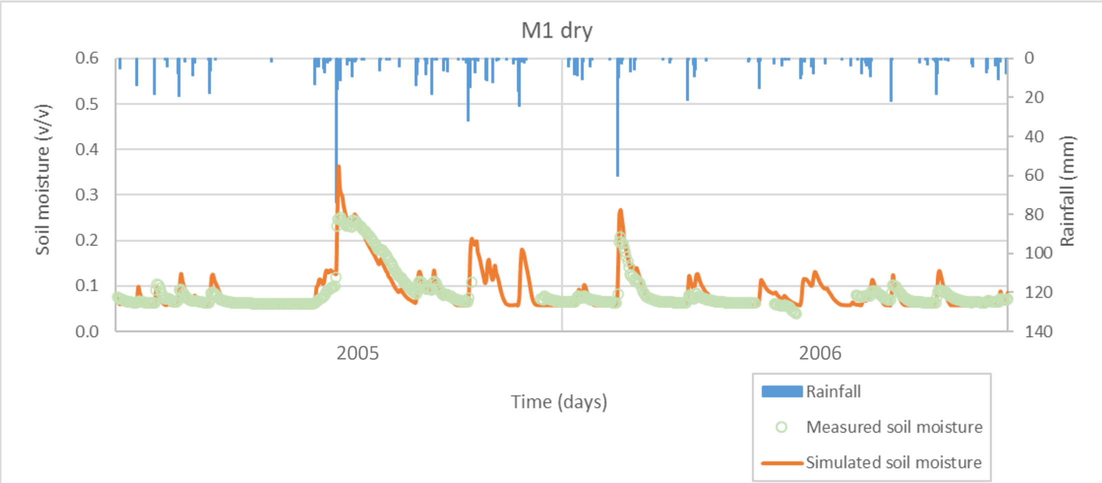

Figure 3.42 – Dry calibration (2005-2006) in M1 station.

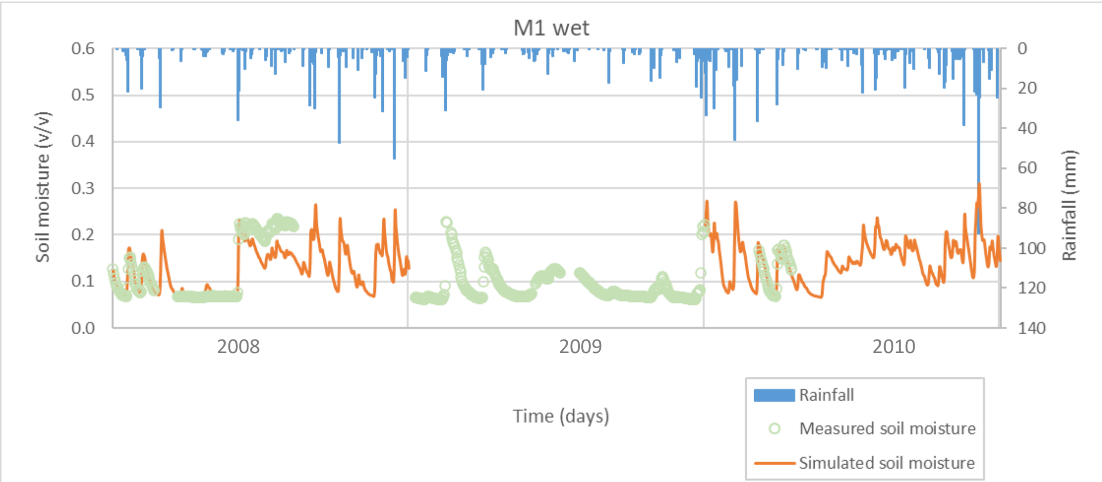

Figure 3.43 – Wet calibration (2008 and 2010) in M1 station.

Table 3.16 – Best parameter set for Merriwa (M1) sandy station for dry (2005-2006) and wet (2008 and 2010) calibration period.

Calibration period	**θr (v/v)**	**θs (v/v)**	**α (cm^{-1})**	**n (-)**	**log Ks (m/s)**	**L (-)**	**LAI (-)**
Dry	0.033	0.554	0.079	1.478	-3.857	2.344	2.39
Wet	0.024	0.561	0.090	1.286	-3.014	-1.880	0.54

The best parameter set for dry and wet calibrations had close values for almost all the parameters and the difference relied on the LAI and tortuosity parameter (L) (Table 3.16). As mentioned before, LAI and L tend to compensate each other in the calculation of the water balance, and once again, the dry period was characterised by a high LAI, which is counterintuitive. This high LAI makes more water come out of the soil by transpiration and reach the lower levels of soil moisture that are found in the dry period. The NSE for the two wetness periods was the same (Table 3.17) and the other goodness-of-fit values were similar.

Table 3.17 – Goodness-of-fit values for Merriwa (M1) sandy station for dry (2005-2006) and wet (2008 and 2010) calibration periods.

Calibration period	**R**	**RMSE (v/v)**	**sRMSE**	**NSE**
Dry	0.879	0.023	0.284	0.690
Wet	0.840	0.035	0.262	0.690

The parameters from the dry calibration obtained suitable goodness-of-fit values when applied to the eleven-year period, and the NSE was only slightly affected. The wet calibration parameters had their NSE a bit more affected when applied to the whole period but still showed satisfactory values (Table 3.18). The eleven-year simulation using the dry calibration parameter set could match the soil moisture recessions well but overestimated the peaks throughout the whole period (Figure 3.44). When running the eleven-year simulation with the wet calibration parameter set, the recessions and peaks were well matched (Figure 3.45). Despite the better visual fit of the wet parameters, the dry parameters obtained higher NSE in the eleven-year period. The scatter plot of the eleven-year simulation period shows that the dry and wet simulations have a very similar behaviour and the wet simulation is only slightly higher than the dry simulation, although the dry simulation reached higher values of soil moisture in the peaks, i.e., soil moisture greater than 0.3 v/v (Figure 3.46).

Table 3.18 – Goodness-of-fit values for Merriwa (M1) for the period 2005-2015 using parameter set from the dry (2005-2006) and wet (2008 and 2010) calibration period.

Calibration period	**R**	**RMSE (v/v)**	**sRMSE**	**NSE**
Dry calibration	0.852	0.036	0.258	0.678
Wet calibration	0.795	0.039	0.273	0.622

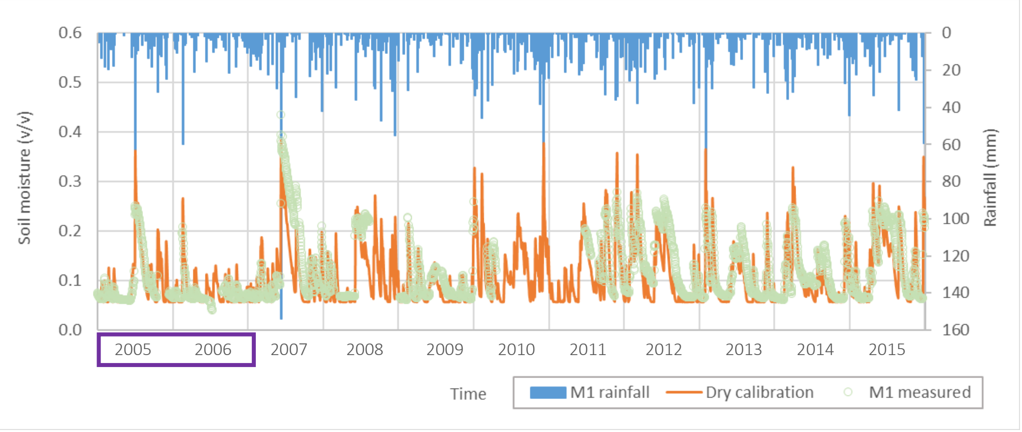

Figure 3.44 – Measured and simulated soil moisture (0-30 cm) at Merriwa station M1 for the period 2005-2015, using parameters from the dry calibration (2005-2006).

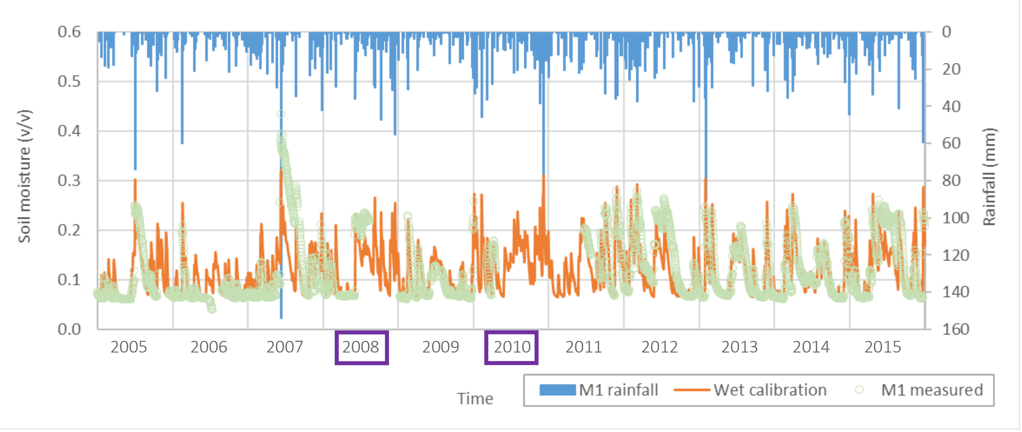

Figure 3.45 – Measured and simulated soil moisture (0-30 cm) at Merriwa station M1 for the period 2005-2015, using parameters from the wet calibration (2008 and 2010).

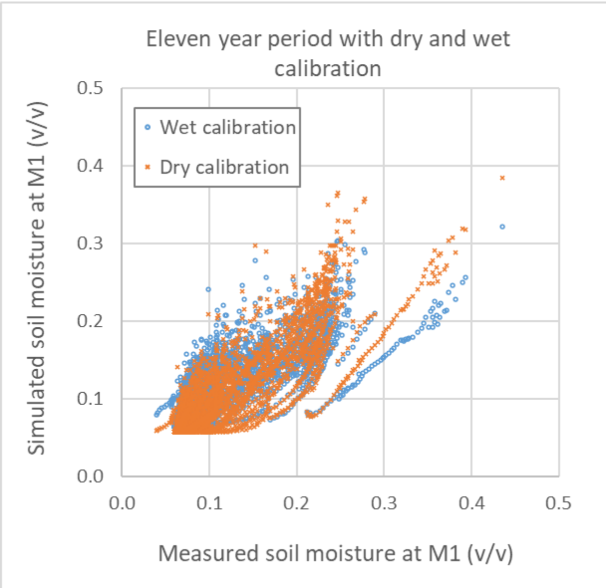

Figure 3.46 – Scatter plot of the measured and simulated soil moisture (0-30 cm) at Merriwa station M1 for the period 2005-2015, using parameters from the dry calibration (2005-2006) and from the wet calibration (2008 and 2010).

3.4.2.3 Clay and sandy station comparison

To facilitate the comparison among stations and between the dry and wet period of calibration, Table 3.19 shows the best parameter set for the stations analysed in this study (S2, S3, K2 and M1) and their respective goodness-of-fit index (NSE).

Table 3.19 – Best parameter set and goodness-of-fit index (NSE) for all stations (S2, S3, K2 and M1) for dry (2005-2006) and wet (2008 and 2010) calibration period.

Station and calibration period		**θr (v/v)**	**θs (v/v)**	**α (cm^{-1})**	**n (-)**	**log Ks (m/s)**	**L (-)**	**LAI (-)**	**NSE**
C	S2 dry	0.133	0.580	0.118	1.245	-4.702	2.476	1.416	0.785
L	S2 wet	0.102	0.599	0.067	1.186	-3.568	-0.655	0.607	0.597
A	S3 dry	0.088	0.561	0.184	1.282	-4.455	2.898	1.381	0.750
Y	S3 wet	0.016	0.558	0.022	1.138	-3.127	-1.453	0.376	0.575

S	K2 dry	0.053	0.306	0.145	1.412	-3.488	2.519	1.413	0.417
A	K2 wet	0.073	0.336	0.147	1.463	-3.222	2.245	1.054	0.727
N	M1 dry	0.033	0.554	0.079	1.478	-3.857	2.344	2.392	0.690
D	M1 wet	0.024	0.561	0.090	1.286	-3.014	-1.880	0.539	0.690

In the clay stations (S2 and S3) the dry calibration period obtained higher NSE than in the wet but in the sandy stations (K2 and M1) the wet period obtained higher NSE for K2, and the dry and wet periods obtained the same NSE for M1 (Table 3.19). The saturated hydraulic conductivity was high in all stations in both periods. The majority of the runs were between -3 and -3.9 log(m/s), which is 8640 and 1088 cm/d, except for S2 and S3 in the dry period, which had lower Ks, 172 and 303 cm/d, respectively. For all stations, LAI was higher during dry periods than during wet, which was not expected, since wet periods have better conditions for vegetation development, thus a higher LAI.

3.4.2.4 Investigating LAI

Because the LAI was higher in the dry period in all stations and this is not an expected behaviour (Grohs et al., 2019), an analysis was carried out by selecting the best dry and wet runs of the four soils moisture stations (S2, S3, M1 and K2) that satisfy the condition: higher LAI for the wet period. The results were used to assess how much the simulations were impacted by this conditioning and are shown in Table 3.20.

Table 3.20 – Best parameter set for dry and wet periods that have higher LAI for the wet period for all stations (S2, S3, K2 and M1).

Station and calibration period		**θr (v/v)**	**θs (v/v)**	**α (cm^{-1})**	**n (-)**	**log Ks (m/s)**	**L (-)**	**LAI (-)**	**NSE**
C	S2 dry	0.125	0.581	0.078	1.230	-4.899	-2.083	0.601	0.746
L	S2 wet	0.022	0.588	0.024	1.118	-3.047	0.020	1.000	0.581
A	S3 dry	0.104	0.588	0.018	1.318	-5.818	-2.478	0.845	0.744
Y	S3 wet	0.049	0.572	0.194	1.176	-4.399	-0.390	0.939	0.559

S	K2 dry	0.061	0.407	0.136	1.584	-3.111	0.814	1.097	0.367
A	K2 wet	0.074	0.356	0.064	1.489	-3.142	2.445	1.295	0.708
N	M1 dry	0.020	0.550	0.074	1.393	-3.597	1.332	1.582	0.676
D	M1 wet	0.042	0.551	0.095	1.468	-3.564	2.969	2.379	0.637

The NSE dropped on average 0.027 from the best parameter set (Table 3.19) to the best parameter set with higher LAI in the wet period (Table 3.20). The highest difference in NSE was 0.053 for M1 wet, and the lower differences occurred in S3 dry (0.006) followed by M1 dry (0.014). The increase of LAI in the wet period was accompanied by a decrease of Ks in S2, S3 and K2. The higher LAI deploys water from the soil and it is compensated with a lower Ks that slows the drainage, allowing the water to stay longer in the soil. In the dry period the LAI decreased in all stations but only for the sandy ones, K2 and M1, was this followed by an increase in Ks. The soil moisture behaviour using these updated parameter sets is shown in Figure 3.47 (a to h).

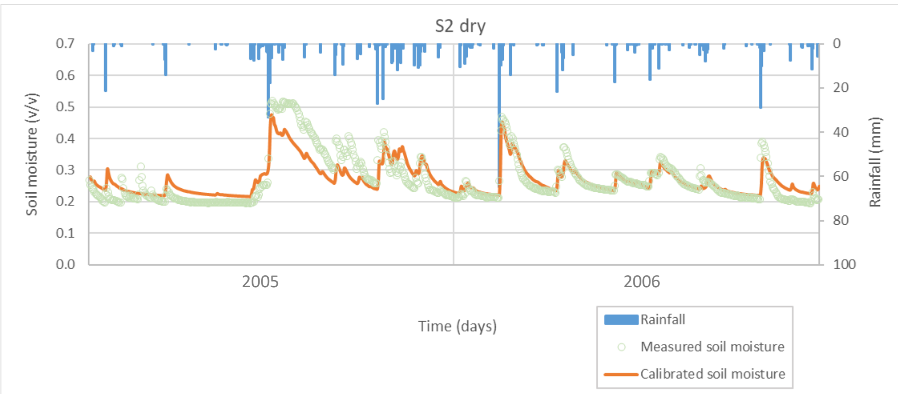

(a)

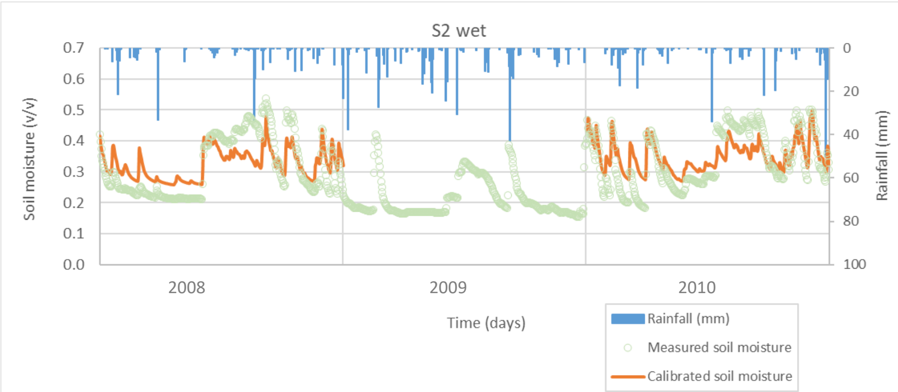
S2 wet
0.7
0.6
0.5
0.4
0.3
0.2
0.1
0.0
Soil moisture (v/v)
0
20
40
60
80
100
Rainfall (mm)
2008
2009
2010
Time (days)
Rainfall (mm)
Measured soil moisture
Calibrated soil moisture

(b)

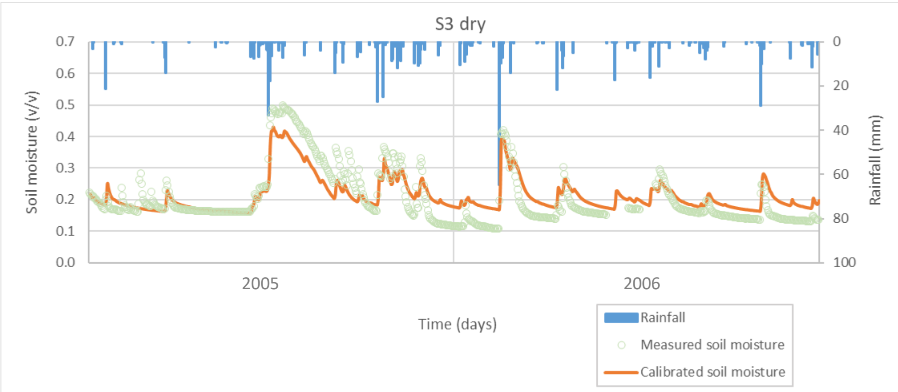
S3 dry
0.7
0.6
0.5
0.4
0.3
0.2
0.1
0.0
Soil moisture (v/v)
0
20
40
60
80
100
Rainfall (mm)
2005
2006
Time (days)
Rainfall
Measured soil moisture
Calibrated soil moisture

(c)

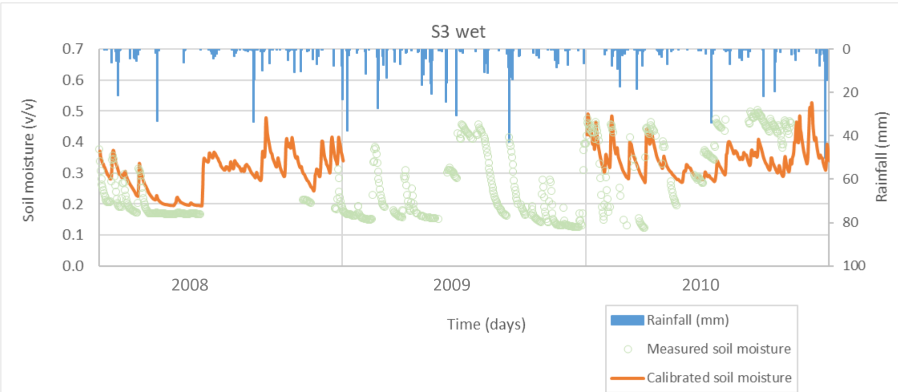
S3 wet
0.7
0.6
0.5
0.4
0.3
0.2
0.1
0.0
Soil moisture (v/v)
0
20
40
60
80
100
Rainfall (mm)
2008
2009
2010
Time (days)
Rainfall (mm)
Measured soil moisture
Calibrated soil moisture

(d)

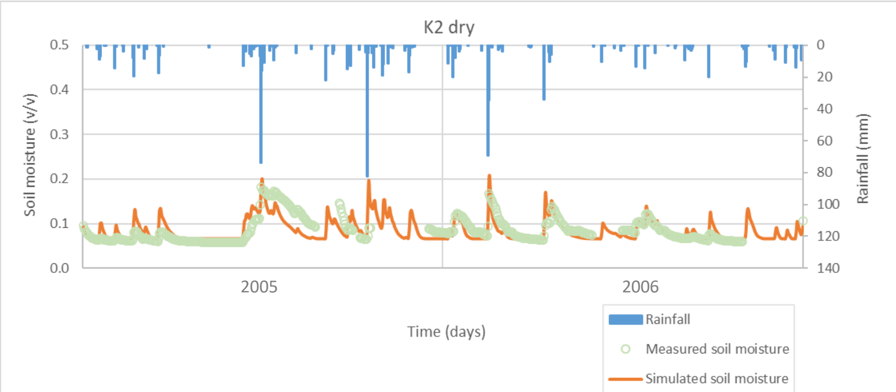
K2 dry
Soil moisture (v/v)
Rainfall (mm)
2005
2006
Time (days)
Rainfall
Measured soil moisture
Simulated soil moisture

(e)

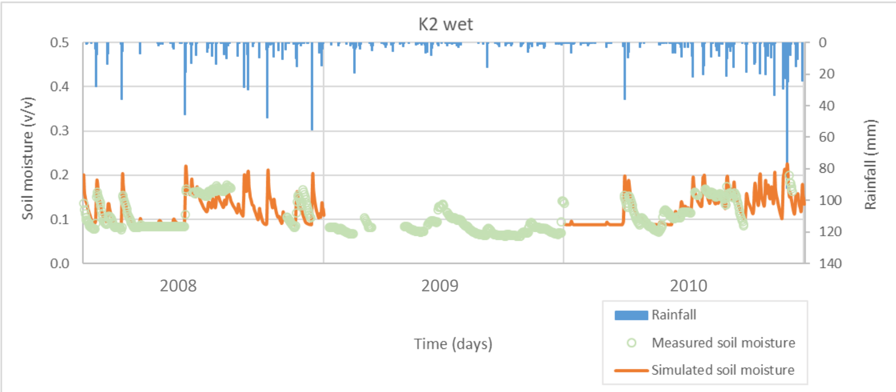
K2 wet
Soil moisture (v/v)
Rainfall (mm)
2008
2009
2010
Time (days)
Rainfall
Measured soil moisture
Simulated soil moisture

(f)

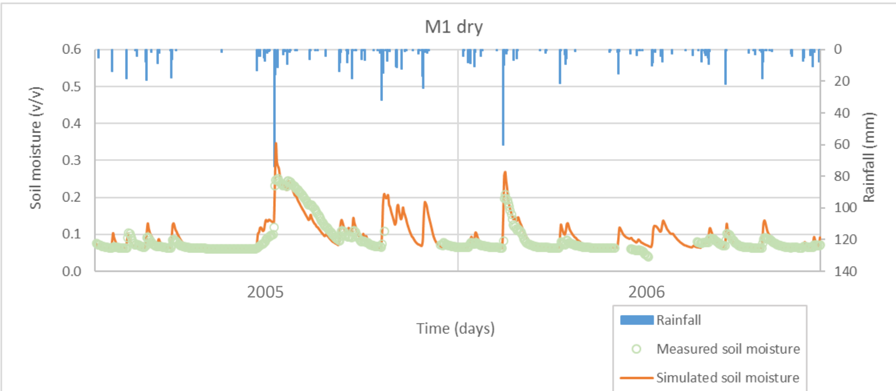
M1 dry
Soil moisture (v/v)
Rainfall (mm)
2005
2006
Time (days)
Rainfall
Measured soil moisture
Simulated soil moisture

(g)

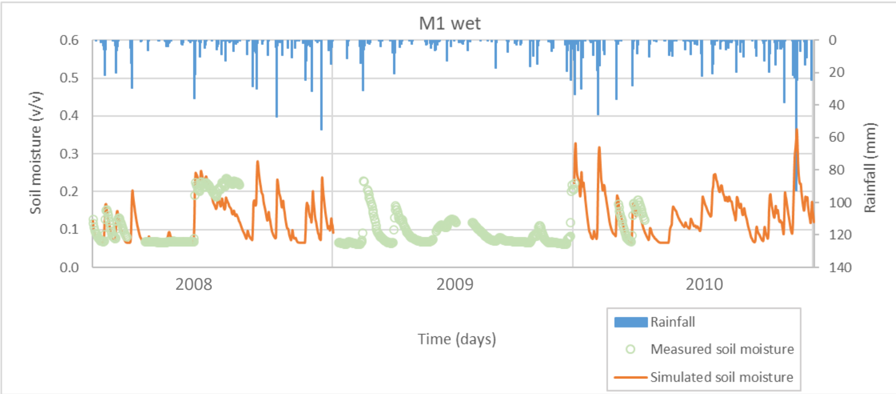

(h)

Figure 3.47 – Best dry and wet calibrations that have higher LAI in the wet period.

The parameter sets from the re-analysis, i.e., LAI in the wet period higher than in the dry (Table 3.20), when used to simulate the eleven-year period (2005-2015) generated the NSE values shown in Table 3.21.

Table 3.21 – NSE for the eleven-year period (2005-2015) using dry and wet parameter sets from LAI re-analysis for all stations (S2, S3, K2 and M1).

Station and calibration period		**NSE for the eleven-year period (2005-2015)**
C	S2 dry	0.617
L	S2 wet	0.528
A	S3 dry	0.562
Y	S3 wet	0.550
S	K2 dry	0.272
A	K2 wet	0.485
N	M1 dry	0.719
D	M1 wet	0.726

3.4.3 Predominance of vertical fluxes

The graphs with potential and actual evapotranspiration assist in interpreting the results of the dry and wet simulations. The parameter sets from the re-analysis, i.e., LAI in the wet period higher than in the dry (Table 3.20), were used in HYDRUS-1D to generate the graphs for actual and potential evapotranspiration for the clay and sand soil moisture stations (Figure 3.48 to Figure 3.55). Table 3.22 shows that the potential evapotranspiration (PET) is higher than actual evapotranspiration (AET) a large part of the time, even in the wet period, in all stations. This indicates that there is not enough water in the soil for evapotranspiration.

The evapotranspiration regime can be characterised by a soil moisture-limited and an energy-limited regime (Seneviratne et al., 2010; Alexander, 2011; Lo et al., 2021). In the soil moisture-limited regime, actual evapotranspiration is predominantly controlled by the available soil moisture, whereas in the energy-limited regime, there is enough moisture in the soil but evapotranspiration is governed by the available input energy, that is, net radiation, vapour pressure deficit, and wind speed (Seneviratne et al., 2010; Lo et al., 2021). The analysis of evapotranspiration at the four stations (Figure 3.48 to Figure 3.55 and Table 3.22) indicates that evapotranspiration in the region is mainly soil moisture-limited.

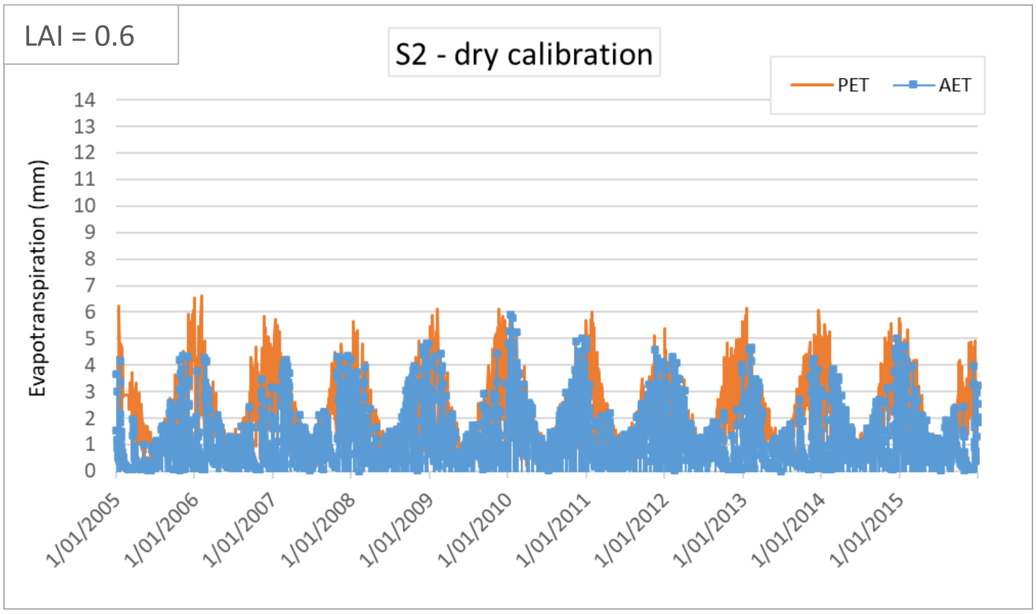

Figure 3.48 – Actual and potential evapotranspiration from the clay station S2 with dry calibration period (2005-2006) over the eleven-year period (2005-2015).

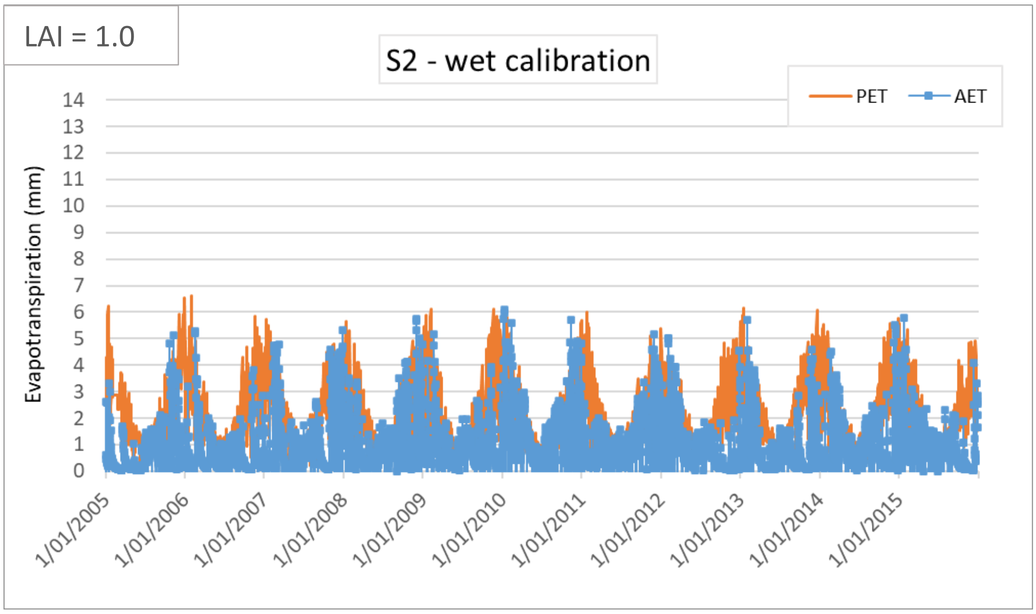

Figure 3.49 – Actual and potential evapotranspiration from the clay station S2 with wet calibration period (2008 and 2010) over the eleven-year period (2005-2015).

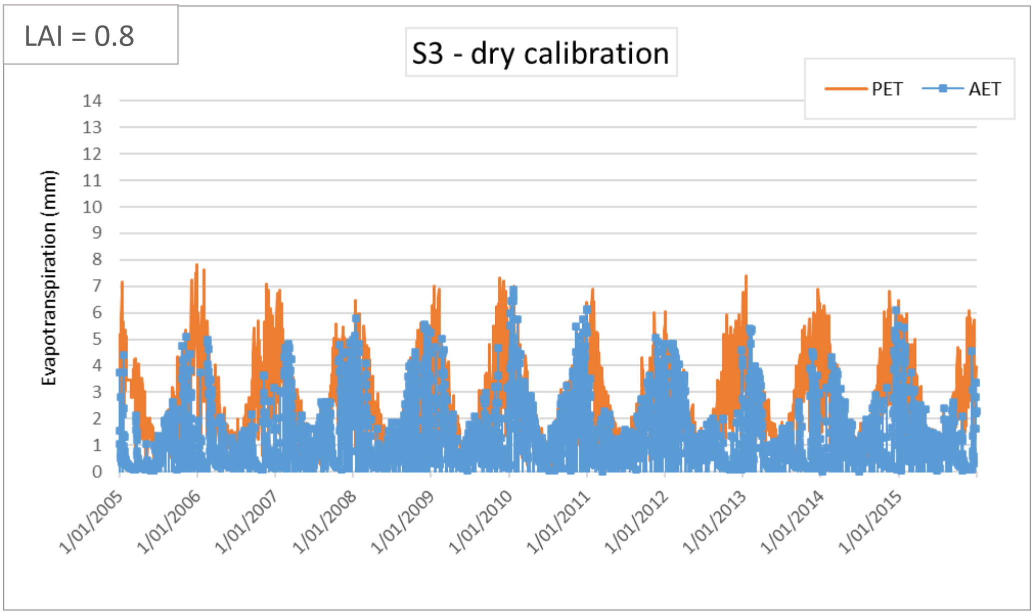

Figure 3.50 – Actual and potential evapotranspiration from the clay station S3 with dry calibration period (2005-2006) over the eleven-year period (2005-2015).

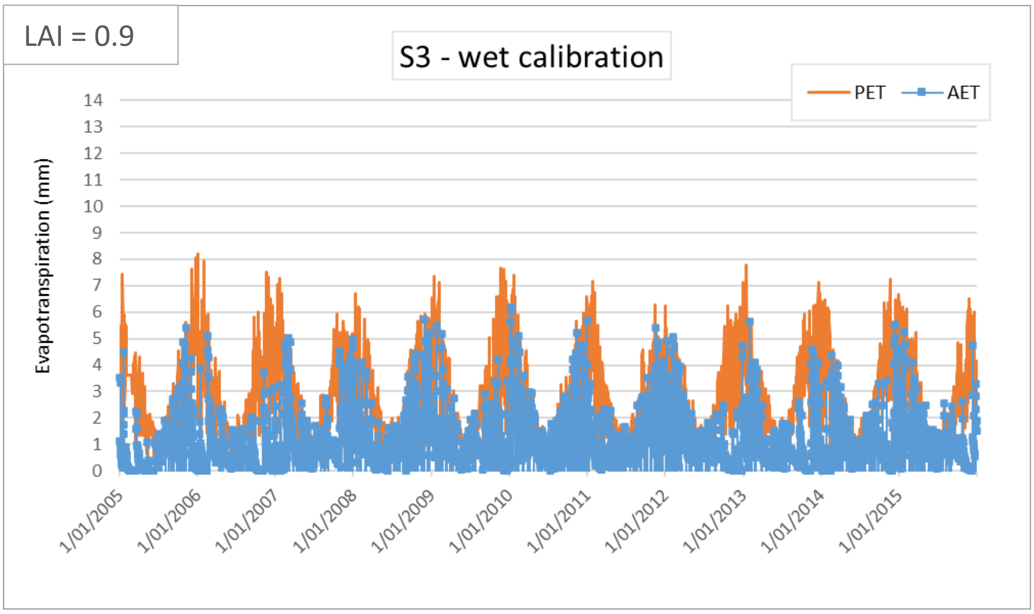

Figure 3.51 – Actual and potential evapotranspiration from the clay station S3 with wet calibration period (2008 and 2010) over the eleven-year period (2005-2015).

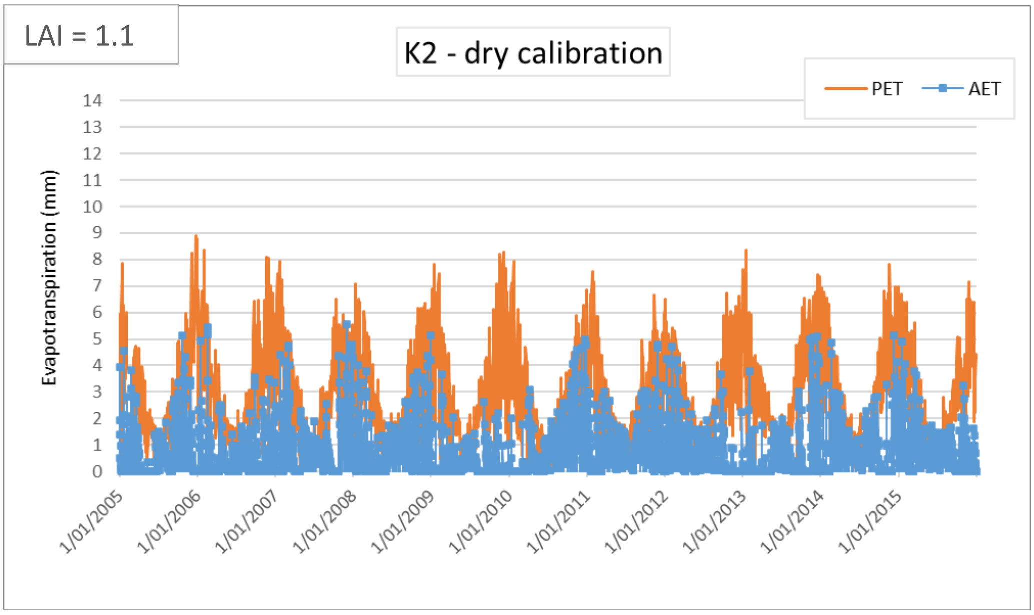

Figure 3.52 – Actual and potential evapotranspiration from the sandy station K2 with dry calibration period (2005-2006) over the eleven-year period (2005-2015).

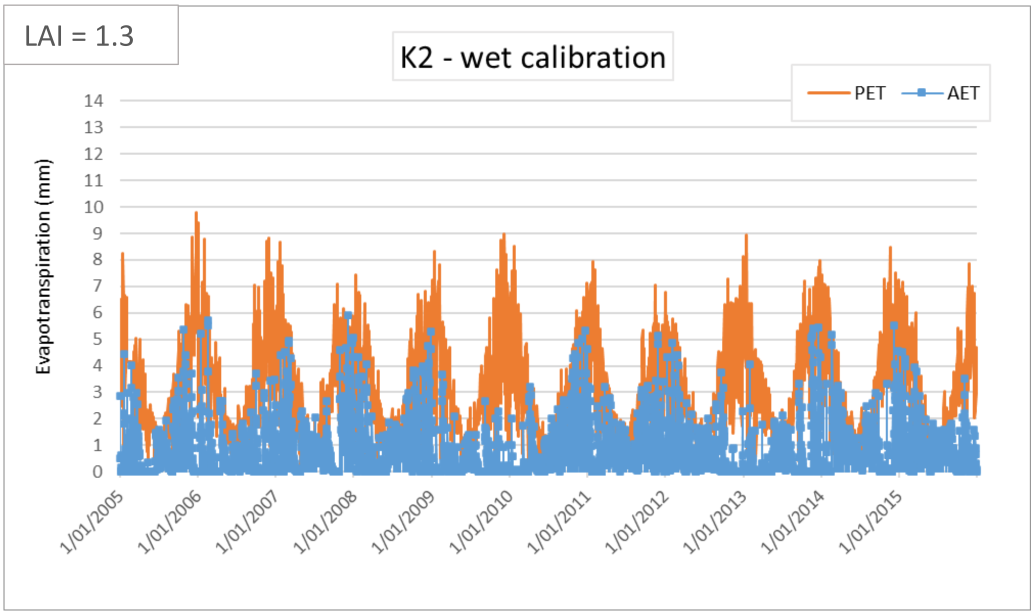

Figure 3.53 – Actual and potential evapotranspiration from the sandy station K2 with wet calibration period (2008 and 2010) over the eleven-year period (2005-2015).

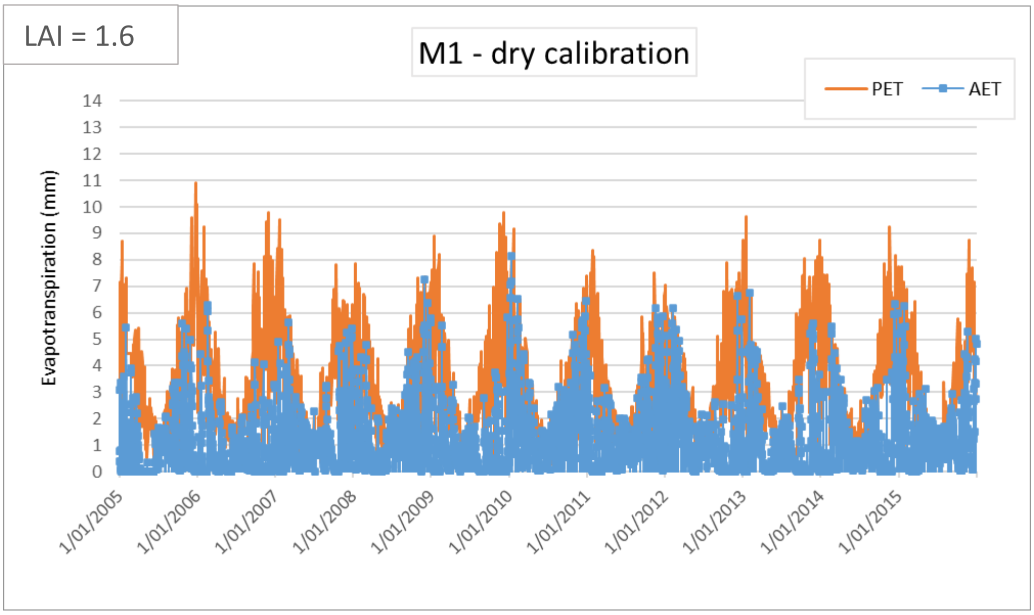

Figure 3.54 – Actual and potential evapotranspiration from the sandy station M1 with dry calibration period (2005-2006) over the eleven-year period (2005-2015).

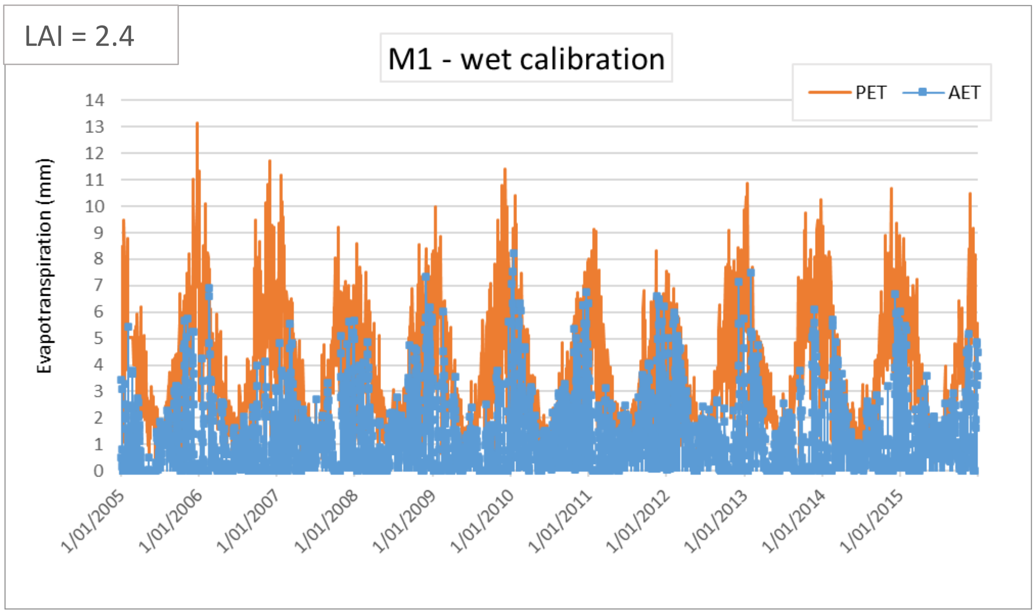

Figure 3.55 – Actual and potential evapotranspiration from the sandy station M1 with wet calibration period (2008 and 2010) over the eleven-year period (2005-2015).

Table 3.22 – Percentage of time that the potential evapotranspiration (PET) is higher than actual evapotranspiration (AET) in the eleven-year period, in the dry and wet periods for all stations (S2, S3, K2 and M1) using dry and wet calibration parameters.

Station and calibration period		**Percentage (%) of time PET is higher than AET**		
		2005-2015	Dry period (2005-2006)	Wet period (2008 and 2010)
C	S2 dry	82	89	75
L	S2 wet	80	89	72
A	S3 dry	84	92	76
Y	S3 wet	88	93	83
S	K2 dry	93	95	91
A	K2 wet	93	95	91
N	M1 dry	89	94	85
D	M1 wet	92	85	88

Graphs from actual and potential evapotranspiration for the clay and sandy soil moisture stations (Figure 3.48 - Figure 3.55) show that LAI is a key parameter to determine actual and potential evapotranspiration in HYDRUS-1D and, consequently, the amount of moisture in the soil. A high LAI, which indicates more vegetation per unit area, results in more water being extracted from the soil by transpiration. Most of the time, potential evapotranspiration (PET) is higher than actual evapotranspiration (AET) in both dry and wet periods (Table 3.22), but in the wet period this percentage is lower, i.e., AET reaches PET, because there is more water in the soil available for evapotranspiration.

For a further investigation, a lateral sub-surface flux was estimated with a mass balance calculation. A plan area of 1 m×1 m multiplied by the soil depth was considered the control volume. The Darcy equation was applied to the soil profile (Equation 3-18).

$$\text{Lateral flux} = K(h) \times H \times \lambda \qquad \text{3-18}$$

where K(h) is the downslope hydraulic conductivity, H is the depth of the soil and λ is the topographic slope in the downslope direction. The soil depth in the stations is around 1 meter, so it was adopted as 1 meter, and the maximum slope was 0.2 m/m. Using the parameters from Table 3.20 to calculate K(h) (Equation 3-4), the daily lateral flux was calculated. The total PET over the eleven-year period (2005-2015) was in average 2 orders of magnitude higher than lateral flux. For the sand stations, the percentage of time that PET was higher than the lateral flux, was higher than for the clay soil stations which is expected since sandy soils have lower water holding capacity than clay soils.

Table 3.23 – Total lateral flux and potential evapotranspiration in the eleven-year period in all stations (S2, S3, K2 and M1) using dry and wet calibration parameters.

Station and calibration period		**Over eleven-year period (2005-2015)**		
		Percentage (%) of time PET is higher than lateral flux	Total lateral flux (mm)	Total PET (mm)
CLAY	S2 dry	96	80	1649
	S2 wet	91	425	1876
	S3 dry	100	17	1981
	S3 wet	98	95	1820
SAND	K2 dry	98	37	2240
	K2 wet	100	11	2067
	M1 dry	100	5	2597
	M1 wet	100	2	2832

3.5 Discussion

This study explored soil moisture temporal variation by comparing the differences in soil moisture dynamics between wet and dry periods through the analysis of changes in soil properties (e.g., saturated water content, pore-size distribution, saturated conductivity), and vegetation (Leaf Area Index - LAI). It also investigated spatial variability by analysing soil moisture behaviour in different soil types (clay and sand). A Monte Carlo (GLUE) approach associated with HYDRUS-1D was used to obtain parameter sets and soil moisture simulations. Visual analysis and goodness-of-fit indices, including the Pearson Correlation Coefficient (R), scaled Root Mean Squared Error (sRMSE), and Nash–Sutcliffe Efficiency (NSE), were applied to evaluate the simulation performances. Another part of this study was to test if the parameter set identified by Chen et al. (2014a) on a HYDRUS-1D calibration for 2005-2007 at the Stanley S2 station could be validated and represent the soil moisture dynamics for a longer simulation period (2008-2015) at that same station.

By exploring soil moisture temporal variation between wet and dry periods through the analysis of changes in soil properties and vegetation it was expected to find a strong relationship between soil moisture and vegetation and soil moisture and soil properties in the two wetness periods. For instance, to have high values of LAI in the wet period, and low values of LAI in the dry periods, or high values of residual soil water content for wet periods and low values for the dry period. What happened instead is that, overall, there were not significant differences in soil moisture behaviour between dry and wet periods.

The soil moisture behaviour was explored by the dotty plots of the simulations that showed the parameters versus the simulations' performances using the NSE. Three parameters behaved differently between wet and dry periods: the soil pore distribution (n) in clay soil stations (S2 and S3), the residual water content (θr) in sandy soils (M1 and K2) and LAI in both soil types. The soil-pore distribution (n) in the dry period of S2 and S3 (clay soils) had a peak around 1.25 and there were simulations in all the soil pore distribution range, i.e., 1 to 2.5. In the wet period, on the other hand, there were no simulations for n>2 and only a few simulations for n>1.5. This parameter (n) has a small value for fine-textured soils (Simunek et al., 2013), so it was expected that the simulations would be concentrated in low values for S2 and S3. Low values of n hold more water in the soil, so in the dry period, high values of n were used to reach the low values of soil moisture. For sandy stations (M1 and K2) the dry period showed a lower range (0.01-0.09) of valid simulations for residual water content (θr), i.e., the moisture content where water flow ceases (Van Genuchten, 1980; Kirkham, 2014), in comparison to the wet period (0.01-0.13). This result tries to account for more water in the soil for the wet period by assigning a higher capacity of water storage in the soil. When analysing this difference between the wet and dry periods of the best parameter set (Table 3.20) the differences between dry and wet periods is not significant.

In regard to the LAI, the difference between dry and wet periods appeared in both clay and sandy soil stations. The best simulations for the dry period had higher LAI values than in wet periods. This is counterintuitive since we would expect higher LAI, i.e., greener conditions, in wet periods. The model tried to obtain the low values of soil moisture that appear in the dry period by allowing more water to get out of the soil by evaporation, i.e., higher LAI. When retrieving LAI from MODIS in a 500 m pixel, it was possible to see that the average LAI for the wet period was only slightly higher than for the dry in all stations. An average LAI among the stations was 0.79 for the dry period and 1.13 for the wet period. The simulations were re-analysed by choosing the best run from the wet and dry periods that satisfied the condition: higher LAI in wet period. From this re-analysis it was found that the simulations had their performance minimally affected; on average the NSE dropped 0.027 and the LAI from the wet period was, on average, 0.37 higher than in the dry period. All dry LAI values decreased when compared to the previous best-parameter set and all wet LAI increased. The difference between LAI in wet and dry periods was more expressive in sandy station M1, with a difference of LAI of 0.8, and least expressive at clay S3, where the difference between LAI in dry and wet periods was 0.09 (Table 3.20).

This lack of difference between dry and wet periods can indicate that the soils do not effectively change state between dry and wet, but that the spatiotemporal patterns have a ‘local control’, that is, are driven by local soil and local vegetation characteristics (Grayson et al., 1997). In wet areas, lateral distribution is present (Western et al., 2002; Brocca et al., 2007), whereas in dry conditions lateral distribution is almost non-existent and vertical fluxes predominate (Grayson et al., 1997; Western et al., 2004; Korres et al., 2015). In our catchments, even in the wet period of the study, the soils remained in a fairly dry state; that is, there was no lateral flow during most of the time and evapotranspiration was limited by soil moisture availability (Table 3.22 and Table 3.23). Although the purpose of this work was to analyse the dry and wet periods under the dominance of vertical water fluxes, thus the choice of the 1D model, it is likely that only if there was a change in the regime (i.e., to lateral flow and non-local control) would significant differences in the dry and wet dynamics occur.

A common behaviour among the dotty plots for clay and sandy soils in wet and dry periods was a concentration of simulations in high saturated hydraulic conductivity (Ks), i.e., higher than 864 cm/d. (or -4 log(m/s)). These are values much higher than those found by Carsel and Parrish (1988) for clay loam (6.24 cm/d), loamy sand (336 cm/d) and sandy loam soils (96 cm/d). Despite the range of saturated hydraulic conductivity found in Hillel (1998), which indicated low values of Ks for clay soils, 0.086 to 86.4 cm/d (or -8 to -5 log(m/s)) and high values for sandy soils, 864 to 8640 cm/d (or -4 to -3 log(m/s)), the dotty plots indicated similar behaviour for clay and sandy soils. This indicates a tendency of the model to regulate soil moisture by permitting a high drainage that makes the water percolate, which generates lower values of soil moisture along the simulation.

Part of this study was to validate the calibration by Chen et al. (2014a) for 2005-2007 at Stanley S2 station. The same hydrological model, HYDRUS-1D, was used and the parameter set found in their calibration was applied to a longer period (2008-2015) at the same station. The overall soil moisture behaviour was matched by the simulated soil moisture, despite the overestimation of some of the extreme peaks and lows. The NSE coefficient was 0.857 in the calibration period and dropped to 0.512 in the validation (2008-2015). During the simulation there was a short period of time (0.3%) when the difference between measured and simulated soil moisture was higher than 0.2 v/v, but 84% of the time this difference was less than 0.1 v/v, which can be considered a good match. Chen et al. (2014a) found good correlations between observed and simulated soil moisture when calibrations for one site were applied to the other; they claimed that it would be possible to extrapolate soil moisture calibration at a single site to other sites for a catchment with an area of up to 1000 km^2 given similar soils and vegetation and using local rainfall data. The validation of the calibrated soil moisture model can be interpreted as an enforcement of Chen et al. (2014a) conclusion.

3.6 Conclusion

There were not many great differences in soil moisture behaviour in dry and wet period in the four soil moisture stations analysed. This result suggests that despite the difference on rainfall of the dry and wet periods, there was no change in the preferential state of the soil, the vertical fluxes were predominant in both periods and local characteristics (i.e., local vegetation and local soil properties) were responsible for driving patterns of soil moisture (Grayson et al., 1997; Western et al., 2002).

Leaf Area Index (LAI) appeared to be higher in dry periods, which indicated that the model was trying to reach low values of soil moisture by assigning a high LAI that increased the PET. There was a dominance of simulations in all stations and in both soil types (clay and sand) towards high saturated hydraulic conductivity values. After a re-analysis of simulations, where the best run had higher LAI in wet periods, it was found that LAI from dry and wet periods were similar, demonstrating that the change in vegetation is not so expressive between dry and wet periods.

The soil moisture spatial differences between clay and sandy soils were mainly represented by changes in residual and saturated water content (θr and θs) and soil-pore distribution (n), which indicated that the model could simulate well the differences in soil water-holding capacities of the two soil types.

The hydrological model calibrated for Stanley S2 station for the period 2005-2007 (Chen et al., 2014a) was validated for the period 2008-2015 with satisfactory goodness-of-fit indices and visual assessment.

Chapter 4. Assessing a dual-porosity model in a clay soil catchment in Australia

4.1 Introduction

Stanley catchment is located in an area characterised by Vertisols, that is, soils rich in expansive clay. The presence of cracks in the soil of the Stanley catchment has been mentioned in other studies (Rüdiger, 2006; Martinez, 2010). Chen et al. (2014a) pointed out that macropores, together with soil type and vegetation, are the main drivers of soil moisture in the Stanley catchment. Macropore flow is a type of preferential flow that can be caused by earthworm burrows, root channels, or fissures and cracks due to the desiccation of clay soils (Beven & Germann, 1982; Hendrickx & Flury, 2001; Gerke, 2006). Preferential flow is characterised by water and solutes moving along certain pathways and bypassing a fraction of the porous soil matrix (Hendrickx & Flury, 2001; Simunek et al., 2003; Gerke, 2006).

In order to investigate the preferential flow through macropores in the clay soil of the region, this study aims to apply a dual-porosity model to Stanley S2 and S3 soil moisture stations to assess how a model that accounts for preferential paths performs at these sites. A dual-porosity model represents a non-equilibrium flow that explicitly accounts for preferential paths (Simunek et al., 2003; Gerke, 2006). In order to allow a direct comparison between the results obtained with the uniform flow model, this chapter will apply the same methodology as in Chapter 3. A Monte Carlo (GLUE) approach associated with HYDRUS-1D will be used to obtain the parameter set (i.e., soil properties and vegetation) for calibration of the HYDRUS-1D model in two wetness periods: wet and dry. The best parameter set will be selected by applying goodness-of-fit indices, including NSE and visual analysis, and an evaluation of the dual-porosity model will be carried out and compared with the uniform flow model (or single porosity model).

4.2 Materials and Methods

To assess macroporosity flow, the dual-porosity model of HYDRUS-1D was applied to the clay soil stations, Stanley-S2 and S3. This section presents the field data, the numerical model and the method used to assess the results. Precipitation and meteorological data are used as input to simulate soil moisture in the HYDRUS-1D model. A Monte Carlo GLUE approach was used to assess the distribution of the model parameters, and the evaluation of the model calibrations against measured soil moisture data was done by visual analysis and applying goodness-of-fit indices.

4.2.1 Field data

4.2.1.1 Soil moisture data

The study area is part of the Scaling and Assimilation of Soil Moisture and Streamflow (SASMAS) project (Rüdiger et al., 2007). In this chapter, only the clay soil stations (S1 and S2) from Stanley catchment (Figure 3.1), located in the Upper Hunter Valley (NSW), will be used. Soil moisture data is from water content reflectometers (Campbell Scientific CS616; Campbell Scientific, 2002) (Rüdiger et al., 2010).

4.2.1.2 Soil data

The area where the Stanley catchment is located is characterised by Vertisols, or soils rich in expansive clay (Hillel, 1998; Martinez, 2010). Soils in the study area consists mainly of Tertiary basalt (Story et al., 1963; Rüdiger, 2006) and cracks in the clay soil of the region have been pointed out in previous studies (Rüdiger, 2006; Martinez, 2010; Chen et al., 2014a). The soil texture and soil type was obtained based on laboratory analyses (Rüdiger et al., 2010), Stanley-S2 and S3 are both clay loam soils (Table 3.1). In clay soils, the porosity is highly variable because the soil alternately swells and shrinks, but it generally ranges from 0.3 to 0.6 (Hillel, 1998). According to Carsel and Parrish (1988), the typical saturated and residual soil water content values for clay loam soil are 0.41 v/v and 0.095 v/v, respectively.

4.2.1.3 Meteorological data

Meteorological data was obtained from the weather station located in the Stanley microcatchment (at station S2) at an elevation of 376 m. The meteorological weather station measures air temperature, relative humidity, wind speed and direction, rainfall and soil temperature. The station includes a pyranometer and measures the soil temperature at eight depths (25, 50, 100, 150, 300, 450, 600, and 750 mm) (Rüdiger et al., 2007). Tipping bucket rain gauges are present at two stations in Stanley (S1 and S2), rainfall from S2 was used as the input for S3 due to their proximity, as they are 230 metres apart.

4.2.2 HYDRUS-1D – Dual-porosity model

4.2.2.1 Model structure

The version of HYDRUS-1D used in this study is V4.14 (Simunek et al., 2013), the same version used by Chen (2013). In this chapter, the dual-porosity model of HYDRUS-1D was applied. In the dual-porosity model, water flow is limited to the fractures (i.e., inter-aggregate pores and macropores), and water in the matrix (i.e., intra-aggregate pores) can only be exchanged with the macropores (Simunek et al., 2013). The dual-porosity model is also known as a mobile-immobile model (MIM), in which the soil matrix is the immobile water content (θim) domain, which can exchange water with the mobile water content (θmo), i.e., macropores, where the water flows. This configures a nonequilibrium flow condition (between mobile and immobile domains) (Simunek et al., 2003), as shown in Figure 4.1.

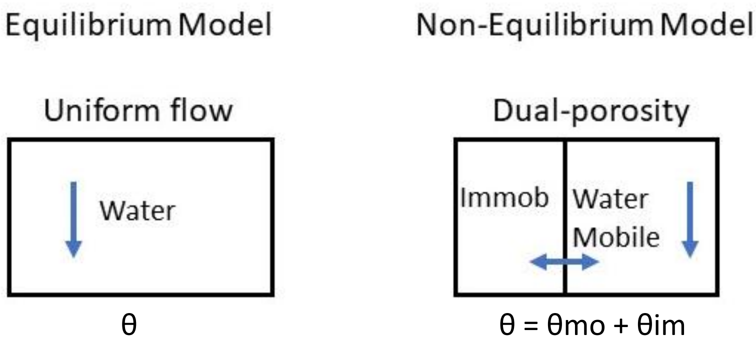

Figure 4.1 – Physical concept of equilibrium and non-equilibrium models for water flow. In the uniform flow model, θ is the water content, and in the dual-porosity model, θmo and θim are water contents of the mobile and immobile flow regions, respectively. Source: modified from Simunek et al. (2013).

The water flow in the mobile fraction (fractures or macropores) (Equation 4-1) is described by Richards equation (Equation 3-1) and a mass balance describes moisture dynamics in the matrix (Equation 4-2) (Simunek et al., 2003). The model describing the soil hydraulic properties in terms of soil water retention parameters for the mobile part of the soil, as well as the calculation of evapotranspiration, are described in Equations 3-1 to 3-12 of Section 3.3.2 in Chapter 3 of this thesis.

$$\frac{\partial \theta_{mo}}{\partial t} = \frac{\partial}{\partial x}\left[K(h)\left(\frac{\partial h}{\partial x}+1\right)\right] - S_{mo} - \Gamma_w \qquad 4\text{-}1$$

$$\frac{\partial \theta_{im}}{\partial t} = - S_{im} + \Gamma_w \qquad 4\text{-}2$$

where S_{mo} and S_{im} are sink terms (for root water uptake) for mobile and immobile regions, respectively. S_{im} is assumed to be zero in the current HYDRUS version (Simunek et al., 2013), which means that the water extracted by the plants is from the macropores and not the matrix. Γw is the transfer rate for water from the inter- to the intra-aggregate pores.

The mass transfer rate, Γw is proportional to the difference in effective saturation of the two regions using the first-order rate equation (Equation 4-3).

$$\Gamma_w = \frac{\partial \theta_{im}}{\partial t} = \omega \left[S_e^{mo} - S_e^{im} \right] \qquad 4\text{-}3$$

where θim is the matrix water content, ω is a first-order rate coefficient (T^{-1}), and S_e^{mo} and S_e^{im} are effective fluid saturations of the mobile (fracture) and immobile (matrix) regions, respectively (Simunek et al., 2013). The mass transfer rate (Γw) is proportional to the difference in effective water content between the mobile and immobile domains, instead of being proportional to the difference of pressure heads. This is because the mass transfer rate proportional to water content should provide a more realistic description of the exchange rate between the fracture and matrix regions (Simunek et al., 2013). Also, the mass transfer rate proportional to the difference in the pressure heads generates two extra parameters that can complicate the calibration process. A fundamental assumption of Equation 4-3 is that the water retention properties of the matrix and the fracture domains (i.e., α, Ks, n and L) are identical (Simunek et al., 2013).

The effective saturation (Se) in Equation 4-3 is a function of the residual and saturated volumetric water content (Equation 4-4).

$$S_e^{mo} = \frac{\theta_{Mo} - \theta_{rMo}}{\theta_{sMo} - \theta_{rMo}}$$

$$S_e^{im} = \frac{\theta_{Im} - \theta_{rIm}}{\theta_{sIm} - \theta_{rIm}} \qquad 4\text{-}4$$

4.2.2.2 Input parameters

The HYDRUS-1D dual-porosity nonequilibrium flow model has the usual soil hydraulic parameters of the equilibrium model, i.e., residual soil water content (θr), saturated soil water content (θs), inverse of the air-entry value (α), saturated hydraulic conductivity (Ks), pore-size distribution (n) and pore discontinuity (L), and it adds three parameters. Two added parameters are to characterise the matrix region (residual and saturated soil water contents of the immobile domain, θrIm and θsIm), and one parameter represents the first-order mass transfer coefficient (ω) (Table 4.1). The water retention properties (α, n, Ks and L) of the matrix (immobile) and the fracture (mobile) domains are identical and are described in Table 3.3.

Table 4.1 – Soil parameters of the dual-porosity model in HYDRUS

Parameter	**Symbol**	**Unit**	**Description**
Residual soil water content for the immobile region	θrIm	$[L^3L^{-3}]$	It is the residual soil water content for the immobile region.
Saturated soil water content for the immobile region	θsIm	$[L^3L^{-3}]$	It is the maximum moisture content of the immobile region.
Mass transfer coefficient	ω	$[T^{-1}]$	It is the first-order mass transfer coefficient from the mass transfer rate (Γw) of water between the fracture and matrix regions in dual-porosity studies (e.g., (Philip, 1968; Simunek et al., 2003).

4.2.3 HYDRUS GLUE calibration

For the HYDRUS-1D calibration using the Monte Carlo GLUE approach, there is a range for each parameter, i.e., a minimum and a maximum value. The parameter range for the dual-porosity parameters are shown in Table 4.2. The water retention properties (α, n, Ks and L) and the vegetation (LAI) have the same range as the uniform flow model application (Table 3.4) in Chapter 3.

Table 4.2 – Parameter range for GLUE analysis – dual-porosity application

	θrMo **[L^3L^{-3}]**	**θsMo** **[L^3L^{-3}]**	**θrIm** **[L^3L^{-3}]**	**θsIm** **[L^3L^{-3}]**	**ω** **[T^{-1}]**
Min	0.01	0.25	0.01	0.10	0
Max	0.15	0.50	0.15	0.15	0.1
	α **[L^{-1}]**	**n** **[-]**	**Ks** **[LT^{-1}]**	**L** **[-]**	**α** **[L^{-1}]**
Min	0.01	1	10^{-8}	-3	0.01
Max	0.2	2.5	10^{-4}	3	0.2

The residual water content (θr), that is the moisture content where water flow ceases (Van Genuchten, 1980), ranges between 0.01 to 0.15 v/v for the mobile (or macropore) domain (θrMo). For the immobile domain (matrix), θrIm varies between 0.01 to 0.15 v/v, which makes the total residual soil water content (θrMo+ θrIm) vary between 0.02 to 0.30 v/v. The saturated water content, that is maximum moisture content of a soil (Van Genuchten et al., 1991), varies from 0.25 and 0.50 v/v in the mobile domain (θsMo) and it ranges from 0.10 and 0.15 v/v in the immobile domain (θsIm). As a result, the total saturated water content (θsMo + θsIm) varies between 0.35 to 0.65 v/v. Both the total residual and saturated water content ranges are slightly higher than in the single porosity model, where θr was set to vary between 0.01 to 0.20 v/v and θs was set to range between 0.30 and 0.60 v/v. These slight increases of 0.01, 0.05 and 0.1 v/v were set to reflect a model with more water storage capacity.

The first-order mass transfer coefficient (ω) from the mass transfer rate (Equation 4-3) represents the transfer of water between the fracture and matrix domains. In the literature, the first-order mass transfer coefficient (ω) was applied with an average value of 0.05 day^{-1} (Zhang et al., 2004; Garg et al., 2009; Pontedeiro et al., 2010). Based on the first-order mass transfer coefficient (ω) found in the literature, and after finding that an increase in ω further than 0.1 day^{-1} did not reflect in changes in the simulated soil moisture, the first-order mass transfer coefficient (ω) was set to range between 0 to 0.1 day^{-1}. Despite the first-order mass transfer coefficient (ω) assuming only positive values, the mass transfer rate (Γw - Equation 4-3) can have both positive or negative values which corresponds to the water flowing either from the mobile domain to the immobile, or from immobile to mobile.

4.3 Results

This section shows the performance of a dual-porosity model applied to two clay loam soil stations, Stanley S2 and S3. A Monte Carlo GLUE analysis was applied to generate a large number of simulations that were assessed by the Nash-Sutcliffe Efficiency (NSE). The simulations that reached the highest NSE were used to further investigate the HYDRUS-1D dual-porosity flow model. Using the methodology applied to the uniform flow model (i.e., single-porosity model) (Chapter 3) enables a comparison of the models on the site.

4.3.1 Dual-porosity simulation

The Monte Carlo GLUE analysis for Stanley-S2 station using the HYDRUS-1D dual-porosity model is shown in Figure 4.2.

Dry simulations

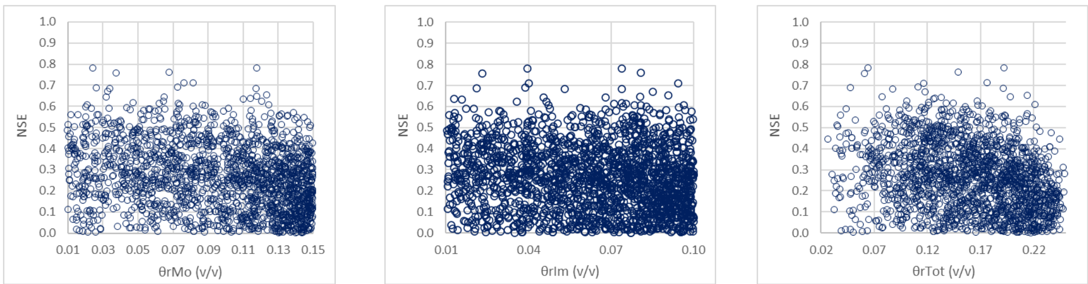

(a) (b) (c)

Wet simulations

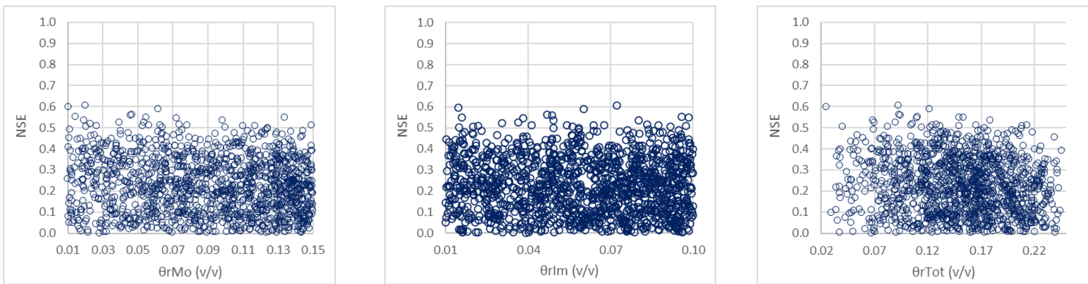

(d) (e) (f)

Dry simulations

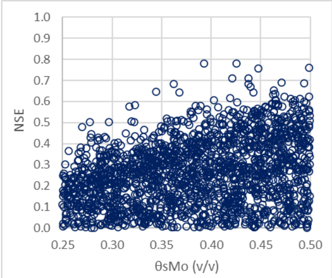

(g)

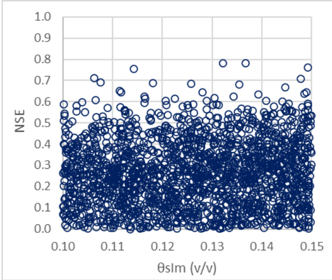

(h)

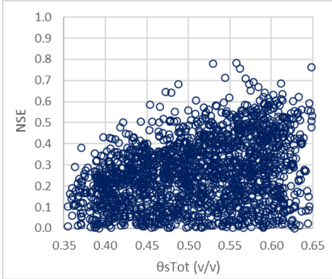

(i)

Wet simulations

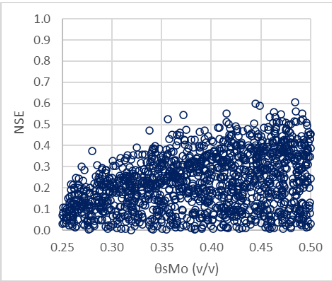

(j)

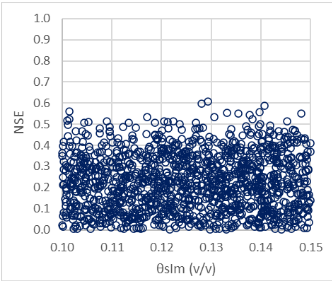

(k)

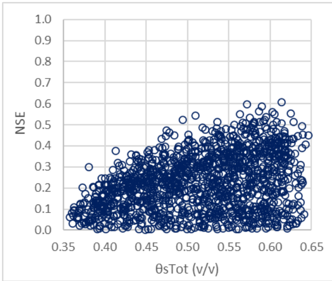

(l)

Dry simulations

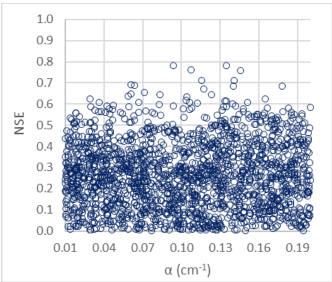

(m)

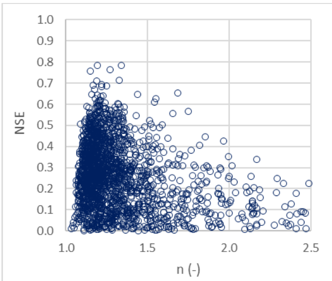

(n)

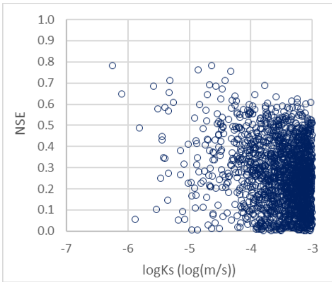

(o)

Wet simulations

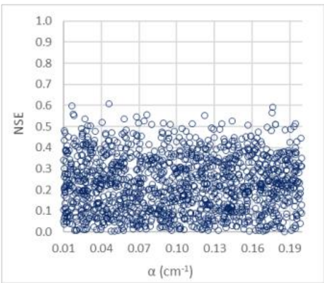

(p)

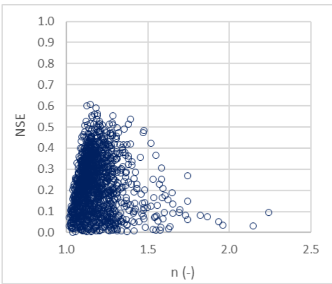

(q)

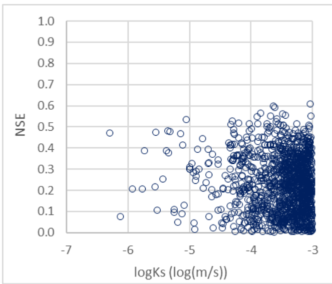

(r)

Dry simulations

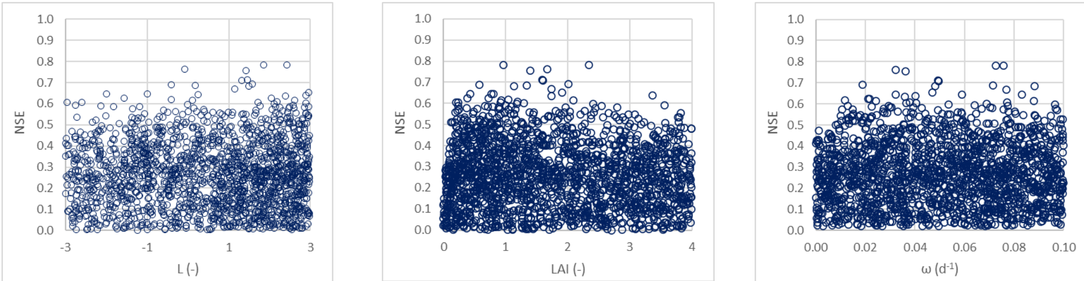

(s) (t) (u)

Wet simulations

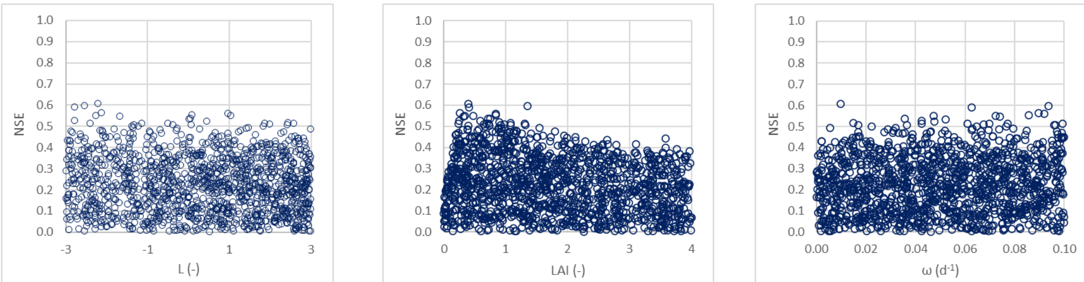

(v) (x) (z)

Figure 4.2 – Dotty plots from Monte Carlo GLUE analysis for the dry (2005-2006) and wet (2008-2010) calibration periods at Stanley-S2 for the parameters: (a, d) residual mobile soil water content – θrMo, (b, e) residual immobile soil water content – θrIm, (c, f) residual total soil water content – θrTot, (g, j) saturated mobile soil water content – θsMo, (h, k) saturated immobile soil water content – θsIm, (i, l) saturated total soil water content – θsTot, (m, p) inverse of the air-entry value – α, (n, q) pore-size distribution – n (o, r) logarithm of saturated hydraulic conductivity – logKs, (s, v) pore discontinuity – L, (t, x) Leaf Area Index – LAI, and (u, z) first-order mass transfer coefficient – ω.

The dry simulations reached higher NSE than the wet simulations, as 20% of the valid runs for the dry simulations had NSE above 0.4, whereas in the wet simulations 10% of the valid runs had NSE above 0.4. The most sensitive parameter in both dry and wet periods was the soil pore distribution (n), with a defined peak around 1.2 (Figure 4.2–n and q), the same parameter as when using the single-porosity model in S2 (Figure 3.19

– g and j). This parameter is linked to the water-holding capacity of the soil and appears to be sensitive not only when using single and dual-porosity models but among clay and sandy soils as well. There was a concentration of simulations in the higher range of Ks, between -4 to -3 log(m/s) (i.e., 864 to 8640 cm/d) for both wet and dry periods (Figure 4.2 – o and r), which was also observed when using the single-porosity model (Figure 3.19 – h and k). In the dry period there was a tendency to obtain high NSE with lower values of Ks, despite there being only a few simulations in the lower ranges of Ks. The opposite occurred in the wet period, where NSE deteriorated with lower values of Ks.

The total saturated soil moisture content (θsTot), which represents the sum of the saturated soil moisture content of the mobile and the immobile (matrix) domains, presented higher values of NSE towards the high values of θs for the dry and wet simulations (Figure 4.2 – i and l). This was also observed in the single-porosity simulations (Figure 3.19 – b and e), which indicates that soils with more space for water, and consequently that need more water to reach the saturated condition, better represent S2. The total residual soil moisture content (θrTot) did not show a well-defined peak, although there was a slight tendency to higher NSE for lower θrTot, and a concentration of runs towards higher values of θr (i.e., greater than 0.12 v/v), for dry and wet periods (Figure 4.2 – c and f). Two parameters related to the water retention properties (α and L) did not show a well-defined peak for either dry or wet periods (Figure 4.2 – m, p, s and v), and the first-order mass transfer coefficient (ω) was not shown to be a sensitive parameter in either dry or wet periods (Figure 4.2 – u and z).

As also occurred when applying the single-porosity model (Chapter 3), simulations with higher NSE corresponded to higher values of Leaf Area Index (LAI) in the dry calibration period than in the wet calibration period. LAI presented a peak between 0.9 and 2.4 in the dry calibration period (Figure 4.2 – t), whereas in the wet calibration period this peak was between 0.2 and 0.9 (Figure 4.2 – x). This was not expected, since wet periods are linked with greener conditions, i.e., higher LAI than dry periods. The reason for this behaviour is in the calibration of LAI is that a high LAI draws water from the soil at a higher rate, reaching lower levels of soil moisture. As the dry period has a lower quantity of water in the soil, a good matching of simulation and measured soil moisture is obtained with high LAI in drier periods. From MODIS data it was possible to see that LAI underwent a modest change from dry to wet periods, as the average LAI for S2 and S3 was 0.8 for the dry period and 1.1 for the wet period. In order to respect this observed condition, the analysis of the dual-porosity simulations was carried out with the best parameter set that also satisfied the condition of higher LAI for wet period than for the dry period.

A good match between simulated and measured values (Figure 4.3) was obtained using the best parameter set of the dry calibration period for Stanley-S2 with the dual-porosity model. The recession periods were well fitted and the peaks were slightly underestimated; the highest difference between a measured and a simulated peak was 0.13 v/v in July 2005. The wet calibration obtained a satisfactory fit of simulated and measured values (Figure 4.4), although NSE was 23% worse than in the dry calibration. Overall, the peaks were well captured, with two underestimations in July and August 2008 and July and August 2010. In both cases the peak was not a single peak, but an extended period (~1 month) with high values of soil moisture where the model drained the water instead of retaining it, as had occurred with the measured values. This also occurred with the single-porosity model. The recession periods were also well captured despite three events that happened around February and March 2010. The highest difference between simulated and measured peak was 0.14 v/v in August 2008. The parameter sets that generated the best dry and wet calibrations are shown in Table 4.3.

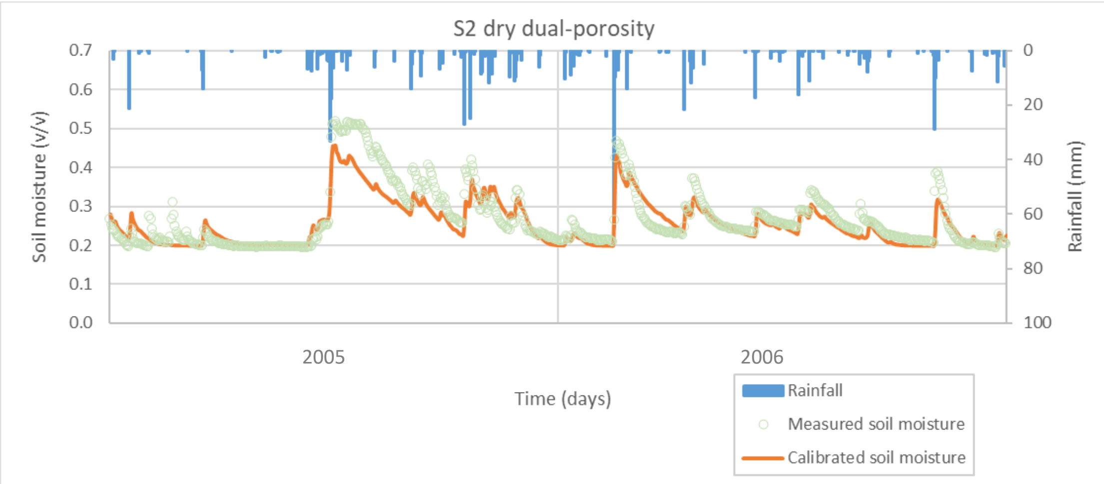

Figure 4.3 – Dual-porosity dry calibration (2005-2006) in Stanley-S2.

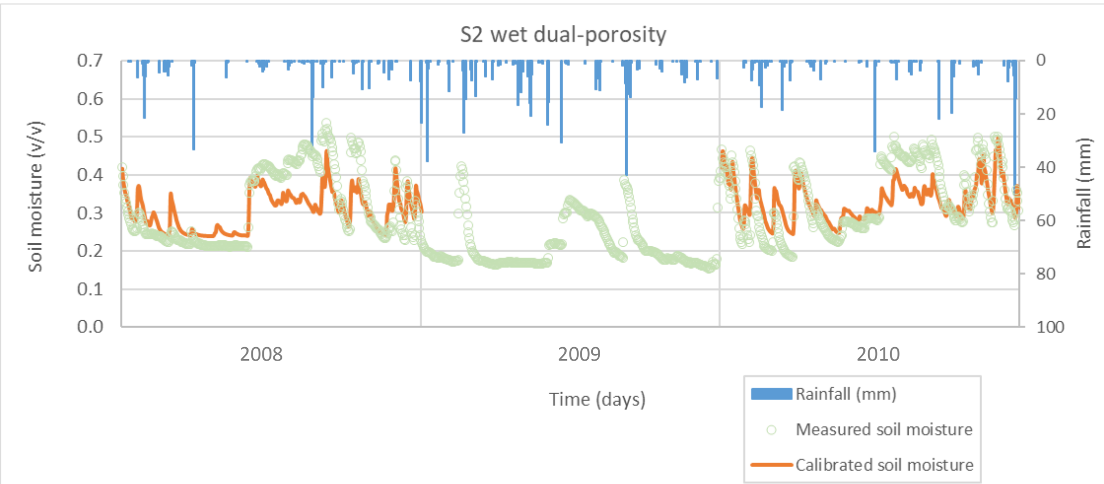

Figure 4.4 – Dual-porosity wet calibration (2008 and 2010) in Stanley-S2.

Table 4.3 – Best parameter set for Stanley (S2) with dual-porosity dry (2005-2006) and wet (2008 and 2010) calibration period.

Period	**θrMo (v/v)**	**θsMo (v/v)**	**θrIm (v/v)**	**θsIm (v/v)**	**θrTot (v/v)**	**θsTot (v/v)**
Dry	0.025	0.426	0.040	0.132	0.065	0.558
Wet	0.010	0.444	0.015	0.128	0.025	0.572
	α (cm^{-1})	**n (-)**	**log Ks (m/s)**	**L (-)**	**Ω (day^{-1})**	**LAI (-)**
Dry	0.094	1.196	-4.630	1.859	0.073	0.961
Wet	0.017	1.127	-3.626	-2.530	0.094	1.350

The parameters that generated the best dry and wet calibrations with the dual-porosity model (Table 4.3) are similar, with the exception of the saturated conductivity (Ks) and tortuosity parameter (L). In the dry period, both the higher tortuosity parameter and the lower saturated conductivity (203 cm/d or -4.630 log(m/s)) work towards making the water stay longer in the soil, which generates higher values of soil moisture. The opposite occurred in the wet period, with higher Ks (2044 cm/d) and lower L. Differently from what was found using the single-porosity model, there were no parameters counterbalancing. The dual-porosity model in the dry calibration period reached considerably better indices, e.g., higher R and NSE, than in the wet period (Table 4.4).

Table 4.4 – Goodness-of-fit values for Stanley (S2) for the dual-porosity model in the dry (2005-2006) and wet (2008 and 2010) calibration period.

Period	**R**	**RMSE (v/v)**	**sRMSE**	**NSE**
Dry	0.919	0.036	0.106	0.781
Wet	0.824	0.060	0.171	0.598

The calibration parameters from the dry period and wet period generated similar goodness-of-fit indices when applied to the eleven-year period at station S2 in Stanley (Table 4.5). Although the NSE from the dry calibration period was only slightly higher than the wet calibration period, visually the dry calibration period (Figure 4.5) generated a considerable better fit than the wet calibration period (Figure 4.6). In particular, the recession periods were better captured by the dry calibration parameters, while the wet calibration parameters overestimated them throughout the eleven-year period. The peaks were overall well captured by both set of parameters, despite underestimations in 2012, 2013 and 2015.

Table 4.5 – Goodness-of-fit values for Stanley (S2) for the period of 2005-2015 using the dual-porosity model with parameter set from the dry (2005-2006) and wet (2008 and 2010) calibration period.

Eleven-year period simulation	R	RMSE (v/v)	sRMSE	NSE
Dry calibration period	0.793	0.064	0.227	0.614
Wet calibration period	0.812	0.067	0.240	0.568

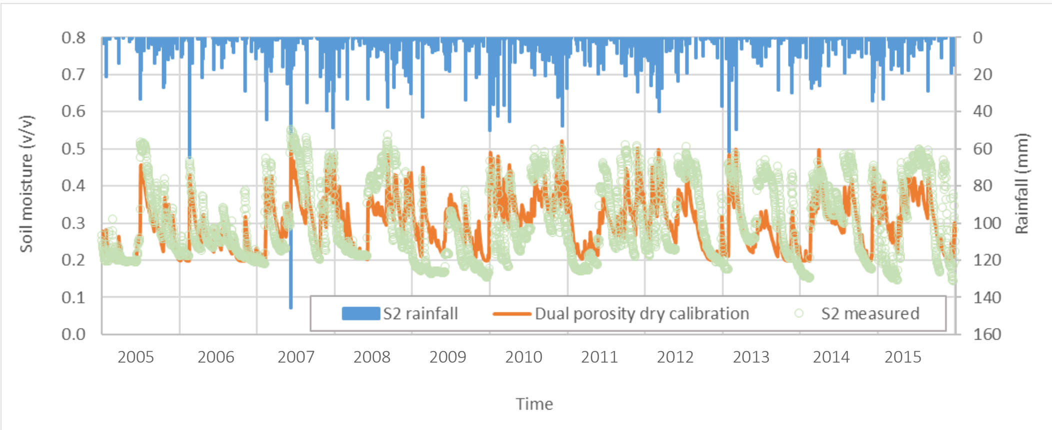

Figure 4.5 – Eleven-year period with dual-porosity dry calibration (2005-2006) for Stanley (S2).

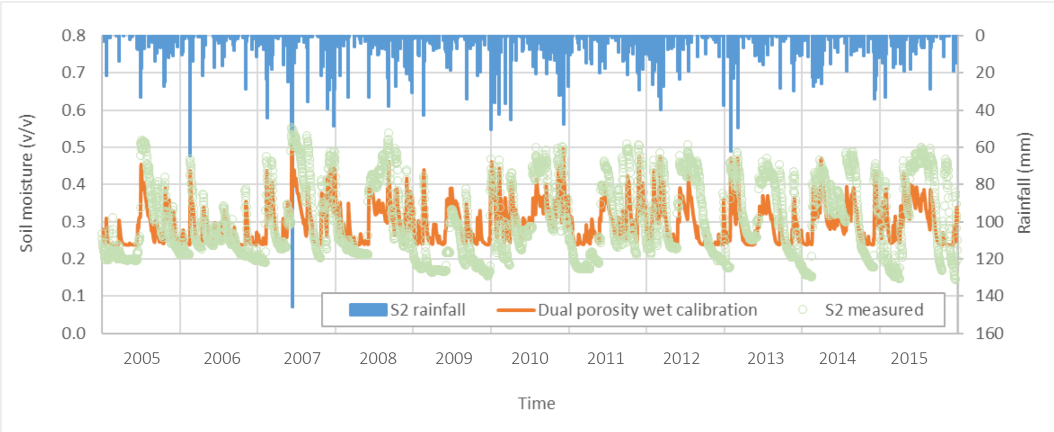

Figure 4.6 – Eleven-year period with dual-porosity wet calibration (2008 and 2010) for Stanley (S2).

The Monte Carlo GLUE analysis for Stanley-S3 station using the HYDRUS-1D dual-porosity model are shown in Figure 4.7.

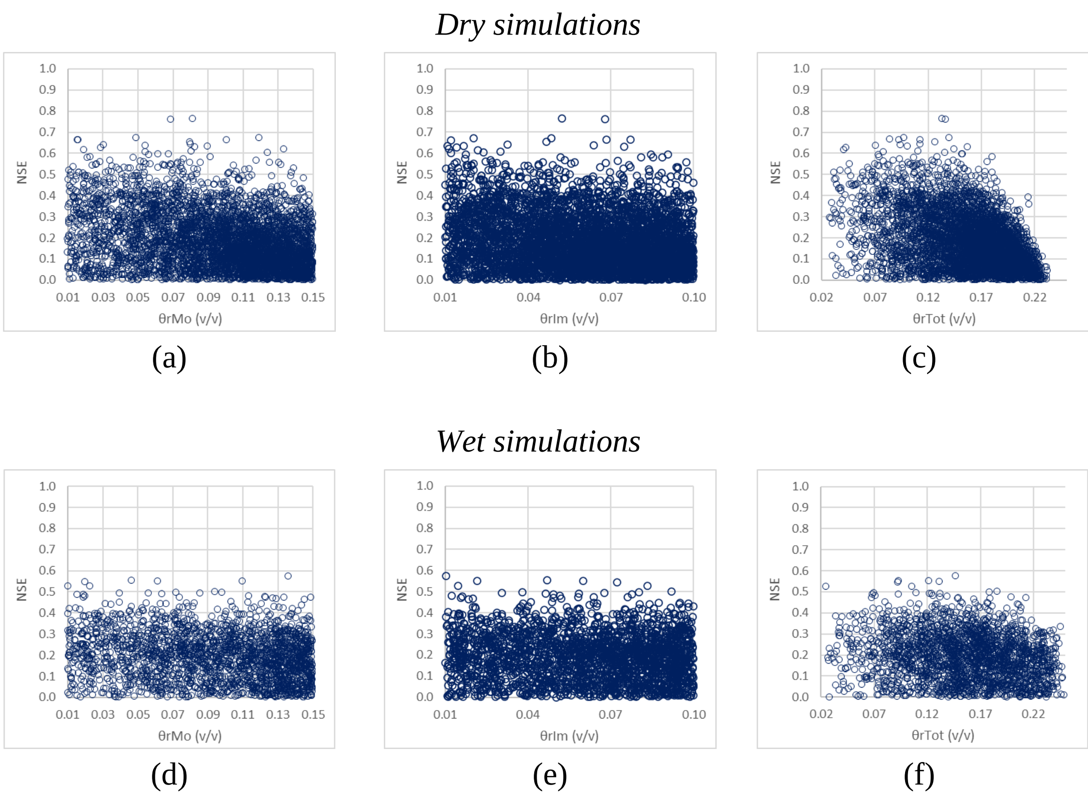

Dry simulations

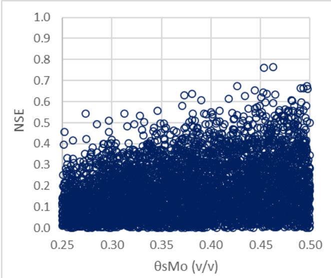

(g)

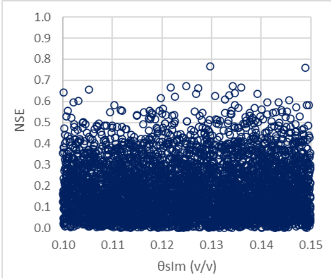

(h)

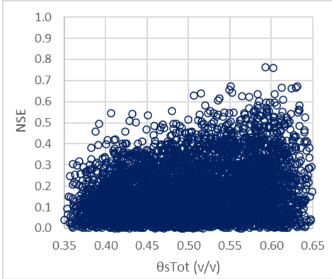

(i)

Wet simulations

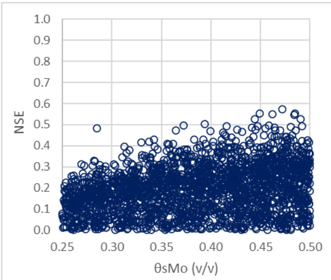

(j)

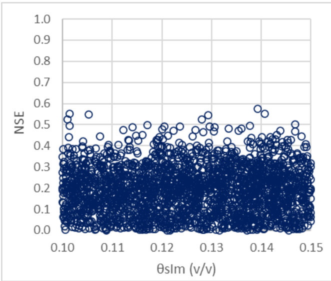

(k)

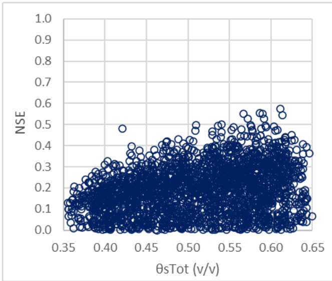

(l)

Dry simulations

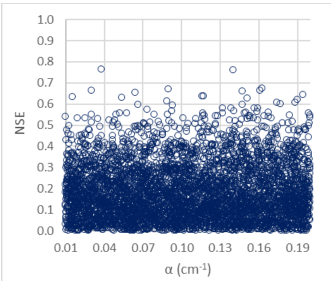

(m)

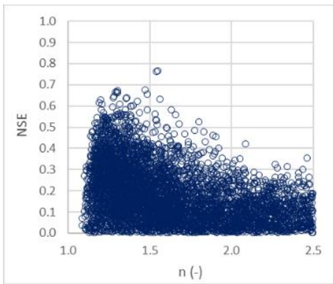

(n)

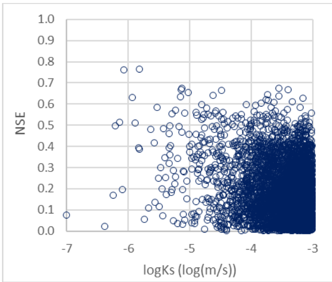

(o)

Wet simulations

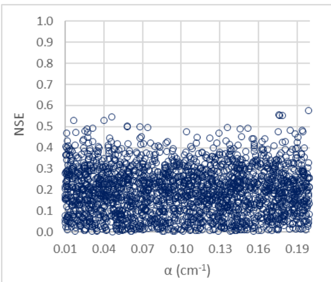

(p)

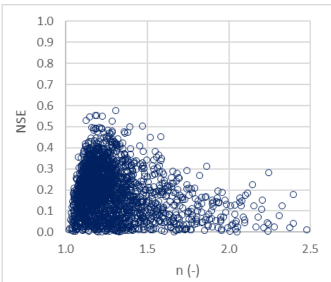

(q)

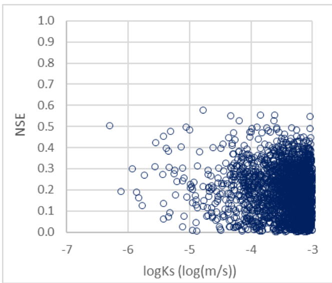

(r)

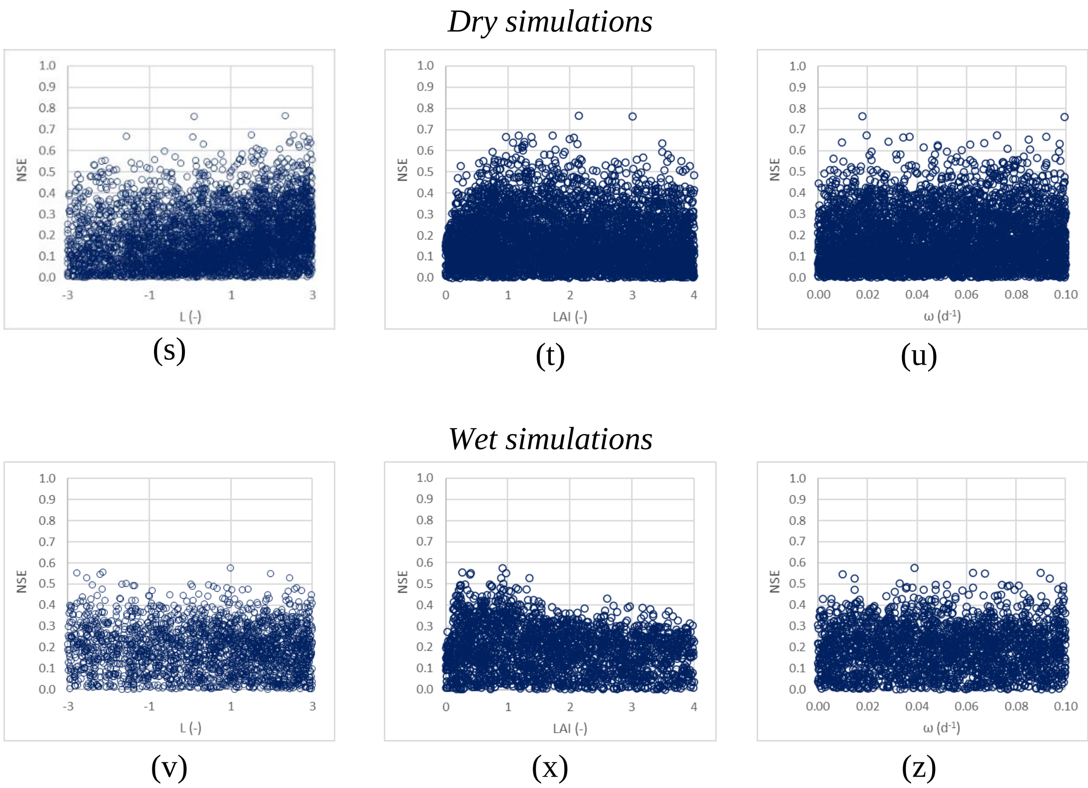

Figure 4.7 – Dotty plots from Monte Carlo GLUE analysis for the dry (2005-2006) and wet (2008-2010) calibration periods at Stanley-S3 for the parameters: (a, d) residual mobile soil water content – θrMo, (b, e) residual immobile soil water content – θrIm, (c, f) residual total soil water content – θrTot, (g, j) saturated mobile soil water content – θsMo, (h, k) saturated immobile soil water content – θsIm, (i, l) saturated total soil water content – θsTot, (m, p) inverse of the air-entry value – α, (n, q) pore-size distribution – n, (o, r) logarithm of saturated hydraulic conductivity – logKs, (s, v) pore discontinuity – L, (t, x) Leaf Area Index – LAI, and (u, z) first-order mass transfer coefficient – ω.

For S3 station, the results from the Monte Carlo simulations show that the parameter sets from the dry period generated a higher NSE coefficient than the wet period (Figure 4.7). LAI showed a peak around 0 and 1 for the wet period (Figure 4.7 – x) but for the dry period the peak was not well defined (Figure 4.7 – t). As had occurred for S2 and when applying the single-porosity model (Chapter 3), simulations with higher NSE corresponded to higher values of Leaf Area Index (LAI) in the dry calibration period than in the wet calibration period. This is because a high LAI depletes more water from the soil, consequently reaching lower levels of soil moisture that are better matched with measured soil moisture in the dry period. The analysis of the dual-porosity simulation was conducted with the parameter set that satisfied the condition of higher LAI for wet period.

The total residual soil moisture content ($\theta rTot$) did not show a well-defined peak in the wet period (Figure 4.7 – f) and showed a slight peak between 0.1 and 0.14 v/v in the dry period (Figure 4.7 – c). The total saturated soil moisture content ($\theta sTot$) showed higher values of NSE towards high values of θs for the dry and wet simulations (Figure 4.7 – i and l) which was also observed in the single-porosity simulations (Figure 3.19 – b and e) and at S2 station. The tortuosity parameter (L) had a flat response in the wet period (Figure 4.7 – v) but generated higher NSE towards high values of L in the dry period (Figure 4.7 – s). The inverse of the air-entry value (α) and the first-order mass transfer coefficient (ω) did not show a well-defined peak for either dry or wet periods (Figure 4.7 – m, p, u and z).

Soil pore distribution (n) and saturated hydraulic conductivity (Ks) were the most sensitive parameters (Figure 4.7), as occurred with S2 (Figure 4.2). The soil pore distribution (n) had a defined peak around 1.3 in dry simulations and around 1.2 in wet simulations (Figure 4.7 – n and q). S3 presented a concentration of simulations in high values of Ks, between -4 to -3 log(m/s) for both wet and dry periods (Figure 4.7 – o and r) that was also noted in S2 and in the single-porosity model application. Similarly to S2, the dry period showed high NSE for lower values of Ks, and the wet period NSE decreased with lower values of Ks.

Even though simulation with the best parameter set for the dry calibration period matched the measured soil moisture in the beginning of 2005, it underestimated soil moisture in mid-2005 and it overestimated all 2006 (Figure 4.8). The wet calibration in S3 could meet the peaks in the beginning of 2008 and beginning of 2010 but the recessions were overestimated throughout the simulation (Figure 4.9). The parameter sets that generated the best dry and wet calibrations are shown in Table 4.6. A visual comparison between S2 and S3 simulations show that S3 was considerably worse in both periods. In the dry period, there was a good match between simulated and measured values in S2 (Figure 4.3), whereas in S3, the model overestimated all the recession periods throughout 2006. The wet period also had a better match in S2 (Figure 4.4) than S3, that showed overestimation in the recessions throughout the period.

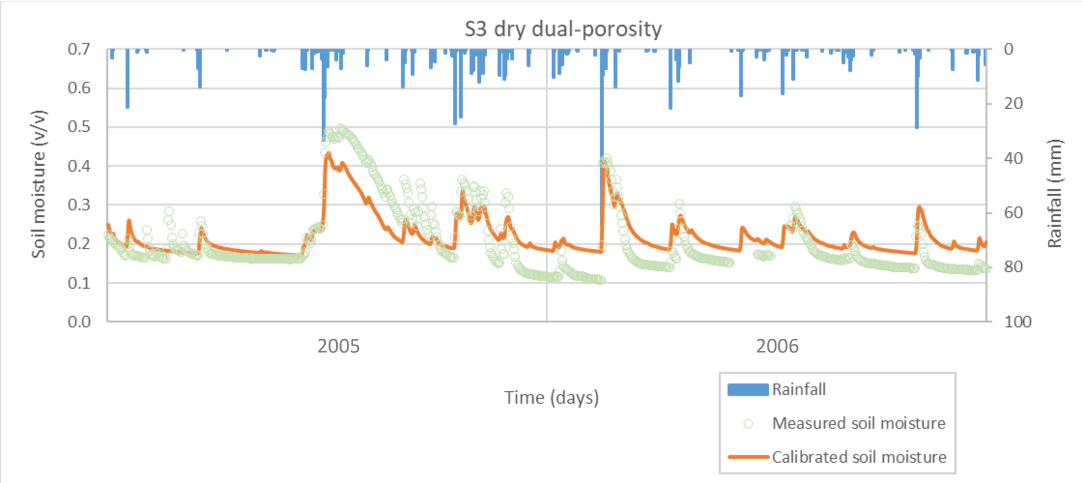

Figure 4.8 – Dual-porosity dry calibration (2005-2006) in Stanley-S3.

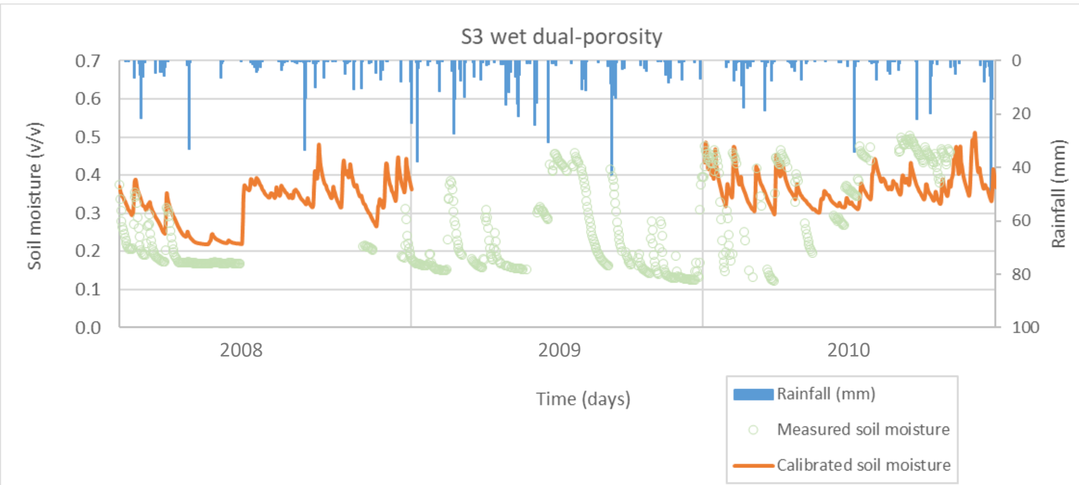

Figure 4.9 – Dual-porosity wet calibration (2008 and 2010) in Stanley-S3.

Table 4.6 – Best parameter set for Stanley (S3) with dual-porosity dry (2005-2006) and wet (2008 and 2010) calibration period.

Period	**θrMo (v/v)**	**θsMo (v/v)**	**θrIm (v/v)**	**θsIm (v/v)**	**θrTot (v/v)**	**θsTot (v/v)**
Dry	0.016	0.491	0.077	0.122	0.093	0.613
Wet	0.110	0.462	0.022	0.105	0.132	0.567
	α (cm^{-1})	**n (-)**	**log Ks (m/s)**	**L (-)**	**Ω (day^{-1})**	**LAI (-)**
Dry	0.030	1.294	-5.136	-1.558	0.092	0.967
Wet	0.179	1.225	-4.321	1.988	0.067	0.978

In the dual-porosity simulations, dry and wet periods obtained similar parameter sets (Table 4.6) apart from inverse of the air-entry value (α), saturated conductivity (Ks) and tortuosity parameter (L). The low α and the low Ks (63 cm/d), in the dry period make the water stay longer in the soil and they are counterbalanced by the low L that facilitates water percolation, making the soil dry faster. The opposite occurs in the wet period, where higher α and Ks speed the water percolation and the high tortuosity, L, slows the water percolation. The dry calibration period obtained better goodness-of-fit indices than the wet period (Table 4.7).

Table 4.7 – Goodness-of-fit values for Stanley (S3) for the dual-porosity model in the dry (2005-2006) and wet (2008 and 2010) calibration period.

Period	**R**	**RMSE (v/v)**	**sRMSE**	**NSE**
Dry	0.891	0.052	0.302	0.665
Wet	0.797	0.081	0.407	0.550

The dry calibration parameters generated better goodness-of-fit indices when applied to the eleven-year period than the wet calibration parameters (Table 4.8). Neither the dry calibration period (Figure 4.10) nor the wet calibration period (Figure 4.11) could capture the recession periods of S3 during the eleven years. Except for the recession in the beginning of 2005, which was captured by the dry calibration period, all recessions were overestimated by both calibration periods. The peaks were well captured by both calibration parameter sets by the dual-porosity model, although the dry period overestimated one peak in 2007 and 2014.

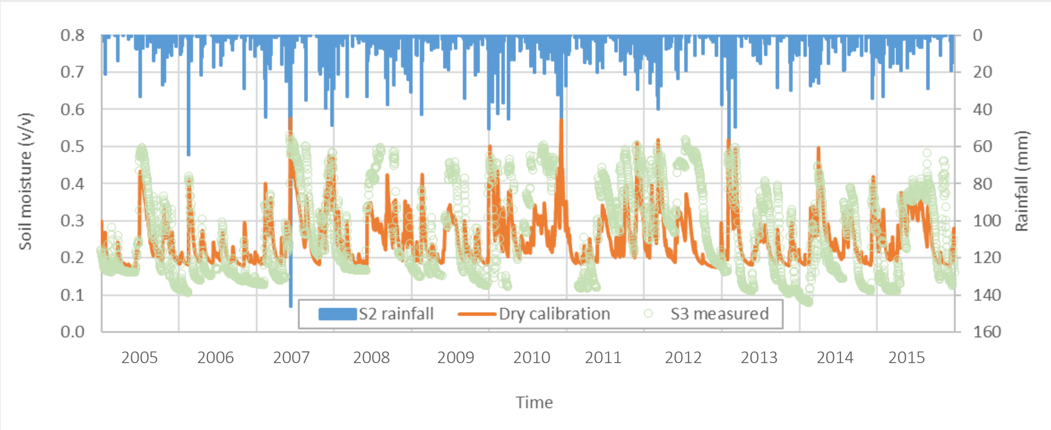

Figure 4.10 – Eleven-year period with dual-porosity dry calibration (2005-2006) for Stanley (S3).

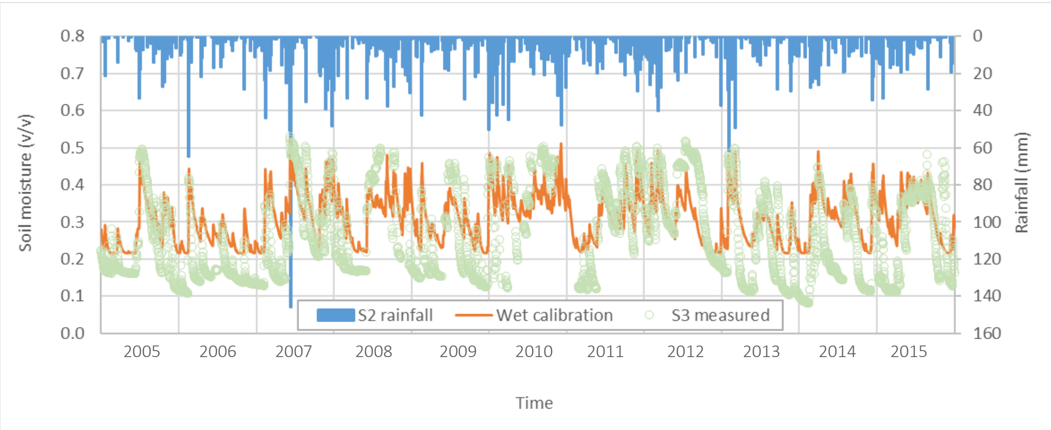

Figure 4.11 – Eleven-year period with dual-porosity wet calibration (2008 and 2010) for Stanley (S3).

Table 4.8 – Goodness-of-fit values for Stanley (S3) for the period of 2005-2015 using parameter set from the dry (2005-2006) and wet (2008 and 2010) calibration period.

Eleven-year period simulation	**R**	**RMSE (v/v)**	**sRMSE**	**NSE**
Dry calibration period	0.760	0.081	0.365	0.527
Wet calibration period	0.779	0.092	0.580	0.403

4.3.2 Dual-porosity model versus single-porosity model simulations

The dual-porosity model simulations were very similar to what was generated by the single-porosity model in S2 station in the dry (Figure 4.12) and wet periods (Figure 4.13). During the simulation period, soil moisture values generated by the single and dual-porosity models were on average 0.02 v/v different for both dry and wet periods. The maximum difference from single to dual-porosity simulations was 0.04 v/v for the dry period and 0.03 v/v for the wet period. In the dry period, the dual-porosity model obtained lower peaks of soil moisture compared to the single-porosity model, although still very close, and on average only 0.02 v/v lower. In the recession periods the dual-porosity model reached lower values and on average it made the soil dry faster than the single-porosity model did (Figure 4.12). There were only two occasions where the soil dried faster with the single-porosity model and they were following the two highest peaks, in July 2005 and March 2006, which was probably because the water was held in the micropore (matrix) and was released to the macropores at a slower rate. For the wet period, the soil moisture simulations had very similar wetting and drying behaviour in single and dual-porosity models, but the dual-porosity simulations appear to be shifted down (Figure 4.13). Only on a few occasions (Feb, Mar and Nov 2008 and Mar and Apr 2010) did the soil seem to be drying faster with the dual-porosity model.

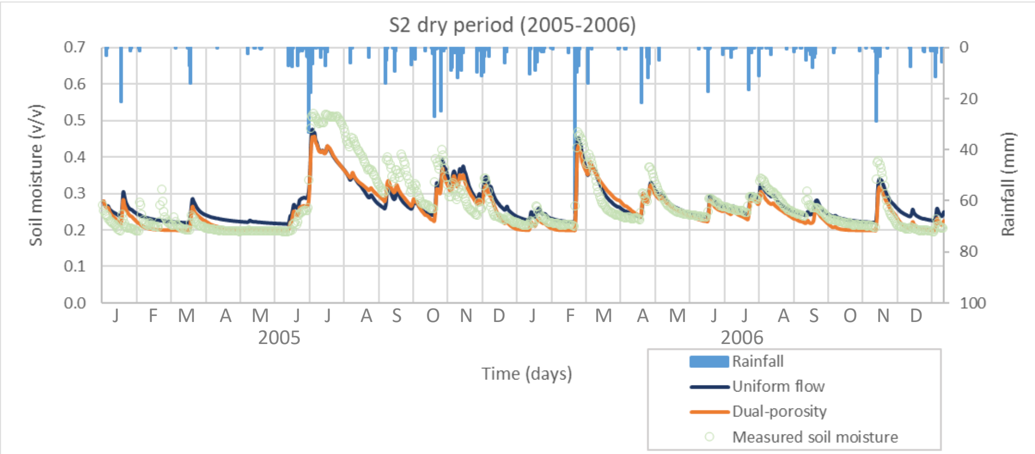

Figure 4.12 –Dry calibration (2005-2006) using the uniform flow model and the dual-porosity model in Stanley (S2).

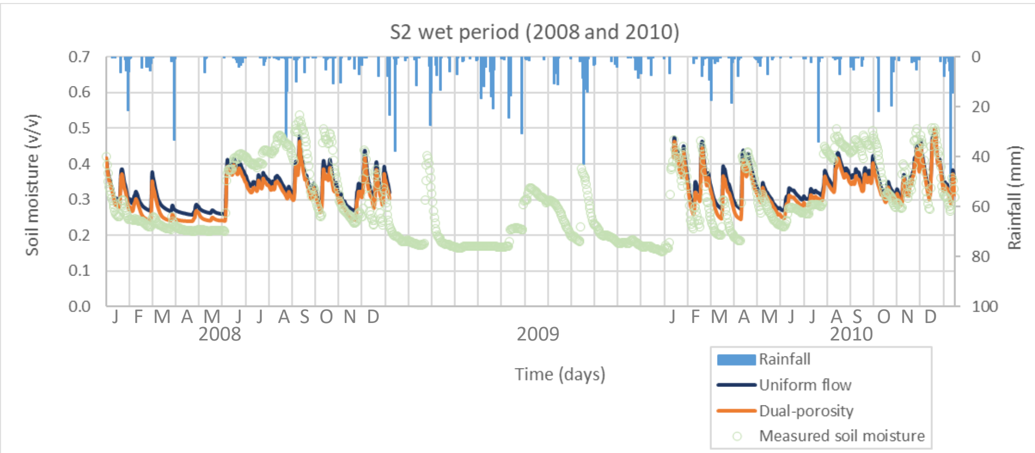

Figure 4.13 –Wet calibration period (2008 and 2010) using the uniform flow model and the dual-porosity model in Stanley (S2).

The single and dual-porosity models generated similar simulations for S3 in the dry period (Figure 4.14) and wet period (Figure 4.15), but the dual-porosity simulations shifted up in both periods. In the dry period the dual-porosity simulation was very close to the single-porosity simulation, with the average difference between the simulations at 0.009 v/v (Figure 4.14). Both models underestimated the soil moisture peaks throughout the period. Recessions and drying curves were also overestimated during most of the period (August 2005 – October 2006). In average the dual-porosity simulation was 0.025 v/v higher than the single-porosity simulation in the wet period (Figure 4.15). For S3, the drying curves were the same when using single or dual-porosity models.

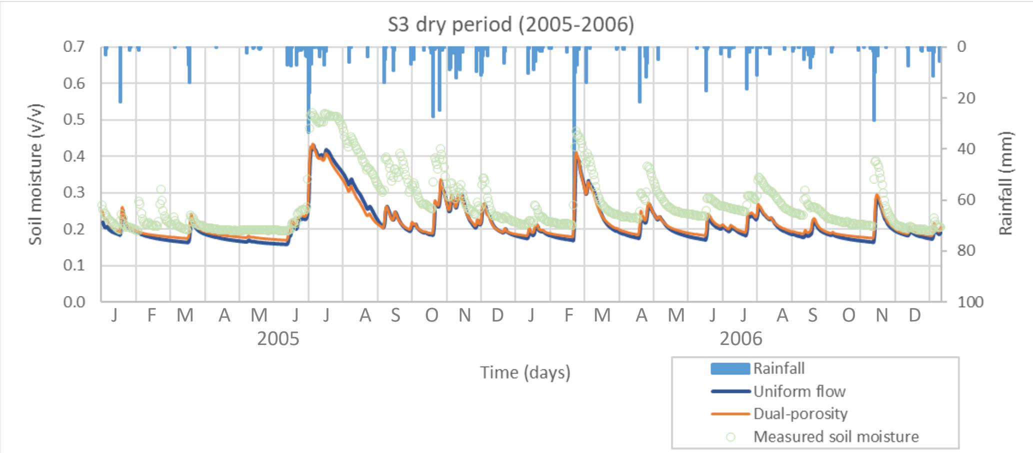

Figure 4.14 –Dry calibration period (2005-2006) using the uniform flow model and the dual-porosity model in Stanley (S3).

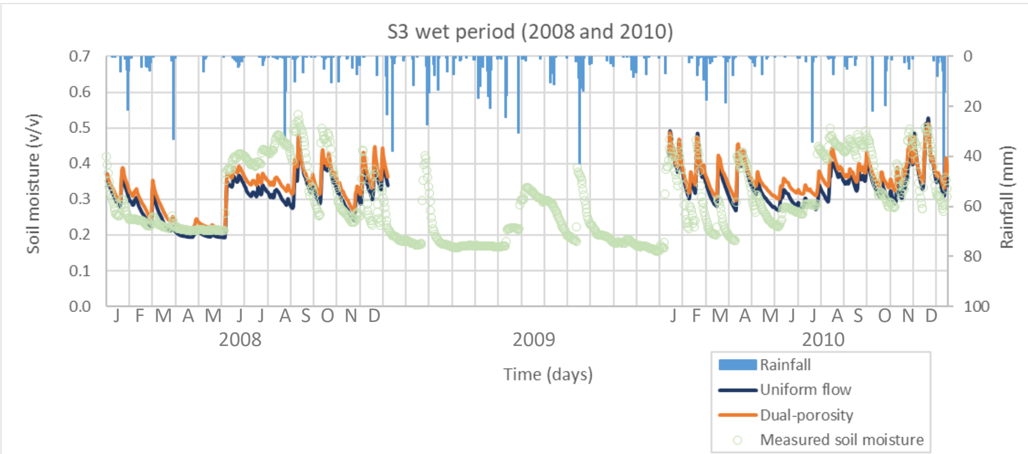

Figure 4.15 –Wet calibration period (2008 and 2010) using the uniform flow model and the dual-porosity model in Stanley (S3).

A comparison of the NSE obtained when using the single-porosity and dual-porosity model shows that there was an overall decrease in the NSE when using the dual-porosity model in the region. Five out of eight simulations, or 63%, saw the NSE diminished with the dual-porosity model. For the S3 station this reduction in NSE occurred for the four simulations: dry calibration, wet calibration, dry calibration applied to eleven-year period and wet calibration applied to eleven-year period. The opposite occurred for S2 station, where three out of four simulations had their NSE improved with the dual porosity model. This slight improvement was observed in S2 station in three simulations: S2 dry calibration, S2 wet calibration and S2 wet calibration applied to eleven-year period. The biggest improvement when using the dual-porosity model was in S2 dry calibration, where the NSE increased 5%. The S3 wet calibration applied to the eleven-year period generated the largest difference between NSE, with NSE from the single-porosity model being 27% higher than with the dual-porosity model.

Table 4.9 – NSE coefficients for dry and wet calibration periods using the single-porosity model and the dual-porosity model.

Station and calibration period		**Single-porosity model**		**Dual-porosity model**	
		NSE in calibration period	**NSE in 11-year period**	**NSE in calibration period**	**NSE in 11-year period**
C L A Y	S2 dry	0.746	0.617	0.781	0.614
	S2 wet	0.581	0.528	0.598	0.568
	S3 dry	0.744	0.562	0.665	0.527
	S3 wet	0.559	0.550	0.550	0.403

4.4 Discussion

An investigation of preferential flow was conducted in Stanley catchment, located in the Upper Hunter Valley region in New South Wales (Australia). Stanley catchment is located in an area characterised by Vertisols, that is, soils rich in expansive clay. The presence of cracks in the soil of Stanley catchment has been mentioned in other studies (Rüdiger, 2006; Martinez, 2010). Chen et al. (2014a) pointed out that macropores, together with soil type and vegetation, are the main drivers of soil moisture in Stanley catchment. In order to assess preferential flow through macropores in the clay soil of the region, this study applied a dual-porosity model to Stanley S2 and S3 soil moisture stations. A dual-porosity model represents a non-equilibrium flow that explicitly accounts for preferential paths (Simunek et al., 2003; Gerke, 2006). In order to allow a direct comparison between the results obtained with the uniform flow model, this chapter applied the same methodology of Chapter 3. From a Monte Carlo (GLUE) approach associated with HYDRUS-1D, the simulations that generated the highest NSE for S2 and S3 were chosen and compared with the uniform flow model (or single porosity model) simulations.

The results pointed to a slight decline in the simulations' performance (NSE) when using the dual-porosity model in five out of eight simulations. The average improvement in the five simulations when keeping the single-porosity model was 9%, whereas the average improvement in the three simulations when using the dual-porosity model was 5%. The differences in simulation performances were only marginal when comparing both models, and the differences in the soil moisture simulations, i.e., the drying and wetting curves, were also minimal. This was also found by Garg et al. (2009) in a study on preferential flow in rice fields, where similar good results for water flow simulations were found when using HYDRUS-1D single (uniform flow) and dual-porosity flow models. Another study that investigated salt leaching in a loamy sand soil under irrigation scenarios found that increasing irrigation accelerated salt leaching but had an insignificant effect on soil water storage (Zeng et al., 2014). This can indicate that the dual-porosity model does not affect water movement in as significant a way as it impacts solute transportation. In the dual-porosity model the soil matrix has its own microporosity and it can dry out or rewet during drying and wetting processes (Šimůnek & van Genuchten, 2008); this allows the soil to dry at a slower or faster rate than with the single-porosity model. The dual-permeability model could probably better describe preferential flow, but it is considerably more complex due to the large number of parameters involved (17 input parameters instead of 10 in the dual-porosity model).

4.5 Conclusion

Overall, the simulations for Stanley S2 and S3 stations had their NSE slightly diminished when using a dual-porosity model. The best parameter sets obtained using the single and the dual-porosity model were similar within each station and period (e.g., S2-dry). The difference between the best parameter set of Stanley-S2 using the single-porosity model or the dual-porosity model was in the LAI and L (tortuosity parameter) for both dry and wet periods. LAI for both dry and wet periods were higher using the single-porosity model, and L was higher using the single-porosity model in the dry period and lower in the wet period comparing to L when applying the dual-porosity model. For Stanley-S3, the difference between parameter sets when using the two models was even smaller, the only noticeable difference was in the parameter L in the wet period.

The average difference in NSE between the use of single-porosity and the dual-porosity models was low, only 0.04. From this evaluation it is possible to conclude that there is no need to use a more complex model in this area, i.e., with more soil input parameters, because the performance of the dual-porosity model is slightly worse to very similar to the single-porosity model. Although the area is characterised by soils rich in expansive clay, and the presence of macropores was pointed to as one of the main drivers of soil moisture in Stanley catchment (Chen et al., 2014a), the HYDRUS-1D dual-porosity model did not add improvements to the understanding and simulation of soil moisture dynamics in the region.

Chapter 5. Long-term variability of soil moisture in New South Wales

5.1 Introduction

Soil moisture is of great importance in global hydrologic and climate cycles due to its influence on vegetation, agriculture, water distribution and carbon land–atmosphere exchange (Jung et al., 2010; Dorigo et al., 2012). Evapotranspiration, i.e., evaporation from bare soil and transpiration from plants, and the partitioning of the incoming energy into latent and sensible heat, are part of the effect of soil moisture on climate processes (Seneviratne et al., 2010; Lo et al., 2021). Further examination of soil moisture behaviour is of interest for hydrologists, climatologists, the agricultural sector and governments to help to identify solutions to global water security challenges (McDonough et al., 2020). Because of soil moisture's importance in the global climate and for its high spatial and temporal variability, it has gained the attention of hydrologists and climatologists over the years. With a general increase in global temperatures, the consequences for soil moisture distribution, droughts and water availability remain uncertain (Goodrich et al., 2000; Dai, 2013; Lockart et al., 2020; Nguyen et al., 2020).

Numerous studies have examined global trends in soil moisture and the results have pointed to different directions; while some studies pointed to the dominance of a drying trend (Dai, 2011; Dorigo et al., 2012; Gu et al., 2019; Deng et al., 2020), others found that dry locations will become drier and wet regions will become wetter (Held & Soden, 2006; Albergel et al., 2013; Greve et al., 2014; Feng & Zhang, 2015). Studies of long-term soil moisture trends have been predominantly carried out on a global scale, with a coarse spatial resolution dataset (25 to 100 km pixel) (Sheffield & Wood, 2008a; Dorigo et al., 2012; Albergel et al., 2013; Deng et al., 2020) that masks local and regional trends. Regional trends are driven by small-scale land–atmosphere interactions, and it is important to understand the patterns of regional soil moisture trends for local agricultural and industrial needs (McDonough et al., 2020).

The global-scale studies of soil moisture trends usually analyse surface soil moisture (to 10 cm) trends (Sheffield & Wood, 2008a; Dorigo et al., 2012; Feng & Zhang, 2015; Deng et al., 2020), and not the profile layer (to 100 cm). The surface and profile layers represent different processes that happen in the soil, which makes the analysis of temporal trends important in both layers. Surface soil moisture is representative of climatic processes due to the flux of mass and energy with the atmosphere that occurs there (Brocca et al., 2009), while profile soil moisture has a longer memory and is a better representation of vegetation (Cai et al., 2009; Santos et al., 2014).

It is not only studies of soil moisture trends, but studies that focus on understanding trends in temperature, evapotranspiration, precipitation, vegetation and floods (Allan et al., 2010; Jung et al., 2010; Alexander, 2011; King et al., 2013; Liu & Allan, 2013; Chen et al., 2014b; Wasko & Nathan, 2019; Nguyen et al., 2020) that are helpful for a better understanding of soil moisture spatial and temporal variability. The abovementioned factors influence and are influenced by soil moisture. This chapter will investigate the long-term variability of soil moisture in the state of New South Wales for the period 1990-2019, for surface (0-10 cm) and profile (0-100 cm) soil layers. This study uses modelled soil moisture data from AWRA-L in a 5×5 km pixel and a temporal decomposition model (BFAST) to compute the soil moisture long-term variability. Soil moisture long-term variability in both surface and profile layers are compared to the physical characteristics of the area, including the elevation, temperature, rainfall and land coverage.

5.2 Study area

The study area encompasses the state of New South Wales (NSW) located in southeast Australia, a continental country surrounded by the Pacific and Indian Oceans (Figure 5.1). New South Wales is Australia's most populous state with 8.3 million people (Australian Bureau of Statistics, 2020) and includes economically important cities for the country, including Sydney (Figure 5.1).

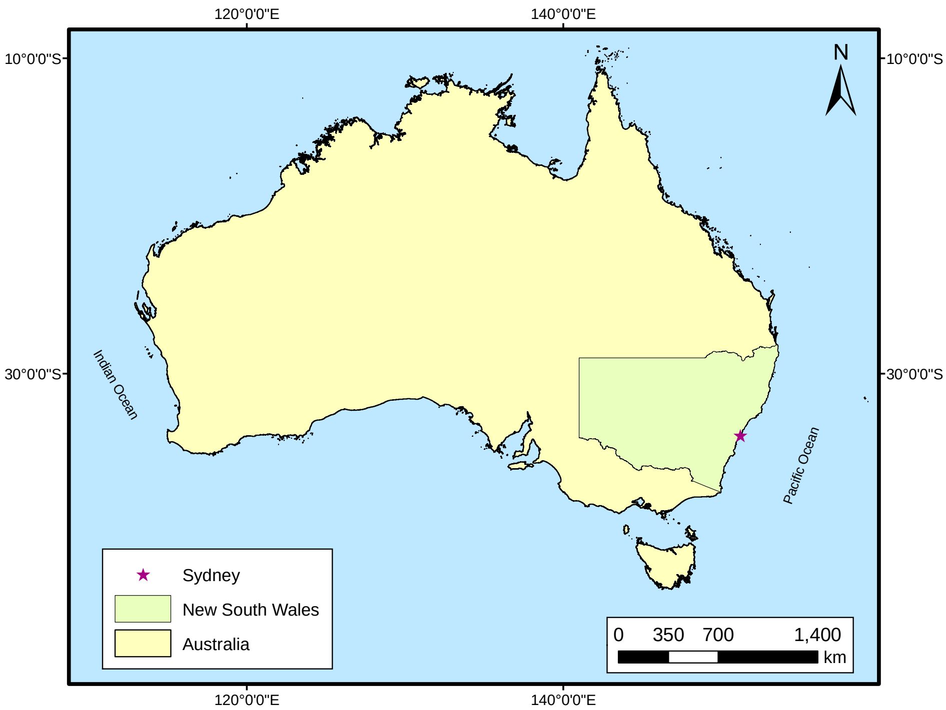

Figure 5.1 – Location map and study area.

The elevation of New South Wales is shown in Figure 5.2 with the highest point in the Great Dividing Range at 2250 m. The Great Dividing Range runs north to south, roughly parallel to the eastern coast, approximately 150 km from the coast of New South Wales (Johnson, 2009). The Great Dividing Range is a chain of mainly basaltic volcanoes (there are no active volcanoes in Australia), typically 300-1600 m above sea level (Johnson, 2009), and is known to separate climate types in south-east Australia (Gibson et al., 2020). The Digital Elevation Model (DEM) was derived from Shuttle Radar Topography Mission (SRTM) data acquired by NASA in a 1sec resolution (~ 30 m) (Gallant et al., 2011).

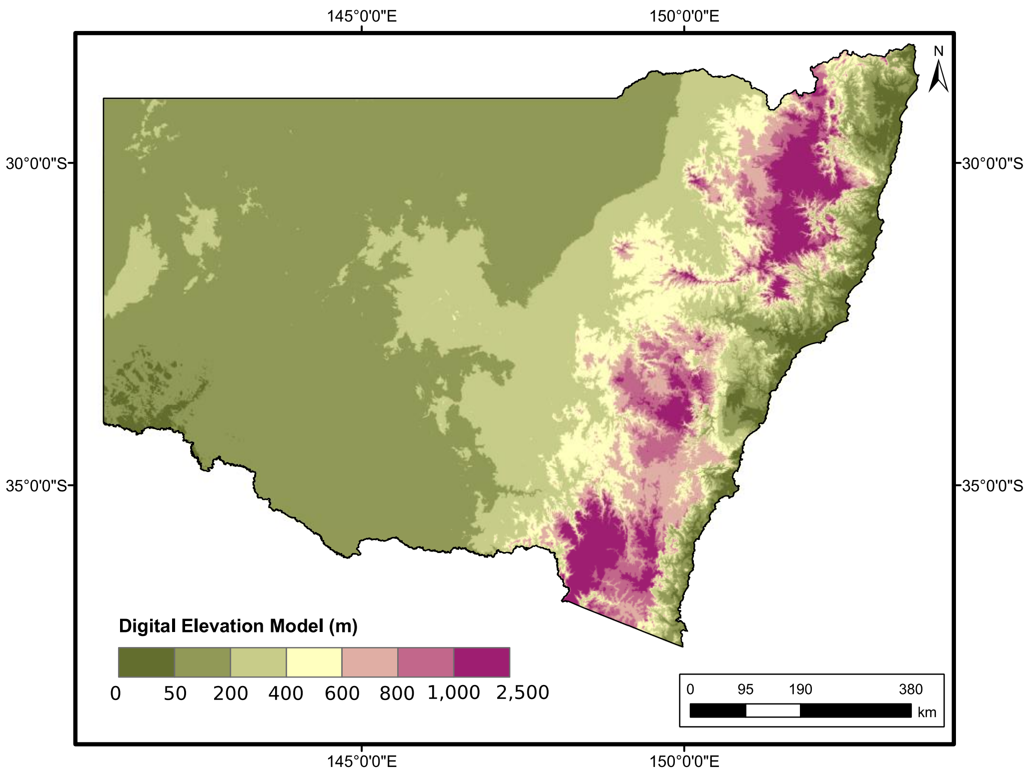

Figure 5.2 – Digital Elevation Model of New South Wales. The Great Dividing Range is shown in pink, representing areas of higher elevations in the figure *(Source: Gallant et al, 2011).*

The main river networks of New South Wales (Figure 5.3) are separated by the Great Dividing Range (Johnson, 2009). West of the Great Dividing Range is the Murray-Darling Basin that covers 75% of New South Wales and is a very important basin as it is the source of 40% of Australia's agricultural produce (Murray-Darling Basin Authority, 2020). The Murray-Darling Basin extends beyond the borders of New South Wales, encompassing large areas of Victoria, all of the Australian Capital Territory, and some of

Queensland and South Australia, comprising some 14% of Australia's total land area (Murray-Darling Basin Authority, 2020). The headwaters of the Darling River are located in the north central region of NSW, whereas the Murray River begins in the south of NSW, at the border with Victoria (Figure 5.3).

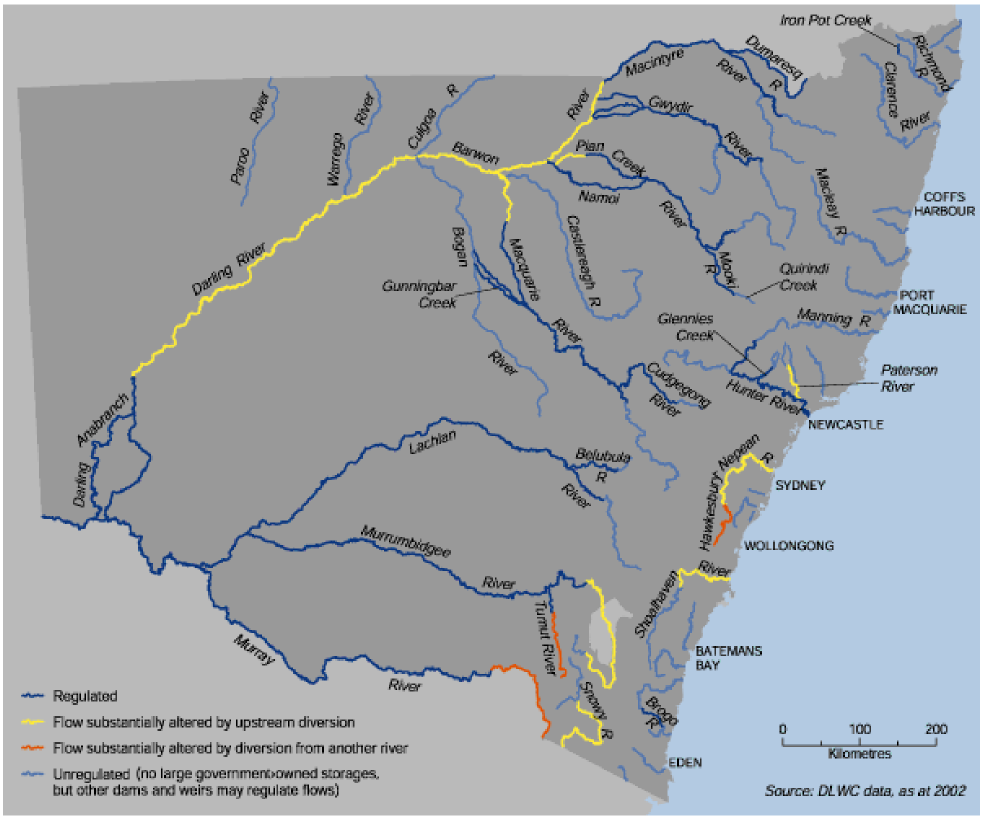

Figure 5.3 – Main river network in New South Wales (Source: State of the Environment 2003, EPA NSW).

The land use in New South Wales is mostly covered by grazing vegetation (~61%), although cropland covers approximately 17% and urban areas represent around 7% of the area (Figure 5.4). The coastal area of New South Wales is characterised by forests (including national parks) and urban development, particularly surrounding Sydney.

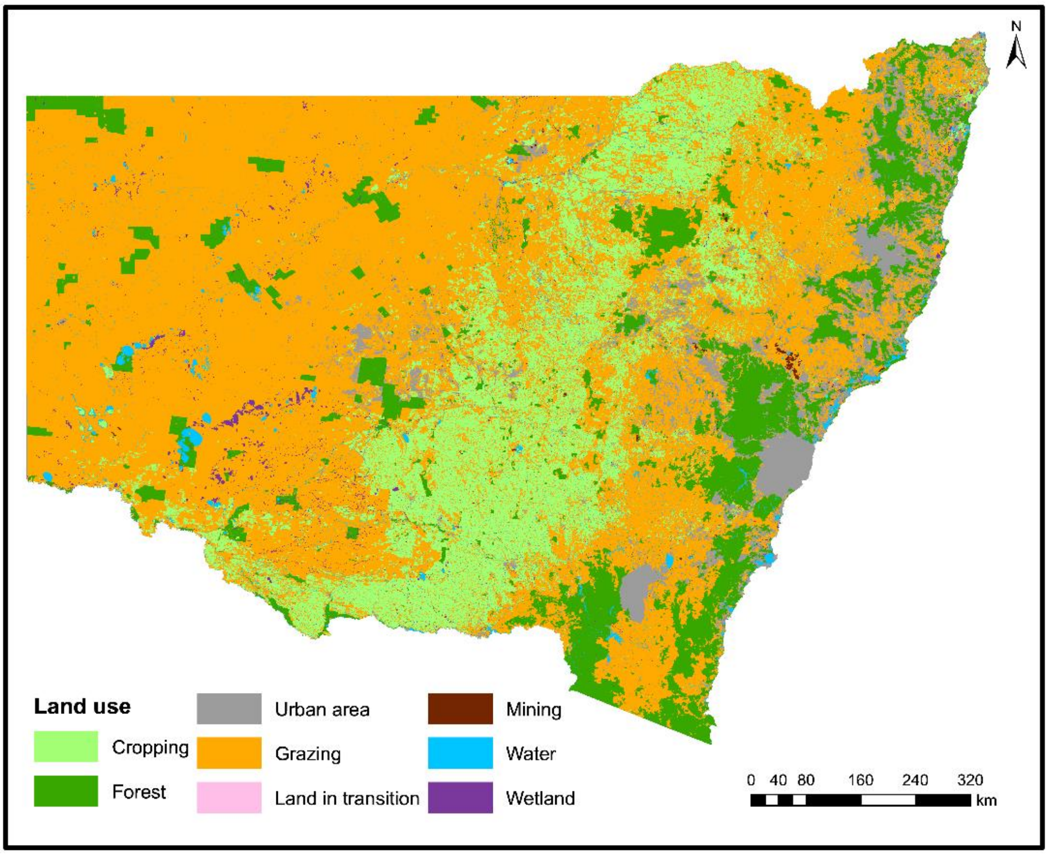

Figure 5.4 – Main land uses in NSW (*Source: Department of Planning, Industry and Environment, NSW*).

The soil texture of New South Wales, represented by the individual clay, silt, and sand fractions, are shown at two depths: 0-5 cm and 60-100 cm (Figure 5.5). The concentration of clay in the surface layer (0-5 cm) is in the same areas of the deeper layer (60-100 cm), and this happens for sand and silt as well. Clay is typically concentrated in areas where rivers are located (Figure 5.3; Figure 5.5). Sand is dominant across the state in the top 5 cm of land, as approximately 68% of the area has more than 50% of sand in its soil texture (Figure 5.5 - c). Data describing the soil texture of New South Wales was obtained from the Commonwealth Scientific and Industrial Research Organisation (CSIRO) in 3 arcsec spatial resolution (~90 m x 90 m) (Viscarra Rossel et al., 2014a, 2014b, 2014c).

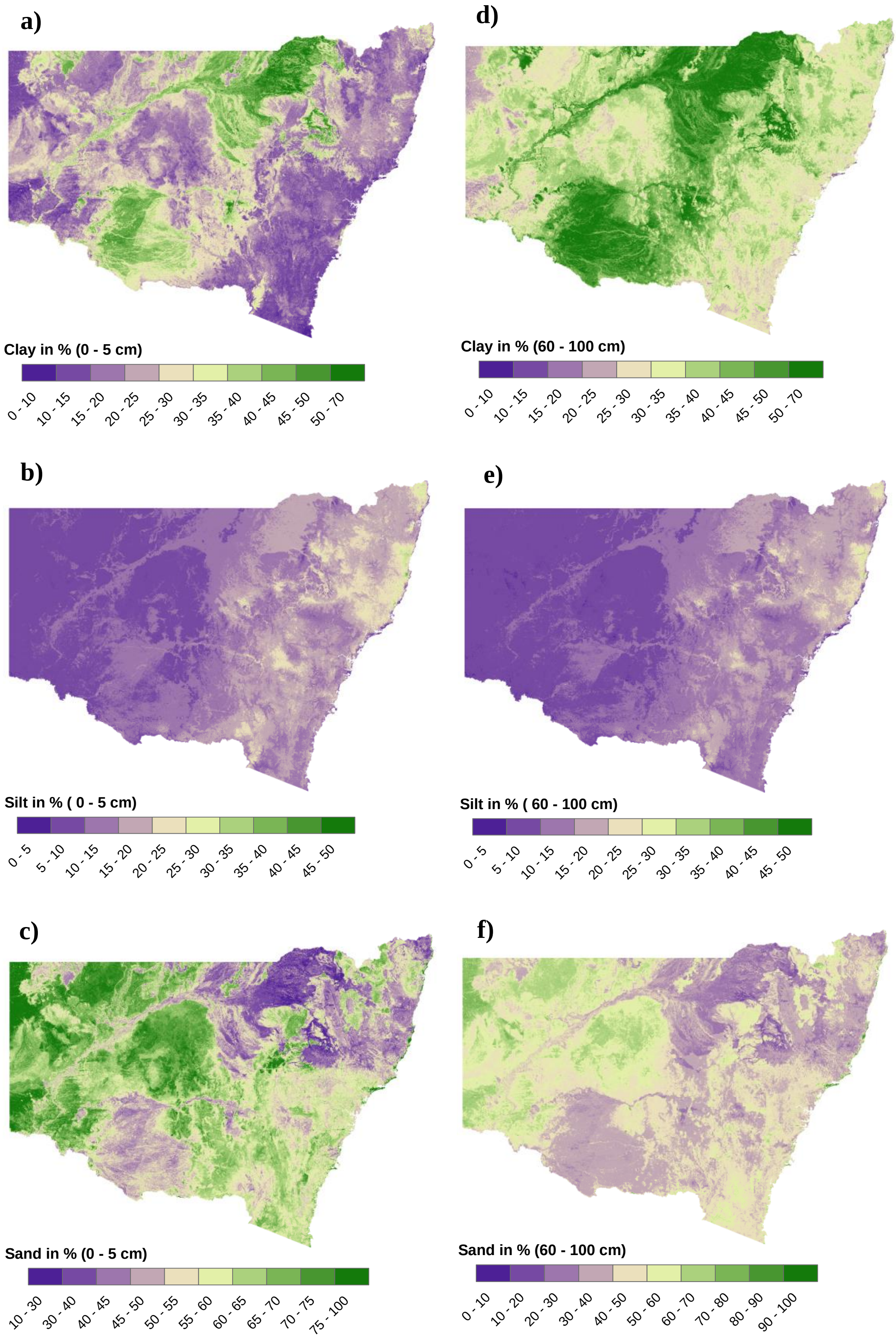
a)
Clay in % (0 - 5 cm)
0 - 10
10 - 15
15 - 20
20 - 25
25 - 30
30 - 35
35 - 40
40 - 45
45 - 50
50 - 70
d)
Clay in % (60 - 100 cm)
0 - 10
10 - 15
15 - 20
20 - 25
25 - 30
30 - 35
35 - 40
40 - 45
45 - 50
50 - 70
b)
Silt in % (0 - 5 cm)
0 - 5
5 - 10
10 - 15
15 - 20
20 - 25
25 - 30
30 - 35
35 - 40
40 - 45
45 - 50
e)
Silt in % (60 - 100 cm)
0 - 5
5 - 10
10 - 15
15 - 20
20 - 25
25 - 30
30 - 35
35 - 40
40 - 45
45 - 50
c)
Sand in % (0 - 5 cm)
10 - 30
30 - 40
40 - 45
45 - 50
50 - 55
55 - 60
60 - 65
65 - 70
70 - 75
75 - 100
f)
Sand in % (60 - 100 cm)
0 - 10
10 - 20
20 - 30
30 - 40
40 - 50
50 - 60
60 - 70
70 - 80
80 - 90
90 - 100

Figure 5.5 – Soil texture of New South Wales. a), b), c) clay, silt and sand (%) in the top layer (0-5 cm), respectively; d), e), f) clay, silt and sand (%) in the deep layer (60-100 cm), respectively *(Source: Viscarra Rossel et al., 2014a, 2014b, 2014c).*

The average rainfall for the most recent climate period (1999-2019) in New South Wales ranges from 140-1900 mm per year (Figure 5.6). The western half of New South Wales is considerably drier (less than 300 mm/year) than the coastal region of the state (more than 800 mm/year), with the average annual rainfall increasing west to east, towards the coast. More than half (58%) of the state has an average rainfall total under 500 mm per year and only 9% above 950 mm per year. The less vegetated west of NSW and the denser vegetated area along the coast (Figure 5.4) are consistent with the low annual rainfall in the west and the higher annual precipitation on the coast, respectively. Data describing the total annual rainfall for New South Wales was obtained from the AWRA model at a 0.05° resolution (~5×5 km).

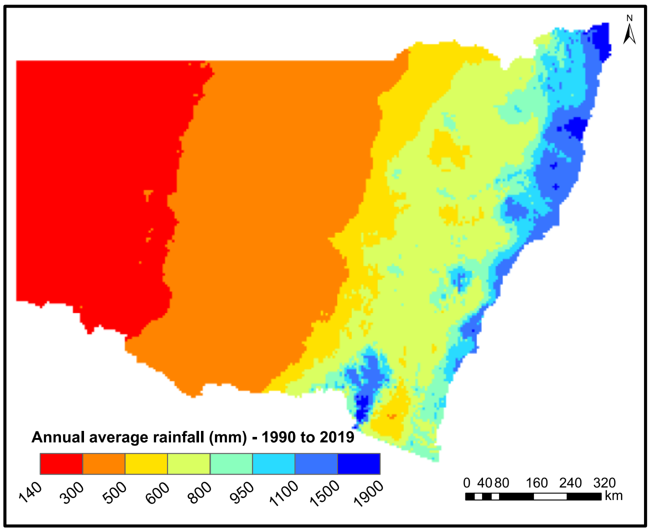

Figure 5.6 – Annual rainfall average for New South Wales (1990-2019) (*Source: AWRA*).

The average maximum temperature in NSW ranges from 9 to 30 C (Figure 5.7 – a) and the average minimum temperature varies between 0.9 and 16°C (Figure 5.7 – b). The spatial distribution of the maximum and minimum temperatures is similar, but on the coast the ocean acts as a temperature regulator, making the temperature vary less, i.e., higher minimum and lower maximum. The north-west part of the state presents the higher annual maximum values (> 27°C) (Figure 5.7 – a), and 44.5% of the state has maximum average between 18°C and 25°C. Colder temperatures are evident in the high altitudes of the Great Dividing Range, where the annual minimum average is lower than 8°C (Figure 5.7 – b), representing 12% of the state area. Data describing the maximum and minimum temperature for New South Wales was obtained from the AWRA model at a 0.05° resolution (~5×5 km) (http://www.bom.gov.au/water/landscape).

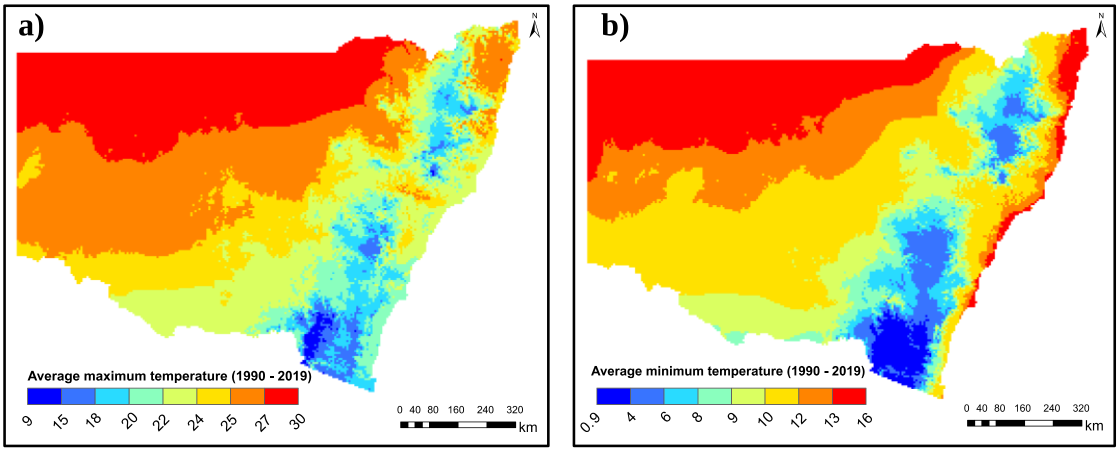

Figure 5.7 – Average maximum (a) and average minimum (b) temperatures for New South Wales (1990-2019) (*Source: AWRA*).

5.3 Materials and Methods

Soil moisture plays a key role in the hydrologic cycle and in land–atmosphere interactions. It acts as a reservoir for soil water storage and as an indicator of water availability for vegetation growth, agriculture and food production. Studies of long-term soil moisture variability are important to manage and allocate water, and to be able to develop strategies for water security (McDonough et al., 2020). Following this logic, we investigate soil moisture long-term in the state of New South Wales, Australia. We used modelled soil moisture data for the period 1990-2019 and a temporal decomposition model to compute the long-term variability of soil moisture. We then relate the long-term variability of soil moisture to the physical characteristics of the area, including elevation, temperature, rainfall and land coverage.

5.3.1 AWRA-L

The modelled soil moisture data used in this study is from the Australian Water Resources Assessment (AWRA) (http://www.bom.gov.au/water/landscape), at a 0.05° spatial resolution (an approximately 5 km by 5 km pixel). The AWRA model has been calibrated and validated against an extensive observational dataset (Frost & Wright, 2018), and for this reason it was the dataset chosen for this study. The use of the modelled outputs from AWRA is common in Australia (Frost et al., 2018), as they have been applied to numerous climatological, flood, water and agricultural studies (Hill et al., 2016; Gibson et al., 2019; Wasko & Nathan, 2019; Khan et al., 2020).

AWRA was developed from a collaboration between the Bureau of Meteorology (BoM) and the Commonwealth Scientific and Industrial Research Organisation (CSIRO) through the Water Information Research and Development Alliance (WIRADA) (Van Dijk, 2010; Viney et al., 2015). In this study we use soil moisture data from AWRA-L (Landscape), a distributed water balance model conceptualised as a small catchment and taking into consideration hydrological processes, starting from the partitioning of rainfall into interception, infiltration and runoff due to saturation or infiltration excess (Van Dijk, 2010; Viney et al., 2015; Frost et al., 2018).

AWRA-L is a grid-based model that covers the entirety of Australia at a 0.05° spatial resolution, in a daily timestep from 1911 to the present (Van Dijk, 2010). For each grid cell there are three soil layers (top: 0-10 cm, shallow: 10-100 cm, deep: 100-600 cm) and two hydrological response units (HRUs) (Frost et al., 2018). The HRUs represent the shallow rooted vegetation (grass) that reaches the two upper soil layers only (0-100 cm), and the deep rooted vegetation (trees), which have access to moisture stored in the deeper layers (0-600 cm) (Viney et al., 2015; Frost et al., 2016). AWRA-L uses climate data as input: air temperature (daily minimum and maximum) and daily precipitation from the Australian Water Availability Project (AWAP), daily solar exposure produced from geostationary satellites, solar radiation from satellite, and daily average wind speed from the Bureau of Meteorology (from 1975) (Frost et al., 2018).

AWRA-L v6.0, the version of AWRA used in this study, has 49 optimisable parameters, although 28 were fixed based on previous experience, leaving only 21 parameters for optimisation (Frost et al., 2018). The parameter optimisation aims to improve the objective function, combining the performance in accordance with streamflow, evapotranspiration and soil moisture at catchments across Australia (Figure 5.8) (Frost et al., 2018; Frost & Wright, 2018). The soil moisture calibration uses the soil moisture product from the passive Advanced Microwave Scanning Radiometer (AMSR-E) from the Earth Observing System orbiting satellite covering the period 2002-2011 (Frost & Wright, 2018).

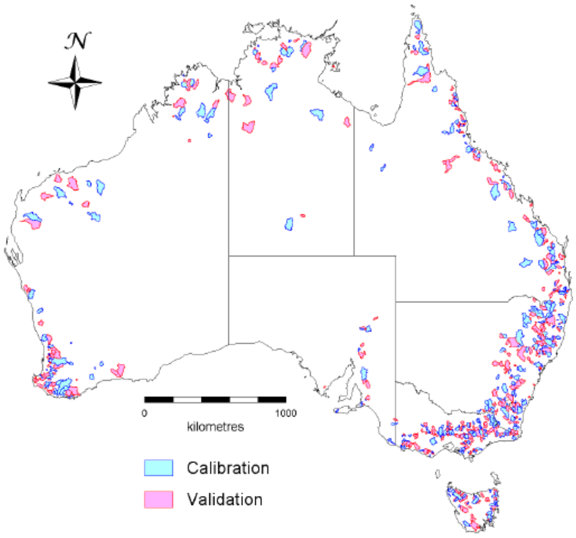

Figure 5.8 – AWRA-L calibration and validation catchments (*Source: Vaze et al., 2013*).

5.3.2 BFAST

A temporal decomposition model separates seasonal trend and noise from the temporal component, allowing the data to be analysed without the interference of abnormal wet or dry years or any possible noise. The temporal trend for soil moisture was computed using the Breaks For Additive Seasonal and Trend (BFAST) model (Verbesselt et al., 2010). BFAST determines the temporal trend of a dataset using the temporal decomposition approach from Cleveland et al. (1990), known as the Seasonal-Trend decomposition procedure (STL), which was initially proposed on a LOcally wEighted regreSsion Smoother (LOESS) (Cleveland, 1979).

For each pixel, BFAST uses an additive model (Equation 5-1) that decomposes the time series (Yt) into trend (Tt), seasonal (St), and remainder components (et) (Figure 5.9), for time (t = 1, … ,n) (Verbesselt et al., 2010; Hutchinson et al., 2015; McDonough et al., 2020).

$$Y_t = T_t + S_t + e_t \qquad (5\text{-}1)$$

The temporal trend represents a smooth change in the dataset, which is typically driven by a long-term driver such as interannual climate variability or a gradual change in land management (Verbesselt et al., 2010). The temporal trend is the component of BFAST that will be examined in this study (Equation 5-2). To determine the trend component, BFAST fits a piecewise linear trend model with break points, $t_1^*, \ldots, t_m^*$, where, $t_0^* = 0$ (Verbesselt et al., 2010).

$$T_t = \alpha_j + \beta_j t \qquad 5\text{-}2$$

For $t_{j-1}^* < t \leq t_j^*$, and where $j = 1, \ldots, m$. α_j is the intercept of the linear model and β_j is the slope of the linear trend. For each pixel, the sign and magnitude of the linear slope of Tt (Equation 5-2) represent the gradual long-term trend in soil moisture (Verbesselt et al., 2010; Hutchinson et al., 2015; McDonough et al., 2020). The statistical significance ($p=0.05$) of the long-term trend was estimated using simple linear regression for each pixel, following the analysis used by McDonough et al. (2020).

The seasonal trend typically exhibits a cyclical behavioural pattern because it is driven by seasonal changes in temperature, rainfall, and evapotranspiration. Analogous to the temporal trend, the seasonal component can vary across breakpoints but it is the same between breakpoints (Verbesselt et al., 2010). The seasonal trend breakpoints are $t_{j-1}^{\#}, \ldots, t_j^{\#}$, and $t_0^{\#}=0$. For $t_{j-1}^{\#} < t \leq t_j^{\#}$, it is assumed that:

$$S_t = \begin{cases} \gamma_{i,j} & \text{if time t is in season i, i = 1, …, s-1} \\ -\sum_{i=1}^{s-1} \gamma_{i,j} & \text{if time t is in season 0} \end{cases} \qquad 5\text{-}3$$

In Equation 5-4, s is the period of seasonality (e.g., the number of observations per year) and $\gamma_{i,j}$ indicates the effect of season i. The sum of the seasonal component, S_t across s successive times is exactly zero for $t^{\#}_{j-1}<t\leq t^{\#}_{j}$ (Verbesselt et al., 2010). This prevents apparent changes in trend being induced by seasonal breaks happening in the middle of a seasonal cycle. The seasonal term is rearranged by:

$$S_t = \sum_{i=1}^{s-1} \gamma_{i,j}\ (d_{t,i} - d_{t,0}) \qquad 5\text{-}4$$

In Equation 5-4, $d_{t,i}= 1$ when t is in season i and 0 otherwise. Therefore, if t is in season 0, then $d_{t,i}-d_{t,0} = -1$. For all other seasons, $d_{t,i}-d_{t,0} = 1$ when t is in season $i\neq0$. The remainder component is the "remaining variation in the data beyond that in the seasonal and trend component" (Cleveland et al., 1990; Verbesselt et al., 2010). Neither the seasonal component (St) or the remainder (et) were utilised in this study.

Time series decomposition methods consider that the seasonal and trend components are smooth and slow changes (interannual), while abrupt changes (intra-annual) are known as breakpoints. Abrupt changes can be characterised as disturbances, such as deforestation, urbanisation, floods and fires (Verbesselt et al., 2010). Despite BFAST having the ability to detect and characterise both slow and abrupt changes, the focus of this study is the long-term variability of soil moisture (i.e., temporal trend) and thus abrupt changes (i.e., the breakpoints) will not be considered.

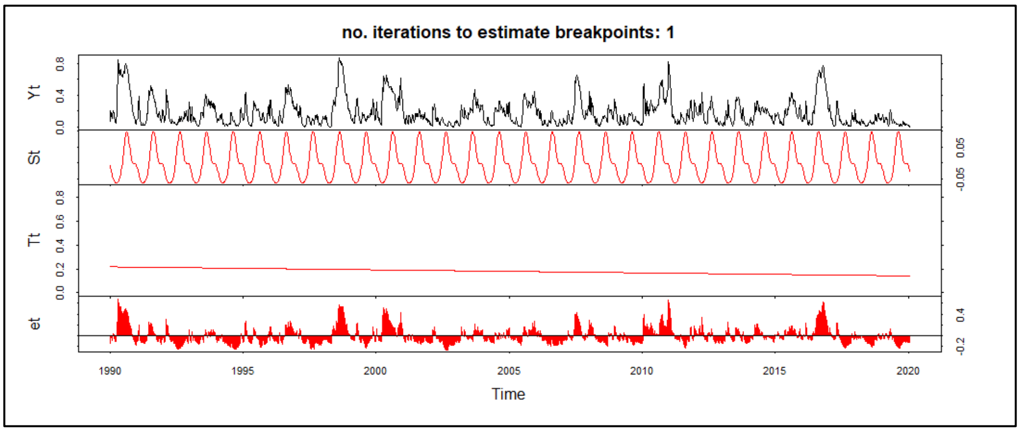

Figure 5.9 – A BFAST generated graph for one pixel of soil moisture. This figure shows the profile soil moisture (0-100 cm) from 1990-2019 with the raw data (Yt), seasonal component (St), temporal trend (Tt), and remainder (et).

The BFAST model has been mainly applied to understand the long-term trend in vegetation from satellite data (Verbesselt et al., 2010; Forkel et al., 2013; Watts & Laffan, 2014; Hutchinson et al., 2015). BFAST was also applied to detect breaks (abrupt changes) in vegetation maps (Buchhorn, 2020), and a study in the United States has recently applied BFAST to investigate the temporal trend of soil moisture in the Great Plains, USA (McDonough et al., 2020).

5.4 Results

The results of the long-term soil moisture regional variability in the state of New South Wales for the period 1990-2019 for surface (0-10 cm) and profile (0-100 cm) layers are shown below. Profile and surface moisture, maximum temperature, minimum temperature and precipitation long-term variability, represent the temporal trend term calculated using the decomposition model (BFAST).

5.4.1 Surface soil moisture

The average surface soil moisture for the study period (1990-2019) varies from 0.3 to 20% (Figure 5.10). Low values of surface soil moisture are prominent throughout New South Wales, as more than half (63.5%) of the area has surface soil moisture values under 3%. The semi-arid western part of NSW presents low values of precipitation (< 500 mm/year) (Figure 5.6), which is consistent with low values of surface soil moisture (< 3%) (Figure 5.10). This is also true for temperature distribution in the west, where both maximum (Figure 5.7-a) and minimum (Figure 5.7-b) have high temperature values (25-30°C and 10-16°C, respectively) corresponding to low surface soil moisture (< 3%) areas (Figure 5.10).

The surface soil moisture pattern (Figure 5.10) coincides with the major hydrological features of the state (Figure 5.3), where wetter areas (15-20% average surface soil moisture) correspond to the headwaters of the Darling River in the north-central part of New South Wales. Regions that have higher surface soil moisture content, like the headwaters of the Darling River and the south-west (8-10% surface soil moisture), coincide with areas of high surface (0-5 cm) clay content (> 45%) (Figure 5.5 - a). Clay has higher water-holding capacity, which can be related to the higher surface soil moisture content found in those areas. Sand, on the other hand, is a very porous soil, and in places where the surface sand concentration (0-5 cm) is high (> 60% of sand) (Figure 5.5 - c) the average surface soil moisture is low (< 3%). Besides the fact that in the west, where low surface soil moisture values match with low precipitation and high temperature values, surface soil moisture is impacted overall by hydrological features and soil texture in the top 5 cm (Figure 5.3).

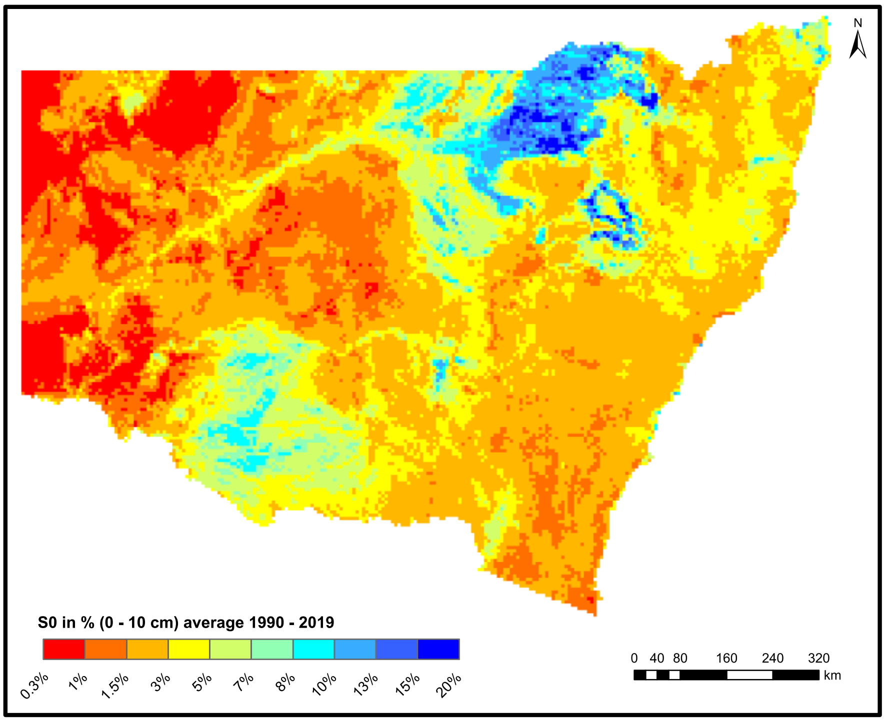

Figure 5.10 – Average surface (0-10 cm) soil moisture (in percentage) for the 30-year study period (1990-2019).

The long-term variability of surface soil moisture (0-10 cm) (Figure 5.11) in NSW is negative across 96% of the area, which indicates that there is a drying tendency for almost the whole state, with values between -0.05 to 0% over 30 years. Only 4% of NSW has a wetting surface soil moisture variability (between 0 and 0.06% over 30 years). The bigger concentration of positive trends is in the north-east, near the coast, and the rest are small pockets spread over NSW (Figure 5.11).

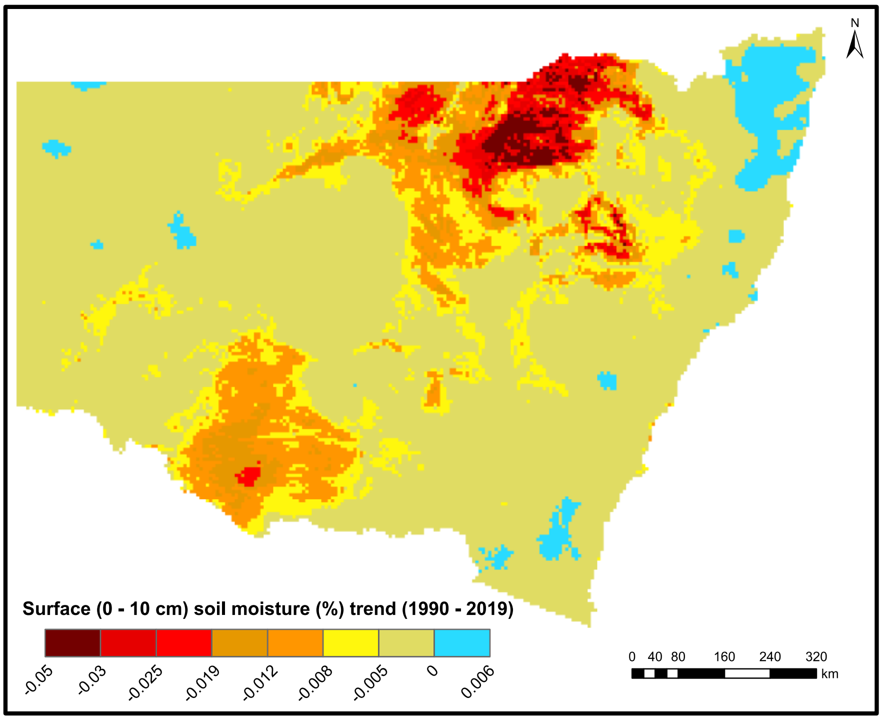

Figure 5.11 – Long-term variability in surface (0-10 cm) soil moisture (in percentage) over the study period (1990-2019).

The largest negative long-term variability (i.e., drying trend) (between -0.03 and -0.05% over 30 years) is located north-west of the Great Dividing Range (Figure 5.2), which corresponds to the headwaters of the Darling River. This area has high surface soil moisture content (8-20%) (Figure 5.10), and represents a large area covered with agricultural (cropping) land use (Figure 5.4). All other areas immediately west of the Great Dividing Range that are also covered by cropping (Figure 5.4) did not exhibit high values of the drying soil moisture trend, so it cannot be concluded that agricultural cropping is a substantial driver of soil drying. Interestingly, the south-west, as in the head waters of the Darling River (north-west of NSW), has high values of surface soil moisture content (5-10%) (Figure 5.10) that correspond to high rates of drying soil moisture (-0.008 and -0.025% over 30 years), which could point to higher values of soil moisture that have higher chances of drying.

5.4.2 Profile soil moisture

The average profile (0-100 cm) soil moisture for the thirty-year period of study (1990-2019) ranges from 5-55% (Figure 5.12). The profile soil moisture distribution closely follows the rainfall distribution pattern (Figure 5.6), where the western part of the state is dry and New South Wales gets wetter heading towards the eastern coast. From the rainfall distribution map (Figure 5.6) the western part of NSW has an annual average of 140 to 300 mm of rainfall, which corresponds to the area of 3-10% of average profile soil moisture (Figure 5.12). Approximately half (57%) of the area of New South Wales has less than 15% of profile soil moisture content, and only 17% is above the 30% profile soil moisture content. As well as in surface soil moisture, lower values of profile soil moisture can be associated with areas of high sand content (> 60%) (Figure 5.5 - f). Areas with a high concentration of clay (> 50%) (Figure 5.5 - d), like the heading of the Darling River (north-central) (Figure 5.3), correspond to areas of high values of profile soil moisture (10-20%).

In general, areas with forest (Figure 5.4), e.g., areas near the coast, are coincident to areas with higher profile soil moisture values (> 45%). The higher permeability of the forest soils summing to the lower soil evaporation, when comparing to non-forested soils, contribute to higher profile soil moisture in those areas (Craib, 1929). The high permeability of forested soils enables a larger volume of water to infiltrate and be stored in the soil profile, in comparison to sandy soils which have a low water-holding capacity and high percolation. The low values of soil moisture located in areas of sandy soil, and the high values of soil moisture associated with areas of high vegetation density, were also observed in the Upper Colorado River (USA) by Tang and Piechota (2009).

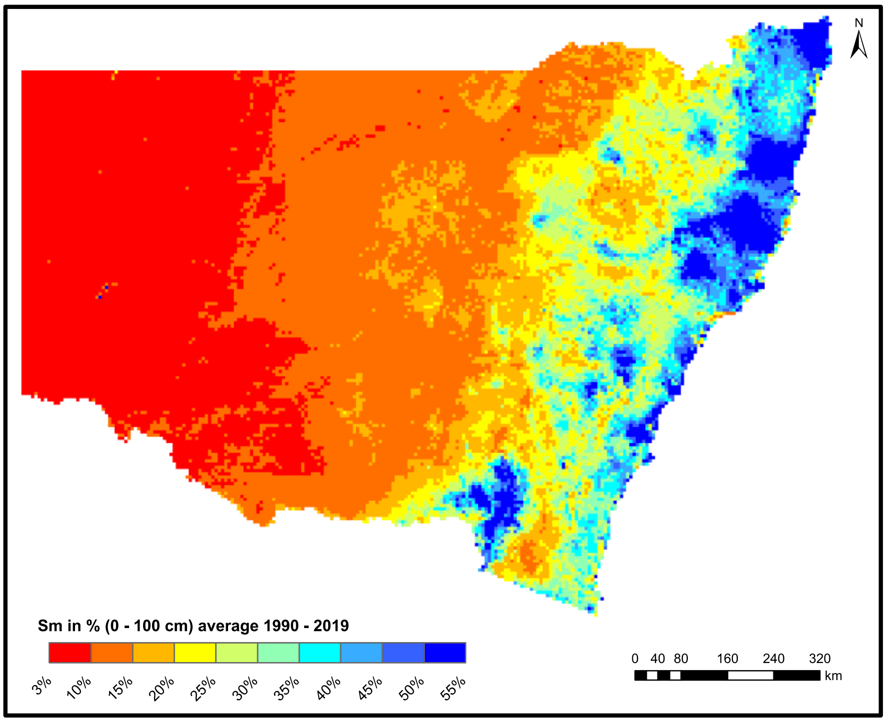

Figure 5.12 – Average profile (0-100 cm) soil moisture (in percentage) for the 30-year study period (1990-2019).

The long-term variability of profile soil moisture (1990-2019) is negative (drying) for 78% of NSW (Figure 5.13). As it happens to surface soil moisture, the majority of the state presents a drying profile soil moisture tendency; however, the spatial pattern of the long-term variability of profile soil moisture substantially from the spatial pattern of the average profile soil moisture. The only region that exhibits similar behaviour between the profile soil moisture and the surface soil moisture is on the north-east coast of the state, where both presented a positive trend, 0-0.08% for profile and 0-0.006% for surface over the study period. The higher values of profile soil moisture drying trend (-0.11 to -0.3 % over 30 years) are found in the high altitudes of the Great Dividing Range (600-2500 m) (Figure 5.2).

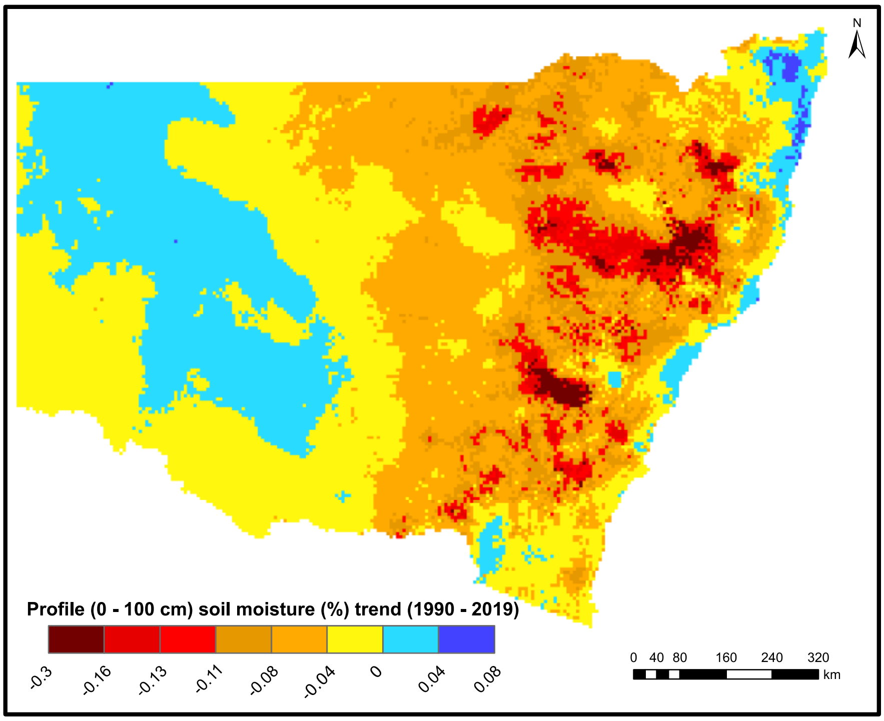

Figure 5.13 – Long-term variability profile (0-100 cm) soil moisture (in percentage) over the study period (1990 -2019).

5.4.3 Temperature and precipitation

The long-term variability of the maximum temperature is positive for all New South Wales (Figure 5.14 - a), which means that there was an increase in the maximum temperature for the study period (1990-2019). In general, along the coast the increase in maximum temperature was milder (0.1 to 1.1°C over 30 years) which can be related to the moderating influence of the ocean. Although in the west there is a pocket of mild increase that is not related to the ocean.

The long-term variability in minimum temperature is positive for 95% of the state (Figure 5.14 - b), which indicates that the minimum temperature experienced by NSW is warming. The rate by which the minimum temperature is increasing is lower than the rate of increase in the maximum temperature, and this would generate a temperature amplitude (difference between the maximum and minimum temperature) increase. Seven pockets of negative trend appear in NSW, indicating that the minimum temperature is cooling in these small regions of NSW. The largest negative trend pocket, in the middle southwest, corresponds to a cropping area (Figure 5.4) in the mid-altitudes (50-200 m) (Figure 5.2). These negative values indicate that there was a decrease in the minimum temperature which corroborates climate change predictions of more extreme temperatures (Meehl & Tebaldi, 2004; Sillmann & Roeckner, 2007; Stott, 2016).

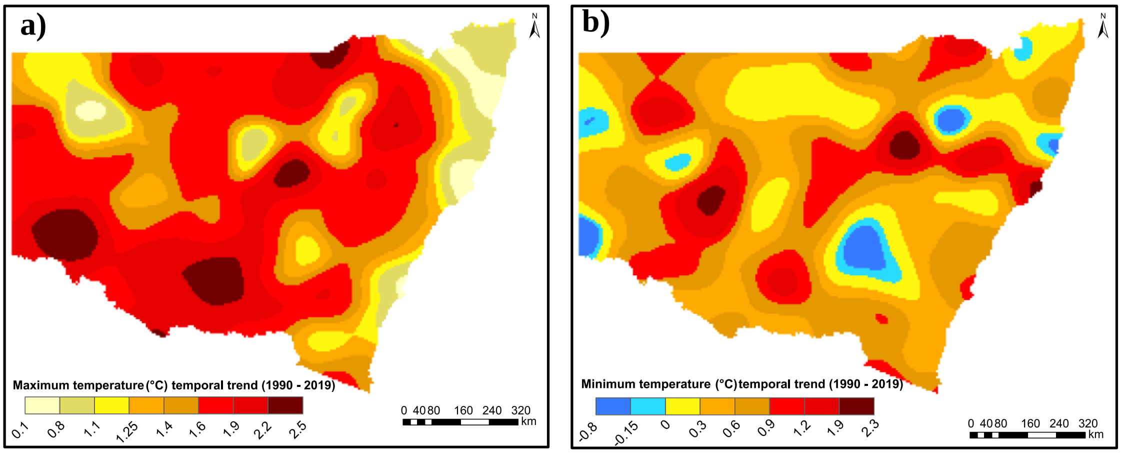

Figure 5.14 – Long-term variability of maximum (a) and minimum (b) temperature (°C) over the study period (1990-2019).

For the precipitation long-term variability, 91% of the results are negative, which indicated a decrease of precipitation in this period (1990-2019) (Figure 5.15). The higher values for the positive trend are found on the northern part of the coast, where the average rainfall is already higher (> 1100 mm/year) (Figure 5.6). Some of the western parts of the state that get 140 to 300 mm of rainfall per year (Figure 5.6), have the highest drying trend (-0.5 to -0.8 mm/30 years).

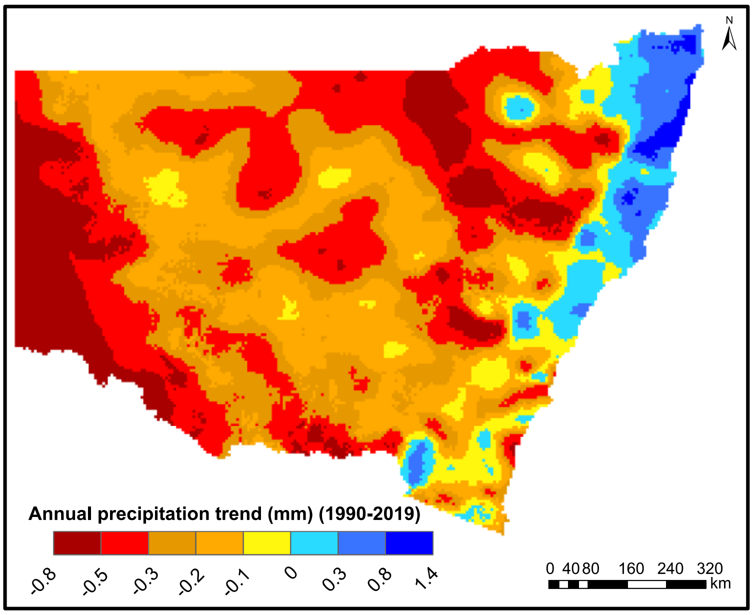

Figure 5.15 – Long-term variability of precipitation (mm) over the study period (1990-2019).

High long-term variability values in maximum temperature (1.9 to 2.5°C over 30 years) (Figure 5.14) in the south-west of NSW (Figure 5.11) are coincident to an area of high surface soil moisture drying trend (between -0.012 and -0.025% over 30 years). Apart from this area, there is no other clear spatial pattern between surface soil moisture and maximum or minimum temperature trend. Comparing to profile soil moisture, there are two regions of positive profile soil moisture trend – the west of NSW and the north-east coast – that are coincident with an area of low increase in maximum temperature (0.1 to 1.8°C over the study period) (Figure 5.14).

An area of negative precipitation long-term variability ranging from -0.3 to -0.8 mm over 30 years. (Figure 5.15), corresponding to the headwaters of the Darling River, is in accordance with the largest negative (drying) surface soil moisture trend (between -0.03 and -0.05% over 30 years) (Figure 5.10). In the north-east, the increase in precipitation trend (0.3 to 1.4 mm over 30 years) (Figure 5.15) is related to a positive (wetting) surface soil moisture long-term variability (Figure 5.10). The increase in precipitation (Figure 5.15) near the coast spatially agrees with the positive trend of profile soil moisture, although the area with a positive trend in precipitation is larger. A decrease in precipitation (-0.3 to -0.8 mm over 30 years) (Figure 5.15) in high altitudes of the Great Dividing Range (600-2500 m) (Figure 5.2) corresponds to the higher values of profile soil moisture drying variability (-0.11 to -0.3% over 30 years) (Figure 5.13). This can indicate an influence of precipitation on soil moisture in high altitudes. Interestingly, in the west of NSW there is an area of increase in profile soil moisture (large blue area in Figure 5.13) that corresponds to an area of decrease in precipitation, -0.1 to -0.3 mm over the study period (Figure 5.15).

5.5 Discussion

5.5.1 Surface soil moisture long-term variability

The results found for surface soil moisture agree with what has been previously reported for the region in global studies (Dorigo et al., 2012; Albergel et al., 2013; Deng et al., 2020). Using data from the AWRA-L model at a 0.05° pixel resolution (approximately 5 km), a negative (drying) trend in surface soil moisture (0-10 cm) was identified for 96% of NSW (Figure 5.11). Similarly, Dorigo et al. (2012) and Albergel et al. (2013) reported a drying trend in southeastern Australia, a region which encompasses NSW, using surface soil moisture at a spatial resolution ranging from 27 km to 111 km for the period 1988 to 2000. Dai (2011) also found a long-term drying trend for eastern Australia (1950-2008) using a drought index that was shown to be closely related to soil moisture.

Although 96% of NSW demonstrated a drying surface soil moisture trend, the northern coast of NSW showed a positive (wetting) trend, as did four pockets in the west, and seven pockets along the coast. Those areas of wetting trends were not large and were probably masked by the larger spatial resolution of the data used by Dorigo et al. (2012) and Albergel et al. (2013). It is also worth mentioning that Dorigo et al. (2012) used three datasets to examine soil moisture trends, and although two showed a drying trend for south-east Australia, the merged microwave surface soil moisture dataset (SM-MW) indicated a wetting trend. Despite this contradiction, the majority of the studies reported a drying trend for south-eastern Australia.

In a recent global study using surface soil moisture (0-7 cm) from the ERA Interim reanalysis dataset (Dee et al., 2011) at a spatial scale of 55 km for the period 1979-2017, Deng et al. (2020) reported a wetting trend along the coast of New South Wales, which aligns better with what was found in this study, which is a wetting trend in small regions along the northern coast of NSW (Figure 5.11). However, Deng et al. (2020) result differs from the drying trend reported by Dorigo et al. (2012) and Albergel et al. (2013) for the area. This difference could be attributed to the period of study utilised, 1988-2000 (Dorigo et al., 2012; Albergel et al., 2013) versus 1979-2017 (Deng et al., 2020), but not to the soil moisture data or spatial resolution, since the three studies used the ERA Interim reanalysis dataset.

The surface soil moisture in areas of higher average surface soil moisture content (> 8%) i.e., north-west and south-west (Figure 5.10), presented the strongest drying trends (-0.012 to -0.05% over 30 years) (Figure 5.11). This drying trend in the north-west corresponds to a cropping area that is located at the headwaters of the Darling River, therefore, it can affect local agriculture and flow in the downstream rivers, which could result in serious consequences for agriculture and for people who live close to the river. The role of soil moisture on streamflow and flood was shown to be crucial (Ivancic & Shaw, 2015; Bennett et al., 2018; Wasko & Nathan, 2019). In the United States, Ivancic and Shaw (2015) reported that very heavy rainfall resulted in 36% of very high discharge across watersheds in the country, and that this percentage decreased to 13% when the soil got drier. A study in Australia conducted by Wasko and Nathan (2019) found visual and statistical correlation between decrease in peak flow and decrease in soil moisture and, in addition to that, they pointed to soil moisture as the main influence on observed flood trends. Soil moisture levels below normal characterise an agricultural drought with consequence of crop failure (Mishra & Singh, 2010; Kiem et al., 2016). Agricultural drought takes longer to develop and to recover from compared to a meteorological drought that is caused by precipitation deficit (Mishra & Singh, 2010; Lockart et al., 2020).

Extreme weather caused by the increase in temperature has shown to be linked with soil moisture deficit by either high temperature leading to decreasing soil moisture trends (Mueller & Seneviratne, 2012; Deng et al., 2020) or soil moisture deficit leading to hotter temperatures (Alexander, 2011). In this study, there was an increase in the maximum temperature in NSW and an increase in the average minimum temperature in 95% of the state territory. The soil moisture long-term variability showed a drying trend in 96% of NSW for the surface layer (0-5 cm) and in 78% of the NSW for the profile layer (0-100 cm). Despite the consistency of a dominant increase in temperature in NSW and a predominant decrease in soil moisture in the studied period, no obvious spatial correlation of temperature and soil moisture trend (surface and profile) was observed in this regional scale study.

5.5.2 Profile soil moisture long-term variability

The profile soil moisture trend is mostly negative in NSW (Figure 5.13), covering 78% of the area. However, there are two areas that presented a wetting trend, one on the north coast and a large area in the west. On the north part of the coast, the wetting soil moisture trend (0 to 0.08% over 30 years, Figure 5.13) corresponds to a wetting precipitation trend (0 to 1.4 mm over 30 years, Figure 5.15). The precipitation trend also agrees with the profile soil moisture trend in the area surrounding the Great Dividing Range, from north to south, where high rates of drying trend (-0.11 to -0.3% over 30 years, Figure 5.13) correspond to high rates of drying precipitation (-0.3 to -0.8 mm over 30 years, Figure 5.15). However, in the west there is an opposite behaviour between soil moisture and precipitation. This area goes from north-west to south-east and corresponds to a slow increase in profile soil moisture (0 to 0.04% per 30 years, Figure 5.13), and a decrease in precipitation (0 to -0.2 mm per 30 years) (Figure 5.15). The relationship of precipitation and profile soil moisture for the study area is thus ambiguous.

This area of a wetting profile soil moisture trend in the west (large blue area in Figure 5.12) could be linked to the maximum temperature trend (Figure 5.14). Especially in the north-west (top left), which has a low rate of increase (-0.1 to -1.4 C over 30 years) when compared to its surroundings (-1.8 to -2.5°C over 30 years). Despite the contrary trend, soil moisture increasing and temperature increasing, it is possible that this area, which is less influenced by the ocean, has more available water in the soil because it is not being depleted by high evapotranspiration rates caused by high temperatures. To summarise, profile soil moisture is increasing at a low rate (0 to 0.04% over 30 years) in the west (Figure 5.13) and this area corresponds to a decrease in precipitation and an increase in temperature, which is opposite to what is expected. However, both temperature and precipitation showed trends at lower rates compared to their surroundings, where the profile soil moisture is drying. This could indicate that it is necessary that higher rates of temperature increase and precipitation decrease for the profile soil moisture to dry.

The profile soil moisture wetting trend on the coast and in the west disagree with the drying trend found by Albergel et al. (2013) for profile soil moisture (0-100 cm) for the whole of New South Wales in two datasets. The difference in the results could be due to the period used by Albergel et al. (2013), 1988 to 2000, or due to the spatial resolution of the dataset used (ERA ~ 80 km and MERRA 55 km latitude by 74 km longitude) that could be masking the area corresponding to the wetting trend. To mask the wetting trend on the coast is a possibility, but the wetting trend in the west occupies a large area, larger than the dataset resolution, so it is unlikely that it would be masked.

A wetting trend in the north-west of NSW was detected by Wasko et al. (2021); it goes from west to east, stopping before the Great Dividing Range, and a discreate wetting trend was found on the coast. The wetting trend in the west for this study overlaps with the western part of Wasko et al. (2021), and then the wetting trend continues towards the south and towards the east, respectively. The difference in the study result is likely to be related to the period analysed by Wasko et al. (2021), 1960 to 2017, rather than the dataset, which is the same (AWRA-L, 5 km resolution). Studies that analysed the temperature or soil moisture trend using different time windows revealed considerable differences in their results (Shi et al., 2016; Stalenberg et al., 2018; Deng et al., 2020).

A study conducted in two catchments (Merriwa and Krui) located in the Hunter region (north-west NSW) found a strong correlation between cumulative deviation rainfall (from BoM stations) and profile soil moisture (from AWRA-L) (Gibson et al., 2019). They applied the Augmented Dicky-Fueller test and did not find any significant trend for profile soil moisture (0-100 cm) for the catchments in the period analysed (1908-2015) (Gibson et al., 2019). However, the catchments are located in an area that corresponds to a profile soil moisture drying trend in this study. This difference in soil moisture trend between studies could be either due to the method Gibson et al. (2019) used, to the different period they analysed or because they used catchment averages calculated from grid cell values.

5.5.3 Comparison of surface and profile soil moisture long-term variability

The surface (0-10 cm) and profile (0-100 cm) soil moisture long-term variability presented in this study (1990-2019) revealed differences in spatial distribution (Figure 5.11 and Figure 5.13), although both were dominated by a general drying trend. The strongest drying trends are located south-west and north-west for surface soil moisture and in the Great Dividing Range area, from north to south, for profile soil moisture. In a global study, Albergel et al. (2013) identified root-zone (0-100 cm) and surface (0-7 cm) soil moisture trends (1988-2010) with similar spatial distribution. Using soil moisture reanalysis data (ERA-Land and MERRA), Albergel et al. (2013) found marked drying trends in the United States, Mongolia, and south-eastern Australia, and pronounced positive trends in northern Canada and north-east Siberia for both root-zone and surface soil moisture. The fact that this study identified the surface soil moisture trend and profile soil moisture trend in different areas could be due to differences in the spatial resolution of data. The finer spatial resolution in this study (5 km) compared to the coarser-scale data utilised by Albergel et al. (2013) (27 km, 55 km and 80 km) could reveal local and regional trends driven by small-scale land–atmosphere interactions and microclimate phenomena that are often masked by spatial data with larger scales.

This study analysed both surface and profile soil moisture layers because the mechanisms governing them are different (Brocca et al., 2009; Cai et al., 2009; Albergel et al., 2013). The profile soil moisture describes more processes than the surface, and it is a better indicator of moisture changes in the soil (Albergel et al., 2013). The profile soil moisture has a longer memory of what happens in the soil and it can represent the vegetation (Cai et al., 2009; Santos et al., 2014). Surface soil moisture is affected by quick drying and rewetting (Cai et al., 2009; Albergel et al., 2013), which makes the surface soil moisture highly spatio-temporally variable (Brocca et al., 2009). The surface soil moisture represents climatic processes because the fluxes of mass and energy with the first layer of the atmosphere occur there (Brocca et al., 2009). The surface layer is captured by the remote sensing data, which facilitates comparison of the results with global studies (Dee et al., 2011; Liu et al., 2011; Dorigo et al., 2012; Albergel et al., 2013; Dai, 2013; Tian et al., 2019). To sum up, analysing the soil moisture long-term variability in both surface (0-10 cm) and profile (0-100 cm) layers is important, since the first is a better representation of atmosphere–land processes and the second of vegetation.

5.5.4 Linking soil moisture to other climate variables

There is general agreement that there has been a global increase in temperature over recent decades (Sheffield & Wood, 2008a; Dai, 2011; Deng et al., 2020), and a similar result was found for NSW in this study. The average maximum temperature for NSW increased for the entire state for the period 1990-2019 (Figure 5.14 - a), whereas the increase in the average minimum temperature was dominant across the state as well (95%) (Figure 5.14 - b). Many studies have highlighted the close relationship of temperature and soil moisture trends (Alexander, 2011; Mueller & Seneviratne, 2012; Deng et al., 2020; McDonough et al., 2020). The soil moisture long-term variability in NSW is in accordance with temperature variability, since 96% of NSW demonstrates a drying surface soil moisture trend and 78% reveals a drying trend in profile soil moisture. The increase in average maximum and minimum temperatures could be leading to an increase in soil evaporation, thus depleting a larger volume of available water from the soil. Drier places, such as the west of NSW, have evaporation limited by soil moisture, whereas humid places, such as coastal NSW, experience evaporative regimes regulated by net radiative energy (Seneviratne et al., 2010; Alexander, 2011; Lo et al., 2021).

Despite this consensus on the relationship between temperature and soil moisture, there was no obvious visual relationship between the spatial distribution of the average minimum temperature trend and soil moisture trend (surface and profile) in this study. However, the average maximum temperature trend (Figure 5.14) and the profile soil moisture trend (Figure 5.13) appeared to have a spatial relationship. Although the trend in average maximum temperature trend is positive for all of NSW, which means that NSW is experiencing hotter extreme temperatures, places with lower trend values – i.e., the rate of the maximum temperature increase is slower – are coincident with wetting profile soil moisture trends. The areas that exhibit a wetting profile soil moisture trend encompass a large area in the west of NSW, which spans from the north-west to the south-east and the north-east coast. It is possible that in this area, especially towards the west that is less influenced by the ocean, there is more water available in the soil due to lower evapotranspiration rates compared to the rest of NSW (which is experiencing higher evapotranspiration rates, due to a larger increase in the maximum temperature trend over the study period).

In numerous global studies, precipitation has also been identified as having a substantial influence on the soil moisture trend (Mueller & Seneviratne, 2012; Feng & Zhang, 2015; Deng et al., 2020). In the temporal period examined in this study (1990-2019), NSW underwent a decrease in precipitation throughout almost all of the state (91%), except for the northern coast (Figure 5.15). A similar pattern occurred in the surface (Figure 5.11) and profile (Figure 5.12) soil moisture trends, with a decrease in 96% and 78% of NSW, respectively. In comparison, Wasko et al. (2021) found a wetting trend in precipitation in the northern half of NSW, except for some spots of drying trend mainly near the coast.

Apart from both precipitation and soil moisture presenting a decreasing trend, there was no clear relationship between the spatial distribution of the precipitation trend and the surface or most of the profile soil moisture trend in this study. Profile soil moisture and precipitation trends are spatially related in the northern part of the coast, where both presented a wetting trend, 0 to 0.08% over 30 years for the profile soil moisture trend (Figure 5.13) and 0 to 1.4 mm over 30 years for the precipitation trend (Figure 5.15). Also, in the higher peaks (> 800 m) of the Great Dividing Range (Figure 5.2), profile soil moisture trend and precipitation trend spatially agree, especially in regions of stronger drying trends, -0.11 to -0.3% for profile soil moisture and -0.3 to -0.8 mm for precipitation. In comparison, Wasko et al. (2021) found a wetting trend in precipitation in the northern half of NSW, except for some spots of drying trend mainly near the coast. Again, this difference is probably due to the different time window used in their studies i.e., 58 years versus 30 years, which can generate considerable differences in trend results (Shi et al., 2016; Stalenberg et al., 2018; Deng et al., 2020). Deng et al. (2020) highlighted that the persistence of a global drying trend in soil moisture points to a future dominated by a drying trend. Sheffield and Wood (2008a) identified that temperature was increasing for the period 1950-2000 and that its effect on drought was also increasing, especially in the later years, despite precipitation's main role in drought.

It is worth mentioning that all long-term variabilities shown here – surface soil moisture, profile soil moisture, minimum temperature, maximum temperature and precipitation – are significant ($p<0.05$) and were calculated using a temporal decomposition analysis. The BFAST model (Verbesselt et al., 2010) decomposes the raw data into seasonal pattern, noise and trend components. This method helps to analyse the temporal trend without the interference of abnormal wet or dry years or any possible noise in the dataset (McDonough et al., 2020). All other studies used in the discussion section applied other methods to calculate the trends that did not account for the decomposition of the raw data. Had abnormal wet or dry years been considered (i.e., the breakpoints) the temporal trend (Tt) would have resulted in a shorter period and a steeper inclination of Tt (Figure 5.9). The BFAST model considers an abnormal event as a breakpoint, thus the trend would have been cut into a smaller period. Because of that, it would not have been possible to analyse a long-term variability, and this shorter trend would not have represented the characterisation of the gradual change in soil moisture in NSW. For instance, 2007 was an abnormal wet year due to an event in June, known as the Pasha-Bulker storm, and if taken into account, this event would have influenced the result of the long-term variability of soil moisture and it could have masked a drying trend.

5.6 Conclusion

Uncertainties about future water availability is one of the main concerns behind the study of long-term soil moisture variability. The objective of this study was to understand the surface and profile soil moisture dynamics, the long-term variability and the drivers of this change in NSW to enable better future water management and food security. To do this, we investigated the long-term regional soil moisture variability in the state of New South Wales in both surface (0-10 cm) and profile (0-100 cm) layers for the period 1990-2019 and compared it to physical characteristics of NSW, e.g., land use, elevation, hydrography, soil composition, trends in temperature (maximum and minimum) and precipitation trends.

A predominance of soil moisture drying trends in New South Wales was found for this period (1990-2019) in the surface and profile layer, in 96% and 78% of NSW, respectively. Even though both layers were dominated by a drying trend, they were not spatially correlated. The surface layer appeared to be related to hydrological components and soil composition, whereas the profile soil moisture appeared to correlate better with trends on maximum temperature and precipitation. The study that explored trends in soil moisture in both profile and surface layers (Albergel et al., 2013) found similar spatial behaviour between them. This study was made at a global scale, i.e., using a coarser dataset (25-80 km), whereas here it was applied at a finer scale (5 km), which showed local and regional trends driven by small-scale land–atmosphere interactions and microclimate phenomena that were probably masked by spatial data in the global study, i.e., at larger scales.

Surface soil moisture had a stronger drying trend in areas of higher surface soil moisture content, i.e., it dried more in areas that had more moisture. The area of stronger surface soil trends corresponds to a cropping area and to the headwaters of the Darling River, in the north of NSW, just west of the Great Diving Range. This could result in lower flow in downstream rivers, which could have serious consequences for agriculture and for people who live close to the river, as soil moisture was shown to have an important role in streamflow (Ivancic & Shaw, 2015; Bennett et al., 2018; Wasko & Nathan, 2019).

An obvious spatial correlation between the profile soil moisture trend and other physical characteristics was not identified. In some areas of NSW, we found that maximum temperature trend and precipitation trend were spatially correlated with profile soil moisture trend. Positive profile soil moisture trends agreed with an increase in precipitation on the coast, and negative profile soil moisture trends corresponded to decreased precipitation in the Great Dividing Range. In the west, however, a large area with a slight profile soil moisture wetting trend was the opposite of the precipitation drying trend. It was not clear what could have caused this disagreement between profile soil moisture and precipitation trends in the west. It was found that lower increase rates in maximum temperature corresponded to an increase in the profile soil moisture trend, whereas in areas in the Great Dividing Range (higher altitude), higher rates of maximum temperature increase corresponded to areas of decrease in soil moisture. This could indicate that it is necessary to see higher rates of temperature increase and precipitation decrease for the profile soil moisture to dry.

This study can help the New South Wales Government and stakeholders to devise strategies and make better decisions for a water-secure future. This study focused on a regional soil moisture trend that represents small-scale land–atmosphere interactions and microclimate phenomena that can reflect soil moisture behaviour in agricultural sites. Agricultural production is an important economic activity in New South Wales, representing 19% of the total gross value of agricultural production in Australia, a gross value of $11.7 billion in 2018-2019 (Australian Bureau of Statistics, 2019). Future work could analyse long-term vegetation trends using LAI and compare these to soil moisture trends to explore their correlation.

Chapter 6. Conclusions

6.1 Key findings

Soil moisture is crucial to the hydrologic cycle and land-atmosphere interactions, it affects evapotranspiration, water distribution, and food production. Soil moisture is highly variable in space and time, and because of its impact on agriculture, lack of in-situ measurements and uncertainties on future availability, studies on soil moisture spatial and temporal variability is important. This study investigates soil moisture temporal variability by analysing the how the main drivers of soil moisture dynamics are affecting the temporal differences in soil moisture in a semi-arid subhumid catchment in New South Wales, Australia. The spatial variability is explored by analysing soil moisture dynamics in two different soil types, clay and sandy. It is hypothesised that a strong relationship will exist, driving soil moisture dynamics, between soil moisture and vegetation (Leaf Area Index - LAI) and soil moisture and soil properties (e.g., saturated and residual soil water content) in dry and wet periods, and in sand and clay soils. The soil moisture monitoring stations located in an area characterised by Vertisols (Rüdiger, 2006; Martinez, 2010), and one of the main drivers of soil moisture are the macropores (Chen et al., 2014a). The macropores can contribute to spatial soil moisture variability since water bypasses a fraction of the porous soil matrix (Hendrickx & Flury, 2001; Simunek et al., 2003; Gerke, 2006). Macropore flow was never assessed in the region and this study evaluates whether a dual-porosity model is able to better simulate the profile soil moisture dynamics to improve the understanding of soil moisture physics and preferential flow in that area. Along with soil moisture temporal and spatial variability, climate change adds uncertainty to climate and consequently to soil moisture modelling, since soil moisture has an important role in land-atmosphere feedback mechanisms (Koster et al., 2004; Zhang et al., 2008; Seneviratne et al., 2010; Whan et al., 2015; Lo et al., 2021). The last portion of the study explores the temporal variability of soil moisture in a long period in the state of New South Wales, in both surface and the profile layers of soil. The long-term soil moisture variability can show where the soil was drying or wetting and relate to soil moisture main drivers – temperature and precipitation.

On the investigation of temporal soil moisture variability in wet and dry periods in a semi-arid subhumid catchment in Australia, no expressive difference in soil parameters and vegetation affecting soil moisture behaviour was found. Despite the difference in total rainfall of the dry and the wet period, there was no change in the preferential state of the soil, vertical fluxes were predominant in both periods and local characteristics (i.e., local vegetation and local soil properties) were responsible for driving patterns of soil moisture (Grayson et al., 1997; Western et al., 2002), which is likely the cause of the lack of difference between dry and wet soil moisture dynamics.

The Leaf Area Index (LAI) appeared to be higher in dry periods, which indicated that the model was trying to reach low values of soil moisture by assigning high LAI that increased the PET. There was a dominance of simulations in all stations and in both soil types (clay and sand) towards high saturated hydraulic conductivity values. After a re-analysis of simulations, where the best run had higher LAI in wet periods, it was found that LAI from dry and wet periods were similar, demonstrating that the change in vegetation is not so meaningful between dry and wet periods.

The soil moisture spatial differences between clay and sandy soils appeared in residual and saturated water content (θr and θs) and soil-pore distribution (n) and indicated that the model could demonstrate well the differences in soil-water holding capacities of the two soil types.

The evaluation of a dual-porosity model applied to a clay-loam soil in a semi-arid subhumid catchment to improve the understanding of soil moisture physics and preferential flow in that area showed that there was an overall decrease on NSE when using a dual-porosity model. From this assessment it was concluded that there is no need to use a more complex model, i.e., with more soil input parameters, because the performance of the dual-porosity model is slightly worse or very similar to the single-porosity model. Although the area is characterised by soils rich in expansive clay, and the presence of macropores was pointed to as one of the main drivers of soil moisture in Stanley catchment (Chen et al., 2014a), the HYDRUS-1D dual-porosity model did not add improvements to the understanding and simulation of soil moisture dynamics in the region.

The analysis of the long-term soil moisture variability in New South Wales for both profile and surface layers showed a predominance of long-term soil moisture drying variability in the period 1990–2019 in the surface and profile layer, in 96% and 78% of NSW, respectively. Even though both layers were dominated by a drying trend, they were not spatially correlated. The surface layer appeared to be related to hydrological components and soil composition, whereas the profile soil moisture appeared to correlate better with trends on maximum temperature and precipitation.

An obvious spatial correlation was not identified between long-term profile soil moisture variability and other physical characteristics. In some areas of NSW, maximum temperature and precipitation long-term variability were spatially correlated with profile soil moisture long-term variability. A positive profile soil moisture trend agreed with an increase in precipitation on the coast, and a negative profile soil moisture trend corresponded to a decrease in precipitation in the Great Dividing Range. In the west, however, a large area with a slight profile soil moisture wetting trend was opposite to the precipitation drying trend. It was not clear what could have caused this disagreement between profile soil moisture and precipitation trends in the west. It was found that lower increase rates in maximum temperature corresponded to an increase in profile soil moisture trend, whereas in areas in the Great Dividing Range (higher altitude) higher rates of maximum temperature increase corresponded to areas of decrease in soil moisture. This could indicate that it is necessary to have higher rates of temperature increase and precipitation decrease for the profile soil moisture to dry.

6.2 Study implications

Study implications are presented below:

- No improvements were noted when applying a dual-porosity model to the clay soil stations (S2 and S3), thus a uniform flow model (single porosity model), that is less complex to apply due to smaller number of parameters, is recommended. This recommendation can be extended to locations of similar soil composition, climate and rainfall regime.
- The analysis of soil moisture dynamics in dry and wet periods showed that similar soil and vegetation characteristics (i.e., parameter sets) were able to describe the soil moisture dynamics in both wetness periods. This may have been because the difference of dry and wet period was not large enough, therefore a separation of dry and wet period would not be necessary for sites with similar climate and rainfall regime of Krui and Merriwa catchments.
- The soil moisture long-term variability for the period of 1990-2019 showed a decline in both surface and profile layers the Goulburn River Catchment, where Krui and Merriwa are inserted. The precipitation also showed a decrease in this period and the maximum and minimum temperature increased. This indicates that the region, that is already dominated by vertical fluxes, will become even drier and an analysis with wet and dry periods will be irrelevant.

6.3 Study limitations and future work

Some limitations of this study are as follows:

- The temporal soil moisture variability in dry and wet periods investigation was applied to one region with predominantly grassland vegetation, constrained to one climate and in an eleven-year time window.
- The use of meteorological data from a single meteorological station.
- The analysis of macroporosity dynamics in the region was carried in only two soil moisture stations and without in-situ measurements of soil properties.
- The model applied in the in dry and wet periods investigation and in the macroporosity is a 1D model and although it was shown that the vertical fluxes predominate in the region, the model could be omitting some water-soil processes.

Recommendation for future work is listed below:

- To investigate the temporal soil moisture variability in dry and wet periods in a region with a more diverse vegetation to be able to analyse the change in dynamics among vegetation types.
- Explore the temporal soil moisture variability in dry and wet periods in other period and climatic region, with more seasonal rainfall difference and with drier and wetter temperatures.
- A deeper investigation on the macroporosity dynamics in the region would benefit from in-situ measurements of soil properties to be able to apply other models that capture the preferential flow in a more detailed method.
- Analyse vegetation long-term variability using LAI and compare this to soil moisture trends to explore their correlation.

Chapter 7. References

Ahmed, I., Rudra, R., McKague, K., Gharabaghi, B., & Ogilvie, J. (2007). Evaluation of the Root Zone Water Quality Model (RZWQM) for Southern Ontario: Part I. Sensitivity Analysis, Calibration, and Validation. *Water Quality Research Journal*, *42*(3), 202-218. doi:10.2166/wqrj.2007.024

Albergel, C., Dorigo, W., Reichle, R. H., Balsamo, G., de Rosnay, P., Muñoz-Sabater, J., Isaksen, L., de Jeu, R., & Wagner, W. (2013). Skill and Global Trend Analysis of Soil Moisture from Reanalyses and Microwave Remote Sensing. *Journal of Hydrometeorology*, *14*(4), 1259-1277. doi:10.1175/jhm-d-12-0161.1

Albergel, C., Rüdiger, C., Carrer, D., Calvet, J. C., Fritz, N., Naeimi, V., Bartalis, Z., & Hasenauer, S. (2009). An evaluation of ASCAT surface soil moisture products with in-situ observations in Southwestern France. *Hydrol. Earth Syst. Sci.*, *13*(2), 115-124. doi:10.5194/hess-13-115-2009

Albergel, C., Rüdiger, C., Pellarin, T., Calvet, J. C., Fritz, N., Froissard, F., Suquia, D., Petitpa, A., Piguet, B., & Martin, E. (2008). From near-surface to root-zone soil moisture using an exponential filter: an assessment of the method based on in-situ observations and model simulations. *Hydrology & Earth System Sciences Discussions*, *5*(3), 1603-1640. doi:10.5194/hessd-5-1603-2008

Alexander, L. (2011). Extreme heat rooted in dry soils. *Nature Geoscience*, *4*(1), 12-13. doi:10.1038/ngeo1045

Allan, R., Soden, B., John, V., Ingram, W., & Good, P. (2010). Current changes in tropical precipitation. *Environ. Res. Lett.*, *5*. doi:10.1088/1748-9326/5/2/025205

Arora, B., Mohanty, B. P., & McGuire, J. T. (2011). Inverse estimation of parameters for multidomain flow models in soil columns with different macropore densities. *Water Resources Research*, *47*(4). doi:10.1029/2010wr009451

Arora, B., Mohanty, B. P., & McGuire, J. T. (2012). Uncertainty in dual permeability model parameters for structured soils. *Water Resources Research*, *48*(1). doi:doi:10.1029/2011WR010500

Asner, G. P., Scurlock, J. M. O., & A. Hicke, J. (2003). Global synthesis of leaf area index observations: implications for ecological and remote sensing studies. *Global Ecology and Biogeography*, *12*(3), 191-205. doi:https://doi.org/10.1046/j.1466-822X.2003.00026.x

Banks, R. G. (1998). *Soil Landscapes of the Blackville 1:100 000 Sheet*. Sydney, Australia: Department of Land and Water Conservation.

Bell, K. R., Blanchard, B. J., Schmugge, T. J., & Witczak, M. W. (1980). Analysis of surface moisture variations within large-field sites. *Water Resources Research*, *16*(4), 796-810. doi:10.1029/WR016i004p00796

Benesty, J., Chen, J., Huang, Y., & Cohen, I. (2009). Pearson correlation coefficient. In *Noise reduction in speech processing* (pp. 1-4): Springer.

Bennett, B., Leonard, M., Deng, Y., & Westra, S. (2018). An empirical investigation into the effect of antecedent precipitation on flood volume. *Journal of Hydrology*, *567*, 435-445. doi:https://doi.org/10.1016/j.jhydrol.2018.10.025

Beven, K. (2006). A manifesto for the equifinality thesis. *Journal of Hydrology*, *320*(1), 18-36. doi:https://doi.org/10.1016/j.jhydrol.2005.07.007

Beven, K. (2012). Parameter Estimation And Predictive Uncertainty. In *Rainfall-runoff modelling: the primer* (2 ed.). UK: John Wiley & Sons,.

Beven, K., & Binley, A. (1992). The future of distributed models: model calibration and uncertainty prediction. *Hydrological Processes, 6*, 279-298.
Beven, K., & Binley, A. (2014). GLUE: 20 years on. *Hydrological Processes, 28*(24), 5897-5918. doi:10.1002/hyp.10082
Beven, K., & Germann, P. (1982). Macropores and Water Flow in Soils. *Water Resources Research - WATER RESOUR RES, 18*, 1311-1325. doi:10.1029/WR018i005p01311
Beven, K., & Germann, P. (2013). Macropores and water flow in soils revisited. *Water Resources Research, 49*(6), 3071-3092. doi:https://doi.org/10.1002/wrcr.20156
Blackmore, S., Pedretti, D., Mayer, K. U., Smith, L., & Beckie, R. D. (2018). *Evaluation of single- and dual-porosity models for reproducing the release of external and internal tracers from heterogeneous waste-rock piles* (Vol. 214).
Blasone, R.-S., Vrugt, J. A., Madsen, H., Rosbjerg, D., Robinson, B. A., & Zyvoloski, G. A. (2008). Generalized likelihood uncertainty estimation (GLUE) using adaptive Markov Chain Monte Carlo sampling. *Advances in Water Resources, 31*(4), 630-648. doi:https://doi.org/10.1016/j.advwatres.2007.12.003
Blöschl, G. (2006). Hydrologic synthesis: Across processes, places, and scales. *Water Resources Research, 42*(3). doi:10.1029/2005WR004319
Bogena, H. R., Herbst, M., Huisman, J. A., Rosenbaum, U., Weuthen, A., & Vereecken, H. (2010). Potential of Wireless Sensor Networks for Measuring Soil Water Content Variability All rights reserved. No part of this periodical may be reproduced or transmitted in any form or by any means, electronic or mechanical, including photocopying, recording, or any information storage and retrieval system, without permission in writing from the publisher. *Vadose Zone Journal, 9*(4), 1002-1013. doi:10.2136/vzj2009.0173
Brady, N. C., & Weil, R. R. (1999). *The nature and properties of soils* (12th ed.). Upper Saddle River, N.J: Prentice Hall,.
Brocca, L., Ciabatta, L., Massari, C., Camici, S., & Tarpanelli, A. (2017). Soil Moisture for Hydrological Applications: Open Questions and New Opportunities. *Water, 9*(2), 140.
Brocca, L., Hasenauer, S., Lacava, T., Melone, F., Moramarco, T., Wagner, W., Dorigo, W., Matgen, P., Martínez-Fernández, J., Llorens, P., Latron, J., Martin, C., & Bittelli, M. (2011). Soil moisture estimation through ASCAT and AMSR-E sensors: An intercomparison and validation study across Europe. *Remote Sensing of Environment, 115*(12), 3390-3408. doi:https://doi.org/10.1016/j.rse.2011.08.003
Brocca, L., Melone, F., Moramarco, T., & Morbidelli, R. (2009). Soil moisture temporal stability over experimental areas in Central Italy. *Geoderma, 148*(3), 364-374. doi:https://doi.org/10.1016/j.geoderma.2008.11.004
Brocca, L., Melone, F., Moramarco, T., & Morbidelli, R. (2010). Spatial-temporal variability of soil moisture and its estimation across scales. *Water Resources Research, 46*(2), n/a-n/a. doi:10.1029/2009WR008016
Brocca, L., Morbidelli, R., Melone, F., & Moramarco, T. (2007). Soil moisture spatial variability in experimental areas of central Italy. *Journal of Hydrology, 333*(2), 356-373. doi:https://doi.org/10.1016/j.jhydrol.2006.09.004

Brocca, L., Tullo, T., Melone, F., Moramarco, T., & Morbidelli, R. (2012). Catchment scale soil moisture spatial–temporal variability. *Journal of Hydrology, 422*(Supplement C), 63-75. doi:https://doi.org/10.1016/j.jhydrol.2011.12.039

Brocca, L., Zucco, G., Mittelbach, H., Moramarco, T., & Seneviratne, S. I. (2014). Absolute versus temporal anomaly and percent of saturation soil moisture spatial variability for six networks worldwide. *Water Resources Research, 50*(7), 5560-5576. doi:10.1002/2014WR015684

Brooks, R. H., & Corey, A. T. (1964). *Hydraulic properties of porous media.* Colorado State University. Libraries,

Buchhorn, M. S., B.; Bertels, L.; De Roo, B.; Lesiv, M.; Tsendbazar, N.E., Linlin, L., Tarko, A. (2020). Copernicus Global Land Service: Land Cover 100m: Version 3 Globe 2015-2019: Product User Manual. doi:10.5281/zenodo.3938963

Cai, W., Cowan, T., Briggs, P., & Raupach, M. (2009). Rising temperature depletes soil moisture and exacerbates severe drought conditions across southeast Australia. *Geophysical Research Letters, 36*(21). doi:10.1029/2009gl040334

Carsel, R. F., & Parrish, R. S. (1988). Developing joint probability distributions of soil water retention characteristics. *Water Resources Research, 24*(5), 755-769. doi:10.1029/WR024i005p00755

Castillo, V. M., Gómez-Plaza, A., & Martínez-Mena, M. (2003). The role of antecedent soil water content in the runoff response of semiarid catchments: a simulation approach. *Journal of Hydrology, 284*(1), 114-130. doi:https://doi.org/10.1016/S0022-1694(03)00264-6

Chan, S. K., Bindlish, R., O'Neill, P., Jackson, T., Njoku, E., Dunbar, S., Chaubell, J., Piepmeier, J., Yueh, S., Entekhabi, D., Colliander, A., Chen, F., Cosh, M. H., Caldwell, T., Walker, J., Berg, A., McNairn, H., Thibeault, M., Martínez-Fernández, J., Uldall, F., Seyfried, M., Bosch, D., Starks, P., Holifield Collins, C., Prueger, J., van der Velde, R., Asanuma, J., Palecki, M., Small, E. E., Zreda, M., Calvet, J., Crow, W. T., & Kerr, Y. (2018). Development and assessment of the SMAP enhanced passive soil moisture product. *Remote Sensing of Environment, 204*, 931-941. doi:https://doi.org/10.1016/j.rse.2017.08.025

Chen, F., Crow, W. T., Bindlish, R., Colliander, A., Burgin, M. S., Asanuma, J., & Aida, K. (2018). Global-scale evaluation of SMAP, SMOS and ASCAT soil moisture products using triple collocation. *Remote Sensing of Environment, 214*, 1-13. doi:https://doi.org/10.1016/j.rse.2018.05.008

Chen, G., Jiao, L., & Li, X. (2016). Sensitivity Analysis and Identification of Parameters to the Van Genuchten Equation. *Journal of Chemistry, 2016*, 9879537. doi:10.1155/2016/9879537

Chen, M. (2013). *On the predictability of hydrology in using land surface models and field soil moisture data.* (PhD thesis), University of Newcastle, Australia.

Chen, M., Willgoose, G. R., & Saco, P. M. (2014a). Spatial prediction of temporal soil moisture dynamics using HYDRUS-1D. *Hydrological Processes, 28*(2), 171-185. doi:10.1002/hyp.9518

Chen, M., Willgoose, G. R., & Saco, P. M. (2015). Investigating the impact of leaf area index temporal variability on soil moisture predictions using remote sensing vegetation data. *Journal of Hydrology, 522*(Supplement C), 274-284. doi:https://doi.org/10.1016/j.jhydrol.2014.12.027

Chen, T., de Jeu, R. A. M., Liu, Y. Y., van der Werf, G. R., & Dolman, A. J. (2014b). Using satellite based soil moisture to quantify the water driven variability in NDVI: A case study over mainland Australia. *Remote Sensing of Environment, 140*, 330-338. doi:https://doi.org/10.1016/j.rse.2013.08.022

Cleveland, R. B., Cleveland, W. S., & Terpenning, I. (1990). STL: A Seasonal-Trend Decomposition Procedure Based on Loess. *Journal of Official Statistics, 6*(1), 3.

Cleveland, W. S. (1979). Robust Locally Weighted Regression and Smoothing Scatterplots. *Journal of the American Statistical Association, 74*(368), 829-836. doi:10.1080/01621459.1979.10481038

Cosh, M. H., Jackson, T. J., Bindlish, R., & Prueger, J. H. (2004). Watershed scale temporal and spatial stability of soil moisture and its role in validating satellite estimates. *Remote Sensing of Environment, 92*(4), 427-435. doi:https://doi.org/10.1016/j.rse.2004.02.016

Cosh, M. H., Jackson, T. J., Moran, S., & Bindlish, R. (2008). Temporal persistence and stability of surface soil moisture in a semi-arid watershed. *Remote Sensing of Environment, 112*(2), 304-313. doi:https://doi.org/10.1016/j.rse.2007.07.001

Cosh, M. H., Jackson, T. J., Starks, P., & Heathman, G. (2006). Temporal stability of surface soil moisture in the Little Washita River watershed and its applications in satellite soil moisture product validation. *Journal of Hydrology, 323*(1), 168-177. doi:https://doi.org/10.1016/j.jhydrol.2005.08.020

Craib, I. J. (1929). Some Aspects of Soil Moisture in the Forest. *Yale School of Forestry Bulletin 25. 62 pp. + figures.*

Cromer, M. V. (1996). *Geostatistics for environmental and geotechnical applications: A technology transferred*: American Society for Testing and Materials, West Conshohocken, PA (United States).

Crow, W. T., Ryu, D., & Famiglietti, J. S. (2005). Upscaling of field-scale soil moisture measurements using distributed land surface modeling. *Advances in Water Resources, 28*(1), 1-14. doi:https://doi.org/10.1016/j.advwatres.2004.10.004

CSIRO, & BoM. (2020). *State of the Climate 2020*. Retrieved from https://www.csiro.au/en/research/environmental-impacts/climate-change/State-of-the-Climate

Dai, A. (2011). Characteristics and trends in various forms of the Palmer Drought Severity Index during 1900–2008. *Journal of Geophysical Research: Atmospheres, 116*(D12). doi:10.1029/2010jd015541

Dai, A. (2013). Increasing drought under global warming in observations and models. *Nature Climate Change, 3*(1), 52-58. doi:10.1038/nclimate1633

Daly, E., & Porporato, A. (2005). A Review of Soil Moisture Dynamics: From Rainfall Infiltration to Ecosystem Response. *Environmental Engineering Science, 22*, 9-24. doi:10.1089/ees.2005.22.9

Das, N. N., Entekhabi, D., Dunbar, R. S., Colliander, A., Chen, F., Crow, W., Jackson, T. J., Berg, A., Bosch, D. D., Caldwell, T., Cosh, M. H., Collins, C. H., Lopez-Baeza, E., Moghaddam, M., Rowlandson, T., Starks, P. J., Thibeault, M., Walker, J. P., Wu, X., O'Neill, P. E., Yueh, S., & Njoku, E. G. (2018). The SMAP mission combined active-passive soil moisture product at 9 km and 3 km spatial resolutions. *Remote Sensing of Environment, 211*, 204-217. doi:https://doi.org/10.1016/j.rse.2018.04.011

de Jeu, R. A. M., Holmes, T. R. H., Parinussa, R. M., & Owe, M. (2014). A spatially coherent global soil moisture product with improved temporal resolution. *Journal of Hydrology, 516*, 284-296. doi:https://doi.org/10.1016/j.jhydrol.2014.02.015

Dee, D. P., Uppala, S. M., Simmons, A. J., Berrisford, P., Poli, P., Kobayashi, S., Andrae, U., Balmaseda, M. A., Balsamo, G., Bauer, P., Bechtold, P., Beljaars, A. C. M., van de Berg, L., Bidlot, J., Bormann, N., Delsol, C., Dragani, R., Fuentes, M., Geer, A. J., Haimberger, L., Healy, S. B., Hersbach, H., Hólm, E. V., Isaksen, L., Kållberg, P., Köhler, M., Matricardi, M., McNally, A. P., Monge-Sanz, B. M., Morcrette, J.-J., Park, B.-K., Peubey, C., de Rosnay, P., Tavolato, C., Thépaut, J.-N., & Vitart, F. (2011). The ERA-Interim reanalysis: configuration and performance of the data assimilation system. *Quarterly Journal of the Royal Meteorological Society, 137*(656), 553-597. doi:https://doi.org/10.1002/qj.828

Deng, Y., Wang, S., Bai, X., Luo, G., Wu, L., Cao, Y., Li, H., Li, C., Yang, Y., Hu, Z., & Tian, S. (2020). Variation trend of global soil moisture and its cause analysis. *Ecological Indicators, 110*, 105939. doi:https://doi.org/10.1016/j.ecolind.2019.105939

Dingman, S. L. (1994). *Physical Hydrology* (1 ed.). New York: Macmilla Publishing Company.

DIP. (2013). *Upper Hunter Region Agricultural Profile*. Retrieved from Department of Primary Industries: https://www.dpi.nsw.gov.au/__data/assets/pdf_file/0018/471024/Upper-hunter-region-agricultural-profile.pdf

Dirmeyer, P. A. (2011). A History and Review of the Global Soil Wetness Project (GSWP). *Journal of Hydrometeorology, 12*(5), 729-749. doi:10.1175/jhm-d-10-05010.1

Dooge, J. C. I. (1986). Looking for hydrologic laws. *Water Resources Research, 22*(9S), 46S-58S. doi:10.1029/WR022i09Sp0046S

Dorigo, W., de Jeu, R., Chung, D., Parinussa, R., Liu, Y., Wagner, W., & Fernández-Prieto, D. (2012). Evaluating global trends (1988–2010) in harmonized multi-satellite surface soil moisture. *Geophysical Research Letters, 39*(18). doi:10.1029/2012gl052988

Dorigo, W. A., Gruber, A., De Jeu, R. A. M., Wagner, W., Stacke, T., Loew, A., Albergel, C., Brocca, L., Chung, D., Parinussa, R. M., & Kidd, R. (2015). Evaluation of the ESA CCI soil moisture product using ground-based observations. *Remote Sensing of Environment, 162*, 380-395. doi:https://doi.org/10.1016/j.rse.2014.07.023

Efstratiadis, A., & Koutsoyiannis, D. (2010). One decade of multi-objective calibration approaches in hydrological modelling: a review. *Hydrological Sciences Journal, 55*(1), 58-78. doi:10.1080/02626660903526292

Entekhabi, D., Njoku, E., Neill, P. O., Spencer, M., Jackson, T., Entin, J., Im, E., & Kellogg, K. (2008, 7-11 July 2008). *The Soil Moisture Active/Passive Mission (SMAP).* Paper presented at the IGARSS 2008 - 2008 IEEE International Geoscience and Remote Sensing Symposium.

Entekhabi, D., Njoku, E. G., Neill, P. E. O., Kellogg, K. H., Crow, W. T., Edelstein, W. N., Entin, J. K., Goodman, S. D., Jackson, T. J., Johnson, J., Kimball, J., Piepmeier, J. R., Koster, R. D., Martin, N., McDonald, K. C., Moghaddam, M., Moran, S., Reichle, R., Shi, J. C., Spencer, M. W., Thurman, S. W., Tsang, L., &

Zyl, J. V. (2010). The Soil Moisture Active Passive (SMAP) Mission. *Proceedings of the IEEE, 98*(5), 704-716. doi:10.1109/JPROC.2010.2043918

Famiglietti, J. S., Devereaux, J. A., Laymon, C. A., Tsegaye, T., Houser, P. R., Jackson, T. J., Graham, S. T., Rodell, M., & van Oevelen, P. J. (1999). Ground-based investigation of soil moisture variability within remote sensing footprints During the Southern Great Plains 1997 (SGP97) Hydrology Experiment. *Water Resources Research, 35*(6), 1839-1851. doi:10.1029/1999WR900047

Famiglietti, J. S., & Rodell, M. (2013). Water in the Balance. *Science, 340*(6138), 1300-1301. doi:10.1126/science.1236460

Famiglietti, J. S., Rudnicki, J. W., & Rodell, M. (1998). Variability in surface moisture content along a hillslope transect: Rattlesnake Hill, Texas. *Journal of Hydrology, 210*(1), 259-281. doi:https://doi.org/10.1016/S0022-1694(98)00187-5

Famiglietti, J. S., Ryu, D., Berg, A. A., Rodell, M., & Jackson, T. J. (2008). Field observations of soil moisture variability across scales. *Water Resources Research, 44*(1), n/a-n/a. doi:10.1029/2006WR005804

Feddes, R. A., P. J. Kowalik, and H. Zaradny. (1978). *Simulation of Field Water Use and Crop Yield* (J. W. Sons Ed.). New York, NY.

Feng, H., & Zhang, M. (2015). Global land moisture trends: drier in dry and wetter in wet over land. *Scientific Reports, 5*(1), 18018. doi:10.1038/srep18018

Feng, S., Bai, Z., Chen, H.-X., Cao, B., Lu, S., & Chen, Y.-M. (2018). *A dual-permeability hydro-biodegradation model for leachate recirculation and settlement in bioreactor landfills* (Vol. 25).

Fitzjohn, C., Ternan, J. L., & Williams, A. G. (1998). Soil moisture variability in a semi-arid gully catchment: implications for runoff and erosion control. *CATENA, 32*(1), 55-70. doi:https://doi.org/10.1016/S0341-8162(97)00045-3

Flury, M., Flühler, H., Jury, W. A., & Leuenberger, J. (1994). Susceptibility of soils to preferential flow of water: A field study. *Water Resources Research, 30*(7), 1945-1954. doi:doi:10.1029/94WR00871

Forkel, M., Carvalhais, N., Verbesselt, J., Mahecha, M. D., Neigh, C. S. R., & Reichstein, M. (2013). Trend Change Detection in NDVI Time Series: Effects of Inter-Annual Variability and Methodology. *Remote Sensing, 5*(5), 2113-2144.

Frost, A. J., Ramchurn, A., & Smith, A. (2016). *The Bureau's Operational AWRA Landscape (AWRA-L) Model. Technical Description of AWRA-L version 5*. Retrieved from

Frost, A. J., Ramchurn, A., & Smith, A. (2018). The Australian Landscape Water Balance model (AWRA-L v6). Technical Description of the Australian Water Resources Assessment Landscape model version 6. . *Bureau of Meteorology Technical Report*.

Frost, A. J., & Wright, D. P. (2018). *The Australian water resource assessment landscape model - AWRA-L: Improved performance and regional calibration*. Paper presented at the Hydrology and Water Resources Symposium (HWRS 2018): Water and Communities, Melbourne.

Gallant, J., Wilson, N., Dowling, T., Read, A., & Inskeep, C. (2011). SRTM-derived 1 Second Digital Elevation Models Version 1.0. Record 1. *Geoscience Australia*.

Garg, K. K., Das, B. S., Safeeq, M., & Bhadoria, P. B. S. (2009). Measurement and modeling of soil water regime in a lowland paddy field showing preferential

transport. *Agricultural Water Management, 96*(12), 1705-1714. doi:https://doi.org/10.1016/j.agwat.2009.06.018
Gerke, H. H. (2006). Preferential flow descriptions for structured soils. *Journal of Plant Nutrition and Soil Science, 169*(3), 382-400. doi:doi:10.1002/jpln.200521955
Gibson, A. J., Hancock, G., Verdon-Kidd, D., & Wells, T. (2019). *Centennial-scale variability of soil moisture in Eastern Australia*. Paper presented at the MODSIM, Canberra.
Gibson, A. J., Verdon-Kidd, D. C., Hancock, G. R., & Willgoose, G. (2020). Catchment-scale drought: capturing the whole drought cycle using multiple indicators. *Hydrol. Earth Syst. Sci., 24*(4), 1985-2002. doi:10.5194/hess-24-1985-2020
Goodrich, D. C., Chehbouni, A., Goff, B., MacNish, B., Maddock, T., Moran, S., Shuttleworth, W. J., Williams, D. G., Watts, C., Hipps, L. H., Cooper, D. I., Schieldge, J., Kerr, Y. H., Arias, H., Kirkland, M., Carlos, R., Cayrol, P., Kepner, W., Jones, B., Avissar, R., Begue, A., Bonnefond, J. M., Boulet, G., Branan, B., Brunel, J. P., Chen, L. C., Clarke, T., Davis, M. R., DeBruin, H., Dedieu, G., Elguero, E., Eichinger, W. E., Everitt, J., Garatuza-Payan, J., Gempko, V. L., Gupta, H., Harlow, C., Hartogensis, O., Helfert, M., Holifield, C., Hymer, D., Kahle, A., Keefer, T., Krishnamoorthy, S., Lhomme, J. P., Lagouarde, J. P., Lo Seen, D., Luquet, D., Marsett, R., Monteny, B., Ni, W., Nouvellon, Y., Pinker, R., Peters, C., Pool, D., Qi, J., Rambal, S., Rodriguez, J., Santiago, F., Sano, E., Schaeffer, S. M., Schulte, M., Scott, R., Shao, X., Snyder, K. A., Sorooshian, S., Unkrich, C. L., Whitaker, M., & Yucel, I. (2000). Preface paper to the Semi-Arid Land-Surface-Atmosphere (SALSA) Program special issue. *Agricultural and Forest Meteorology, 105*(1), 3-20. doi:https://doi.org/10.1016/S0168-1923(00)00178-7
Grayson, R. B., & Western, A. W. (1998). Towards areal estimation of soil water content from point measurements: time and space stability of mean response. *Journal of Hydrology, 207*(1), 68-82. doi:https://doi.org/10.1016/S0022-1694(98)00096-1
Grayson, R. B., Western, A. W., Chiew, F. H. S., & Blöschl, G. (1997). Preferred states in spatial soil moisture patterns: Local and nonlocal controls. *Water Resources Research, 33*(12), 2897-2908. doi:10.1029/97WR02174
Greve, P., Orlowsky, B., Mueller, B., Sheffield, J., Reichstein, M., & Seneviratne, S. I. (2014). Global assessment of trends in wetting and drying over land. *Nature Geoscience, 7*(10), 716-721. doi:10.1038/ngeo2247
Grohs, R. D., Willgoose, G., & Saco, P. (2019). *The impact of dry and wet periods on profile soil moisture calibration and validation in catchments characterised by vertical fluxes.* Paper presented at the EGU General Assembly 2019, Vienna.
Gu, X., Zhang, Q., Li, J., Singh, V. P., Liu, J., Sun, P., & Cheng, C. (2019). Attribution of Global Soil Moisture Drying to Human Activities: A Quantitative Viewpoint. *Geophysical Research Letters, 46*(5), 2573-2582. doi:https://doi.org/10.1029/2018GL080768
Hall, M. J. (2001). How well does your model fit the data? *Journal of Hydroinformatics, 3*(1), 49-55. doi:10.2166/hydro.2001.0006
Hardie, M., Lisson, S., Doyle, R., & Cotching, W. (2013). Determining the frequency, depth and velocity of preferential flow by high frequency soil moisture

monitoring. *Journal of Contaminant Hydrology, 144*(1), 66-77. doi:https://doi.org/10.1016/j.jconhyd.2012.10.008
Hardie, M. A., Cotching, W. E., Doyle, R. B., Holz, G., Lisson, S., & Mattern, K. (2011). Effect of antecedent soil moisture on preferential flow in a texture-contrast soil. *Journal of Hydrology, 398*(3), 191-201. doi:https://doi.org/10.1016/j.jhydrol.2010.12.008
He, Y., Guo, X., & Wilmshurst, J. F. (2007). Comparison of different methods for measuring leaf area index in a mixed grassland. *Canadian Journal of Plant Science, 87*(4), 803-813. doi:10.4141/cjps07024
Held, I. M., & Soden, B. J. (2006). Robust Responses of the Hydrological Cycle to Global Warming. *Journal of Climate, 19*(21), 5686-5699. doi:10.1175/jcli3990.1
Hendrickx, J. M. H., & Flury, M. (2001). Uniform and preferential flow, mechanisms in the vadose zone, . In *Conceptual Models of Flow and Transport in the Fractured Vadose Zone* (pp. 149–187). Washington, DC: National Academies Press.
Hill, P., Nathan, R., & Zhang, J. (2016). *Application of AWRA-L gridded soil moisture data for flood estimation [online]*. Paper presented at the 37th Hydrology & Water Resources Symposium 2016: Water, Infrastructure and the Environment, Barton, ACT. https://search.informit.com.au/documentSummary;dn=684424744481799;res=IELENG
Hillel, D. (1998). *Environmental soil physics*. San Diego, CA: Academic Press.
Hossain, F., Anagnostou, E. N., Dinku, T., & Borga, M. (2004a). Hydrological model sensitivity to parameter and radar rainfall estimation uncertainty. *Hydrological Processes, 18*(17), 3277-3291. doi:https://doi.org/10.1002/hyp.5659
Hossain, F., Anagnostou, E. N., & Lee, K. H. (2004b). A non-linear and stochastic response surface method for Bayesian estimation of uncertainty in soil moisture simulation from a land surface model. *Nonlin. Processes Geophys., 11*(4), 427-440. doi:10.5194/npg-11-427-2004
Huang, X., Shi, Z. H., Zhu, H. D., Zhang, H. Y., Ai, L., & Yin, W. (2016). Soil moisture dynamics within soil profiles and associated environmental controls. *CATENA, 136*, 189-196. doi:https://doi.org/10.1016/j.catena.2015.01.014
Hutchinson, J. M. S., Jacquin, A., Hutchinson, S. L., & Verbesselt, J. (2015). Monitoring vegetation change and dynamics on U.S. Army training lands using satellite image time series analysis. *Journal of Environmental Management, 150*, 355-366. doi:https://doi.org/10.1016/j.jenvman.2014.08.002
Ivancic, T. J., & Shaw, S. B. (2015). Examining why trends in very heavy precipitation should not be mistaken for trends in very high river discharge. *Climatic Change, 133*, 681-693.
Iversen, B., Børgesen, C., Lægdsmand, M., Greve, M., Heckrath, G., & Kjaergaard, C. (2011). *Risk Predicting of Macropore Flow using Pedotransfer Functions, Textural Maps, and Modeling* (Vol. 10).
Jackson, R., Jg, C., Ehleringer, J., Mooney, H., Sala, O., & Schulze, E. (1996). A Global Analysis of Root Distributions for Terrestrial Biomes. *Oecologia, 108*, 389-411. doi:10.1007/BF00333714
Jackson, T. J., Vine, D. M. L., Hsu, A. Y., Oldak, A., Starks, P. J., Swift, C. T., Isham, J. D., & Haken, M. (1999). Soil moisture mapping at regional scales using

microwave radiometry: the Southern Great Plains Hydrology Experiment. *IEEE transactions on geoscience and remote sensing, 37*(5), 2136-2151. doi:10.1109/36.789610

Jaynes, D. B., Ahmed, S. I., Kung, K.-J., & Kanwar, R. S. (2001). Temporal dynamics of preferential flow to a subsurface drain. *Soil Science Society of America Journal, 65*(5), 1368-1376.

Jaynes, D. B., B. Moorman, T., B. Parkin, T., & Kaspar, T. (2016). *Simulating Woodchip Bioreactor Performance Using a Dual-Porosity Model* (Vol. 45).

Jeffrey, S. J., Carter, J. O., Moodie, K. B., & Beswick, A. R. (2001). Using spatial interpolation to construct a comprehensive archive of Australian climate data. *Environmental Modelling & Software, 16*(4), 309-330. doi:https://doi.org/10.1016/S1364-8152(01)00008-1

Jiang, S., Pang, L., Buchan, G. D., Šimůnek, J., Noonan, M. J., & Close, M. E. (2010). Modeling water flow and bacterial transport in undisturbed lysimeters under irrigations of dairy shed effluent and water using HYDRUS-1D. *Water Research, 44*(4), 1050-1061. doi:https://doi.org/10.1016/j.watres.2009.08.039

Johnson, D. (2009). *The Geology of Australia* (2nd ed.). Australia: Cambridge University Press.

Jung, M., Reichstein, M., Ciais, P., Seneviratne, S., Sheffield, J., Goulden, M., Bonan, G., Cescatti, A., Chen, J., de Jeu, R., Dolman, H., Eugster, W., Gerten, D., Gianelle, D., Gobron, N., Heinke, J., Kimball, J., Law, B., & Montagnani, L. (2010). Recent Decline in the Global Land Evapotranspiration Trend Due to Limited Moisture Supply. *Nature, 467,* 951-954. doi:10.1038/nature09396

Kerr, Y. H. (2007). Soil moisture from space: Where are we? *Hydrogeology Journal, 15*(1), 117-120. doi:10.1007/s10040-006-0095-3

Kerr, Y. H., Waldteufel, P., Wigneron, J., Martinuzzi, J., Font, J., & Berger, M. (2001). Soil moisture retrieval from space: the Soil Moisture and Ocean Salinity (SMOS) mission. *IEEE transactions on geoscience and remote sensing, 39*(8), 1729-1735. doi:10.1109/36.942551

Khan, M. S., Baik, J., & Choi, M. (2020). Inter-comparison of evapotranspiration datasets over heterogeneous landscapes across Australia. *Advances in Space Research, 66*(3), 533-545. doi:https://doi.org/10.1016/j.asr.2020.04.037

Kiem, A., Johnson, F., Westra, S., Dijk, A., Evans, J., O'Donnell, A., Rouillard, A., Barr, C., Tyler, J., Thyer, M., Jakob, D., Woldemeskel, F., Sivakumar, B., & Mehrotra, R. (2016). Natural hazards in Australia: droughts. *Climatic Change, 139*(1), 37-54. doi:10.1007/s10584-016-1798-7

King, A. D., Alexander, L. V., & Donat, M. G. (2013). The efficacy of using gridded data to examine extreme rainfall characteristics: a case study for Australia. *International Journal of Climatology, 33*(10), 2376-2387. doi:10.1002/joc.3588

Kirkham, M. B. (2014). Chapter 10 - Field Capacity, Wilting Point, Available Water, and the Nonlimiting Water Range. In M. B. Kirkham (Ed.), *Principles of Soil and Plant Water Relations (Second Edition)* (pp. 153-170). Boston: Academic Press.

Kirono, D. G. C., Round, V., Heady, C., Chiew, F. H. S., & Osbrough, S. (2020). Drought projections for Australia: Updated results and analysis of model simulations. *Weather and Climate Extremes, 30*, 100280. doi:https://doi.org/10.1016/j.wace.2020.100280

Kladivko, E. J., Brown, L. C., & Baker, J. L. (2001). Pesticide Transport to Subsurface Tile Drains in Humid Regions of North America. *Critical Reviews in Environmental Science and Technology, 31*(1), 1-62. doi:10.1080/20016491089163

Kodešová, R., Josef, K., & Jiři, Š. (2006). *Numerical Study of Macropore Impact on Ponded Infiltration in Clay Soils* (Vol. 1).

Kohne, J., Kohne, S., Mohanty, B., & Simunek, J. J. (2004). Inverse Mobile-Immobile Modeling of Transport During Transient Flow: Effects of Between-Domain Transfer and Initial Water Content. *Vadose Zone Journal - VADOSE ZONE J, 3*, 1309-1321. doi:10.2113/3.4.1309

Köhne, J. M., & Mohanty, B. P. (2005). Water flow processes in a soil column with a cylindrical macropore: Experiment and hierarchical modeling. *Water Resources Research, 41*(3). doi:https://doi.org/10.1029/2004WR003303

Köhne, J. M., Mohanty, B. P., & Šimůnek, J. (2006). Inverse Dual-Permeability Modeling of Preferential Water Flow in a Soil Column and Implications for Field-Scale Solute Transport. *Vadose Zone Journal, 5*(1), 59-76. doi:10.2136/vzj2005.0008

Köhne, J. M., Mohanty, B. P., Simunek, J., & Gerke, H. H. (2004). Numerical evaluation of a second-order water transfer term for variably saturated dual-permeability models. *Water Resources Research, 40*(7). doi:doi:10.1029/2004WR003285

Korres, W., Reichenau, T. G., Fiener, P., Koyama, C. N., Bogena, H. R., Cornelissen, T., Baatz, R., Herbst, M., Diekkrüger, B., Vereecken, H., & Schneider, K. (2015). Spatio-temporal soil moisture patterns – A meta-analysis using plot to catchment scale data. *Journal of Hydrology, 520*(Supplement C), 326-341. doi:https://doi.org/10.1016/j.jhydrol.2014.11.042

Koster, R. D., Dirmeyer, P. A., Guo, Z., Bonan, G., Chan, E., Cox, P., Gordon, C. T., Kanae, S., Kowalczyk, E., Lawrence, D., Liu, P., Lu, C.-H., Malyshev, S., McAvaney, B., Mitchell, K., Mocko, D., Oki, T., Oleson, K., Pitman, A., Sud, Y. C., Taylor, C. M., Verseghy, D., Vasic, R., Xue, Y., & Yamada, T. (2004). Regions of Strong Coupling Between Soil Moisture and Precipitation. *Science, 305*(5687), 1138-1140. doi:10.1126/science.1100217

Koster, R. D., Suarez, M. J., Higgins, R. W., & Van den Dool, H. M. (2003). Observational evidence that soil moisture variations affect precipitation. *Geophysical Research Letters, 30*(5). doi:https://doi.org/10.1029/2002GL016571

Legates, D., & McCabe, G. (1999). Evaluating the Use Of "Goodness-of-Fit" Measures in Hydrologic and Hydroclimatic Model Validation. *Water Resources Research, 35*, 233-241. doi:10.1029/1998WR900018

Liu, C. l., & Allan, R. (2013). Observed and simulated precipitation responses in wet and dry regions 1850–2100. *Environmental Research Letters, 8*, 034002. doi:10.1088/1748-9326/8/3/034002

Liu, Y. Y., Parinussa, R., Dorigo, W., de Jeu, R., Wagner, W., van Dijk, A., McCabe, M., & Evans, J. (2011). Developing an improved soil moisture dataset by blending passive and active microwave satellite-based retrievals. *Hydrology and Earth System Sciences, 15*. doi:10.5194/hess-15-425-2011

Lo, M.-H., Wu, W.-Y., Tang, L. I., Ryu, D., Rashid, M., & Wu, R.-J. (2021). Temporal Changes in Land Surface Coupling Strength: An Example in a Semi-Arid Region of Australia. *Journal of Climate, 34*(4), 1503-1513. doi:10.1175/jcli-d-20-0250.1

Lockart, N., Kiem, A., Chiong, R., Askland, H., & Rich, J. (2020). Projected change in meteorological drought characteristics using regional climate model data for the Hunter region of Australia. *Climate Research*. doi:10.3354/cr01596

Mahmood, R., & Hubbard, K. G. (2007). Relationship between soil moisture of near surface and multiple depths of the root zone under heterogeneous land uses and varying hydroclimatic conditions. *Hydrological Processes, 21*(25), 3449-3462. doi:https://doi.org/10.1002/hyp.6578

Marquardt, D. W. (1963). An Algorithm for Least-Squares Estimation of Nonlinear Parameters. *Journal of the Society for Industrial and Applied Mathematics, 11*(2), 431-441.

Martinez, C. (2010). *Soil carbon dynamics at hillslope and catchment scales.* (PhD thesis), University of Newcastle, Australia.

Martinez, C., Hancock, G. R., Kalma, J. D., & Wells, T. (2008). Spatio-temporal distribution of near-surface and root zone soil moisture at the catchment scale. *Hydrological Processes, 22*(14), 2699-2714. doi:10.1002/hyp.6869

McCabe, M. F., Franks, S. W., & Kalma, J. D. (2005). Calibration of a land surface model using multiple data sets. *Journal of Hydrology, 302*(1), 209-222. doi:https://doi.org/10.1016/j.jhydrol.2004.07.002

McCuen, R. H., Knight, Z., & Cutter, A. G. (2006). Evaluation of the Nash–Sutcliffe Efficiency Index. *Journal of Hydrologic Engineering, 11*(6), 597-602. doi:doi:10.1061/(ASCE)1084-0699(2006)11:6(597)

McDonough, K. R., Hutchinson, S. L., & Hutchinson, S. (2020). Declining Soil Moisture Threatens Water Availability in the U.S. Great Plains. *Transactions of the ASABE, 63*(5), 1147-1156. doi:https://doi.org/10.13031/trans.13773

Meehl, G. A., & Tebaldi, C. (2004). More Intense, More Frequent, and Longer Lasting Heat Waves in the 21st Century. *Science, 305*(5686), 994-997. doi:doi:10.1126/science.1098704

Mishra, A. K., & Singh, V. P. (2010). A review of drought concepts. *Journal of Hydrology, 391*(1), 202-216. doi:https://doi.org/10.1016/j.jhydrol.2010.07.012

Mitchell, M. (2002). *Native grasses : an identification handbook for temperate Australia / Meredith Mitchell ; photographs by John Schneider*. Collingwood, Vic: Landlink Press.

Mo, X., & Beven, K. (2004). Multi-objective parameter conditioning of a three-source wheat canopy model. *Agricultural and Forest Meteorology, 122*(1), 39-63. doi:https://doi.org/10.1016/j.agrformet.2003.09.009

Mualem, Y. (1976). A new model for predicting the hydraulic conductivity of unsaturated porous media. *Water Resources Research, 12*(3), 513-522. doi:10.1029/WR012i003p00513

Mueller, B., & Seneviratne, S. (2012). Hot days induced by precipitation deficits at the global scale. *Proceedings of the National Academy of Sciences of the United States of America, 109*, 12398-12403. doi:10.1073/pnas.1204330109

Nash, J. E., & Sutcliffe, J. V. (1970). River flow forecasting through conceptual models part I — A discussion of principles. *Journal of Hydrology, 10*(3), 282-290. doi:https://doi.org/10.1016/0022-1694(70)90255-6

Nguyen, H., Mehrotra, R., & Sharma, A. (2020). Assessment of Climate Change Impacts on Reservoir Storage Reliability, Resilience, and Vulnerability Using a

Multivariate Frequency Bias Correction Approach. *Water Resources Research, 56*(2), e2019WR026022. doi:https://doi.org/10.1029/2019WR026022

Nimmo, J. (2012). Preferential flow occurs in unsaturated conditions. *Hydrological Processes, 26*, 786-789. doi:10.1002/hyp.8380

Nimmo, J. (2013). Porosity and Pore Size Distribution. *Reference Module in Earth Systems and Environmental Sciences*. doi:10.1016/B978-0-12-409548-9.05265-9

Parinussa, R. M., Holmes, T. R. H., & de Jeu, R. A. M. (2012). Soil Moisture Retrievals From the WindSat Spaceborne Polarimetric Microwave Radiometer. *IEEE transactions on geoscience and remote sensing, 50*(7), 2683-2694. doi:10.1109/TGRS.2011.2174643

Paulik, C., Dorigo, W., Wagner, W., & Kidd, R. (2014). Validation of the ASCAT Soil Water Index using in situ data from the International Soil Moisture Network. *International Journal of Applied Earth Observation and Geoinformation, 30*, 1-8. doi:https://doi.org/10.1016/j.jag.2014.01.007

Peischl, S., Walker, J. P., Rüdiger, C., Ye, N., Kerr, Y. H., Kim, E., Bandara, R., & Allahmoradi, M. (2012). The AACES field experiments: SMOS calibration and validation across the Murrumbidgee River catchment. *Hydrology and Earth System Sciences, 16*(6).

Philip, J. R. (1968). The theory of absorption in aggregated media. *Australian Journal of Soil Research - AUST J SOIL RES, 6*. doi:10.1071/SR9680001

Pontedeiro, E. M., van Genuchten, M. T., Cotta, R. M., & Simunek, J. (2010). The effects of preferential flow and soil texture on risk assessments of a NORM waste disposal site. *Journal of Hazardous Materials, 174*(1), 648-655. doi:https://doi.org/10.1016/j.jhazmat.2009.09.100

Prihodko, L., Denning, A. S., Hanan, N. P., Baker, I., & Davis, K. (2008). Sensitivity, uncertainty and time dependence of parameters in a complex land surface model. *Agricultural and Forest Meteorology, 148*(2), 268-287. doi:https://doi.org/10.1016/j.agrformet.2007.08.006

Ramírez-García, J., Almendros, P., & Quemada, M. (2012). Ground cover and leaf area index relationship in a grass, legume and crucifer crop. *Plant Soil and Environment, 58*, 385-390. doi:10.17221/195/2012-PSE

Ratto, M., Tarantola, S., & Saltelli, A. (2001). Sensitivity analysis in model calibration: GSA-GLUE approach. *Computer Physics Communications, 136*, 212-224. doi:10.1016/S0010-4655(01)00159-X

Reusser, D. E., Buytaert, W., & Zehe, E. (2011). Temporal dynamics of model parameter sensitivity for computationally expensive models with the Fourier amplitude sensitivity test. *Water Resources Research, 47*(7). doi:https://doi.org/10.1029/2010WR009947

Rhodin, A., Kucharski, F., Callies, U., Eppel, D. P., & Wergen, W. (1999). Variational analysis of effective soil moisture from screen-level atmospheric parameters: Application to a short-range weather forecast model. *Quarterly Journal of the Royal Meteorological Society, 125*(559), 2427-2448. doi:https://doi.org/10.1002/qj.49712555905

Rimon, Y., Nativ, R., & Dahan, O. (2011). *Physical and Chemical Evidence for Pore-Scale Dual-Domain Flow in the Vadose Zone* (Vol. 10).

Rodgers, J., & Nicewander, A. (1988). Thirteen Ways to Look at the Correlation Coefficient. *American Statistician - AMER STATIST, 42*, 59-66. doi:10.1080/00031305.1988.10475524

Romano, N. (2014). Soil moisture at local scale: Measurements and simulations. *Journal of Hydrology, 516*, 6-20. doi:https://doi.org/10.1016/j.jhydrol.2014.01.026

Rosenbaum, U., Bogena, H. R., Herbst, M., Huisman, J. A., Peterson, T. J., Weuthen, A., Western, A. W., & Vereecken, H. (2012). Seasonal and event dynamics of spatial soil moisture patterns at the small catchment scale. *Water Resources Research, 48*(10), 1 - 22. doi:10.1029/2011WR011518

Rüdiger, C. (2006). *Streamflow Data Assimilation for Soil Moisture Prediction.* (PhD thesis), The University of Melbourne, Australia.

Rüdiger, C., Hancock, G., Hemakumara, H. M., Jacobs, B., Kalma, J. D., Martinez, C., Thyer, M., Walker, J. P., Wells, T., & Willgoose, G. R. (2007). Goulburn River experimental catchment data set. *Water Resources Research, 43*(10), n/a-n/a. doi:10.1029/2006WR005837

Rüdiger, C., Western, A. W., Walker, J. P., Smith, A. B., Kalma, J. D., & Willgoose, G. R. (2010). Towards a general equation for frequency domain reflectometers. *Journal of Hydrology, 383*(3), 319-329. doi:https://doi.org/10.1016/j.jhydrol.2009.12.046

Santi, E., Paloscia, S., Pettinato, S., Brocca, L., Ciabatta, L., & Entekhabi, D. (2018). On the synergy of SMAP, AMSR2 AND SENTINEL-1 for retrieving soil moisture. *International Journal of Applied Earth Observation and Geoinformation, 65*, 114-123. doi:https://doi.org/10.1016/j.jag.2017.10.010

Santos, W. J. R., Silva, B. M., Oliveira, G. C., Volpato, M. M. L., Lima, J. M., Curi, N., & Marques, J. J. (2014). Soil moisture in the root zone and its relation to plant vigor assessed by remote sensing at management scale. *Geoderma, 221-222*, 91-95. doi:https://doi.org/10.1016/j.geoderma.2014.01.006

Schaap, M. G., & Leij, F. J. (2000). Improved Prediction of Unsaturated Hydraulic Conductivity with the Mualem-van Genuchten Model. *Soil Science Society of America Journal, 64*(3), 843-851. doi:https://doi.org/10.2136/sssaj2000.643843x

Schaap, M. G., Leij, F. J., & van Genuchten, M. T. (2001). Rosetta: a computer program for estimating soil hydraulic parameters with hierarchical pedotransfer functions. *Journal of Hydrology, 251*(3), 163-176. doi:https://doi.org/10.1016/S0022-1694(01)00466-8

Schulz, K., & Beven, K. (2003). Data-supported robust parameterisations in land surface–atmosphere flux predictions: towards a top-down approach. *Hydrological Processes, 17*(11), 2259-2277. doi:https://doi.org/10.1002/hyp.1331

Seneviratne, S. I., Corti, T., Davin, E. L., Hirschi, M., Jaeger, E. B., Lehner, I., Orlowsky, B., & Teuling, A. J. (2010). Investigating soil moisture–climate interactions in a changing climate: A review. *Earth-Science Reviews, 99*(3), 125-161. doi:https://doi.org/10.1016/j.earscirev.2010.02.004

Shamsi, U. M. S., & Koran, J. (2017). Continuous calibration. *Journal of Water Management Modeling*.

Sheffield, J., & Wood, E. (2008a). Global Trends and Variability in Soil Moisture and Drought Characteristics, 1950 2000, from Observation-Driven Simulations of the

Terrestrial Hydrologic Cycle. *Journal of Climate - J CLIMATE, 21*. doi:10.1175/2007JCLI1822.1

Sheffield, J., & Wood, E. F. (2008b). Projected changes in drought occurrence under future global warming from multi-model, multi-scenario, IPCC AR4 simulations. *Climate Dynamics, 31*(1), 79-105. doi:10.1007/s00382-007-0340-z

Shi, Y., Zhai, P., & Jiang, Z. (2016). Multi-sliding time windows based changing trend of mean temperature and its association with the global-warming hiatus. *Journal of Meteorological Research, 30*(2), 232-241. doi:10.1007/s13351-016-5093-3

Sillmann, J., & Roeckner, E. (2007). Indices for extreme events in projections of anthropogenic climate change. *Climatic Change, 86*, 83-104. doi:10.1007/s10584-007-9308-6

Šimůnek, J., & van Genuchten, M. T. (2008). Modeling Nonequilibrium Flow and Transport Processes Using HYDRUS. *Vadose Zone Journal, 7*(2), 782-797. doi:https://doi.org/10.2136/vzj2007.0074

Simunek, J. J., J. Jarvis, N., Van Genuchten, M., & Gärdenäs, A. (2003). *Review and comparison of models for describing non-equilibrium and preferential flow and transport in the vadose zone* (Vol. 272).

Simunek, J. J., Saito, H., Sakai, M., & Van Genuchten, M. (2008). *The HYDRUS-1D Software Package for Simulating the One-Dimensional Movement of Water, Heat, and Multiple Solutes in Variably-Saturated Media*.

Simunek, J. J., Šejna, M., Saito, H., Sakai, M., & Van Genuchten, M. (2013). The Hydrus-1D Software Package for Simulating the Movement of Water, Heat, and Multiple Solutes in Variably Saturated Media, Version 4.17, HYDRUS Software Series 3, Department of Environmental Sciences, University of California Riverside, Riverside, California. *USA*.

Sivapalan, G. B. M. (1995). Scale issues in hyrological modelling: a review. *Hydrological Processes, 9*, 41.

Smith, A. B., Walker, J. P., Western, A. W., Young, R. I., Ellett, K. M., Pipunic, R. C., Grayson, R. B., Siriwardena, L., Chiew, F. H. S., & Richter, H. (2012). The Murrumbidgee soil moisture monitoring network data set. *Water Resources Research, 48*(7), n/a-n/a. doi:10.1029/2012WR011976

Stalenberg, E., Hutchinson, M. F., & Foley, W. (2018). Using historical normals to improve modern monthly climate normal surfaces for Madagascar. *International Journal of Climatology, 38*. doi:10.1002/joc.5776

Statistics, A. B. o. (2020). "National, state and territory population – March 2020". Retrieved from https://www.abs.gov.au/statistics/people/population/national-state-and-territory-population/mar-2020

Stern, H., Hoedt, G., & Ernst, J. (2000). Objective classification of Australian climates. *Australian Meteorological Magazine, 49*, 87-96.

Story, R., Tweedie, A., van de Graaf, R., & Galloway, R. (1963). No. 8 General Report on the Lands of the Hunter Valley. *CSIRO Land Research Surveys, 2010*(1), 1-156. doi:https://doi.org/10.1071/LRS08

Stott, P. (2016). How climate change affects extreme weather events. *Science, 352*, 1517-1518. doi:10.1126/science.aaf7271

Stumpp, C., Nützmann, G., Maciejewski, S., & Maloszewski, P. (2009). A comparative modeling study of a dual tracer experiment in a large lysimeter under atmospheric conditions. *Journal of Hydrology, 375*(3), 566-577. doi:https://doi.org/10.1016/j.jhydrol.2009.07.010

Sun, M., Zhang, X., Huo, Z., Feng, S., Huang, G., & Mao, X. (2016). Uncertainty and sensitivity assessments of an agricultural–hydrological model (RZWQM2) using the GLUE method. *Journal of Hydrology, 534*, 19-30. doi:https://doi.org/10.1016/j.jhydrol.2015.12.045

Tang, C., & Piechota, T. C. (2009). Spatial and temporal soil moisture and drought variability in the Upper Colorado River Basin. *Journal of Hydrology, 379*(1), 122-135. doi:https://doi.org/10.1016/j.jhydrol.2009.09.052

Teuling, A. J., & Troch, P. A. (2005). Improved understanding of soil moisture variability dynamics. *Geophysical Research Letters, 32*(5). doi:10.1029/2004GL021935

Tian, S., Renzullo, L. J., van Dijk, A. I. J. M., Tregoning, P., & Walker, J. P. (2019). Global joint assimilation of GRACE and SMOS for improved estimation of root-zone soil moisture and vegetation response. *Hydrol. Earth Syst. Sci., 23*(2), 1067-1081. doi:10.5194/hess-23-1067-2019

Timbal, B., Power, S., Colman, R., Viviand, J., & Lirola, S. (2002). Does Soil Moisture Influence Climate Variability and Predictability over Australia? *Journal of Climate - J CLIMATE, 15*, 1230-1238. doi:10.1175/1520-0442(2002)015<1230:DSMICV>2.0.CO;2

Tyner, J., Wright, W., & Yoder, R. (2007). *Identifying Long-Term Preferential and Matrix Flow Recharge at the Field Scale* (Vol. 50).

USDA. (2017). *Soil survey manual USDA Handbook 18*. Washington, D.C.: Government Printing Office.

Vachaud, G., Passerat De Silans, A., Balabanis, P., & Vauclin, M. (1985). Temporal Stability of Spatially Measured Soil Water Probability Density Function1. *Soil Science Society of America Journal, 49*(4), 822-828. doi:10.2136/sssaj1985.03615995004900040006x

Van Dijk, A. I. J. M. (2010). *The Australian Water Resources Assessment System. Technical Report 3. Landscape Model (version 0.5). Technical Description.* Retrieved from

Van Genuchten, M. (1980). A Closed-form Equation for Predicting the Hydraulic Conductivity of Unsaturated Soils1. *Soil Science Society of America Journal, 44*. doi:10.2136/sssaj1980.03615995004400050002x

Van Genuchten, M., Leij, F., Yates, S., & Williams, J. (1991). The RETC Code for Quantifying Hydraulic Functions of Unsaturated Soils. *EPA/600/2-91/065, R.S., 83*.

Vázquez, R. F., Beven, K., & Feyen, J. (2009). GLUE Based Assessment on the Overall Predictions of a MIKE SHE Application. *Water Resources Management, 23*(7), 1325-1349. doi:10.1007/s11269-008-9329-6

Verbesselt, J., Hyndman, R., Newnham, G., & Culvenor, D. (2010). Detecting trend and seasonal changes in satellite image time series. *Remote Sensing of Environment, 114*(1), 106-115. doi:https://doi.org/10.1016/j.rse.2009.08.014

Viney, N., J, V., R, C., B, W., W, D., & A, F. (2015). *AWRA-L v5.0: technical description of model algorithms and inputs*. Retrieved from Canberra:

Viscarra Rossel, R., Chen, C., Grundy, M., Searle, R., Clifford, D., Odgers, N., Holmes, K., Griffin, T., Liddicoat, C., & Kidd, D. (2014a). Soil and Landscape Grid

National Soil Attribute Maps - Clay (3" resolution) - Release 1. v5. CSIRO. Data Collection.
Viscarra Rossel, R., Chen, C., Grundy, M., Searle, R., Clifford, D., Odgers, N., Holmes, K., Griffin, T., Liddicoat, C., & Kidd, D. (2014b). Soil and Landscape Grid National Soil Attribute Maps - Sand (3" resolution) - Release 1. v5. CSIRO. Data Collection.
Viscarra Rossel, R., Chen, C., Grundy, M., Searle, R., Clifford, D., Odgers, N., Holmes, K., Griffin, T., Liddicoat, C., & Kidd, D. (2014c). Soil and Landscape Grid National Soil Attribute Maps - Silt (3" resolution) - Release 1. v5. CSIRO.
Wagener, T., & Gupta, H. V. (2005). Model identification for hydrological forecasting under uncertainty. *Stochastic Environmental Research and Risk Assessment, 19*(6), 378-387. doi:10.1007/s00477-005-0006-5
Wagner, W., Lemoine, G., & Rott, H. (1999). A Method for Estimating Soil Moisture from ERS Scatterometer and Soil Data. *Remote Sensing of Environment, 70*(2), 191-207. doi:https://doi.org/10.1016/S0034-4257(99)00036-X
Warrick, A. W., Mullen, G. J., & Nielsen, D. R. (1977). Scaling field-measured soil hydraulic properties using a similar media concept. *Water Resources Research, 13*(2), 355-362. doi:https://doi.org/10.1029/WR013i002p00355
Wasko, C., & Nathan, R. (2019). Influence of changes in rainfall and soil moisture on trends in flooding. *Journal of Hydrology, 575*, 432-441. doi:https://doi.org/10.1016/j.jhydrol.2019.05.054
Wasko, C., Shao, Y., Vogel, E., Wilson, L., Wang, Q. J., Frost, A., & Donnelly, C. (2021). Understanding trends in hydrologic extremes across Australia. *Journal of Hydrology, 593*, 125877. doi:https://doi.org/10.1016/j.jhydrol.2020.125877
Watson, D. J. (1947). Comparative Physiological Studies on the Growth of Field Crops: I. Variation in Net Assimilation Rate and Leaf Area between Species and Varieties, and within and between Years. *Annals of Botany, 11*(41), 41-76.
Watts, L. M., & Laffan, S. W. (2014). Effectiveness of the BFAST algorithm for detecting vegetation response patterns in a semi-arid region. *Remote Sensing of Environment, 154*, 234-245. doi:https://doi.org/10.1016/j.rse.2014.08.023
Weiler, M., & Flühler, H. (2004). Inferring flow types from dye patterns in macroporous soils. *Geoderma, 120*(1), 137-153. doi:https://doi.org/10.1016/j.geoderma.2003.08.014
Western, A. W., & Blöschl, G. (1999). On the spatial scaling of soil moisture. *Journal of Hydrology, 217*(3), 203-224. doi:https://doi.org/10.1016/S0022-1694(98)00232-7
Western, A. W., Blöschl, G., & Grayson, R. B. (1998). Geostatistical characterisation of soil moisture patterns in the Tarrawarra catchment. *Journal of Hydrology, 205*(1), 20-37. doi:https://doi.org/10.1016/S0022-1694(97)00142-X
Western, A. W., Grayson, R. B., & Blöschl, G. (2002). Scaling of Soil Moisture: A Hydrologic Perspective. *Annual Review of Earth and Planetary Sciences, 30*(1), 149-180. doi:10.1146/annurev.earth.30.091201.140434
Western, A. W., Grayson, R. B., Blöschl, G., Willgoose, G. R., & McMahon, T. A. (1999). Observed spatial organization of soil moisture and its relation to terrain indices. *Water Resources Research, 35*(3), 797-810. doi:10.1029/1998WR900065

Western, A. W., Zhou, S.-L., Grayson, R. B., McMahon, T. A., Blöschl, G., & Wilson, D. J. (2004). Spatial correlation of soil moisture in small catchments and its relationship to dominant spatial hydrological processes. *Journal of Hydrology, 286*(1), 113-134. doi:https://doi.org/10.1016/j.jhydrol.2003.09.014

Whan, K., Zscheischler, J., Orth, R., Shongwe, M., Rahimi, M., Asare, E. O., & Seneviratne, S. I. (2015). Impact of soil moisture on extreme maximum temperatures in Europe. *Weather and Climate Extremes, 9*, 57-67. doi:https://doi.org/10.1016/j.wace.2015.05.001

Wigneron, J.-P., Olioso, A., Calvet, J.-C., & Bertuzzi, P. (1999). Estimating root zone soil moisture from surface soil moisture data and soil-vegetation-atmosphere transfer modeling. *Water Resources Research, 35*(12), 3735-3745. doi:https://doi.org/10.1029/1999WR900258

Willgoose, G. R., & Sharmeen, S. (2006). A one-dimensional model for simulating armouring and erosion on hillslopes: 1. model development and event-scale dynamics. *Earth Surface Processes and Landforms, 31*(8), 970-991. doi:https://doi.org/10.1002/esp.1398

Wu, W., & Dickinson, R. E. (2004). Time Scales of Layered Soil Moisture Memory in the Context ofLand–Atmosphere Interaction. *Journal of Climate, 17*(14), 2752-2764. doi:10.1175/1520-0442(2004)017<2752:Tsolsm>2.0.Co;2

Yan, L., Jin, J., & Wu, P. (2020). Impact of parameter uncertainty and water stress parameterization on wheat growth simulations using CERES-Wheat with GLUE. *Agricultural Systems, 181*, 102823. doi:https://doi.org/10.1016/j.agsy.2020.102823

Yates, S., Van Genuchten, M., Leij, F., & Warrick, A. (1992). Analysis of Measured, Predicted, and Estimated Hydraulic Conductivity Using the RETC Computer Program. *Soil Science Society of America Journal, 56*, 347-354. doi:10.2136/sssaj1992.03615995005600020003x

Yee, M. S., Walker, J. P., Monerris, A., Rüdiger, C., & Jackson, T. J. (2016). On the identification of representative in situ soil moisture monitoring stations for the validation of SMAP soil moisture products in Australia. *Journal of Hydrology, 537*, 367-381. doi:https://doi.org/10.1016/j.jhydrol.2016.03.060

Zacharias, S., Bogena, H., Samaniego, L., Mauder, M., Fuß, R., Pütz, T., Frenzel, M., Schwank, M., Baessler, C., Butterbach-Bahl, K., Bens, O., Borg, E., Brauer, A., Dietrich, P., Hajnsek, I., Helle, G., Kiese, R., Kunstmann, H., Klotz, S., & Vereecken, H. (2013). *A Network of Terrestrial Environmental Observatories in Germany* (Vol. 10).

Zeng, W., Xu, C., Wu, J., & Huang, J. (2014). Soil salt leaching under different irrigation regimes: HYDRUS-1D modelling and analysis. *Journal of Arid Land, 6*(1), 44-58. doi:10.1007/s40333-013-0176-9

Zhang, J., Wang, W.-C., & Leung, L. R. (2008). Contribution of land-atmosphere coupling to summer climate variability over the contiguous United States. *Journal of Geophysical Research: Atmospheres, 113*(D22). doi:https://doi.org/10.1029/2008JD010136

Zhang, P., Šimůnek, J., & Bowman, R. S. (2004). Nonideal transport of solute and colloidal tracers through reactive zeolite/iron pellets. *Water Resources Research, 40*(4). doi:https://doi.org/10.1029/2003WR002445

Zheng, G., & Moskal, L. M. (2009). Retrieving Leaf Area Index (LAI) Using Remote Sensing: Theories, Methods and Sensors. *Sensors, 9*(4), 2719-2745.

Zribi, M., Paris Anguela, T., Duchemin, B., Lili, Z., Wagner, W., Hasenauer, S., & Chehbouni, A. (2010). Relationship between soil moisture and vegetation in the Kairouan plain region of Tunisia using low spatial resolution satellite data. *Water Resources Research, 46*(6), n/a-n/a. doi:10.1029/2009WR008196

Zucco, G., Brocca, L., Moramarco, T., & Morbidelli, R. (2014). Influence of land use on soil moisture spatial–temporal variability and monitoring. *Journal of Hydrology, 516*(Supplement C), 193-199. doi:https://doi.org/10.1016/j.jhydrol.2014.01.043